Award Number: W81XWH-**06-1-0303**

TITLE: BATTLE (Biomarker-based Approaches of Targeted Therapy for Lung Cancer Elimination)

PRINCIPAL INVESTIGATOR:
Waun Ki Hong, M.D.

CONTRACTING ORGANIZATION:
The University of Texas M. D. Anderson Cancer Center
Houston, TX 77030

REPORT DATE: April 2011

TYPE OF REPORT: Annual

PREPARED FOR: U.S. Army Medical Research and Materiel Command
Fort Detrick, Maryland 21702-5012

DISTRIBUTION STATEMENT:

X Approved for public release; distribution unlimited

REPORT DOCUMENTATION PAGE

Form Approved
OMB No. 0704-0188

1. REPORT DATE *(DD-MM-YYYY)*	2. REPORT TYPE	3. DATES COVERED *(From - To)*
30-Apr-2011	Annual	01 APR 2010 - 31 MAR 2011

4. TITLE AND SUBTITLE
BATTLE (Biomarker-based Approaches of Targeted Therapy for

Lung Cancer Elimination)

5a. CONTRACT NUMBER
W81XWH-06-1-0303

5b. GRANT NUMBER

5c. PROGRAM ELEMENT NUMBER

6. AUTHOR(S)
Waun Ki Hong, M.D.

whong@mdanderson.org

5d. PROJECT NUMBER

5e. TASK NUMBER

5f. WORK UNIT NUMBER

7. PERFORMING ORGANIZATION NAME(S) AND ADDRESS(ES)

The University of Texas M.D. Anderson Cancer Center
Houston, TX 77030

8. PERFORMING ORGANIZATION REPORT NUMBER

9. SPONSORING / MONITORING AGENCY NAME(S) AND ADDRESS(ES)
U.S. Army Medical Research and Materiel Command
Fort Detrick, Maryland 21702-5012

10. SPONSOR/MONITOR'S ACRONYM(S)

11. SPONSOR/MONITOR'S REPORT NUMBER(S)

12. DISTRIBUTION / AVAILABILITY STATEMENT

Approved for public release; distribution unlimited

13. SUPPLEMENTARY NOTES

14. ABSTRACT

The Program BATTLE seeks to establish individualized targeted therapy by prospectively examining patients' tumor biomarker profiles and assigning them to corresponding targeted therapies with the expectation to yield a better clinical outcome. Based on common altered signaling pathways in lung cancer, the BATTLE Program proposes to develop four phase II trials for chemorefractory, advanced NSCLC patients: erlotinib, ZD6474, bexarotene with erlotinib, and sorafenib which target, respectively, EGFR, VEGF / VEGFR, retinoid X receptor and cyclin D1, and Ras / Raf signaling pathways. A novel adaptive randomization statistical design will be applied to the clinical trials to accelerate the identification of best-fit treatment for patients. We propose also to study the molecular mechanisms of response or resistance to these targeted agents, identify novel molecular features in tumors and surrogate tissues to correlate with tumor response or resistance to the agents and, finally, explore other novel targeted agents (RAD001 and perifosine) in combination and their mechanisms of action by targeting mTOR and PI3K/Akt signaling, and develop phase I trials to test these combinations.

15. SUBJECT TERMS
Lung cancer, biomarker, targeted therapy, ZD6474, erlotinib, Sorafenib, bexarotene.

16. SECURITY CLASSIFICATION OF: U			17. LIMITATION OF ABSTRACT	18. NUMBER OF PAGES	19a. NAME OF RESPONSIBLE PERSON
a. REPORT	b. ABSTRACT	c. THIS PAGE			USAMRMC
U	U	U	UU	111	19b. TELEPHONE NUMBER *(include area code)*

TABLE OF CONTENTS

INTRODUCTION

Lung cancer is the leading cause of cancer-related death in both men and women in the United States. Chemotherapy has reached its limit in improving the survival of lung cancer patients. Therefore, a different strategy must be waged in the battle against lung cancer. Targeted therapy, a newly emerged therapeutic approach in lung cancer, has succeeded in some cancer types and demonstrated its initial success in the treatment of lung cancer when a class of targeted agents termed epidermal growth factor receptor (EGFR) tyrosine kinase inhibitors, such as gefitinib and erlotinib, improved tumor response rates in patients with advanced non-small cell lung cancer (NSCLC), which was strongly correlated to the presence of *EGFR* mutations in the tumors (Cappuzzo and Hirsch et al., 2004; Cappuzzo and Magrini et al., 2004; Gatzemeier et al., 2004; Herbst and Giaccone et al., 2004; Herbst and Prager et al., 2004; Herbst and Sandler et al., 2004; Lynch et al., 2004; Kobayashi et al., 2005; Miller et al., 2004; Pao et al., 2004; Paez et al., 2004; Shepherd et al., 2004; Shigematsu et al., 2005). This has for the first time demonstrated the importance of selecting patients for individualized targeted therapy in NSCLC.

The Program **BATTLE** (**B**iomarker-integrated **A**pproaches of **T**argeted **T**herapy for **L**ung Cancer **E**limination) seeks to establish individualized targeted therapy by prospectively examining patients' tumor biomarker profiles and assigning them to corresponding targeted therapies with the expectation to yield a better clinical outcome. This novel approach will be a proof-of-principle experiment to test the benefit of molecular-based individualized targeted therapy for lung cancer patients. Specifically, the objectives of the BATTLE program are:

1) To establish a clinical trial program using biomarkers to select individualized targeted therapy for patients with chemorefractory advanced NSCLC through the implementation of molecular classification based on the status of specific targeted biomarkers and adaptive randomization via hierarchical Bayes modeling.
2) To study the molecular mechanisms of response and resistance to targeted agents to discover new signaling pathways for test in future trials.
3) To identify molecular features in tumor tissues to correlate with tumor response or resistance, and identify serum biomarkers as surrogates.
4) To investigate other targeted agents in combination to overcome the resistance due to novel signaling pathways (e.g., mTOR and PI3K/Akt) and improve treatment efficacy.

BATTLE is composed of four Specific Aims with four phase II clinical trials and an umbrella protocol in Aim 1, six research projects in Aims 2 - 4, and two potential phase I trials in Aim 4. Here, we present our scientific progress of the BATTLE program for this fifth grant year.

PROGRESS REPORT

Aim 1 To establish a clinical trial program using biomarker assessment to select individualized targeted therapy for previously treated chemorefractory advanced NSCLC patients.

(PI, Co-PIs, and Investigators: Drs. Waun Ki Hong, Roy Herbst, Edward S. Kim, George Blumenschein, Anne Tsao, Hai Tran, Marshall Hicks, Rodolfo Morice, Bruce Johnson)

Specific Aim 1 has five clinical trials: one umbrella trial and four Phase II open-label trials. After screening, eligible patients are enrolled in the umbrella trial, and tumor biopsies are taken for biomarker analysis conducted by the Biomarker Core. (For details, please see the Biomarker Core section of this report.) Biomarker results are analyzed by the Biostatistics and Data Management Core. (For details, please see the Biostatistics and Data Management Core section of this report.) There are two components of this study: 1) an equal randomization phase, where patients are randomized equally to the four trials after biomarker analysis; and 2) an adaptive randomization phase, where patients are enrolled to one of the four clinical trials based on their tumor biomarker characteristics. The four Phase II clinical trials are presented in the four sub-aims of Aim 1 described below and depicted in Figure 1. An update is provided following the list of subaims.

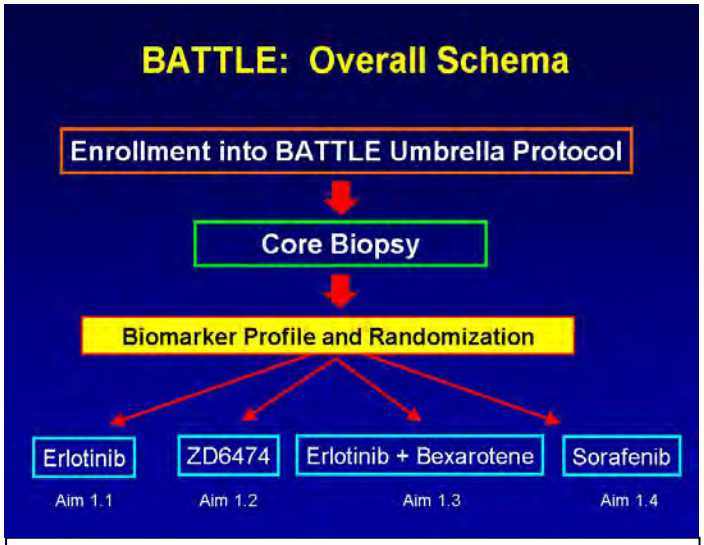

Figure 1. Overall Schema for BATTLE Trials.

Aim 1.1 To conduct a clinical trial with erlotinib in patients with previously treated advanced NSCLC whose tumors have EGFR mutations and / or overrepresentation.

Primary objective is to determine the 8-week progression-free survival (PFS) rate of patients with previously treated advanced NSCLC whose tumors have EGFR mutations and / or overrepresentation who are treated with erlotinib.

Secondary objectives are to 1) determine the overall survival rate, response rate, and toxicity profiles of patients with advanced NSCLC whose tumors have EGFR mutations and / or overrepresentation and treated with erlotinib, 2) determine the plasma and (if available) tumor tissue concentrations of erlotinib and their correlation with response and toxicity by using pharmacokinetics and pharmacodynamic modeling.

Aim 1.2 To conduct a clinical trial with ZD6474 in patients with previously treated advanced NSCLC whose tumors have increased VEGF and / or VEGFR-2.

Primary objective is to determine the 8-week PFS rate in patients with previously treated advanced NSCLC whose tumors have increased VEGF and / or VEGFR-2 who are treated with ZD6474.

Secondary objectives are to 1) determine the overall survival rate, response rates, and toxicity profiles of patients with advanced NSCLC whose tumors express increased VEGF and / or VEGFR-2 and treated with ZD6474, and 2) determine the plasma and (if available) tumor tissue levels of ZD6474 and their correlations with response and toxicity by using pharmacokinetics and pharmacodynamic modeling.

Aim 1.3 To conduct a clinical trial with the combination of bexarotene and erlotinib trial in patients with previously treated advanced NSCLC whose tumors have expressed RXRs and / or increased cyclin D1.

Primary objective is to determine the 8-week PFS rate in patients with previously treated advanced NSCLC whose tumors have expressed RXRs and / or increased cyclin D1 who are treated with the combination of Bexarotene and Erlotinib.

Secondary objectives are to 1) determine the overall survival rate, response rate, and toxicity profiles of patients with advanced NSCLC whose tumors have expressed RXRs and / or increased cyclin D1 and treated with the combination of bexarotene and erlotinib, 2) determine the plasma and (if available) tumor tissue concentrations of bexarotene and erlotinib and their correlation with response and toxicity by using pharmacokinetics and pharmacodynamic modeling.

Aim 1.4 To conduct a clinical trial with sorafenib trial in patients with previously treated advanced NSCLC whose tumors have mutated *K-ras* and / or *B-raf.*

Primary objective is to determine the 8-week PFS rate in patients with previously treated advanced NSCLC whose tumors have mutant *K-ras* and / or *B-raf* who are treated with sorafenib.

Secondary objectives are to 1) determine the overall survival rate, response rate, and toxicity profiles of patients with advanced NSCLC whose tumors have mutated K-ras and / or B-raf and treated with sorafenib, 2) determine the plasma and (if available) tumor tissue concentrations of sorafenib and their correlation with response and toxicity by using pharmacokinetics and pharmacodynamic modeling.

Summary of Research Findings

Results from Specific Aim 1 were detailed in the previous annual report. During this project period, the primary BATTLE primary manuscript and two commentaries were published online in inaugural issue of the newest AACR journal, *Cancer Discovery* (E Kim, R Herbst, I Wistuba, JJ Lee et al., Cancer Discovery 2011). Other manuscripts are currently being prepared for submission during the next unfunded extension period. A detailed list of all manuscripts in progress is attached in the Appendix.

Specific Aim 2: To investigate molecular mechanisms of response and resistance to the targeted agents used in the BATTLE program.

Specific Aim 2.1. To validate the molecular mechanisms of response and resistance to erlotinib for patients with chemorefractory NSCLC.

(PI and Co-PI: Bruce Johnson, M.D., and Pasi Jänne, M.D., Ph.D.)

The association between somatic epidermal growth factor receptor (*EGFR*) mutations and clinical response to gefitinib in patients with non-small cell lung cancer (NSCLC) was published in 2004. This proposal builds on previous findings to further characterize *EGFR* mutations in subjects' tumors and in tumor cell lines and the relationship of these mutations, subject outcome, and *in vitro* behavior to different EGFR inhibitors. The data generated demonstrates that subjects whose NSCLCs have *EGFR* mutations typically respond to single-agent therapy

with gefitinib, are treated for a median of 1 year or longer, and achieve a median overall survival duration longer than 2 years. This survival duration is 3-fold longer than that achieved with conventional chemotherapy in previously untreated subjects with NSCLC. The patients treated with gefitinib or erlotinib with increased copy number assessed by fluorescence in situ hybridization (FISH) have a response rate of 20-30% and the patients live a median of approximately 2 years. The goal of this research is to confirm these initial observations in prospective cohorts of subjects with NSCLC and somatic *EGFR* mutations or increased copy number with erlotinib as the initial therapy. This proposal is generating translational information on somatic mutations and copy number, prospective validation of the outcome of patients with NSCLC and *EGFR* mutations or increased copy number treated with erlotinib, information on activation of the EGFR pathway in NSCLC and NSCLC cell lines, and information about mechanisms of resistance.

Objective 1: Establish estimates of the response and outcome of previously treated patients with prospectively identified somatic *EGFR* mutations treated with erlotinib.

Summary of Research Findings
Results from this aim were detailed in the previous annual report.

Objective 2: Determine effects of TGF-α, EGF, and AR on the growth of *EGFR*-mutant and wild-type cell lines.

Summary of Research Findings
Results from this aim were detailed in the previous annual report.

Objective 3: Determine effects of TGF-α, EGF, and AR on the cell cycle and apoptosis of *EGFR*-mutant and wild-type cell lines.

Summary of Research Findings
Results from this aim were detailed in the previous annual report.

Objective 4: Determine effects of different *EGFR* mutations and EGFR inhibitors on phosphorylation of EGFR and downstream signaling intermediates.

Summary of Research Findings
Results from this aim were detailed in the previous annual report.

Specific Aim 2.2. Insulin-like Growth Factor Receptor Signaling Pathways and Resistance to Gefitinib in Non Small-Cell Lung Cancer Cells

(PI: Ho-Young Lee, Ph.D.)

Non-small cell lung cancer (NSCLC) accounts for about 75%-80% of lung cancer cases and its dismal survival rate has not improved in the past 2 decades. The lack of effective therapy, the high proportion of patients with advanced disease at the time of diagnosis, and the rapidity of tumor progression are major contributors to lung cancer mortality, and raises the urgent need for novel strategies to treat this disease. Of many potential targets in adult solid tumors, the epidermal growth factor receptor (EGFR) has been extensively studied because overexpression of EGFR has been observed in a number of other common solid tumors including 40–80% of NSCLC (Jemal et al, 2003). Therefore, one therapeutic strategy was to use the agents targeting

the EGFR pathway. However, negative results from several large-scale phase III clinical trials in lung cancer have been reported (Giaccone et al, 2002; Johnson, 2002), indicating the need for understanding the mechanisms that induce resistance to EGFR inhibitors. Accumulating evidence has implicated insulin-like growth factor receptor-I (IGF-IR) pathways in resistance to chemotherapy, radiation therapy, and molecularly targeted agents (Kulik et al, 1997; Lin et al, 1999; DiGiovanni et al, 2000; Porras et al, 1998; Toker and Newton, 2000). Our objective is to investigate whether IGF-IR and downstream signaling mediators, such as PI3K/Akt and MAPK, are involved in the resistance to anti-EGFR therapies in NSCLC.

Objective 1: **Determine whether inhibition of the IGF-1R–mediated signaling pathway augments the antiproliferative effects of erlotinib on NSCLC cells *in vitro,* and investigate the mechanism by which erlotinib leads NSCLC cells to activate the IGF-1R signaling pathway.**

Objective 2: **Determine whether inhibition of the IGF-1R–mediated signaling pathway augments effects of erlotinib on the growth of human NSCLC xenograft tumors established in nude mice.**

Objective 1 and 2 have been completed and were reported previously. In the past year, we investigated whether inhibition of the IGF-1R-mediated signaling pathway augments the anti-proliferative effects of IGF-1R antibody, either individually or in combination with EGFR antibodies on NSCLC cells *in vitro* to confirm our findings reported in prior years. We performed multiple target tracing (MTT) analysis but were not able to detect any effects from the treatments. We plan to analyze the anchorage-independent growth of a subset of NSCLC cells after treatment in studies supported by outside funding mechanisms

Objective 3: **Investigate whether IGF-1R activity influences the therapeutic activity of erlotinib in patients with NSCLC.**

Summary of Research Findings

In collaboration with Dr. Ignacio Wistuba, we performed immunohistochemical analysis on IGF-1R expression in patients with NSCLC and found significantly higher expression levels of IGF-1R in male patients compared to female patients ($P<0.0001$) but no difference in pIGF-1R/IR expression. Notably, expression levels of IGF-1R and pIGF-1R/IR were significantly higher in patients with squamous cell carcinoma ($P<0.0001$) than in patients with adenocarcinoma after tissue microarrays analysis was performed. No significant difference in survival has been observed between the high IGF-1R expression and low expression groups in these studies. The correlation between the therapeutic activity of erlotinib and IGF-1R phosphorylation (as an indicator of IGF-1R activity) needs to be further investigated outside the scope of this grant.

Key Research Accomplishments:

- Performed IHC analysis on IGF-1R expression in NSCLC patients and found expression levels of IGF-1R and pIGF-1R/IR were significantly higher in patients with squamous cell carcinoma ($P<0.0001$) than in patients with adenocarcinoma.
- Planned future studies to analyze anchorage-independent growth of NSCLC cells after treatment.

Conclusions

Our findings from the *in vitro* study indicate the potential for integration of IGF-1R-targeted agents into treatment regimens using EGFR TKIs for patients with lung cancer. Future studies are needed to verify our data to allow us to translate these findings into the clinic.

Specific Aim 2.3. To investigate the molecular mechanisms of resistance to and biomarkers of the biologic activity of inhibitors of the VEGF pathway

(PI: John Heymach, M.D., Ph.D.)

The primary goals of this Aim were to develop biomarkers for the activity of VEGF inhibitors and investigate potential markers of therapeutic resistance. Substantial progress has been made towards these goals. The focus of our effort thus far has been in the identification of potential mechanisms of resistance to VEGF inhibitors and development of our methodologies for identification of blood-based biomarkers, in large part because of specimen availability. Notable advances over the past year, detailed below, include the following: 1) Identification of KDR (copy number gain and protein levels) as a marker of both VEGFR inhibitor benefit and resistance to chemotherapy. 2) Identification of tumor endothelial markers (TEM) and development of techniques for assessing circulating TEM+ endothelial cells; 3) Plasma profiling of cytokine and angiogenic factors in the BATTLE patient samples

The objectives of this aim have not been modified since the project began. Progress on these objectives is detailed below.

Objective 1: Quantitatively assess VEGFR phosphorylation, downstream signaling, and biomarkers of angiogenesis in pre- and post-treatment tumor biopsy samples.

Summary of Research Findings

KDR CNGs in NSCLC: frequency and correlation with KDR protein and angiogenesis.

Our preliminary data suggests the KDR copy number gains (CNGs) or protein levels may be associated with both VEGFR inhibitor benefit and resistance to chemotherapy. Dr. Ignacio Wistuba initially reported the presence of CNGs within the 4q12 amplicon (Yang et al, *in preparation*). In that study, CNGs (>4 copies) were observed in 7% of adenocarcinomas and 11% of squamous cell carcinomas. To further investigate the characteristics of these tumors, we evaluated *KDR* copy gains in NSCLC cells microdissected from 139 tumor specimens by qPCR, and detected CNGs in 45 (32%) of tumors examined. *KDR* CN ranged from 4.0 to 11 copies, and no *KDR* CNGs were detected in adjacent normal tissue. All 20 NSCLC specimens positive for *KDR* copy gains by qPCR were also confirmed as positive by FISH. We observed a similar frequency of *KDR* copy gain in adenocarcinoma (26/85, 31%) and squamous cell carcinoma (19/54, 35%) histologies. In addition, *KDR* CNG was associated with increased KDR protein expression by IHC (Figure 2E). We also observed significantly higher microvessel density (MVD) in tumors with *KDR* CNGs than those without (Figure 2F).

We studied the impact of KDR CNGs and protein *in vitro* in 63 NSCLC cell lines through our Lung SPORE effort and found that cell lines with KDR CNGs, assessed by CGH arrays, had significantly greater resistance to cisplatin by MTS assay. We also assessed KDR protein by RPPA and found higher levels of KDR to be significantly correlated with resistance to both cisplatin and carboplatin (Figure 2G, 1H).

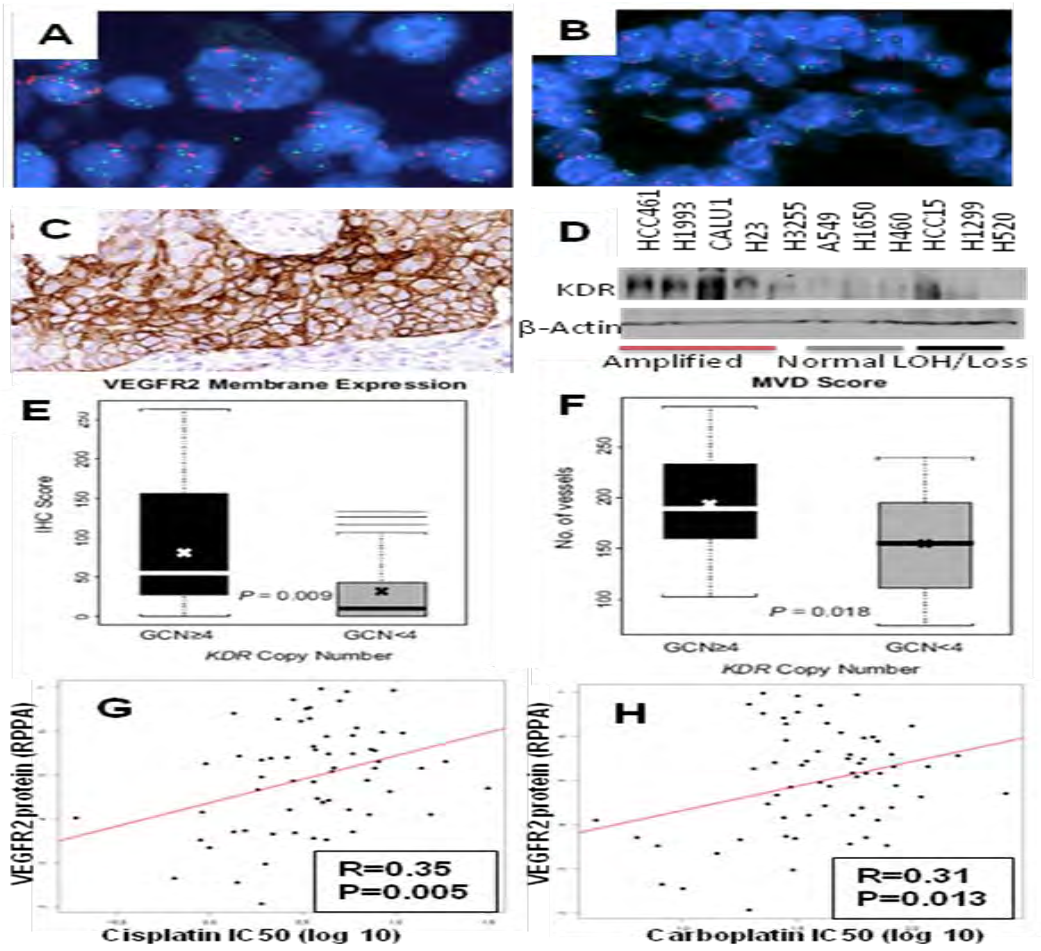

Figure 2. KDR CNGs are associated with increased KDR protein levels, angiogenesis, and *in vitro* chemoresistance. Representative *KDR* FISH in NSCLC tissue specimens ***(A)*** with CNG and ***(B)*** without. *KDR* probe is red, and the chromosome 4 reference probe green. ***C.*** KDR IHC in NSCLC with CNG. Both cytoplasmic and membrane staining of tumor cells was observed (200x). ***D.*** WB for in cell lines with KDR CNG vs normal or LOH, showing higher KDR protein in lines with CNG. ***E.*** KDR IHC score and ***(F)*** MVD were significantly higher in tumors with KDR CNG than those without (p=0.009 and 0.018). ***(G, H)*** CIS and CARBO sensitivity for 63 NSCLC cell lines was assessed by MTS assay *in vitro*. Cells with KDR CNGs were significantly more resistant to CIS (p<0.05; data not shown). KDR protein was assessed by RPPA. There was a significant correlation between KDR levels and drug resistance; p=.005 (CIS) and .013 (CARBO).

<u>KDR CNG predicted worse outcome in NSCLC patients treated with adjuvant chemotherapy.</u> *KDR* CNG was tested in 115 NSCLC patients with or without adjuvant therapy. In the multivariate analysis after adjusting for stage, *KDR* CNG predicted a worse OS (HR=5.16, *p*=0.003) in patients who received adjuvant therapy, but did not predict poor OS (*p*=0.349) in patients without adjuvant therapy (Figure 3A, 2B), suggesting that *KDR* CNG in malignant cells may represent a predictive marker for adjuvant chemotherapy. Together, the data s upport an association of *KDR* CNG and chemoresistance.

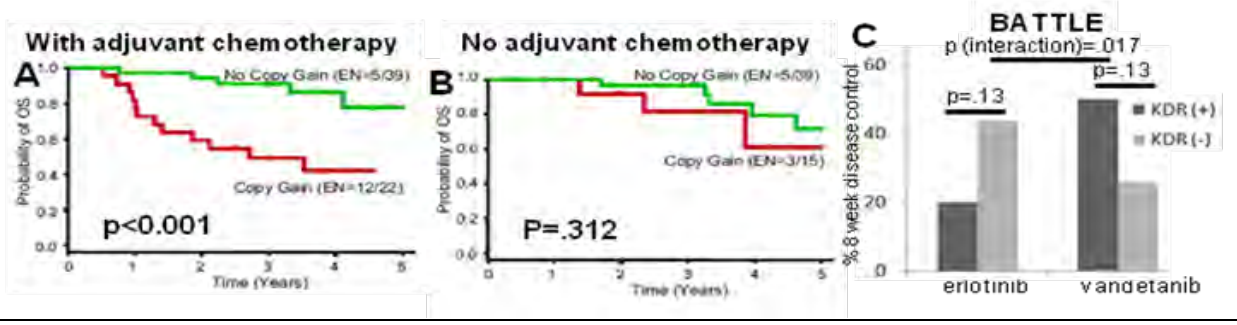

Figure 3. KDR CNGs predict significantly worse OS and RFS (not shown) in resected NSCLC pts with ***(A)*** but not without ***(B)*** adjuvant chemotherapy. In the BATTLE study, high KDR IHC was associated with trends towards worse DC in the erlotinib arm but better DC in vandetanib (*p* interaction)=0.017).

KDR protein is associated with improved disease control (DC) in BATTLE pts treated with vandetanib vs. erlotinib.

Tumor KDR was assessed by IHC. In the vandetanib arm, KDR+ patients had improved 8-week DC, the primary endpoint, compared to KDR- pts (Figure 3C). In the erlotinib arm, the KDR+ patients demonstrated a trend towards worse DC, and was, therefore, predictive of DC (*p* for interaction=0.017). PFS showed a similar trend (not shown). In future work outside the scope of this grant, KDR CNGs will be assessed from these tumors and from the phase III ZEST trial of the same two drugs.

Effect of *KDR* knockdown on platinum sensitivity and cell migration in cell lines.

We observed that cell lines with KDR CNGs had a significantly higher level of HIF-1α in normoxia, consistent with our earlier studies showing regulation of this pathway in normoxia by RTKs. We conducted KDR knockdown and observed decreased migration in cell lines with KDR CNG and also observed that KDR knockdown sensitized H23 cell line to cisplatin chemotherapy. Specifically, siRNA targeting *KDR* significantly decreased *KDR* mRNA expression by RT-PCR, and VEGFR-2 expression by Western blot, compared with control cells transfected with scrambled siRNA and non-transfected cells (Figure 4A). To evaluate the effect of *KDR* overexpression on sensitivity to cisplatin, we inhibited the expression of *KDR* by transfecting H23 and H461 cells with control siRNA or siRNA targeting *KDR* and then treated the cells with increasing concentrations of the chemotherapy drugs. The sensitivity of H23 cells to cisplatin (Figure 4B) was increased in si*KDR* transfected cells when compared with control siRNA-transfected or untransfected cells, suggesting that VEGFR-2 is contributing to chemoresistance in this model. We have also already shown that VEGFR-2 promotes tumor cell migration, as knockdown or reduction of VEGFR-2 expression induced by si*KDR* transfection significantly inhibited the migration of H23 cells compared with siRNA control-transfected or untransfected cells (Figure 4C).

Correlation Between *KDR* CNG and HIF-1α Expression in Cell Lines and Tumors.

The observations that *KDR* CNGs were associated with increased angiogenesis, chemoresistance, and migration suggested that VEGFR-2 may be impacting the HIF-1α pathway, which is known to affect each of these cellular properties. To investigate this finding further, we evaluated HIF-1α levels by ELISA in a panel of NSCLC cell lines with a range of *KDR* copy numbers and expression of VEGFR-2. HIF-1α levels were higher in cell lines with *KDR* CNG, and significantly (*p*=0.02) higher in cells with 6-9 gene copies, compared to cells with no CNG (Figure 4D). In H23 cells that had *KDR* CNG, stimulation with VEGF-A induced a rise in HIF-1α expression. Furthermore, knockdown of *KDR* significantly (*p*=0.01) reduced HIF-1α levels (Figure 4E). These data indicated that VEGFR-2 can regulate HIF-1α in a ligand-

dependent, but hypoxia-independent, manner in NSCLC cells. We have also investigated the potential association between *KDR* CNG and HIF-1α in NSCLC clinical specimens. Similar to the results in the NSCLC cell lines, tumor tissue specimens with *KDR* CNG (n=25) demonstrated a significantly (p=0.037) higher expression of nuclear HIF-1α expression by IHC than tumors without CNG (n=22) (Figure 4F, 4G).

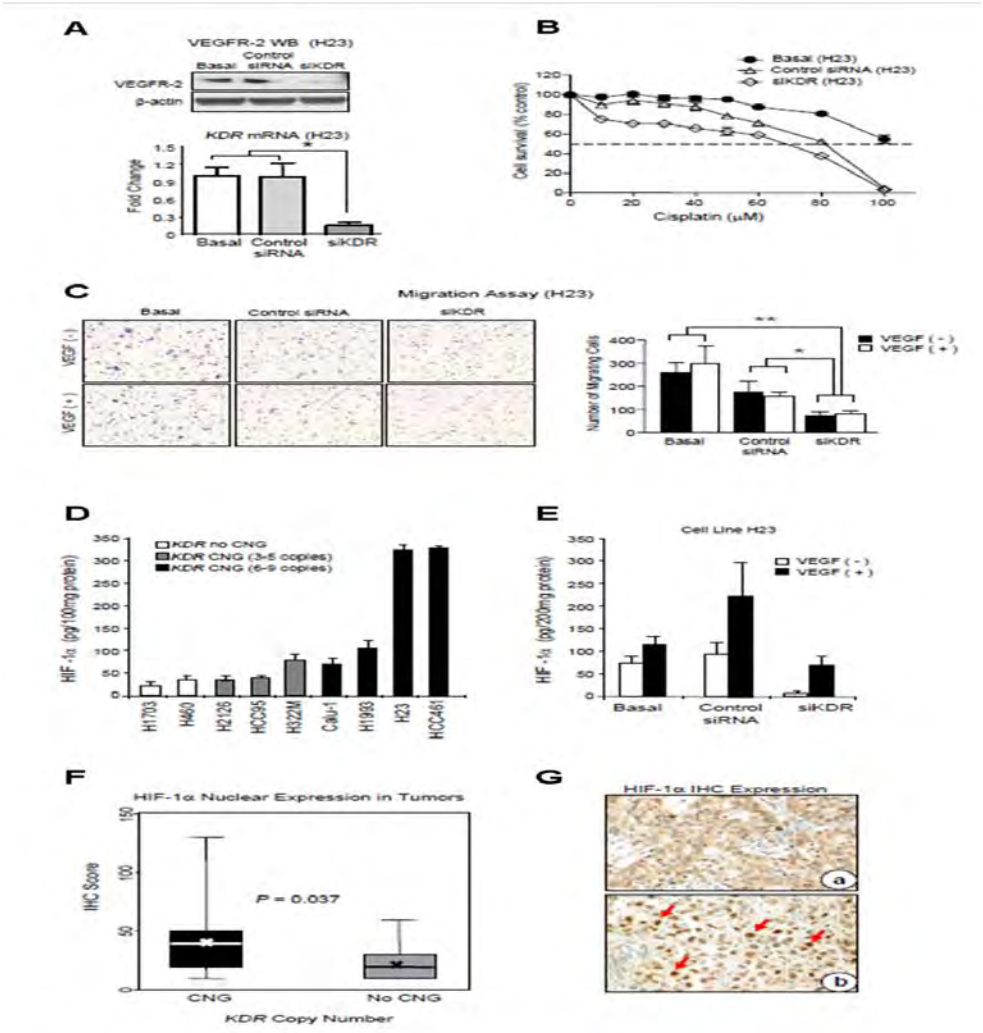

Figure 4. Effect of *KDR* Knockdown on Platinum Sensitivity and Cell Migration in Cell Lines and Correlation Between *KDR* CNG and HIF-1α Expression in Cell Lines and Tumors. ***A.*** siRNA targeting *KDR* (si*KDR*) in NSCLC cell line H23 inhibited significantly the expression of VEGFR-2 by Western-blot (WB) and *KDR* mRNA by qRT-PCR compared with basal and scrambled control siRNA (*p<0.05). ***B.*** knocking down *KDR* using siRNA decreased the viability of NSCLC cell line H23 exposed to cisplatin by MTS assay. Knockdown of *KDR* in H23 cells caused 1.9-fold decrease in the cisplatin IC_{50} (p<0.05). ***C.*** migration of NSCLC cell line H23 was inhibited by knocking down *KDR* using si*KDR* in cells with and without stimulation with VEGF (*p<0.05: **p<0.003). ***D.*** HIF-1α protein expression determined by ELISA correlated with *KDR* CNG in a series of NSCLC cell lines (cell lines with CNG 6-9 copies versus 3-5 copies and no CNG, *p<0.02). ***E.*** HIF-1α expression by ELISA was markedly inhibited by knocking down using si*KDR* in NSCLC H23 cell line with and without stimulation with VEGF (*p<0.01). ***F.*** expression of nuclear HIF-1α in tumors with *KDR* CNG compared with lung cancers without CNG. ***G.*** representative example of low (*a*, adenocarcinoma) and high (*b*, squamous cell carcinoma) IHC expression of HIF-1α in NSCLC tissue specimens (×200). *Red arrows*, positive nuclear HIF-1α immunostaining.

Objective 2: Investigate the utility of circulating endothelial cells (CECs), monocytes, and other cells in peripheral blood as biomarkers for antiangiogenic activity and inhibition of the VEGF pathway.

Summary of Research Findings

Our previous work focused on identifying tumor endothelial markers (TEMs) in preclinical models that would identify a new subset of circulating TEM+ positive endothelial cells (CTECs) derived from tumor endothelium sloughed into the circulation. This sloughing is known to increase after antiangiogenic therapy and therefore, we hypothesized that this population of detectable CTECs may increase after antiangiogenic therapy. Thus, identification of the tumor endothelium-specific CECs would provide a more accurate measure of response to antiangiogenic therapy. Analysis of the samples from the BATTLE clinical study is underway, and will be reported in the final progress report.

Objective 3: Systematically examine changes in the plasma and serum angiogenic profiles consisting of a panel of proangiogenic cytokines, targeted receptors, and potential biomarkers of endothelial damage.

Summary of Research Findings

During the cytokine and angiogenic (CAF) analysis using multiplex magnetic bead assays of the 185 baseline samples obtained from patients whom consented to the optional blood collection and analysis, we detected significant batch effects. The cause was determined to be a fault of the manufacturing of the plates themselves and the analysis of these baseline samples was therefore redone to ensure the collection of satisfactory data. . This analysis incorporated a total of 65 analytes including newly available markers of the EGFR axis such as Amphiregulin, Betacellulin, EGF, EGFR, Epiregulin, FGF-basic, HB-EGF, PDGF-BB, PlGF, Tenascin C, TGF-α. The data was sent to send to Biostatistics/Bioinformatics Core for analysis and a report will be forthcoming on results of this analysis. We are also in the process evaluating available post-treatment samples to determine treatment effects on CAFs.

Key Research Accomplishments:

- Detected KDR CNGs in NSCLC and predicted worse outcome in patients treated with adjuvant chemotherapy.
- Associated KDR CNGs with improved disease control in BATTLE patients treated with vandetanib versus erlotinib.
- Evaluating a new population of circulating TEM+ endothelial cells (CTECs) in a set of clinical BATTLE samples; these CTECs may offer a more specific biomarker for evaluating the effect of angiogenesis inhibitors .
- Re-analyzed CAFs in 185 samples from BATTLE study due to the identification of batch effects in the previous analysis; data analysis is underway.

Conclusions

Our preliminary data suggest that tumor cell KDR may be a potential therapeutic target, and that NSCLC tumors with KDR CNGs may be particularly sensitive to KDR inhibition. Taken together with the BATTLE data and the *in vitro* studies, these data provide evidence that: 1) KDR CNGs occur in NSCLC with relatively high frequency; 2) CNGs result in increased KDR protein; and 3) KDR protein and/or CNGs appear to be associated with relapse after adjuvant chemotherapy, increased angiogenesis, chemoresistance *in vitro*, and potentially, response to VEGF inhibitors or RTKIs. We therefore expect inhibitors to slow tumor growth and sensitize to chemotherapy

but not to induce apoptosis in vitro as seen with EGFR TKIs in *EGFR*-mutant tumors. Our preclinical studies have identified a number of potential markers that predict response to VEGFR inhibitors. It will be interesting to see if these same markers will predict response in patient samples. In addition, our studies have identified a new population of cells that can be detected that identify circulating endothelial cells derived from tumor endothelium. Analysis of this population of cells in patients treated with angiogenesis inhibitors is likely to be a better prognostic marker of response to treatment.

Several plasma CAFs are associated with specific tumor-derived pathway activation. Our preliminary study suggests that broad-based plasma profiling of cytokines and angiogenic factors may be a feasible approach for identifying markers of activation of tumor signaling pathways. In addition to the evaluation of pathway activation using plasma samples, we will be evaluating modulation of CAFs by each treatment arm, evaluating for potential predictive plasma signatures with clinical outcome measures such as progression-free survival (PFS) during the next unfunded extension. The final step will be to validate the plasma predictive signature derived from BATTLE with other randomized clinical studies. These studies can also validate our results that identify circulating VEGF as a predictive marker of response to angiogenic therapies in other clinical studies.

Specific Aim 2.4. To investigate the molecular mechanisms of the effects of the combination of bexarotene and erlotinib on NSCLC cells

(PI: Reuben Lotan, Ph.D.)

The need to discover and introduce more effective treatment agents and combinations is urgent, as is the need to improve the selection of the right agent or combination of agents for each patient on the basis of our understanding of the molecular targets. The combination of the retinoid X receptor (RXR)-selective ligand Bexarotene and the epidermal growth factor receptor (EGFR) tyrosine kinase (TK) inhibitor erlotinib appears to be a promising approach, and it will be tested in patients with NSCLC in the BATTLE program. Some aspects of the mechanisms of action of these two agents are not fully resolved. Therefore, we propose to investigate how they exert their effects on NSCLC cells so as to improve their usefulness in future clinical trials.

The objectives of this project have not changed.

Objective 1: To determine by immunohistochemical analysis the expression of nuclear receptors (retinoic acid receptors [RAR]-α, -β, and -γ; RXR-α, -β, and -γ; and PPAR-γ1 and PPAR-γ2) and cyclin D1 in NSCLC specimens obtained from patients to be enrolled in the BATTLE umbrella trial and from patients whose cancer progresses on treatment.

Summary of Research Findings

This objective was a collaborative work with Dr. Ignacio Wistuba (Director of the Biomarker Core) on the analysis of NSCLC samples from the clinical trial patients continued, facilitated by the robust patient accrual. The progress is detailed in his report (see Biomarker Core).

Objective 2: Examine the effects of bexarotene, erlotinib, and rosiglitazone alone and in combination on the growth and apoptosis of NSCLC cells, cyclin D1 and PPAR-γ levels, and gene expression profiles.

Summary of Research Findings
Results from this aim were detailed previously.

Objective 3: Determine whether RXRs, EGFR, and PPAR-γ are required to mediate the effects of bexarotene, erlotinib, and rosiglitazone, respectively, on cell growth control and apoptosis, and examine the functional significance of changes in gene expression induced by receptor agonists used singly or in combinations.

Summary of Research Findings
Results from this aim were detailed in the previous annual report.

Objective 4: Evaluate the growth inhibitory effects and mechanisms of action of novel RXR ligands AGN194204 and 9cUAB30 alone or combined with erlotinib and rosiglitazone on NSCLC cells.

Summary of Research Findings
This aim was closed as reported previously.

Specific Aim 3: To identify biomarkers as novel predictors of clinical end points and potential therapeutic targets

(PI: Ignacio Wistuba, M.D.)

Objective 1: Identify molecular features in tumor tissues that correlate with patients' responses to individual regimens used in the clinical trials of the proposed program.

Summary of Research Findings
As reported in the previous year, the BATTLE clinical trial completed accrual in October 2009, with subsequent follow-up identifying 244 evaluable patients in December 2009. The patient response data to individual regimens in the clinical trial has been unblinded; during the last year, we performed an extensive bioinformatic and biostatistical analysis of the gene expression profiles obtained by Affymetrix array of a large portion of the lung tumor tissues using mRNA extracted from fresh core needle biopsies (CNBs). These molecular profiles analyses will be completed during the next unfunded year of the grant.

A total of 324 patients were biopsied in the clinical trial, and tumor tissue was detected in 270 cases. Of these, frozen tissue specimens from 257 patients were made available for RNA extraction and for global gene expression analysis. RNA quality was measured using the Nanodrop and Agilent Bioanalyzer, and a total of 187 RNA samples were found to be suitable for amplification using the NuGEN RNA Pico Amplification System. Of these, histology quality control was performed by the Biomarker Core C (Dr. I. Wistuba) in 175 frozen tissues samples, and malignant cells were detected in 143 (82%) of cases.

We selected mRNA from two sets of extractions. From the first extraction, a total of 50 qualified mRNA samples were used for gene expression analysis through the Affymetrix GeneChip array (Human Gene U 133 plus 2.0 array). Among the RNA samples tested, 32 (64%) showed acceptable gene expression profiles and the remaining 18 samples (36%) were labeled as of

poor quality and not suitable for analysis. As reported last year, our data suggested that *MYC* gene downregulation may play an important role in NSCLC resistance to platinum-based chemotherapy, and the role of MYC targeting agents in lung cancer therapy should be re-evaluated for future cancer treatment. These data are being prepared for publication (Saintigny et al., *manuscript in preparation*).

We subsequently adapted a new RNA amplification protocol (WT-Ovation™ RNA Pico Amplification System) developed by NuGEN and a new generation of Affymetrix GeneChips (Human Gene ST 1.0 Array) and analyzed the newly extracted 173 RNA samples. The new strategy generated high quality expression profiles from 139 samples suitable for bioinformatics analyses. Importantly, both the yield and the quality of gene expression profiles obtained from the recent 139 samples were significantly higher than the profiles from the previous 50 samples. During the last year, in collaboration with Drs. John Heymach (BATTLE co-Investigator), J. Jack Lee (Biostatistics Core B), and Kevin Coombes (Bioinformatics), we have developed and tested gene expression (Affymetrix) signatures (Table 1) in the BATTLE trial tissue specimens. As part of the trial, tumor biopsies were obtained for biomarker analysis, including mRNA expression profiling, immediately prior to treatment. Eight-week disease control (8-wk DC; the primary study endpoint) was correlated with signature scores from patients treated in each arm with targeted agents: erlotinib, erlotinib+bexarotene, sorafenib, or vandetanib. We have shown that two of those signatures (referred to as the "epithelial mesenchymal transition (EMT)" and "5-gene" signatures) were predictive of outcome in the BATTLE trial patients, while a third ("EGFR") predicted the presence of EGFR mutations. Currently, we are still in the process of refining and testing two additional signatures ("KRAS" and "Sorafenib") that we hypothesize will be associated with erlotinib and sorafenib treatments, and that we expect to finalize during the next unfunded year of the grant.

Table 1. Gene expression signatures developed and tested in the BATTLE NSCLC tumor specimens.

Signature	Sample Use to Derive Signature	Predictive of DC at 8 weeks in BATTLE		
		Yes/No	Treatment Arms	Type of Tumors
EGFR	Resected tumor tissues	No	None	--
EMT	Cell lines	Yes	Erlotinib	*EGFR* wild-type
5-gene	BATTLE tissues	Yes	Erlotinib	*EGFR* wild-type
KRAS*	Cell lines	No	None	--
"Sorafenib"*	BATTLE tissues	Yes	Sorafenib	--

* Signatures still being refined.

A brief description of the most developed signatures, EGFR, EMT and 5-gene, is provided:

EGFR Signature: *EGFR*-mutated NSCLCs bear hallmarks including sensitivity to EGFR tyrosine kinase inhibitors (TKIs); however, the biology of EGFR dependence is still poorly understood. In our DoD PROSPECT grant, we have developed a 72-gene signature using a training cohort of surgically resected lung adenocarcinomas that predicted tumors' *EGFR* mutation status in three independent datasets of tumors and cell lines. The signature correlated with sensitivity to erlotinib in cell lines *in vitro*, and improved survival, even in the wild-type *EGFR* subgroup, in surgically resected NSCLC tumors. In the EGFR signature, we identified 62 up-regulated and 29 down-regulated probesets in *EGFR* mutant and wild-type adenocarcinomas, with a 2-fold-change, and a false discovery rate of 4.7%. Our gene profiling studies showed that *EGFR* mutant tumors had significantly increased levels of endocytosis-related genes and lower levels of mitosis-related genes including *MYC* and the phosphatase *DUSP4*.

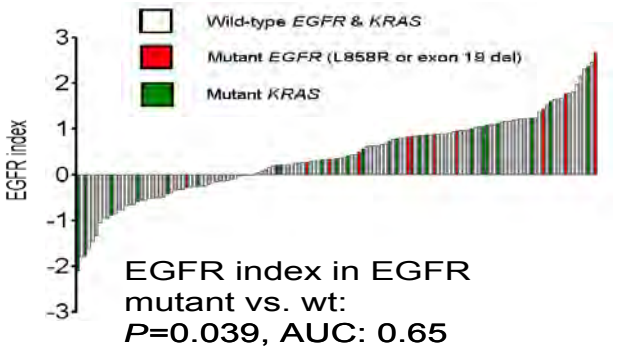

Figure 5. The EGFR signature, expressed as an index, significantly predicted EGFR mutation status in BATTLE tumors.

We then examined the performance of the EGFR signature as predictor of response in patients treated in the BATTLE trial. For analysis in the clinical specimens, including the BATTLE tumor samples, the signature was computed as an index, subsequently called EGFR index. 8-wk DC was correlated with the EGFR index score in patients with *EGFR* wild-type. In the BATTLE specimens (Figure 5), the EGFR signature predicted the presence of *EGFR* mutation in tumors, but did not predict response to any therapy in patients with *EGFR* wild-type tumors, including the EGFR TKI erlotinib (Figure 6). These data were presented (*Heymach et al*) in a late-breaking oral presentation in the 102nd Annual Meeting of the AACR, Orlando, April 2-6, 2011 (Saintigny et al, submitted).

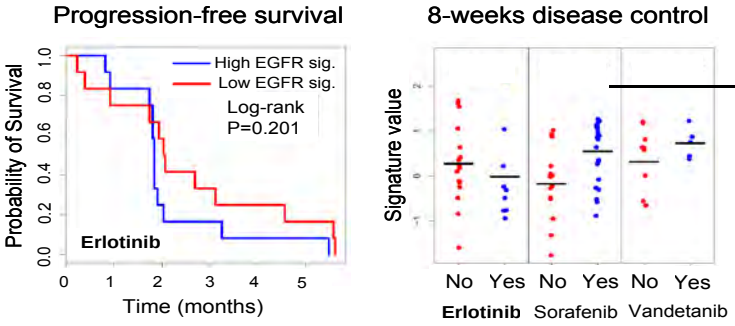

Figure 6. The EGFR Signature did not predict progression-free survival and 8-wk DC in BATTLE patients, including the erlotinib-treated ones.

EMT Signature: EMT is associated with loss of cell adhesion molecules, such as E-cadherin, and increased invasion, migration, and proliferation. In NSCLC, EMT is associated with resistance to EGFR inhibitors. In our DoD PROSPECT grant, we aimed to develop a robust EMT gene expression signature that could predict drug response and facilitate the identification of new, potentially therapeutic EMT markers. The EMT signature was originally derived in 54 NSCLC cell lines and tested in independent sets of NSCLC and head and neck squamous cell carcinomas lines. We identified 76 genes (the EMT signature) whose expression was highly correlated with one or more of four known EMT markers (E-cadherin [*CDH1*], vimentin [*VIM*], N-cadherin [*CDH2*], or fibronectin [*FN1*]) and bimodally distributed across the NSCLC cell line training set. Importantly, epithelial-like EMT scores predicted erlotinib sensitivity *in vitro* (*P*=0.028).

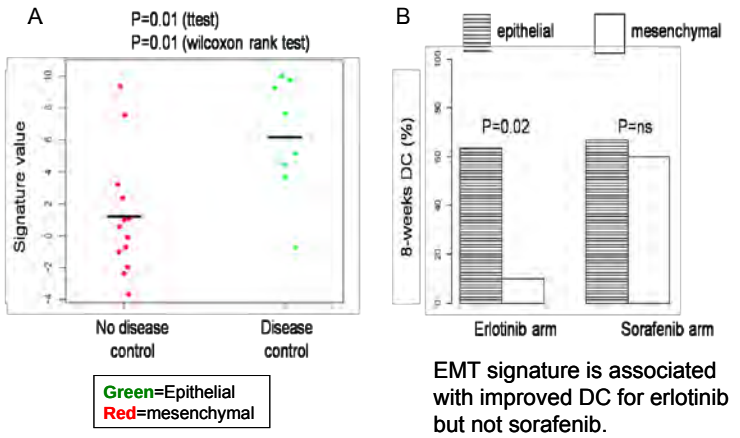

Figure 7. ***A***, EMT signature score associated with 8-wk DC in BATTLE patients with *EGFR* wild-type tumors and treated with erlotinib. ***B***, Patients with tumors having epithelial phenotype showed higher frequency of disease control in the erlotinib-treated, but not sorafenib-treated arm.

As noted above, we next analyzed the EMT signature in tumor specimens from patients with advanced NSCLC treated in the BATTLE trial. 8-wk DC was correlated with the EMT score in patients with *EGFR* wild-type and *KRAS* wild-type disease. Disease control following treatment with erlotinib was significantly associated with an epithelial-like phenotype, as determined by the first principal component (Figure 7). The difference in disease control predicted by the EMT score was not observed in other treatment arms, suggesting that EMT score is a marker of erlotinib activity in *EGFR* wild-type/*KRAS* wild-type tumors, not merely a prognostic marker of a less aggressive tumor phenotype. We have developed a novel predictor of response to EGFR tyrosine kinase inhibitors in NSCLC with wild-type *EGFR*, and also identified novel EMT markers with potential as therapeutic targets (see Goal 2).

Five-gene signature: Despite a low response rate, erlotinib improves survival in a subset of NSCLC patients with wild-type *EGFR,* but there are no established markers for identifying patients likely to have clinical benefit. We hypothesized that a gene expression signature could be used for this purpose. We used pretreatment gene expression profiles from 101 BATTLE patients treated in all arms of the trial. Twenty-four cases of wild-type *EGFR* and *KRAS* tumors from patients treated with erlotinib or erlotinib/bexarotene were compared to test the signature (two-sided t-test), using the primary end-point of the trial (8-wk DC). Principal component (PC) analysis and a logistic regression model were used to develop the signature. Gene expression profiles from 108 NSCLC cell lines, with available erlotinib IC50s (N=94) and DNA methylation profiling (N=66, Illumina), were used for *in vitro* studies.

We found that 113 genes were differentially expressed between patients with or without 8-wk DC (false discovery rate 30%; *P*=0.004). Leave-one-out cross validation with various gene list lengths produced a 5-gene signature, including lipocalin 2 gene (*LCN2*), with a specificity, sensitivity and accuracy of 80% to predict 8-wk DC (Figure 8). In patients treated with erlotinib or erlotinib+bexarotene, using the median signature score, the 8-wk DC rate in the signature-positive group was 83% compared with 0% in the signature-negative group; the

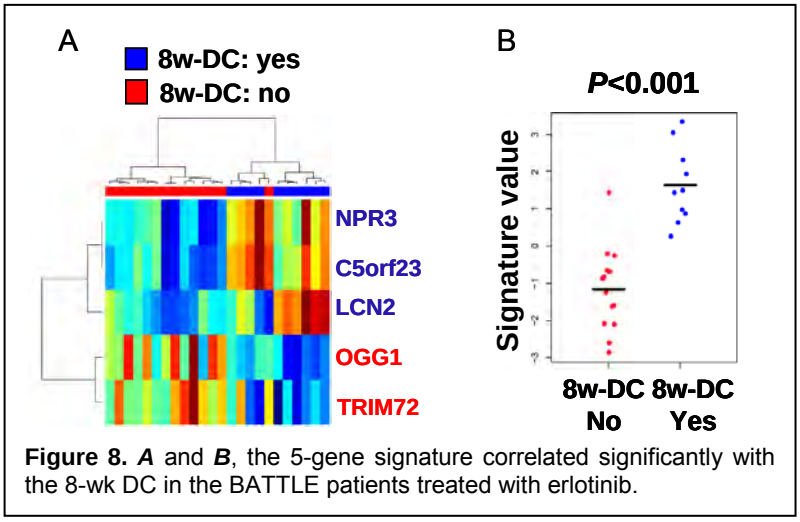

Figure 8. ***A*** and ***B***, the 5-gene signature correlated significantly with the 8-wk DC in the BATTLE patients treated with erlotinib.

signature did not predict 8-wk DC in patients treated with sorafenib or vandetanib (Mantel-Haenszel chi-squared test *P*=0.023).

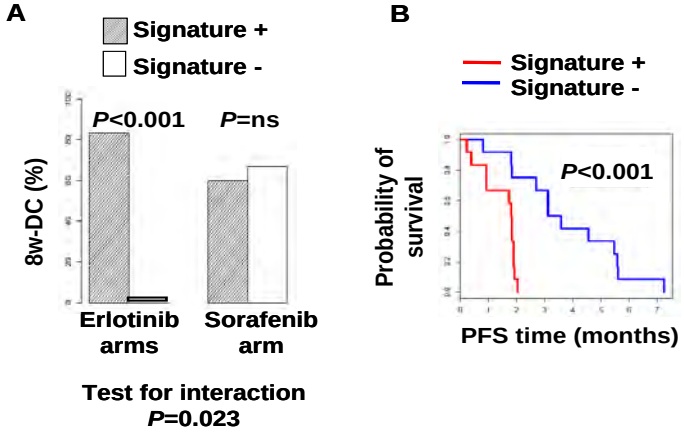

Figure 9. ***A***, the 5-gene signature correlated significantly with the 8-wk DC in the BATTLE patients treated with erlotinib and not in patients treated with sorafenib. ***B***, the signature associated significantly with recurrence free survival (RFS).

The improvement in 8-wk DC in the signature-positive group translated to an increased progression-free survival (PFS) (hazard ratio=0.12, 95% confidence interval: 0.03-0.46, *P*=0.001; log-rank *P*=0.0004; median PFS: 12.5 weeks vs. 7.2 weeks) (Figure 9).

We conclude that we have identified a 5-gene signature predictive of DC and PFS benefit in NSCLC patients with wild-type *EGFR* and *KRAS* treated with erlotinib, but not sorafenib or vandetanib. The signature was also predictive of erlotinib sensitivity *in vitro*. *LCN2* was the strongest individual marker of sensitivity and may be epigenetically regulated.

We have demonstrated that gene expression profiling from CNBs is a feasible approach for predicting response and identifying potential therapeutic targets in refractory NSCLC patients treated with targeted therapy. We have identified that an EGFR signature predicted mutation status but, in wild-type *EGFR* patients, did not predict 8-wk DC. Interestingly, the EMT and the novel 5-gene signatures were predictive of disease control in patients with wild-type *EGFR* and treated with the EGFR TKI erlotinib.

Additionally, in collaboration with the Biomarker Core C (Dr. I. Wistuba), proteomic analysis using the reverse phase protein array (RPPA) platform from of 215 BATTLE CNBs tumor specimens has been recently completed by Dr. Lauren Byers' lab, and the data are being subjected to quality control analysis. This proteomic analysis will be performed during the next unfunded year of the grant (an additional no-cost extension has been approved by the DoD).

Objective 2: Determine the effect of targeted agents in tumor tissues, and identify novel molecular mechanisms of tumor response or progression.

Summary of Research Findings

The gene mutation and expression profiling analyses performed in the BATTLE tumor tissue specimens in collaboration with the Biomarker Core C (Dr. I. Wistuba), and with several BATTLE investigators and collaborators, have provided information on several potential novel molecular mechanisms of NSCLC tumor response and resistance to targeted therapy. A description of 3 of those novel molecular mechanisms, and new potential molecular targets, is provided below.

1. Novel mechanisms of EGFR TKI response in EGFR wild-type NSCLC: Our gene profiling analyses of the BATTLE tumor specimens coupled with NSCLC cell line studies have resulted in the identification of at least 2 potential mechanisms of response to EGFR TKIs in *EGFR* wild-

type refractory NSCLC, as well as the development of potential new molecular targets in this disease.

a. EMT-related novel mechanisms and targets: An integrated analysis of the EMT signature scores (see Objective 1), including the BATTLE-derived data, and protein profiles of non-BATTLE-related samples, identified higher levels of Rab25 and activated EGFR pathway proteins in epithelial-like cell lines, and higher levels of Axl, PARP1, cRaf, and telomerase in mesenchymal-like lines. Of these, the Axl protein seems of great interest. *AXL* mRNA expression was shown to be strongly associated with *VIM* (r=0.6) and *N-Cadherin* (r=0.54) expression, and Axl protein was significantly higher in mesenchymal cell lines (P=0.002 by t-test). Interestingly, Axl expression has been associated with EMT and/or therapeutic resistance in other epithelial cancers, such as breast and colon cancer, and may represent a novel therapeutic target in mesenchymal-type or EGFR TKI-resistant NSCLC.

b. 5-gene signature-derived novel mechanisms and targets: We tested the 5-gene signature derived from the BATTLE tumor tissue specimens in an independent set of 47 wild-type *EGFR* and *KRAS* NSCLC cell lines. The signature predicted erlotinib sensitivity with an area under the curve of 78% (P=0.002). The first principal component of the signature and the IC50 for erlotinib were correlated (r=-0.47, P=0.0009). From the 5 genes, the range of *LCN2* expression was large with a bimodal expression pattern. The other genes (*NPR3*, *C5orf23*, *OGG1* and *TRIM72*) were expressed at very low levels *in vitro*. Interestingly, *LCN2* correlated significantly with the IC50 for erlotinib (r=-0.46, P=0.001) in 108 NSCLC cell lines tested (Figure 10). Then, we identified that the degree of methylation and expression level of *LCN2* were inversely correlated in wild-type *EGFR* and *KRAS* NSCLC cells (r=-0.79, P<0.0001, N=33). Cell lines with completely unmethylated *LCN2* were more sensitive to erlotinib compared to those with fully methylated *LCN2* (N=36; P=0.006); the difference remained significant in wild-type *EGFR* and *KRAS* cell lines (P=0.014). Currently, in collaboration with Biomarker Core C (Dr. I. Wistuba), LCN2 immunohistochemical protein expression has been examined in a large set of surgically resected NSCLC and the BATTLE CNB tissue specimens. Our data suggested that *LCN2* was the strongest individual marker of sensitivity from the 5-gene signature derived from the BATTLE tumors, and may be epigenetically regulated.

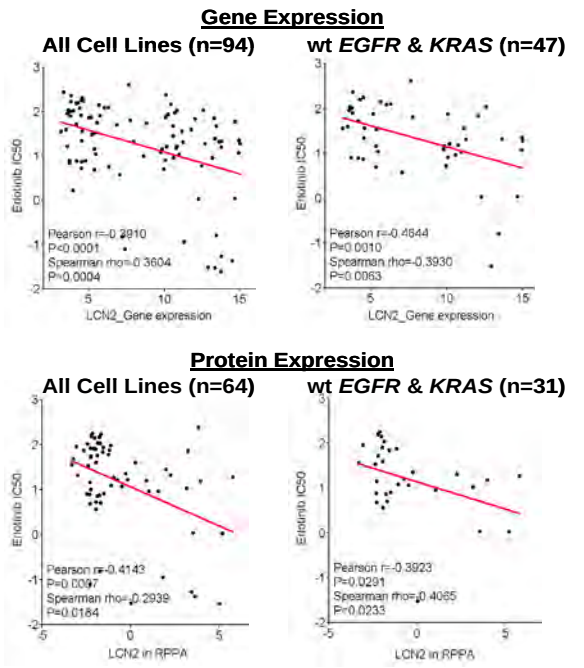

Figure 10. LCN2 gene and protein expression is correlated with *in vitro* sensitivity to erlotinib in NSCLC cell lines.

Subtypes of *KRAS* mutations: Mutant *KRAS* (mut-*KRAS*) is present in 30% of all human cancers and plays a critical role in cancer cell growth and resistance to therapy. There is evidence from colon cancer that mut-*KRAS* is a poor prognostic factor and negative predictor of patient response to molecularly targeted therapy. However, evidence for such a relationship in NSCLC is conflicting. *KRAS* mutations are primarily found at codons 12 and 13, where different base changes lead to alternate amino acid substitutions that lock the protein in an active state.

The patterns of mut-*KRAS* amino acid substitutions in colon cancer and NSCLC are quite different, with aspartate (D) predominating in colon cancer (50%) and cysteine (C) in NSCLC (47%).

In collaboration with Dr. G. Powis and N. Ihle, and through the analysis of 215 evaluable NSCLC patients treated in the BATTLE trial whose tumor specimens have *KRAS* mutation data obtained by the Biomarker Core C (Dr. I. Wistuba; Table 2), we showed that mut-*KRAS*-G12C/V but not total mut-*KRAS* predicts PFS for the overall group and for the sorafenib and vandetanib treatment arms (Figure 11). Mut-*KRAS*-G12C/V was associated with a significantly decreased PFS (*P*= 0.046, median survival 1.84 months) as compared to all other mut-*KRAS* (3.35 months) or wild-type *KRAS* (1.95 months). The effects of other prognostic factors such as age, gender, smoking status, and disease stage were controlled for by Cox regression. The sorafenib treatment arm of the trial showing that mut-*KRAS*-G12C/V was significantly associated with PFS (*P* =0.026, 1.84 months) compared to other mut-*KRAS* (3.55 months) or wild-type *KRAS* (2.83 months).

Table 2. *KRAS* mutation subtypes of 215 evaluable patients in the BATTLE trial.

		Cys/Val	Other	Wil
Total		26	20	258
	G	0	0	206
	A	0	6	0
	D	0	10	0
	C	19	0	0
	V	7	0	0
	Other	0	4	0
Codon		0	0	206
	10	0	1	0
	12	19	24	0
	61	0	2	0

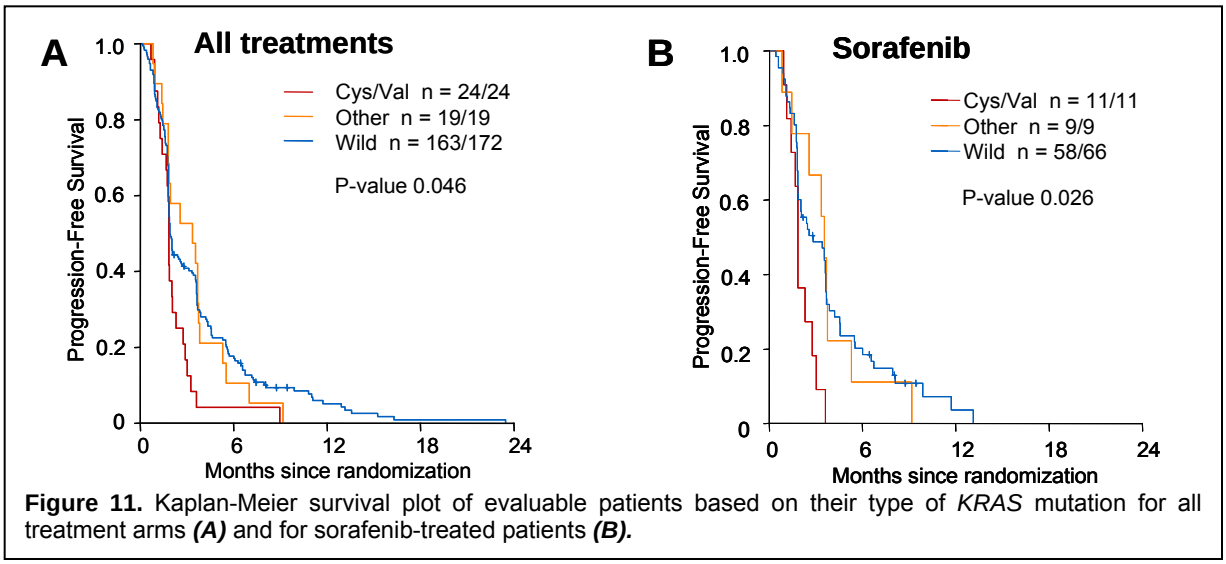

Figure 11. Kaplan-Meier survival plot of evaluable patients based on their type of *KRAS* mutation for all treatment arms ***(A)*** and for sorafenib-treated patients ***(B).***

The gene expression microarray (Affymetrix) data performed in the BATTLE tumor specimens showed differential expression of cell cycle genes between mut-*KRAS*-G12C/V and G12D patient tumors (Figure 12). A panel of NSCLC cell lines with known mut-*KRAS* amino acid substitutions was used to identify pathways activated by the different mut-*KRAS*, showing that mut-*KRAS*-G12D activates both PI-3-K and MEK signaling, while mut-*KRAS* G12C does not, and mut-*KRAS*-G12D alternatively activates RAL signaling. This finding was confirmed using immortalized human bronchial epithelial cells stably transfected with wild-type *KRAS* and different forms of mut-*KRAS*. Our molecular modeling studies show that the different

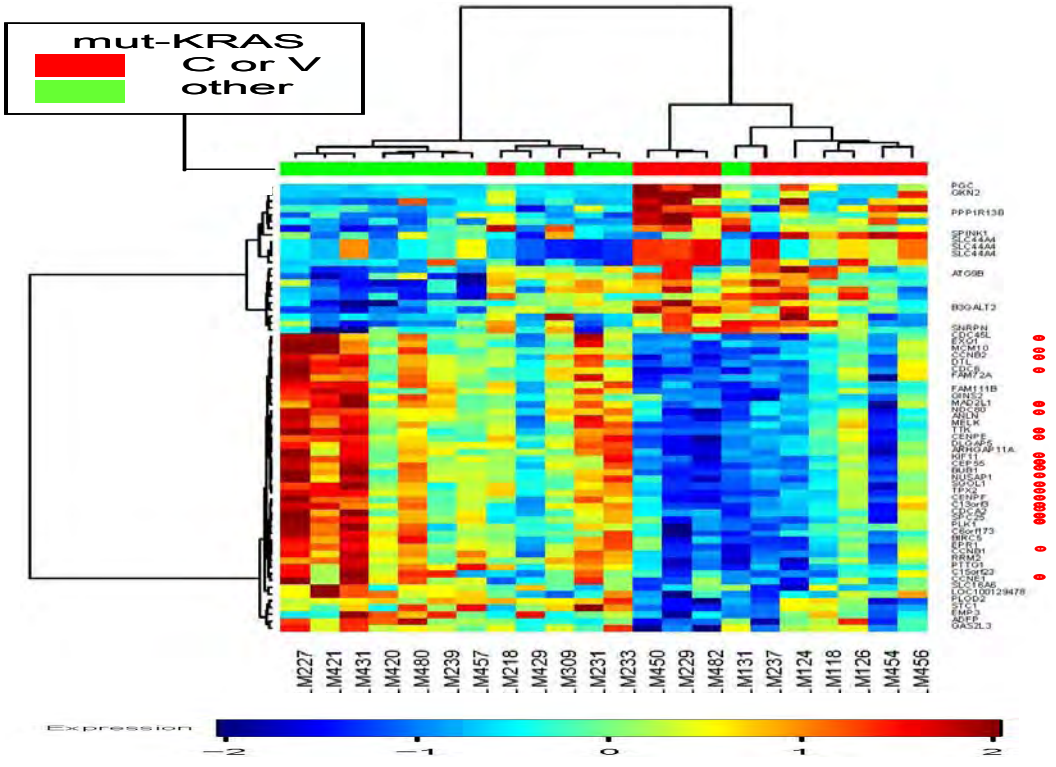

Figure 12. Clustering analysis of microarray data from patients treated in BATTLE trial of genes which most accurately define the differences between of two mut-*KRAS* groups. Red dots: genes involved in cell cycle regulation.

conformation imposed by mut-*KRAS*-G12C could lead to altered association with downstream signaling transducers compared to wild-type and mut-*KRAS*-G12D. The significance of the findings for developing mut-*KRAS* therapies is profound, since it suggests that not all mut-*KRAS* amino acid substitutions signal to effectors in a s imilar way, and may require different therapeutic interventions.

Key Research Accomplishments:

- Demonstrated that gene expression profiling from CNBs is a feasible approach for predicting response and identifying potential therapeutic targets in refractory NSCLC patients treated with targeted therapy.
- Developed and tes ted two gene expression signatures, the EMT and the novel 5-gene, which predicted 8-week disease control in patients with advanced and refractory NSCLC treated with the EGFR TKI erlotinib with wild-type *EGFR* tumors.
- Identified two novel molecular mechanisms of response to EGFR TKIs in patients with *EGFR* and *KRAS* wild-type NSCLC, involving the *AXL* and *LCN2* genes.
- Demonstrated that different therapeutic approaches may be required when treating patients with NSCLC harboring different mutant-*KRAS* amino acid substitutions.

Conclusions

We have demonstrated that gene expression profiling from CNBs is a feasible approach for predicting response and identifying potential therapeutic targets in refractory NSCLC patients

treated with targeted therapy. We have identified that the EGFR signature predicted *EGFR* gene mutation status but, in wild-type *EGFR* patients, did not predict 8-week disease control. Interestingly, an EMT and the novel 5-gene signatures were predictive of disease control in patients with wild-type *EGFR*-tumors in patients treated with EGFR TKIs. In addition, we identified at least two novel molecular mechanisms of response to EGFR TKIs and we discovered that not all mutant-*KRAS* amino acid substitutions signal to effectors in a similar way in NSCLC.

Specific Aim 4: To explore new preclinical combinations and their mechanisms of action by targeting mTOR signaling and develop phase I trials to test these combinations.

(PI and Co-PIs: Suresh Ramalingam, M.D., Shi-Yong Sun, Ph.D., Haian Fu, Ph.D.)

The overall objective of Aim 4 is to study the efficacy of mTOR inhibitor combination therapies that co-target mTOR and PI3K/Akt signaling. Following is a summary of our research progress for Year 3:

Objective 1: To study the efficacy of mTOR inhibitor combination therapies that co-target mTOR and PI3K/Akt signaling.

Summary of Research Findings

We previously demonstrated that the combination of an mTOR inhibitor and a PI3K inhibitor acted as a potential cancer therapeutic strategy. The findings on enhanced anticancer activity by the combination of RAD001 and BEZ235 against human lung cancer *in vitro* and *in vivo* has been summarized in a manuscript and submitted to *PLoS One* for publication.

We further tested the effects of RAD001 in combination with the novel PI3K inhibitor, BKM120, in a panel of human lung cancer cell lines and found that the combination synergistically inhibited the growth of lung cancer cells (the combination indexes are < 1). The combination demonstrated enhanced effects on G1 arrest, but did not exhibit an augmented effect on induction of apoptosis. Using these results as preliminary data, we have submitted a new proposal (Project 1) in our lung cancer PO1 renewal, in which we will elucidate the underlying mechanisms of combination therapies and validate our findings in animal models and in clinical trials.

We also studied whether BEZ235 induces autophagy in lung cancer cells. We found that BEZ235 induced autophagy evidenced by induction of type II LC3 while promoting apoptosis. BEZ235 reduced the levels of $FLIP_S$; and this effect contributes to BEZ235-induced autophagy because enforced expression of $FLIP_S$ abrogated type-II LC3 increase by BEZ235. When BEZ235 was used in combination with the lysosomal or autophagic inhibitor chloroquine (CQ), synergistic inhibitory effects on monolayer growth and colony formation of NSCLC cells was observed. Enhanced induction of apoptosis was also detected in cells exposed to the combination of BEZ235 and CQ. Moreover, the combination of BEZ235 and CQ was more effective than each single agent alone in inhibiting the growth of NSCLC xenografts in nude mice. Thus, BEZ235-induced autophagy appears to be a survival mechanism that may counteract BEZ235's anticancer activity. Accordingly, we suggest a strategy to enhance BEZ235's anticancer efficacy by blockade of autophagy. This research has been submitted to *Molecular Cancer Therapeutics* for publication.

Objective 2: To examine whether rapamycin-induced Akt activation suppresses ASK1-mediated apoptosis and leads to decreased therapeutic efficacy.

Summary of Research Findings

During this research period, we tested the Akt-mediated ASK1 signaling to demonstrate an enhanced therapeutic effect of rapalogs. Through this study, we discovered that Akt regulates ASK1 through a novel mechanism by activating IKK (I-κB kinase) to phosphorylate Ser967 of ASK1. Akt is known to play a pro-survival role in many settings, and is known to downregulate ASK1 activity through phosphorylation of another site, Ser83. Similarly, the region surrounding Ser967 of ASK1 fits nicely within the recognized phosphorylation motif of Akt, and Akt is known to phosphorylate several 14-3-3 client proteins within the 14-3-3 recognition motif, where Ser967 of ASK1 resides. Expression of inactive AktKM led to marked decrease in Ser967 phosphorylation, while AktΔPH resulted in dramatic Ser967 phosphorylation. Surprisingly, however, recombinant Akt was unable to phosphorylate ASK1 in an *in vitro* kinase assay. After confirming the activity of recombinant Akt with an antibody directed against phosphorylated Ser473, a phosphorylation indicative of Akt activity, we came to the conclusion that Akt does not phosphorylate ASK1 directly at Ser967. These data suggest that Akt plays an indirect role in Ser967 phosphorylation.

After discovering Akt is likely to be upstream of the kinase responsible for phosphorylation of ASK1 at Ser967, kinase substrates of Akt were investigated for further activity. Akt has been shown to activate the prominent pro-survival kinase, IKK. Thus, we tested the premise that IKK phosphorylates ASK1 at Ser967. Co-transfection of COS7 cells with wild-type IKK (IKK WT) increased basal levels of ASK1 Ser967 phosphorylation and prevented serum starvation-induced dephosphorylation of the kinase. When cells were co-transfected with a catalytically inactive form of IKK (IKK K44M), an obvious decrease of Ser967 dephosphorylation was observed in cells grown in the presence of serum, suggesting the kinase activity of IKK is critical in maintaining ASK1 Ser967 phosphorylation. To confirm the role for IKK in the phosphorylation of ASK1 at Ser967, an *in vitro* kinase assay was performed. Intriguingly, both IKKβ and IKKα could phosphorylate immunoprecipitated ASK1 *in vitro*. Furthermore, inhibition of IKK activity, whether through expression of a kinase-dead mutant of IKK or through pharmacological inhibition of the kinase, leads to decreased ASK1 Ser967 phosphorylation, even in the presence of AKT expression or IGF-1. These results suggest the exciting possibility that IKK is downstream of Akt in the signaling pathway leading to phosphorylation of ASK1 at Ser967.

Because ASK1 phosphorylation at Ser967 is important for 14-3-3 interaction and subsequent ASK1 inhibition, we sought to examine whether IKK can suppress ASK1-mediated signaling. Expression of IKK WT was sufficient to prevent H_2O_2-induced ASK1 Ser967 dephosphorylation and phosphorylation of downstream ASK1 substrates, including JNK and p38, supporting a role for IKK in the blockade of ASK1-mediated signaling. Finally, we sought to determine with IKK could prevent ASK1-mediated apoptosis. IKK WT, but not IKK K44M, was able to block ASK1-induced apoptosis, as measured by caspase activity. IKK expression also had no effect on the ability of ASK1 S967A to induce apoptosis, suggesting that IKK inhibits the apoptotic activity of ASK1 primarily through inducing phosphorylation at Ser967. Together, our research established a new signaling pathway by which Akt inhibits ASK1 through IKK. Our results point to a new strategy to block the rapamycin/rapalog-triggered feedback Akt activation through the inhibition of IKK in order to enhance the therapeutic efficacy of rapalogs.

Objective 3: To conduct two phase I clinical trials to test the efficacy of the combination of an mTOR inhibitor with an Akt or an EGFR inhibitor in advanced NSCLC patients resistant to the front and second line therapy, and assess the

modulation of targeted biomarkers from tumor tissues before and after the treatment.

Summary of Research Findings

In collaboration with investigators at MD Anderson Cancer Center and Dana Farber Cancer Center, a phase I study was conducted to evaluate the combination of RAD001 with erlotinib. Subsequently, a randomized phase II study was performed to compare the combination against monotherapy with erlotinib alone in patients with advanced stage NSCLC. The combination was tolerated well without undue increase in the incidence of adverse events. There was a trend towards improvement in PFS for the combination therapy, but the differences did not reach statistical significance. The disease control rate at 3 months was 39% for the combination compared to 28% for monotherapy with erlotinib. These results call for the identification of biomarkers for future patient selection. Based on the promising pre-clinical observations in objective 1, we will soon initiate a phase I study of RAD001 with BKM120, a PI3K inhibitor. This study will involve sequential biopsy collection to understand the molecular effects of the combination at the level of the tumor tissue.

Key Research Accomplishments:

- Demonstrated that the combination of RAD001 and BKM120 synergistically inhibits the growth of human lung cancer cells, warranting the clinical testing of this combination.
- Demonstrated that the combination of RAD001 and erlotinib results in modest improvements in efficacy, thus setting the stage for identification of predictive biomarkers with which to select patients who would most benefit from this regimen.

Conclusions

This project has resulted in significant improvement in utilization of mTOR inhibitors for the treatment of lung cancer. Our data with the combination of an mTOR inhibitor with a PI3K inhibitor represents a very promising approach for treating lung cancer. It is clear that monotherapy with mTOR inhibitors is not useful in selected patients, and treatment with novel combinations are the best way forward for future lung cancer patients.

Biostatistics and Data Management Core

(Core Director: J Jack Lee, Ph.D.)

In close collaboration with the Biomarker Core, the clinical research team, and each of the basic science research components, the Biostatistics and Data Management Core (BDMC) for the Department of Defense (DoD) BATTLE lung cancer research program is a comprehensive, multi-lateral resource for designing clinical and basic science experiments; developing and applying innovative statistical methodology, data acquisition and management, and statistical analysis; and publishing translational research generated by this research proposal.

The main objectives of the BDMC are as follows:

1. Develop and implement a novel adaptive randomization scheme for assigning patients into the treatment arms with the highest probability of success.
2. Provide the statistical design, sample size, and power calculations for each project.
3. Develop a secure, internet-driven, web-based database network between UTMDACC and other research centers, including Emory University and the Dana-Farber Cancer

Center, that integrates the clinical data generated by the five proposed clinical trials and relating basic science research efforts of the BATTLE research project.
4. Develop a comprehensive, Web-based database management system for tissue specimen tracking and distribution and for a central repository of all biomarker data.
5. Provide all statistical data analyses, including descriptive analysis, hypothesis testing, estimation, and modeling of prospectively generated data.
6. Provide prospective collection, entry, quality control, and integration of data for the basic science, pre-clinical, and clinical studies in the BATTLE grant.
7. Provide study monitoring and conduct that ensures patient safety by timely reporting of toxicity and interim analysis results to various institutional review boards (IRBs), the UTMDACC data monitoring committee, the DoD, and other regulatory agencies.
8. Generate statistical reports for all projects.
9. Collaborate with all project investigators and assist them in publishing scientific results.
10. Develop and adapt innovative statistical methods pertinent to biomarker-integrated translational lung cancer studies.

Summary of Research Findings

In this unfunded research period, the Biostatistics and Data Management Core continued to work with all project investigators and provide biostatistics and database management support for all projects and cores in the BATTLE program. We have completed the accrual of 341 patients and randomization of 255 of them in October 2009. The clinical trial operations, including treatment, clinical visits, outcome evaluation, and follow-up have progressed as planned. We have completed the clinical trial enrollment and the evaluation of the primary endpoint. Evaluation and analysis of the clinical and scientific secondary endpoints continues.

(A) Biostatistics

We have implemented a novel study design incorporating the hierarchical Bayesian model and adaptive randomization to identify the best treatment for each patient's biomarker profile and to adaptively randomize more patients into more effective treatments accordingly. We have written "R" programs and created videos to illustrate the adaptive randomization process. We provided statistical reports for our monthly project meetings to update the follow-up, toxicity, and outcome evaluation of the patients on trial. The main clinical results were presented at the Opening Plenary Session of the AACR Annual meeting in April, 2010, and published online in Cancer Discovery (E Kim et al. April 2011). Further detailed results of the sorafenib treatment was presented in the ASCO Annual meeting in June, 2010. The statistical design and the experience for conducting the BATTLE trial was presented at Joint Statistical Meetings in August, 2010. We have continued to work with clinical and basic science investigators in data analysis and manuscript writing.

(B) Data Management

Database programming effort:

- Worked closely with the Thoracic/Head and Neck Medical Oncology Nurses to make sure the data is meticulously updated, cleaned, and is accurate. This includes checking patient timelines for consent, randomization, response and off study, etc. Multiple iterations had taken place to achieve the goal.
- Histology reports were generated for the Research Nurses.

- Generated many reports for the Statistical Analyst on virtually all data captured to help with detailed analysis reports and statistics. This includes progression free survival reports, off study reports, medical history data as well as drug compliance data.
- Worked closely with the Thoracic/Head and Neck Labs on Phase II data and identifying patient re-enrollment.

Key Research Accomplishments:

- Performed extensive statistical analysis on the study findings including treatment efficacy, toxicity, compliance, pre-specified biomarkers, and discovery biomarkers, etc.
- Developed and maintained a secured, web-based database application to assist with the data collection and analysis.
- A web-based database application is developed, deployed, and maintained at: https://insidebiostat/DMI_BATTLE/Common/Login.aspx.

Conclusions

In collaboration with clinical investigators, research nurses, the Biomarker Core, and basic scientists, the Biostatistics and Data Management Core has continued to deliver the biostatistics and data management support as proposed.

Biomarker Core: Perform biomarker assessment to stratify patients into a particular arm of clinical trials and coordinate the distribution of clinical samples.

(Core Director: Ignacio Wistuba, M.D.)

The Biomarker Core, in close collaboration with the Biostatistics and Data Management Core, the Clinical Trial team, and Research Project Investigators, has played an important role in achieving the objectives proposed in the aims of the proposed BATTLE program by acquiring and processing lung cancer tissue specimens and performing the biomarker analysis for the stratification of patients into the clinical trials. In addition, the Core has collected and banked tissue specimens to support mechanistic studies of response or resistance to targeted agents used in the BATTLE trials.

The Biomarker Core has successfully combined standard methods of histopathology processing and assessment of lung cancer tissue specimens with more advanced tools of molecular and genetic biomarker analyses.

Objective 1: To acquire, bank, process, and distribute tumor and blood specimens obtained from BATTLE enrolled patients for biomarker analyses and molecular mechanistic studies of targeted agents.

Summary of Research Findings

In the BATTLE clinical trial, the Biomarker Core C collected and banked two types of core needle biopsy (CNB) NSCLC tumor specimens: 1) formalin-fixed and paraffin-embedded (FFPE), and 2) fresh frozen tissues. A description of the tumor specimens collected and distributed for molecular analysis during last year is provided:

FFPE CNB specimens: As reported last year, the Biomarker Core completed the collection and processing of all specimens from patients enrolled in the BATTLE clinical trial in December

2009. The Core collected and processed NSCLC tumor tissue specimens from 324 patients for biomarker analysis. Of the 324 specimens collected, 270 (83%) cases yielded enough tumor cells to examine and report a complete set of biomarkers as proposed. We were not able to detect enough viable tumor cells (higher than 50 cells/slide) for biomarker analysis in 54 (17%) patients; in these specimens, the most frequent findings were necrotic tumor tissue and dense fibrosis. We obtained 171 tissue specimens from lung tumor sites, and the remaining specimens were collected from metastatic sites (including 45 lymph nodes, 36 liver, 30 adrenal glands, 26 soft tissues/skin, 8 mediastinum, and 8 pleura). NSCLC histology types included 197 adenocarcinoma (61%), 30 squamous cell carcinoma (9%), and 40 NSCLC not otherwise specified (12%).

The overall data on the tumor tissue qualification for the molecular biomarker analysis proposed in the BATTLE trial has been reported with the results of the clinical trial (*Kim, Herbst, Wistuba, Lee et al, Cancer Discovery, April 2011*). In addition, a detailed characterization of the histopathological and molecular findings of this large set of CNBs obtained from advanced, refractory, NSCLC lung tumor and metastasis is being prepared (*Wistuba et al, manuscript in preparation*). This manuscript will be finalized during the next unfunded year of the grant.

The residual tissue specimens of formalin-fixed and paraffin-embedded (FFPE) tissues of all the evaluated biopsies are banked in the Biomarker Core, and they represent 588 tissue blocks from 266 cases (2.2 block/case; range 1-4) and 3,965 unstained histology sections from 246 cases (16 slides/case; range 1-36). Of these, during last year, one set of CNB tissue specimens has been distributed for further molecular characterization, including mutation analysis using Sequenom™ methodology of 12 oncogenes that have been shown as mutated in NSCLC (Drs. Wistuba and Kim, V Foundation grant), and for protein expression analysis of LCN2 by immunohistochemistry (see Objective 2), a potential new marker of response to EGFR TKI in patients with *EGFR* wild-type tumors, which is part of the novel 5-gene signature discovered in the molecular profiling of the BATTLE tissues (Drs. Heymach and Wistuba, Aim 3).

In addition, in close collaboration with the Biostatistics Core and the Clinical Trial team, we increased the collection of the diagnostic, pre-chemotherapy tissue specimens from BATTLE patients to 142 specimens. During the next year, we plan to use these diagnostic tissue specimens to compare the expression of molecular markers, particularly through gene mutation profiling by Sequenom™, before and after chemotherapy treatments, as part of a V Foundation grant (PIs: Drs. I. Wistuba and E. Kim).

Fresh frozen CNB specimens: As reported last year, at least one fresh tumor tissue core obtained from 257/270 (95%) cases was snap-frozen, and those specimens were distributed to Dr. Wistuba's lab for RNA and protein extractions and subsequent profiling (Aim 3). Of these, histology quality control was performed in 175 frozen tissues samples, and malignant cells were detected in 143 (82%) of cases. During the last year, the Biomarker Core collaborated closely with investigators of Aim 3 to derive and test 5 gene expression signatures. Two of these signatures, epithelial mesenchymal transition (EMT) and 5-gene, demonstrated to be predictive of response to treatment in the BATTLE trial patients. Currently, we are still in the process of refining and testing two additional signatures ("KRAS" and "Sorafenib") that we hypothesize will be associated with erlotinib and sorafenib treatment outcomes. Several manuscripts reporting these data are in preparation (see Appendix).

In addition, we have extracted microRNA (miR) from residual samples used for mRNA extraction in 50 BATTLE tumor specimens, and they have been successfully examined for miRNA expression using AB Life Technologies arrays. The data are currently under analysis by Dr. Kevin Coombes (Bioinformatics).

Finally, in collaboration with Dr. Lauren Byers' lab, proteins have been extracted from 160 fresh frozen CNBs for proteomic analysis using the reverse phase protein array (RPPA) platform. The RPPA analysis has been recently completed and the data are being subjected to quality control analysis.

Objective 2: **To perform biomarker analyses and report results in a timely fashion for patient stratification in the BATTLE trials and molecular mechanistic studies of the targeted agents.**

Summary of Research Findings

As reported last year, we completed the analysis of the 11 molecular markers proposed in the BATTLE trial from the 270 tumors with adequate malignant cells, and recorded the results in the Web-based clinical trial database within 14 days in more than 99% of cases.

During the last year, we collaborated actively with BATTLE investigators, particularly from Aim 3, for the molecular characterization of the BATTLE tissues. The Biomarker Core participated actively in two main projects using the existing tumor tissue molecular data and the banked tumor tissue specimens: 1) analysis of *KRAS* mutation subtypes, and 2) examination of LCN2 protein expression in NSCLC tumor specimens.

Subtypes of *KRAS* mutations: Through the analysis of 215 evaluable NSCLC patients treated in the BATTLE trial whose tumor specimens have *KRAS* mutation data, we have shown that mut-*KRAS*-G12C/V but not total mut-*KRAS* predicts progression-free survival (PFS) for the overall BATTLE patients group, and for the sorafenib and vandetanib treatment arms. In addition, the gene expression microarray (Affymetrix) data performed in the BATTLE tumor specimens showed differential expression of cell cycle genes between mut-*KRAS*-G12C/V and G12D patient tumors. We believe that the significance of the findings for developing mut-*KRAS* therapies is profound, since it suggests that not all mut-*KRAS* amino acid substitutions signal to effectors in a similar way, and may require different therapeutic interventions.

LCN2 expression in lung cancer specimens: We derived a 5-gene signature from the BATTLE tumor tissue specimens that predicted response (8-week disease control, DC) to erlotinib treatment in collaboration with investigators of Aim 3. From the 5 genes, the data suggested that *LCN2* was the strongest individual marker of sensitivity to this drug. To better examine the expression of LCN2 protein in FFPE archival tissues, including BATTLE samples, we developed an immunohistochemical (IHC) test (Figure 12). Using this IHC test, we first examined the expression in a large set (n=600) of surgically resected NSCLCs (adenocarcinoma and squamous cell carcinoma) placed in tissue microarrays (TMAs). We identified that LCN2 is frequently expressed in the cytoplasm and membrane of malignant NSCLC cells. Then, we completed the examination of the expression of LCN2 in 250 FFPE CNB tissue specimens from BATTLE trial. Currently, collaborators from the Biostatistics Core are correlating the IHC

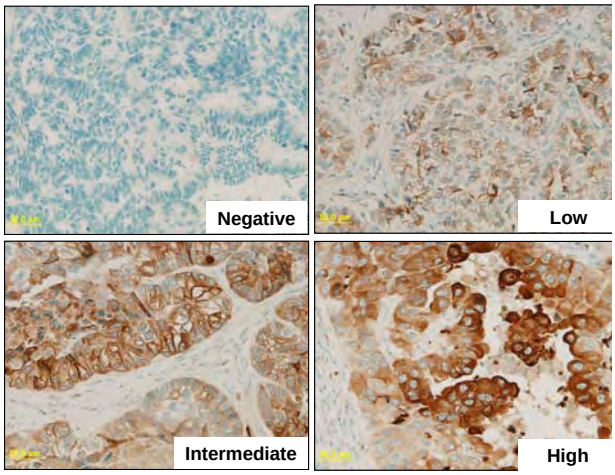

Figure 12. Representative microphotographs depicting LCN2 expression in NSCLC tumor specimens.

expression of LCN2 with clinicopathological features in the surgically resected NSCLC and in BATTLE tumors from patients treated with erlotinib to assess response to therapy.

Key Research Accomplishments:

- Demonstrated that gene expression, miRNA, and protein profiling from CNBs is a feasible approach for predicting response in refractory NSCLC patients treated with targeted therapy.
- Identified that not all mutant-*KRAS* amino acid substitutions signal to effectors in a similar way in NSCLC, and may require different therapeutic approaches.
- Developed an immunohistochemical test to assess the expression of LCN2, one of the members of the 5-gene signature identified in the BATTLE studies that predicted response to erlotinib.

Conclusions

In collaboration with other BATTLE investigators, we demonstrated that gene expression, miRNA, and protein profiling from tumor CNB is a feasible approach for predicting response in refractory NSCLC patients treated with targeted therapy. We contributed significantly to important discoveries by examining molecular abnormalities in the BATTLE tumor tissues, including the identification that in NSCLC not all mutant-*KRAS* amino acid substitutions signal to effectors in a similar way, and may require different therapeutic approaches, and the development of a novel 5-gene signature that predicted response to BATTLE patients treated with erlotinib. In addition, we have developed an IHC test to assess the expression of LCN2, one of the members of this 5-gene signature.

KEY RESEARCH ACCOMPLISHMENTS

Specific Aim 2.2. To investigate whether the resistance to erlotinib is mediated by the activation of type I insulin-like growth factor receptor (IGF-1R) signaling pathway

- Performed IHC analysis on IGF-1R expression in NSCLC patients and found expression levels of IGF-1R and pIGF-1R/IR were significantly higher in patients with squamous cell carcinoma ($P<0.0001$) than in patients with adenocarcinoma.
- Planned future studies to analyze anchorage-independent growth of NSCLC cells after treatment.

Specific Aim 2.3. To investigate the molecular mechanisms of resistance to and biomarkers of the biologic activity of inhibitors of the VEGF pathway

- Detected KDR CNGs in NSCLC and predicted worse outcome in patients treated with adjuvant chemotherapy.
- Associated KDR CNGs with improved disease control in BATTLE patients treated with vandetanib versus erlotinib.
- Evaluating a new population of circulating TEM+ endothelial cells (CTECs) in a set of clinical BATTLE samples; these CTECs may offer a more specific biomarker for evaluating the effect of angiogenesis inhibitors .
- Re-analyzed CAFs in 185 samples from BATTLE study due to the identification of batch effects in the previous analysis; data analysis is underway.

Specific Aim 3: To identify biomarkers as novel predictors of clinical end points and potential therapeutic targets

- Demonstrated that gene expression profiling from CNBs is a feasible approach for predicting response and identifying potential therapeutic targets in refractory NSCLC patients treated with targeted therapy.
- Developed and tested two gene expression signatures, the EMT and the novel 5-gene, which predicted 8-week disease control in patients with advanced and refractory NSCLC treated with the EGFR TKI erlotinib with wild-type *EGFR* tumors
- Identified two novel molecular mechanisms of response to EGFR TKIs in patients with *EGFR* and *KRAS* wild-type NSCLC, involving the *AXL* and *LCN2* genes.
- Demonstrated that different therapeutic approaches may be required when treating patients with NSCLC harboring different mutant-*KRAS* amino acid substitutions.

Specific Aim 4: To explore new preclinical combinations and their mechanisms of action by targeting mTOR signaling and develop phase I trials to test these combinations.

- Demonstrated that the combination of RAD001 and BKM120 synergistically inhibits the growth of human lung cancer cells, warranting the clinical testing of this combination.
- Demonstrated that the combination of RAD001 and erlotinib results in modest improvements in efficacy, thus setting the stage for identification of predictive biomarkers with which to select patients who would most benefit from this regimen.

Biostatistics and Data Management Core:

- Performed extensive statistical analysis on the study findings including treatment efficacy, toxicity, compliance, pre-specified biomarkers, and discovery biomarkers, etc.
- Developed and maintained a secured, web-based database application to assist with the data collection and analysis.
- A web-based database application is developed, deployed, and maintained at: https://insidebiostat/DMI_BATTLE/Common/Login.aspx.

Biomarker Core:

- Demonstrated that gene expression, miRNA, and protein profiling from CNBs is a feasible approach for predicting response in refractory NSCLC patients treated with targeted therapy.
- Identified that not all mutant-*KRAS* amino acid substitutions signal to effectors in a similar way in NSCLC, and may require different therapeutic approaches.
- Developed an immunohistochemical test to assess the expression of LCN2, one of the members of the 5-gene signature identified in the BATTLE studies that predicted response to erlotinib.

REPORTABLE OUTCOMES:

Publications (Attached in Appendix A)

Cascone T, Herynk MH, Xu L, Du Z, Kadara H, Nilsson MB, Oborn CJ, Park YY, Erez B, Jacoby JJ, Lee JS, Lin HY, Ciardiello F, Herbst RS, Langley RR, Heymach JV. Upregulated stromal EGFR and vascular remodeling in mouse xenograft models of angiogenesis inhibitor-resistant human lung adenocarcinoma. *Journal of Clinical Investigation*. 2011 Apr 1;121(4):1313-28. doi: 10.1172/JCI42405. PMID: 21436589

Flores LM, Kindelberger DW, Ligon AH, Capelletti M, Fiorentino M, Loda M, Cibas ES, Janne PA, Krop IE, Improved yields of circulating tumour cells facilitates molecular characterization and recognition of discordant HER2 amplification in breast cancer. *British Journal of Cancer*. 2010 May 11;102(10):1495-502. PMCID: PMC2869174.

Gu X, Lee JJ. A simulation study for comparing testing statistics in response-adaptive randomization. *BMC Medical Research Methodology.* 2010 Jun 5;10:48. PMCID: PMC2911470.

Kadara H, Fujimoto J, Men T, Ye X, Lotan D, Lee JS, Lotan R. A Gprc5a tumor suppressor loss of expression signature is conserved, prevalent, and associated with survival in human lung adenocarcinomas. Neoplasia. 2010 Jun;12(6):499-505. PMCID: PMC2887090

Kim ES, Herbst RS, Wistuba II, Lee JJ, Blumenschein GR, Tsao A, Stewart DJ, Hicks ME, Erasmus J, Gupta S, Alden CM, Liu S, Tang X, Khuri FR, Johnson BE, Heymach JV, Mao L, Fossella F, Kies MS, Papadimitrakopoulou V, Davis SE, Lippman SM, Hong WK. The BATTLE Trial: Personalizing Therapy for Lung Cancer. *Cancer Discovery* 1(1): 42-51, 2011. [Epub ahead of print].

Kim WY, Kim MJ, Moon H, Yuan P, Kim JS, Woo JK, Zhang G, Suh YA, Feng L, Behrens C, Van Pelt CS, Kang H, Lee JJ, Hong WK, Wistuba II, Lee HY. Differential Impacts of Insulin-Like Growth Factor-Binding Protein-3 (IGFBP-3) in Epithelial IGF-Induced Lung Cancer Development. *Endocrinology.* 2011 Mar 29. [Epub ahead of print]. PMID: 21447628.

Lee JJ, Gu X, Liu S. Bayesian adaptive randomization designs for targeted agent development. *Clinical Trials.* 2010 Oct;7(5):584-96. PMID: 20571130.

Rubin EH, Anderson KM, Gause CK. The BATTLE Trial: A Bold Step Toward Improving the Efficiency of Biomarker-Based Drug Development. *Cancer Discovery* 1(1): 17-20, 2011. [Epub ahead of print].

Sequist LV, Muzikansky A, Engelman J. A New BATTLE in the Evolving War on Cancer. *Cancer Discovery* 1(1): 14-16, 2011. [Epub ahead of print].

Abstracts (Attached in Appendix A)

Byers L, Wang J, Diao L, Yordy J, Girard L, Story M, Coombes K, Weinstein J, Minna J, Heymach J. An epithelial to mesenchymal transition (EMT) gene expression signature identifies Axl as an EMT marker in non-small cell lung cancer (NSCL) and head and neck cancer (HNC) lines and predicts response to erlotinib. 22nd EORTC-NCI-AACR Symposium on Molecular Targets and Cancer Therapeutics, Berlin, Germany, 2010. Abstract 37.

Herbst RS, Blumenschein Jr. GR, Kim ES, Lee J, Tsao AS, Alden CM, Liu S, Stewart DJ, Wistuba II, Hong WK. Sorafenib treatment efficacy and KRAS biomarker status in the Biomarker-Integrated Approaches of Targeted Therapy for Lung Cancer Elimination (BATTLE) trial. Journal of Clinical Oncology 28:15s, 2010 (suppl; abstr 7609).

Heymach JV, Saintigny P, Kim ES, Byers LA, Lee JJ, Coombes K, Diao L, Wang J, Tran H, Fan YH, Tsao A, Blumenschein Jr. GR, Papadimitrakopoulou V, Tang X, Story M, Xie Y, Girard L, Weinstein J, Mao L, Minna JD, Herbst R, Lippman SM, Hong WK, Wistuba II. Gene expression signatures predictive of clinical outcome and tumor mutations in refractory NSCLC patients (pts) in the BATTLE trial (Biomarker-integrated Approaches of Targeted Therapy for Lung Cancer Elimination). Proceedings of the 102nd Annual Meeting of the American Association for Cancer Research. Abstract LB-88.

Hong WH, Kim ES, Lee JJ, Wistuba I, Lippman S. The landscape of cancer prevention: Personalized approach in lung cancer. Proceedings of the 102nd Annual Meeting of the American Association for Cancer Research. Abstract PL01-03.

Ihle NT, Herbst RS, Kim ES, Wistuba II, Lee JJ, Blumenschein, Jr GR, Tsao AS, Chen L, Zhang S, Alden CM, Tang X, Liu S, Stewart DJ, Papadimitrakopoulou V, Heymach JV, Tran HT, Hicks ME, Erasmus JJ, Gupta S, Minna JD, Larsen J, Lippman SM, Hong WK, Powis G. Specific forms of mutant *KRAS* predict patient benefit from targeted therapy in the BATTLE-1 clinical trial in advanced non-small cell lung cancer. Proceedings of the 102nd Annual Meeting of the American Association for Cancer Research. Abstract 955.

Kim JS, Kim ES, Liu D, Lee JJ, Solis L, Behrens C, Lippman S, Hong WK, Wistuba II, Lee HY. Insulin receptor expression and survival of patients with non-small cell lung cancer. Proceedings of the 102nd Annual Meeting of the American Association for Cancer Research. Abstract 1122.

Liu S, Lee JJ. Design, Implementation, and Results for a Bayesian Adaptive Randomization Trial for Targeted Therapy in Lung Cancer. Poster Presentation. Joint Statistical Meetings. Vancouver, British Columbia, Canada, 2010. Abstract 307615.

Saintigny P, Diao L, Wang J, Girard L, Lin SH, Coombes KR, Liu S, Lee JJ, Weinstein JN, Xie Y, Fan YH, Tang XM, Kim ES, Herbst RS, Tsao A, Blumenschein GR, Mao L, Lippman SM, Minna JD, Hong WK, Wistuba II, Heymach JV. A 5-gene signature (sig) predicts clinical benefit from erlotinib in non-small cell lung cancer (NSCLC) patients (pts) harboring wild-type (wt) EGFR & KRAS. Proceedings of the 102nd Annual Meeting of the American Association for Cancer Research. Abstract 4109.

CONCLUSIONS

Aim 2.2: Our findings from the *in vitro* study indicate the potential for integration of IGF-1R-targeted agents into treatment regimens using EGFR TKIs for patients with lung cancer. Future studies are needed to verify our data to allow us to translate these findings into the clinic.

Aim 2.3: Our preliminary data suggest that tumor cell KDR may be a potential therapeutic target, and that NSCLC tumors with KDR CNGs may be particularly sensitive to KDR inhibition. Taken together with the BATTLE data and the *in vitro* studies, these data provide evidence that: 1) KDR CNGs occur in NSCLC with relatively high frequency; 2) CNGs result in increased KDR protein; and 3) KDR protein and/or CNGs appear to be associated with relapse after adjuvant chemotherapy, increased angiogenesis, chemoresistance *in vitro*, and potentially, response to VEGF inhibitors or RTKIs. We therefore expect inhibitors to slow tumor growth and sensitize to chemotherapy but not to induce apoptosis in vitro as seen with EGFR TKIs in *EGFR*-mutant tumors. Our preclinical studies have identified a number of potential markers that predict response to VEGFR inhibitors. It will be interesting to see if these same markers will predict response in patient samples. In addition, our studies have identified a new population of cells that can be detected that identify circulating endothelial cells derived from tumor endothelium. Analysis of this population of cells in patients treated with angiogenesis inhibitors is likely to be a better prognostic marker of response to treatment.

Several plasma CAFs are associated with specific tumor-derived pathway activation. Our preliminary study suggests that broad-based plasma profiling of cytokines and angiogenic factors may be a feasible approach for identifying markers of activation of tumor signaling pathways. In addition to the evaluation of pathway activation using plasma samples, we will be evaluating modulation of CAFs by each treatment arm, evaluating for potential predictive plasma signatures with clinical outcome measures such as progression-free survival (PFS) during the next unfunded extension. The final step will be to validate the plasma predictive signature derived from BATTLE with other randomized clinical studies. These studies can also validate our results that identify circulating VEGF as a predictive marker of response to angiogenic therapies in other clinical studies.

Aim 3: We have demonstrated that gene expression profiling from CNBs is a feasible approach for predicting response and identifying potential therapeutic targets in refractory NSCLC patients treated with targeted therapy. We have identified that the EGFR signature predicted *EGFR* gene mutation status but, in wild-type *EGFR* patients, did not predict 8-week disease control. Interestingly, an EMT and the novel 5-gene signatures were predictive of disease control in patients with wild-type *EGFR*-tumors in patients treated with EGFR TKIs. In addition, we identified at least two novel molecular mechanisms of response to EGFR TKIs and we discovered that not all mutant-*KRAS* amino acid substitutions signal to effectors in a similar way in NSCLC.

Aim 4: This project has resulted in significant improvement in utilization of mTOR inhibitors for the treatment of lung cancer. Our data with the combination of an mTOR inhibitor with a PI3K inhibitor represents a very promising approach for treating lung cancer. It is clear that monotherapy with mTOR inhibitors is not useful in selected patients, and treatment with novel combinations are the best way forward for future lung cancer patients.

Biostatistics and Data Management Core: In collaboration with clinical investigators, research nurses, the Biomarker Core, and basic scientists, the Biostatistics and Data Management Core has continued to deliver the biostatistics and data management support as proposed.

Biomarker Core: In collaboration with other BATTLE investigators, we demonstrated that gene expression, miRNA, and protein profiling from tumor CNB is a feasible approach for predicting response in refractory NSCLC patients treated with targeted therapy. We contributed significantly to important discoveries by examining molecular abnormalities in the BATTLE tumor tissues, including the identification that in NSCLC not all mutant-*KRAS* amino acid substitutions signal to effectors in a similar way, and may require different therapeutic approaches, and the development of a novel 5-gene signature that predicted response to BATTLE patients treated with erlotinib. In addition, we have developed an IHC test to assess the expression of LCN2, one of the members of this 5-gene signature.

APPENDIX

Abstracts and Publications

Upregulated stromal EGFR and vascular remodeling in mouse xenograft models of angiogenesis inhibitor–resistant human lung adenocarcinoma

Tina Cascone,[1,2] Matthew H. Herynk,[1] Li Xu,[1] Zhiqiang Du,[1] Humam Kadara,[1] Monique B. Nilsson,[1] Carol J. Oborn,[3] Yun-Yong Park,[4] Baruch Erez,[1] Jörg J. Jacoby,[1] Ju-Seog Lee,[4] Heather Y. Lin,[5] Fortunato Ciardiello,[2] Roy S. Herbst,[1] Robert R. Langley,[3] and John V. Heymach[1,5]

[1]Department of Thoracic/Head and Neck Medical Oncology, University of Texas M.D. Anderson Cancer Center, Houston, Texas, USA.
[2]Division of Medical Oncology, "F. Magrassi — A. Lanzara" Department of Clinical and Experimental Medicine, Second University of Naples, Naples, Italy.
[3]Department of Cancer Biology, [4]Department of Systems Biology, and [5]Department of Biostatistics, University of Texas M.D. Anderson Cancer Center, Houston, Texas, USA.

Angiogenesis is critical for tumor growth and metastasis, and several inhibitors of angiogenesis are currently in clinical use for the treatment of cancer. However, not all patients benefit from antiangiogenic therapy, and those tumors that initially respond to treatment ultimately become resistant. The mechanisms underlying this, and the relative contributions of tumor cells and stroma to resistance, are not completely understood. Here, using species-specific profiling of mouse xenograft models of human lung adenocarcinoma, we have shown that gene expression changes associated with acquired resistance to the VEGF inhibitor bevacizumab occurred predominantly in stromal and not tumor cells. In particular, components of the EGFR and FGFR pathways were upregulated in stroma, but not in tumor cells. Increased activated EGFR was detected on pericytes of xenografts that acquired resistance and on endothelium of tumors with relative primary resistance. Acquired resistance was associated with a pattern of pericyte-covered, normalized revascularization, whereas tortuous, uncovered vessels were observed in relative primary resistance. Importantly, dual targeting of the VEGF and EGFR pathways reduced pericyte coverage and increased progression-free survival. These findings demonstrated that alterations in tumor stromal pathways, including the EGFR and FGFR pathways, are associated with, and may contribute to, resistance to VEGF inhibitors and that targeting these pathways may improve therapeutic efficacy. Understanding stromal signaling may be critical for developing biomarkers for angiogenesis inhibitors and improving combination regimens.

Introduction

Tumor growth and metastasis are dependent on the formation of a vascular supply, i.e., angiogenesis (1–3). Most therapeutic efforts directed toward inhibiting the angiogenic process for the treatment of cancer have focused on the VEGF pathway (4–8). The majority of the mitogenic, angiogenic, and permeability-enhancing properties of VEGF are mediated by VEGF receptor–2 (VEGFR2) (8). Several inhibitors of this pathway have received FDA approval and are currently in clinical use; these include bevacizumab (BV; Avastin; Genentech), a monoclonal antibody that blocks human VEGF (9, 10), and small-molecule inhibitors of the VEGFR2 tyrosine kinase (e.g., sorafenib, sunitinib, and pazopanib) (11). The results from phase III clinical trials demonstrated that the addition of BV to standard therapy prolongs progression-free survival (PFS) and/or overall survival, and improves objective tumor responses, in patients with advanced malignancies including non–small-cell lung cancer (NSCLC) and colon cancer (12, 13). However, not all patients benefit from antiangiogenic therapy, and those tumors that initially respond to treatment will ultimately become refractory and relapse (14, 15). Therefore, the development of more durable cancer therapies requires an improved understanding of the cellular and molecular mechanisms that mediate resistance to antiangiogenic agents.

Recent studies suggest that blockade of the VEGFR2 signaling pathway may prompt some tumors to increase their expression of secondary molecules in order to sustain the neovascularization response (16). Casanovas et al. reported that although anti-VEGFR therapy initially blocks new blood vessel formation and tumor growth in a transgenic model of pancreatic islet cell tumors, both angiogenesis and tumor progression are eventually restored by the increased synthesis of other angiogenic factors from tumor cells (17). There is also evidence suggesting that commonly occurring genetic alterations in tumor cells may uncouple tumor dependency on a vascular blood supply. For example, loss of *p53* enhances the ability of tumor cells to withstand hypoxic conditions (18), which renders p*53*-deficient tumors to be at least partially resistant to antiangiogenic therapy (19). Other tumor cells have been shown to alter their pattern of growth when challenged with antiangiogenic therapy. Instead of recruiting resident ECs to form new vascular networks, these tumor cells meet their metabolic requirements by residing in close proximity to preexisting blood vessels (20). Incomplete target inhibition after treatment with VEGFR antago-

Conflict of interest: J.V. Heymach and R.S. Herbst have served on advisory boards for Genentech and AstraZeneca and receive research support from AstraZeneca.

Citation for this article: *J Clin Invest.* 2011;121(4):1313–1328. doi:10.1172/JCI42405.

nists has been described in orthotopic models of pancreatic cancer, as well as in patients with this type of cancer and with advanced soft tissue sarcomas (21, 22).

Emerging evidence suggests that stromal cells may also play an important role in mediating resistance to antiangiogenic therapies. Shojaei et al. reported that localization of Gr-1$^+$CD11b$^+$ myeloid cells to various murine tumors rendered the neoplasms refractory to anti-VEGF therapy (23). Myeloid cells provide a rich reserve of angiogenic molecules and possess potent immunosuppressive activity (24), both of which favor tumor progression. Similarly, a recent study evaluating the effects of a neutralizing VEGF antibody in murine lymphoma models demonstrated that tumor-associated fibroblasts upregulate expression of PDGF-C when the VEGFR pathway is blocked, ensuring the continued formation of tumor blood vessels when signaling through this pathway is prohibited (25). Together, these studies provide evidence that both tumor cells and stromal cells contribute to VEGF inhibitor resistance, although their respective contributions remain incompletely characterized and are likely to vary based on molecular features of the tumor and its microenvironment.

We hypothesized that there may be additional stromal and tumor cell mechanisms that contribute to the resistant phenotype. To assess this question, we investigated 3 different models with varying de novo responsiveness to BV. In order to discriminate between tumor (human) and stromal (mouse) genes that may be associated with acquired resistance to BV, we performed species-specific gene expression profiling using vehicle-treated (controls) and BV-resistant xenografts. This approach demonstrated that gene expression changes associated with resistance occurred primarily in stromal cells, highlighted different modes of vascular remodeling that may accompany the emergence of resistance, and led to the identification of what we believe to be a previously unrecognized mechanism for acquired resistance to BV involving upregulation of EGFR signaling in vascular pericytes.

Results

NSCLC xenografts exhibit different patterns of resistance to BV. To investigate the mechanisms by which NSCLC xenografts develop resistance to VEGF blockade, we initially injected male nude mice with either H1975 or A549 human NSCLC adenocarcinoma cells. These models were selected because in prior studies, we observed that A549 xenograft tumors were relatively insensitive to VEGF inhibitors de novo (relative primary resistance), whereas H1975 tumors were more initially responsive to these agents, experiencing significant tumor volume reduction typically lasting more than 1 month (26). Furthermore, the tumor cells contain 2 common alterations associated with EGFR tyrosine kinase inhibitor (TKI) resistance: a T790M EGFR mutation (H1975 model; ref. 27) and a KRas mutation (A549 model; ref. 28). Approximately 3 weeks after tumor cell injection, mice bearing tumors with a mean volume of approximately 270 mm^3 were randomized to receive either vehicle control or BV (see Methods). Animals were treated for 2 weeks (short-term treatment) or until they were euthanized due to tumor burden. Tumors were considered to be resistant when they tripled in volume (i.e., tumor progression) compared with the pretreatment tumor size, and PFS was measured as the time from initiation of treatment until tumor progression. In H1975 tumors, as assessed by tumor volume change ratio ($\Delta T/\Delta C$; see Methods), short-term treatment with BV inhibited tumor growth by 77% compared with vehicle-treated control tumors ($\Delta T/\Delta C$ 23.1%; P = 0.015, Mann Whitney test; Figure 1, A and C). In A549 xenografts, in contrast, a nonsignificant 16% reduction in tumor growth was observed ($\Delta T/\Delta C$ 83.8%; P = 0.381, Mann Whitney test; Figure 1, B and C).The individual tumor growth curves shown in Figure 1, D and E, illustrate the growth kinetics of H1975 and A549 xenografts treated with vehicle or BV for a longer period until progression. All H1975 control xenografts progressed within 31 days of treatment onset, with median PFS of 6 days. In contrast, 67% of xenografts (4 of 6) receiving BV developed resistance, and the median PFS was 138 days (P = 0.0007, log-rank test; Figure 1D). A549 tumors were less responsive to BV and had a median PFS of 40 days compared with 29.5 days in control tumors (P = 0.390, log-rank test; Figure 1E). These results showed that H1975 tumors were initially responsive to BV therapy, but eventually acquired resistance after prolonged treatment with the drug, whereas A549 tumors demonstrated relative primary resistance to BV.

Acquired resistance to BV is associated with sustained inhibition of VEGFR2 activation and reduced endothelial apoptosis. To determine whether acquired resistance to BV is the result of increased VEGFR2 signaling, potentially through increased expression of murine VEGF or another mechanism to bypass blockade of human VEGF by this agent, we evaluated the phosphorylation status of VEGFR2 in control-treated (vehicle progression), BV-sensitive (2 weeks BV treatment), and BV-resistant (BV progression) tumors using immunofluorescence (IF) staining. In control tumors, phosphorylated VEGFR2 (p-VEGFR2) was readily detected on CD31$^+$ tumor-associated ECs. However, no p-VEGFR2 was detected on the vasculature of BV-sensitive tumors or the BV progression group (Supplemental Figure 1A; supplemental material available online with this article; doi:10.1172/JCI42405DS1). To evaluate changes in stromal (defined here as nontumor cells derived from the host) and tumor-derived VEGF in H1975 BV-resistant tumors, we quantified mouse *Vegfa* and human *VEGFA* mRNA expression by quantitative real-time PCR (qRT-PCR). We observed no change in mouse *Vegfa* mRNA expression in resistant xenografts, whereas human *VEGFA* mRNA levels were increased in resistant tumors, compared with controls ($P < 0.05$; Supplemental Figure 1B). Despite the increase in VEGF ligand, however, VEGFR2 phosphorylation remained suppressed in BV-resistant tumors.

We then assessed whether the acquisition of resistance was associated with changes in endothelial apoptosis. We performed double IF staining for CD31$^+$ and TUNEL$^+$ cells in H1975 tumors following short-term BV treatment and BV progression and determined the percentage of apoptotic ECs (CD31$^+$TUNEL$^+$; Supplemental Figure 1, C and D). The percentage of apoptotic ECs significantly increased following 2 weeks of BV treatment compared with control xenografts ($P < 0.05$). However, at the time of progression, EC apoptosis diminished significantly ($P < 0.05$ versus short-term BV), to levels comparable to those of vehicle-treated tumors. Thus, EC apoptosis increased while tumors were initially responding to VEGF signaling blockade and returned to levels comparable to those of controls in tumors that acquired BV resistance.

In the same tumors, we also quantified the percentage of total apoptotic cells using laser scanning cytometry (LSC; data not shown). Tumors sensitive to BV showed an increased percentage of total TUNEL$^+$ cells compared with controls (2 weeks vehicle treatment), whereas no significant changes were observed in BV-resistant tumors compared with controls (vehicle progression).

Stromal and tumor cell gene expression changes in H1975 BV-resistant xenografts. To identify changes in stromal and tumor gene expres-

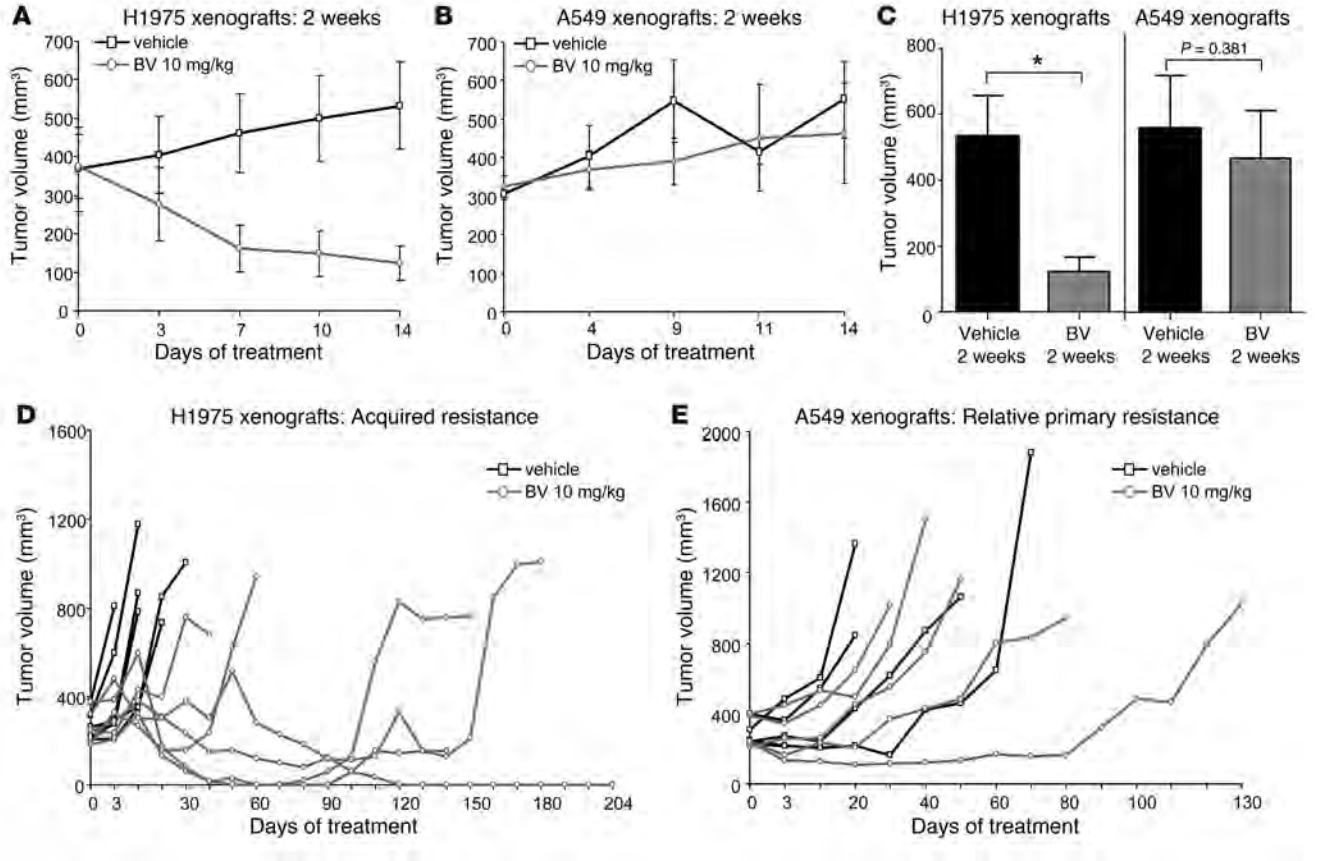

Figure 1

H1975 and A549 NSCLC xenografts show different patterns of resistance to BV treatment. (**A** and **B**) Tumor growth curves of H1975 (**A**; $n = 5$ per group) and A549 (**B**; $n = 6$ per group) xenografts receiving vehicle (control) and BV for 2 weeks. (**C**) Mean tumor volume obtained at the last measurement in H1975 and A549 xenografts treated with BV for 2 weeks compared with controls ($\Delta T/\Delta C$). *$P < 0.05$, Mann-Whitney test. (**D** and **E**) Individual tumor growth curves of H1975 (**D**; $n = 6$ per group) and A549 (**E**; $n = 5$ per group) xenografts treated with vehicle and BV until animals became moribund. Tumors were considered resistant (progression) when tripled in volume compared with the beginning of the treatment.

sion associated with acquired resistance to anti-VEGF therapy, we performed RNA microarray analyses comparing H1975 control and BV-resistant xenografts ($n = 3$ per group) using Illumina mouse-specific (WG-6 v2) and human-specific (WG-6 v3) expression arrays. Probes in these arrays have been designed to minimize cross-species reactivity; consistent with this, essentially no cross-reactivity was observed in experiments mixing human and mouse cell lines (E.S. Park, unpublished observations). We found that a much larger number of stromal mouse genes were significantly modulated in BV progression versus control vehicle progression xenografts compared with human tumor genes (1,385 stromal genes versus 98 tumor genes), according to the statistical criteria described in Methods. We observed significant changes in the expression of genes involved in angiogenesis, lymphangiogenesis, and hypoxia signaling pathway between BV-resistant and control xenografts. Both *Egfr* and *Fgfr2* genes were upregulated in the stromal compartment, but not in tumor cells, of H1975 BV-resistant tumors compared with controls, as well as stromal molecules and ligands associated with these signaling pathways (e.g., *Epgn*, *Areg*, *Fgf13*, and *Fgfbp1*; Figure 2A and Supplemental Table 1). Among human angiogenic or hypoxia-regulated genes, carbonic anhydrase IX (*CA9*) was significantly upregulated in BV-resistant tumors (Figure 2A and Supplemental Table 2).

We next sought to identify pathways potentially important in the acquired resistance phenotype. Functional gene-interaction network analyses of gene features differentially expressed between the mouse stroma of BV-resistant and vehicle-treated H1975 xenografts, using Ingenuity Pathway Analysis, revealed significant modulation in the predicted function of a gene neighborhood and interaction network surrounding *Egfr*, based on the number of focus genes and nodes of interaction ($P < 0.001$; Figure 2B). In addition, the modulated gene network associated with *Egfr* expression included downregulated proapoptotic genes, such as the Bcl-2 family member protein *Bax* and apoptotic peptidase activating factor 1 (*Apaf1*). Genes with prosurvival functions, such as the heat shock protein *Dnajb1*, were upregulated.

Next, to validate the changes in expression of the significantly modulated network-hub gene *Egfr*, we assessed the human and mouse mRNA levels using qRT-PCR. Consistent with the microarray data, we observed a 2.5-fold increase in mouse *Egfr* mRNA levels in H1975 BV-resistant xenografts compared with controls ($P < 0.05$; Figure 2C). Human *EGFR* mRNA levels were not significantly different than those of controls. We also validated the stromal expression of *Fgfr2*, which we noted to be upregulated in BV-resistant H1975 tumors in the microarray analysis. A significant increase in mouse *Fgfr2*, but not human *FGFR2*, mRNA

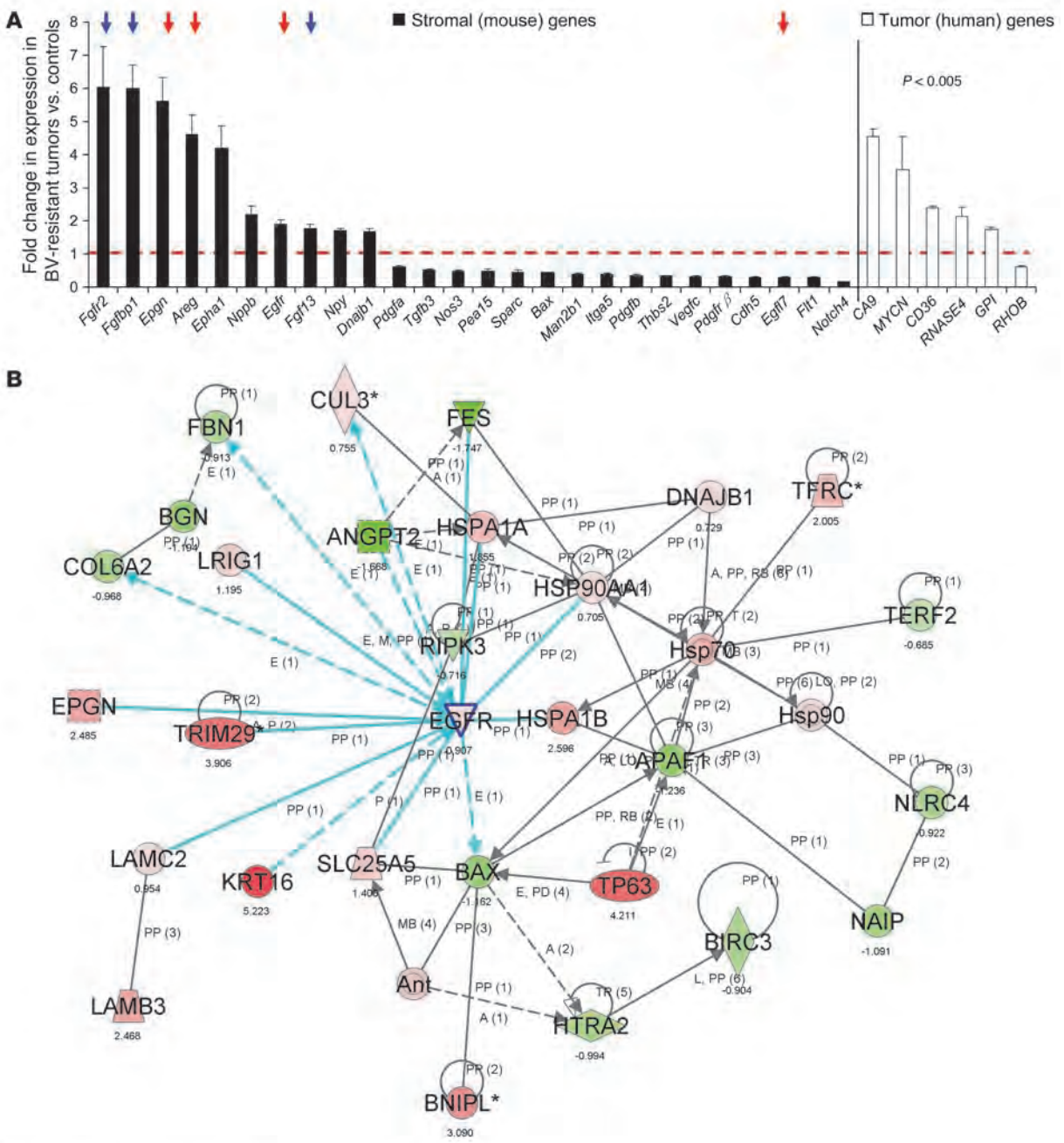
A
Fold change in expression in BV-resistant tumors vs. controls
Stromal (mouse) genes
Tumor (human) genes
P < 0.005
Fgfr2
Fgfbp1
Epgn
Areg
Epha1
Nppb
Egfr
Fgf13
Npy
Dnajb1
Pdgfa
Tgfb3
Nos3
Pea15
Sparc
Bax
Man2b1
Itga5
Pdgfb
Thbs2
Vegfc
Pdgfr β
Cdh5
Egfl7
Flt1
Notch4
CA9
MYCN
CD36
RNASE4
GPI
RHOB
B
FBN1
CUL3*
FES
BGN
ANGPT2
HSPA1A
DNAJB1
TFRC*
COL6A2
LRIG1
HSP90AA1
TERF2
RIPK3
Hsp70
EPGN
TRIM29*
EGFR
HSPA1B
Hsp90
APAF1
NLRC4
LAMC2
KRT16
SLC25A5
BAX
TP63
NAIP
BIRC3
Ant
LAMB3
HTRA2
BNIP3L*
C
Vehcile progression
BV progression
Relative fold change
Human EGFR mRNA
Mouse Egfr mRNA
D
Relative fold change
Human FGFR2 mRNA
Mouse Fgfr2 mRNA

Figure 2
BV resistance is associated with increased expression of stromal genes involved in angiogenesis. (**A**) Stromal and human angiogenic genes were differentially regulated in H1975 BV-resistant xenografts compared with vehicle controls ($n = 3$ per group). $P < 0.005$, 2-sample *t* test with random variance model. Exact permutation *P* values for significant genes were computed based on 10 available permutations. Data represent differences in fold change of genes in BV-resistant tumors versus controls. The dashed red line indicates fold change 1 (i.e., no change versus controls). Red and blue arrows indicate *Egfr* and *Fgfr* family member genes, respectively. (**B**) Functional pathway analysis of selected genes and their interaction nodes in a gene network significantly modulated between the BV-resistant and control xenograft mouse stroma. Network score was calculated by the inverse log of the *P* value and indicates the likelihood of focus genes in a network being found together not by chance. The selected genes (*Egfr*, *Bax*, and *Dnajb1*) and their interaction segments are highlighted by a blue border. Gene expression variation by at least 1.5-fold is indicated by color (red, upregulated; green, downregulated; gray, NS). (**C** and **D**) qRT-PCR showing human *EGFR* and mouse *Egfr* (**C**) and human *FGFR2* and mouse *Fgfr2* (**D**) mRNA expression in H1975 xenografts that progressed on vehicle and BV treatments ($n = 4$ per group). Data are normalized relative to vehicle progression samples and shown as relative fold change. $^*P < 0.05$, *t* test.

expression was observed in H1975 BV-resistant xenografts compared with controls ($P < 0.05$; Figure 2D).

EGFR is activated on stromal cells of H1975 and A549 BV-resistant tumors. Given our observation that mouse *Egfr* mRNA was increased in BV-resistant tumors, we next evaluated EGFR protein expression in H1975 tumors by IF staining using antibodies directed against CD31 and EGFR (Supplemental Figure 2A). Quantification of EGFR staining by LSC analysis revealed that prolonged administration of BV produced a nearly 10-fold increase in the number of EGFR-expressing cells in H1975 BV-resistant tumors compared with control tumors ($P < 0.01$; Figure 3A and Supplemental Figure 2A). We also evaluated EGF ligand by immunohistochemistry (IHC) in H1975 vehicle- and BV-treated xenografts at progression and observed increased levels of EGF immunoreactivity in resistant tumors compared with controls (Supplemental Figure 2B).

We next examined the activation status of EGFR in H1975 and A549 xenografts after treatment with vehicle and BV at progression. Confocal microscopy was used to analyze specimens stained with antibodies directed against CD31 and p-EGFR. As shown in Figure 3B, BV resistance was associated with a marked difference in p-EGFR expression in both H1975 and A549 tumors compared with controls; however, notable differences in the staining pattern were observed between the 2 xenograft models. In the H1975 model, p-EGFR expression was significantly increased on the vascular supporting cells (VSCs) of resistant tumors compared with controls ($P < 0.001$), whereas in A549 BV-resistant xenografts, p-EGFR expression was significantly increased on tumor-associated ECs compared with controls ($P < 0.05$; Figure 3C, right).

To identify the population of VSCs expressing p-EGFR in H1975 BV-resistant tumors, we performed IF staining using antibodies directed against p-EGFR and desmin, a marker for pericytes (Figure 3D). This analysis revealed that the VSCs of H1975 BV-resistant tumors coexpressed p-EGFR and desmin. In addition, the number of pericytes expressing p-EGFR was 8-fold greater in H1975 BV-resistant tumors than in control tumors ($P < 0.01$; Figure 3E). Taken together, our results suggest that upregulation and activation of stromal EGFR is a characteristic feature of BV-resistant tumors in these models and that multiple stromal cell types can express EGFR.

Increased expression of basic FGF and FGFR2 in H1975 xenografts resistant to BV therapy. Based on our observation that mouse *Fgfr2* gene expression was increased in the stromal compartment of BV-resistant H1975 tumors, we performed colocalization studies (IF) on H1975 tumors that progressed while receiving vehicle and BV, using antibodies against CD31 and FGFR2 (Figure 4A). We observed a significant increase in FGFR2 protein expression levels in resistant tumors compared with controls ($P < 0.001$; Figure 4B). Furthermore, to assess changes in the FGFR2 ligand, we next measured the plasma concentration of mouse basic FGF (bFGF). We found a 1.5-fold increase in the level of circulating bFGF in BV-resistant tumors compared with controls ($P = 0.025$; Figure 4C). Consistent with these findings, IHC analysis of H1975 control- and BV-treated xenografts at progression demonstrated increased protein expression of bFGF in BV-resistant tumors compared with controls (Figure 4D).

Resistance to BV is associated with tumor revascularization and morphological changes in the vasculature. Because the primary mechanism of action of BV is directed against blood vessels, we quantified the microvessel density (MVD) of H1975 and A549 xenografts. We initially assessed changes in the vasculature after short-term treatment. There was a 3-fold MVD reduction in initially sensitive H1975 tumors treated with BV for 2 weeks compared with controls ($P < 0.01$; Figure 5, A and B). Vessel density (as an indicator of relative primary resistance) of A549 tumors treated for 2 weeks did not show significant changes compared with controls. To determine whether the vascular effects observed after 2 weeks of BV therapy persisted in tumors receiving long-term BV treatment, we quantified the MVD in BV-resistant H1975 and A549 tumors (Figure 5, A and B). We found that relative primary and acquired resistance were associated with distinct patterns of tumor vascularization. In H1975 BV-treated xenografts, MVD was significantly higher at progression compared with 2 weeks of treatment ($P < 0.01$), then returned to levels comparable to those of vehicle-treated controls. In A549 BV-resistant xenografts, MVD significantly increased compared with A549 vehicle-treated controls ($P < 0.05$). These data suggest that BV therapy has a marked initial antiangiogenic effect on sensitive H1975 xenografts, but the effect is lost after continued exposure to the drug, and that therapeutic resistance is associated with revascularization at levels comparable with or higher than those in vehicle-treated controls.

Previous studies have demonstrated that antiangiogenic therapy can alter the morphology of the tumor-associated vasculature (29–32). To evaluate the tumor vascularization in greater detail, we measured the vascular tortuosity in vehicle and BV-treated H1975 and A549 xenografts. Short-term administration of BV led to a modest, but not statistically significant, reduction in the vessel tortuosity of H1975 tumors (Figure 5, A and C). However, as these tumors developed BV resistance, we noted a 4-fold reduction in vascular tortuosity compared with controls ($P < 0.01$). These blood vessels were also characterized by large-diameter lumens and a greater degree of pericyte coverage (referred to herein as normalized revascularization). In contrast, in A549 xenografts with relative primary resistance to BV, tumor vascularization was associated with smaller, more tortuous vessels with reduced pericyte coverage compared with controls (referred to herein as sprouting vascularization; $P < 0.05$; Figure 5, A and C). Thus, in these mod-

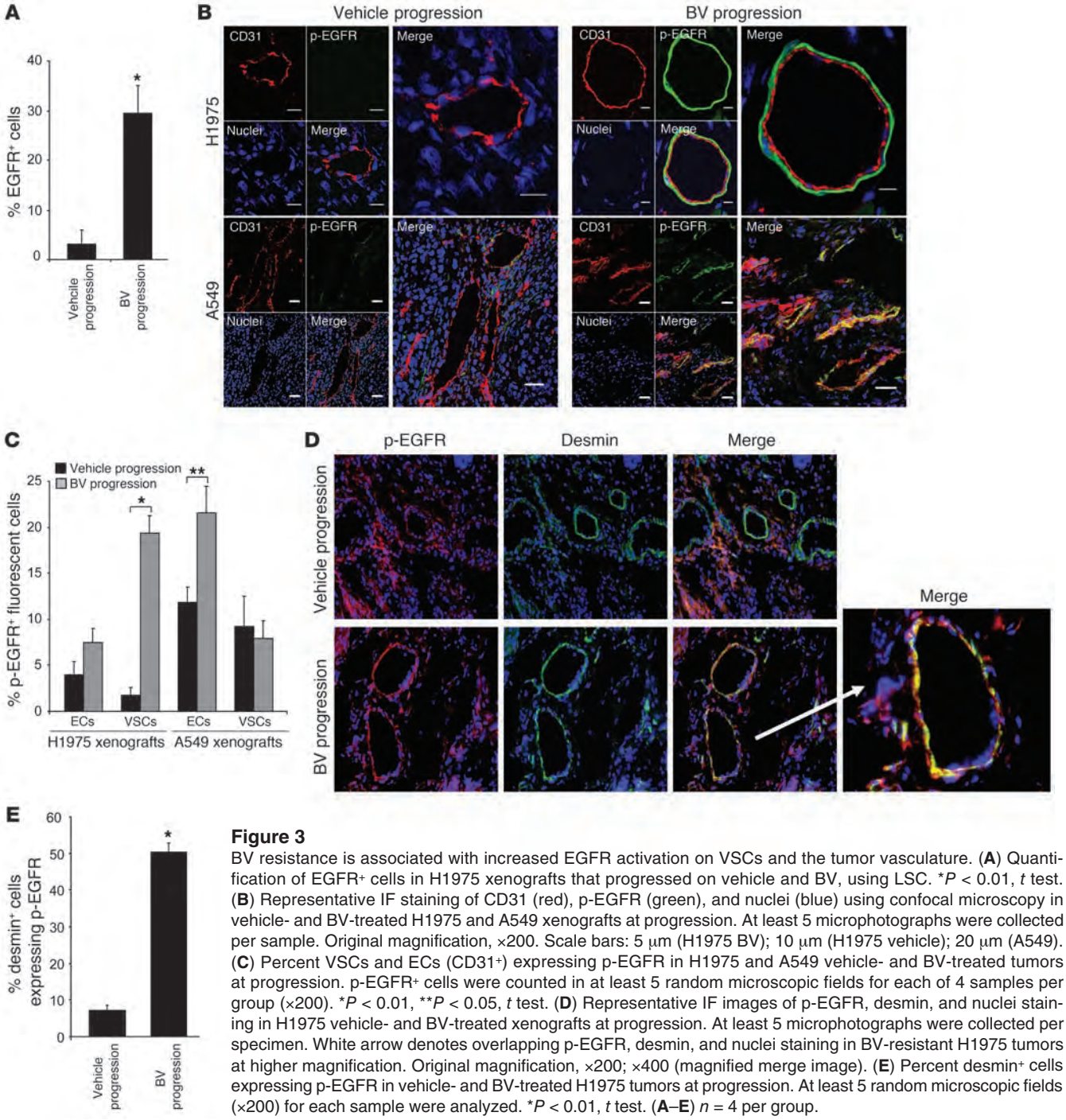

Figure 3

BV resistance is associated with increased EGFR activation on VSCs and the tumor vasculature. (**A**) Quantification of EGFR+ cells in H1975 xenografts that progressed on vehicle and BV, using LSC. *$P < 0.01$, *t* test. (**B**) Representative IF staining of CD31 (red), p-EGFR (green), and nuclei (blue) using confocal microscopy in vehicle- and BV-treated H1975 and A549 xenografts at progression. At least 5 microphotographs were collected per sample. Original magnification, ×200. Scale bars: 5 μm (H1975 BV); 10 μm (H1975 vehicle); 20 μm (A549). (**C**) Percent VSCs and ECs (CD31+) expressing p-EGFR in H1975 and A549 vehicle- and BV-treated tumors at progression. p-EGFR+ cells were counted in at least 5 random microscopic fields for each of 4 samples per group (×200). *$P < 0.01$, **$P < 0.05$, *t* test. (**D**) Representative IF images of p-EGFR, desmin, and nuclei staining in H1975 vehicle- and BV-treated xenografts at progression. At least 5 microphotographs were collected per specimen. White arrow denotes overlapping p-EGFR, desmin, and nuclei staining in BV-resistant H1975 tumors at higher magnification. Original magnification, ×200; ×400 (magnified merge image). (**E**) Percent desmin+ cells expressing p-EGFR in vehicle- and BV-treated H1975 tumors at progression. At least 5 random microscopic fields (×200) for each sample were analyzed. *$P < 0.01$, *t* test. (**A**–**E**) $n = 4$ per group.

els, acquired resistance and relative primary resistance to BV were associated with distinct patterns of vascular remodeling.

Dual blockade of EGFR and VEGFR2 signaling pathways delays tumor growth of NSCLC xenografts. To elucidate whether targeting functioning stromal signaling pathways in BV-resistant tumors abrogates therapeutic resistance, we targeted EGFR using either the EGFR TKI erlotinib in combination with BV, or the dual VEGFR/EGFR inhibitor vandetanib. Both A549 and H1975 tumor cells are known to be resistant to erlotinib and vandetanib in vitro, which is thought to be caused by the presence of a KRas mutation and a secondary EGFR mutation (T790M), respectively (26–28). Consistent with previous results, erlotinib did not inhibit H1975 tumor growth compared with vehicle, as 5 of 6 xenografts progressed, with a median PFS of 12.5 days ($P = 0.33$, erlotinib versus vehicle; Figure 6A). Erlotinib and BV treatment in combination (referred to herein as erlotinib+BV) resulted in prolonged PFS; only 1 of 6 tumors progressed at the end of more than 200 days (median PFS not reached; $P = 0.0009$, erlotinib+BV versus vehicle; $P = 0.19$, erlotinib+BV versus BV; Figure 6, A and B), although after more than 140 days of treatment, 3 mice died of causes unrelated to

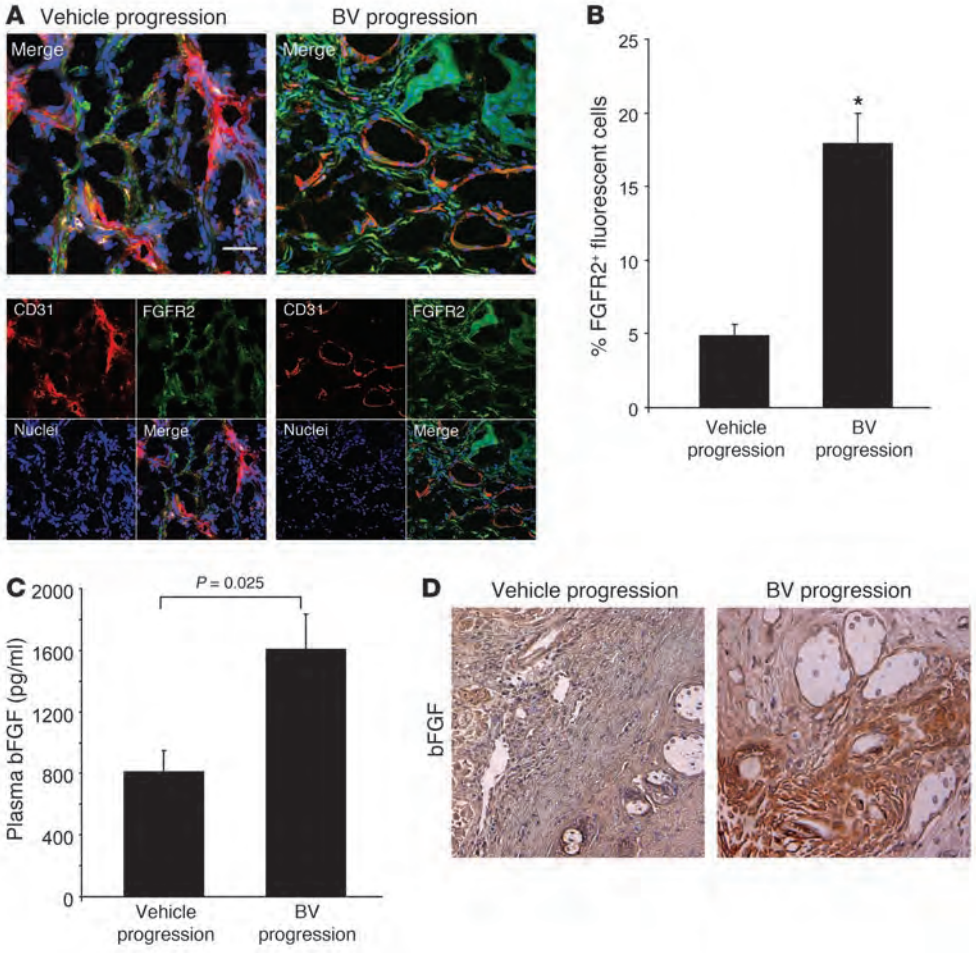

Figure 4
Increase in stromal FGFR2 expression in H1975 BV-resistant xenografts. (**A**) Representative IF images of CD31 and FGFR2 staining in H1975 vehicle- and BV-treated H1975 xenografts at progression, using confocal microscopy. At least 5 microphotographs were collected from 4 specimens per group. Original magnification, ×200. Scale bar: 20 μm. (**B**) Percent FGFR2+ fluorescent cells counted in 5 random microscopic fields (×200) per sample (n = 4 per group). *P < 0.001, t test. (**C**) bFGF levels were measured in plasma of vehicle- and BV-treated H1975 xenografts at progression, using multiplex bead assay (n = 4 per group; each sample tested in duplicate). P value was calculated using t test. (**D**) Representative IHC images showing bFGF protein expression in vehicle- and BV-treated H1975 xenografts. At least 5 random microscopic fields were collected from each of 4 specimens per group. Original magnification, ×200.

tumor growth. Vandetanib treatment inhibited tumor growth in all tumors, and only 2 of 6 progressed after response, displaying a median PFS of 211 days (P = 0.0007, vandetanib versus vehicle; P = 0.295, vandetanib versus BV; Figure 6, A and B).

In A549 xenografts, treatment with erlotinib resulted in a median PFS of 53 days, compared with 29.5 days in vehicle-treated controls (P = 0.34; Figure 6C). Over the course of the experiment, 2 tumors progressed on erlotinib+BV treatment (median PFS not reached), and the addition of erlotinib to BV significantly delayed the onset of resistance compared with BV alone (P = 0.013, erlotinib+BV versus vehicle; P = 0.049, erlotinib+BV versus BV; Figure 6, C and D). On vandetanib treatment, 1 xenograft progressed after 102 days, and the median PFS was not reached (P = 0.017, vandetanib versus vehicle; P = 0.046, vandetanib versus BV; Figure 6, C and D). These findings indicate that EGFR inhibition not only reduced the number of NSCLC xenografts that progressed on therapy compared with BV alone in both our models, but also delayed the onset of resistance to VEGF signaling inhibition in A549 xenografts.

Given the aforementioned EGFR expression in pericytes in the H1975 model, we examined whether targeting EGFR affects vessel maturation and pericyte coverage. Multicolor IF staining was performed using antibodies directed against CD31 and desmin, and pericyte coverage was quantified. In H1975 BV-resistant xenografts, the percentage of blood vessels supported by pericytes was 50% greater than that in control tumors (P < 0.01; Figure 5D). However, pericyte coverage was significantly reduced in tumors receiving long-term treatment with erlotinib+BV or with vandetanib (P < 0.01), consistent with EGFR blockade blunting the increase in pericyte coverage accompanying the normalized revascularization observed with BV in this model. In contrast, A549 xenografts that progressed on BV therapy had significantly fewer blood vessels supported by pericytes than did controls (P < 0.01; Supplemental Figure 3); nevertheless, long-term administration of erlotinib+BV or of vandetanib also decreased the pericyte coverage in this model compared with controls (P < 0.01; Supplemental Figure 3), providing further support for the role of EGFR in tumor-associated stroma.

Lung adenocarcinoma H441 orthotopic tumors acquire resistance to BV, and tumor growth is delayed with dual EGFR/VEGFR2 inhibition. To investigate whether the changes associated with BV resistance in subcutaneous models also occur in tumors growing in the lung, we used an established orthotopic model whereby H441 lung adenocarcinoma cells were injected directly into the lung of male nude mice. These cells harbor wild-type EGFR and mutant KRas and were selected because of their moderate tumor cell resistance to EGFR blockade (33), and also because they display optimal growth kinetics when implanted in the mouse lung (34). At 21 days after injection, an initial cohort of 8 mice was euthanized to evaluate mean tumor volume (approximately 60 mm^3). To evaluate the effects of short-term BV treatment, 2 additional groups of mice were sacrificed after 2 weeks of BV therapy, as in the prior experiments. The remaining animals were then randomized for a

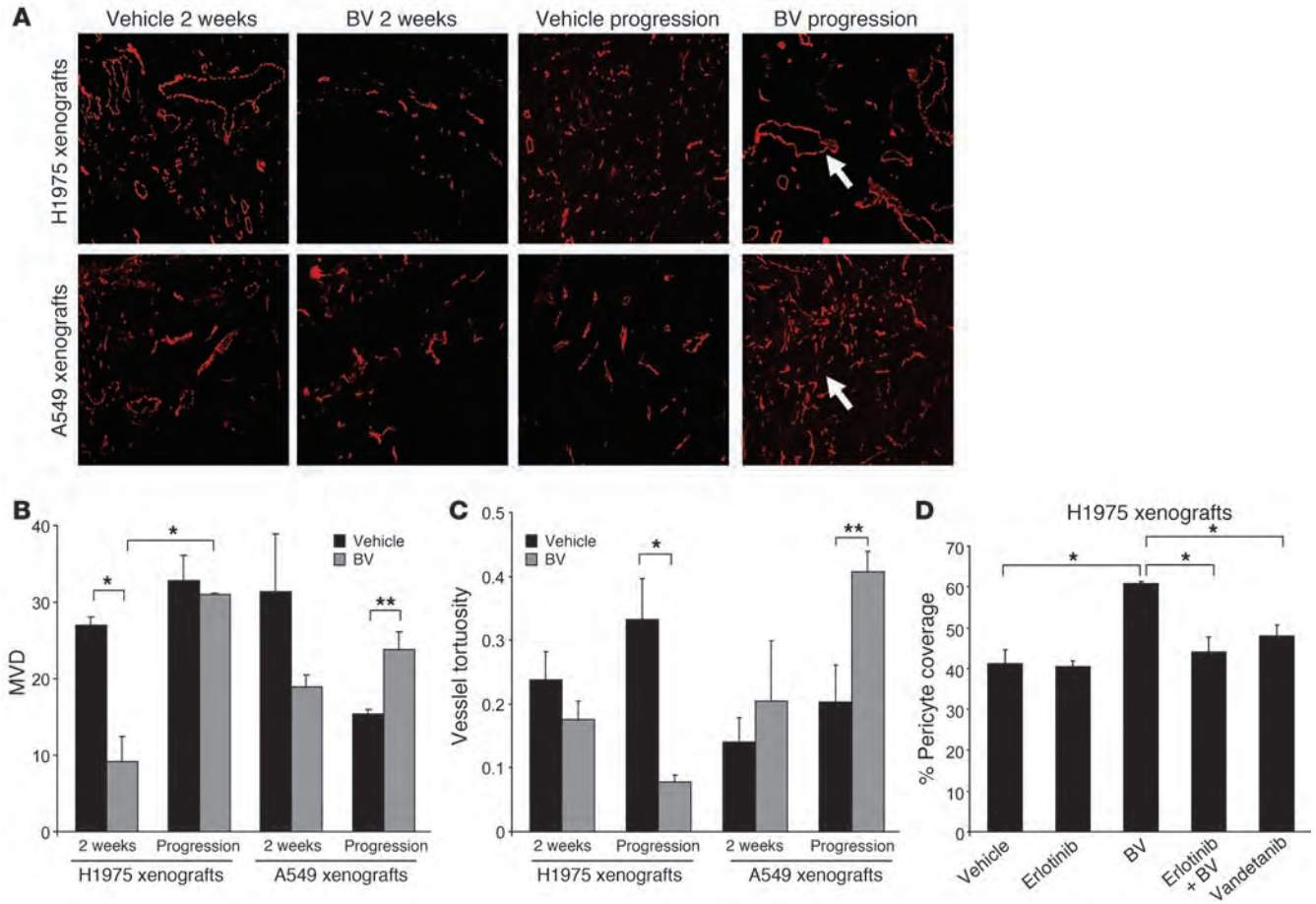

Figure 5

Altered patterns of tumor vascular density, tortuosity, and pericyte coverage in BV-resistant xenograft tumors. (**A**) Microphotographs of CD31$^+$ tumor vessels (red) in H1975 and A549 xenografts treated with vehicle and BV after 2 weeks and at progression. 5–10 microscopic fields were collected from each of 4 specimens per group. Arrows indicate the different vessel morphology in H1975 (top panel) and A549 (lower panel) BV-resistant tumors. Original magnification, ×100. (**B** and **C**) Quantification of MVD (**B**) and vessel tortuosity (**C**) based on CD31-stained tumor sections in H1975 and A549 xenografts treated with vehicle and BV after 2 weeks and at progression. 5 hotspot microscopic fields (×200) per tumor section were analyzed to quantify MVD; 5 random microscopic fields (×100) were quantified for vessel tortuosity analysis. $n = 4$ per group. Units of the y axis for MVD (**B**) represent CD31 + vessels per HPF (high power field). The y axis for vessel tortuosity (**C**) represents the ratio T = (L/S) – 1. (**D**) Pericyte coverage of H1975 xenografts was quantified as percent CD31$^+$ vessels with at least 50% coverage of associated desmin$^+$ cells in at least 5 microscopic fields (×200) in tumors receiving long-term treatment. $n = 2$ (vandetanib); 3 (erlotinib); 4 (vehicle, BV, and erlotinib+BV). (**B**–**D**) $^*P < 0.01$, $^{**}P < 0.05$, t test.

survival analysis ($n \geq 7$ per group) and treated with vehicle, erlotinib, BV, erlotinib+BV, or vandetanib until moribund, at which time they were euthanized. Survival was defined as the time from treatment onset until sacrifice.

Short-term treatment with BV resulted in significant tumor growth inhibition compared with vehicle-treated tumors ($\Delta T/\Delta C$ 45.7%; $P = 0.026$, Mann-Whitney test; Figure 7, A and B). In the long-term treatment analysis, all mice had a large tumor burden at the time of sacrifice (Figure 7C). As shown in Figure 7D and Supplemental Figure 4, erlotinib treatment resulted in a small but significant prolongation of survival compared with vehicle (median survival, 58 versus 50 days; $P = 0.02$, log-rank test). The BV group had a longer survival (median, 77 days) compared with erlotinib alone ($P = 0.00015$), and the combination of erlotinib and BV, or vandetanib, significantly prolonged survival (median, 101 days) compared with BV or erlotinib alone ($P = 0.0001$, erlotinib+BV versus erlotinib; $P = 0.0001$, erlotinib+BV versus BV; $P = 0.022$, vandetanib versus BV; Figure 7D and Supplemental Figure 4, C and D). Similar to our results obtained with the H1975 xenografts, H441 orthotopic tumors were initially sensitive to VEGF signaling pathway blockade, but tumors ultimately progressed. In this orthotopic model, dual targeting of EGFR and VEGF pathways significantly delayed the onset of therapeutic resistance compared with inhibition of either pathway alone.

Characterization of H441 orthotopic tumor stroma after anti-VEGF therapy and dual EGFR/VEGFR2 inhibition. We next sought to more completely characterize the vasculature and stroma of BV-resistant H441 tumors. We found a significant decrease in MVD after 2 weeks of BV treatment compared with vehicle controls ($P = 0.0008$; Figure 7E). Consistent with the revascularization observed in the subcutaneous models, tumors resistant to BV or dual VEGFR/EGFR inhibition showed significantly increased MVD compared with BV-sensitive

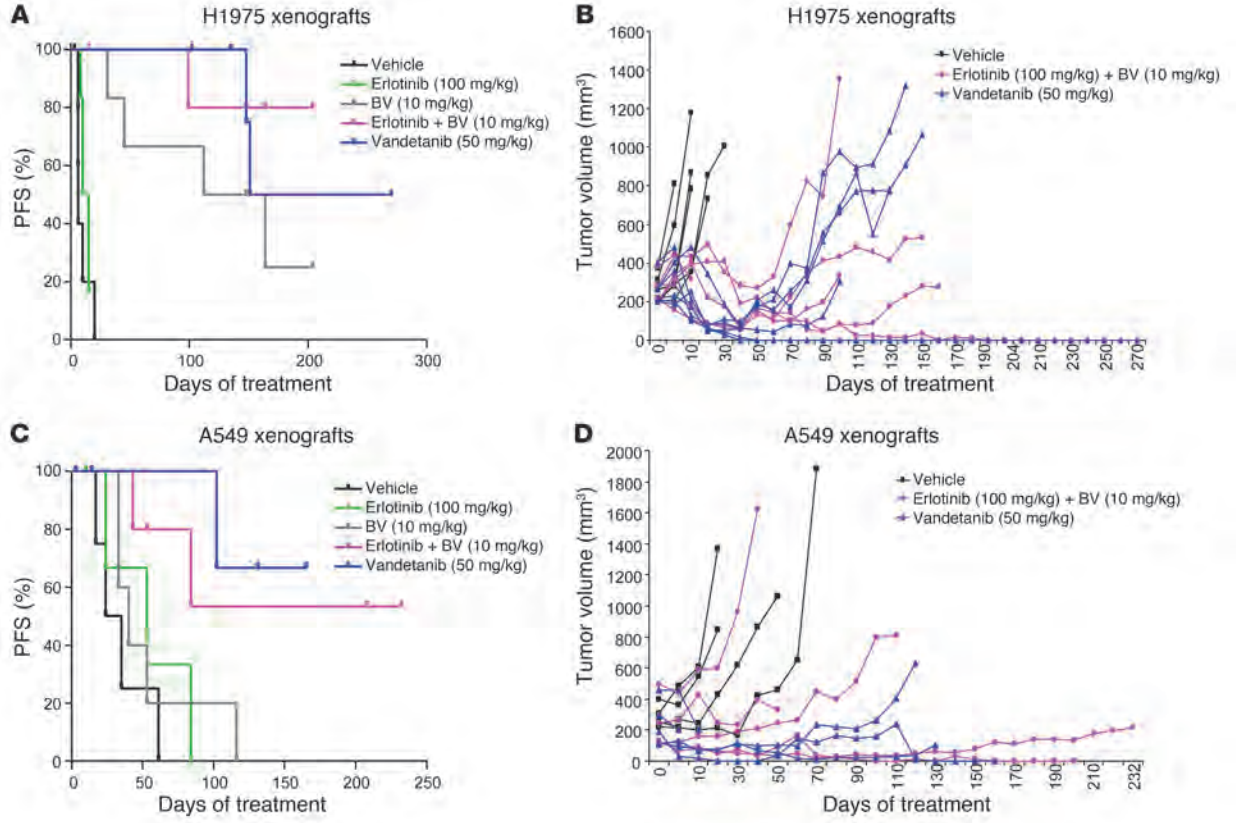

Figure 6
Effect of dual EGFR/VEGFR2 inhibition on H1975 and A549 NSCLC xenograft models. (**A** and **C**) Distribution of PFS, shown by Kaplan-Meier plots, and (**B** and **D**) individual tumor growth curves of H1975 (**A** and **B**) and A549 (**C** and **D**) xenografts receiving long-term treatment as indicated. Log-rank test was used to compare statistical differences in survival among treatment groups.

tumors ($P = 0.045$; Figure 7E). Interestingly, in the erlotinib-resistant group, no revascularization was observed; in fact, MVD was significantly lower than in BV-resistant tumors ($P = 0.034$; Figure 7E). These findings indicate that VEGF inhibitor resistance is associated with revascularization in H441 orthotopic tumors.

We next investigated the EGFR signaling pathway in BV-resistant H441 tumors. Protein levels of total EGFR were not significantly different in tumor and endothelium of vehicle and BV-resistant H441 tumors (data not shown). Levels of p-EGFR, however, were significantly increased in H441 BV-resistant tumors compared with vehicle-treated tumors ($P = 0.039$; Figure 8, A and B), and, consistent with the H1975 subcutaneous model of acquired resistance, the activated receptor colocalized with the stroma, supporting large, normalized vessels in BV-resistant tumors. Furthermore, in tumors resistant to VEGFR/EGFR targeting, the levels of p-EGFR were strongly decreased compared with either vehicle-treated or BV-resistant tumors ($P = 0.0001$, erlotinib+BV versus vehicle; $P = 0.0008$, erlotinib+BV versus BV; $P = 0.011$, vandetanib versus vehicle; $P = 0.009$, vandetanib versus BV; Figure 8, A and B), demonstrating persistent EGFR blockade with treatment. Given these results, we next quantified the percentage of pericyte coverage of the blood vessels supplying H441 orthotopic tumors, as an index of vessel maturations. As shown in Figure 8, C and D, BV-resistant tumors had significantly increased pericyte coverage compared with controls and BV-sensitive tumors ($P = 0.003$, BV progression versus vehicle progression; $P < 0.0001$, BV progression versus BV 2 weeks). Moreover, in tumors that progressed while receiving erlotinib alone, erlotinib+BV, or the dual inhibitor vandetanib, the pericyte coverage was reduced to levels comparable to vehicle-treated tumors ($P = 0.001$, erlotinib versus BV; $P = 0.054$, erlotinib+BV versus BV; $P = 0.007$, vandetanib versus BV; Figure 8, C and D). These findings support our earlier observation that stromal EGFR contributed to acquisition of resistance to VEGF inhibition through signaling activation on VSCs. However, we also noted in BV-resistant H441 tumors a substantial amount of p-EGFR IF staining localized far from the $CD31^+$ vascular structures (Figure 8A), which indicates that apart from VSCs, other components of the tumor stroma may undergo significant changes and contribute to the resistant phenotype, at least in this model. Furthermore, it is worth noting that increases in FGFR2 gene and protein levels were not observed in BV-resistant orthotopic tumors (data not shown), which indicates that there were differences between the orthotopic and subcutaneous models.

Inflammatory cells and tumor-associated fibroblasts in BV-resistant tumors. Because bone marrow–derived inflammatory cells and tumor-associated fibroblasts have previously been shown to play a role in mediating angiogenesis and refractoriness to VEGF blockade (23, 25, 35, 36), we next evaluated the infiltration of inflammatory macrophages and myofibroblasts in the stroma of both our models of acquired resistance. We performed double IF staining

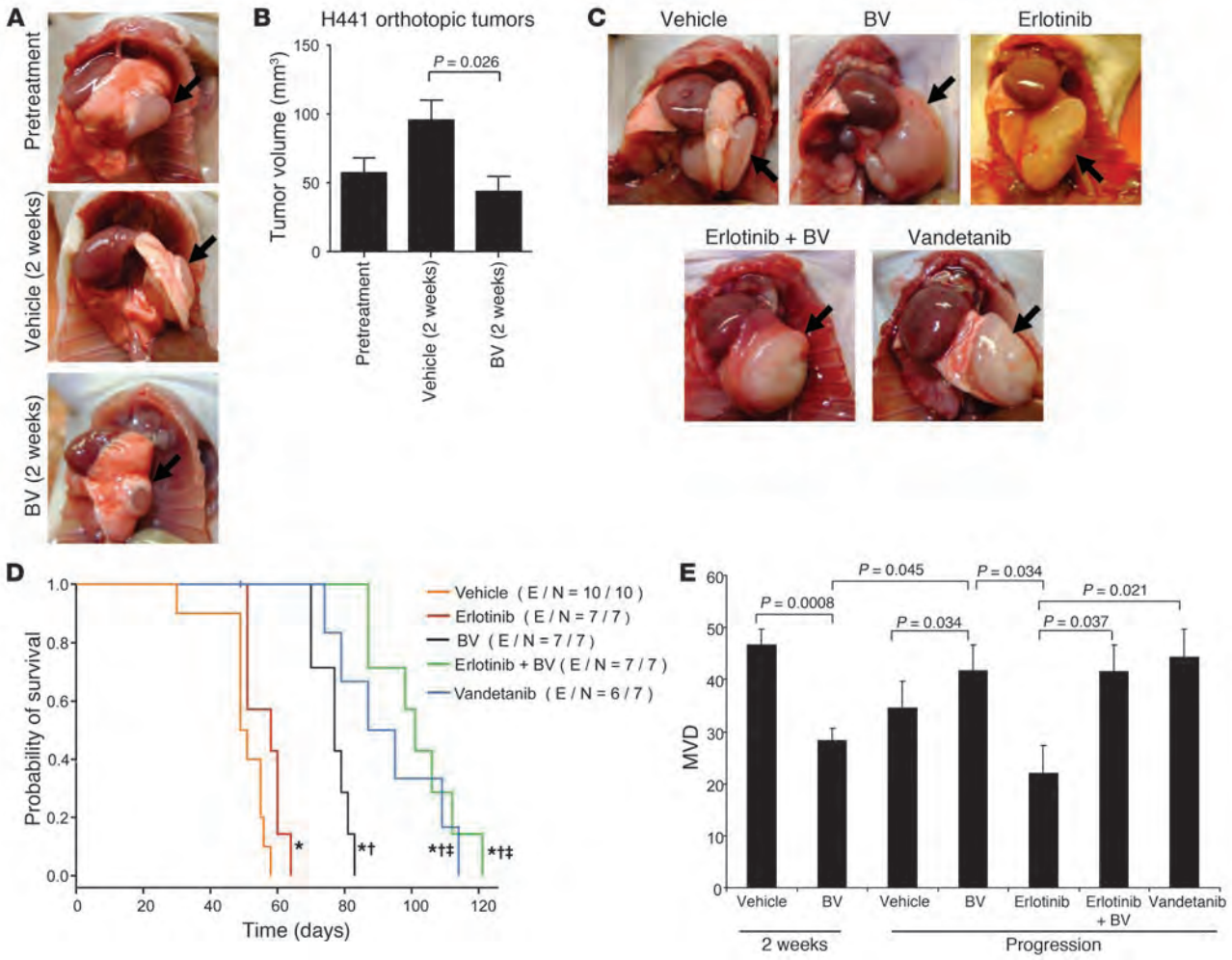

Figure 7

Orthotopic H441 NSCLC tumor growth and MVD after VEGF blockade or dual EGFR/VEGFR pathway inhibition. (**A** and **B**) Representative photographs (**A**) and mean tumor volume obtained at the last measurement (**B**) of H441 orthotopic tumors before or after 2 weeks of treatment. Arrows denote tumor mass in the lung. $n = 8$ (pretreatment); 9 (vehicle); 10 (BV). P value was calculated using Mann-Whitney test. (**C**) Representative photographs of H441 orthotopic tumors after long-term administration. $n = 10$ (vehicle); 7 (erlotinib, BV, and erlotinib+BV); 6 (vandetanib). Arrows denote tumor mass in the lung. (**D**) Kaplan-Meier plots showing survival distribution in H441 orthotopic tumor–bearing mice treated as indicated. Number of events (E) per number in each group (N) is indicated. $^{*}P < 0.05$ versus vehicle, $^{\dagger}P < 0.01$ versus erlotinib, $^{\ddagger}P < 0.05$ versus BV, log-rank test. (**E**) MVD quantification in H441 orthotopic tumors. $n = 4$ (erlotinib); 5 (vehicle 2 weeks and vandetanib); 6 (BV 2 weeks and vehicle progression); 7 (BV progression and erlotinib+BV). Statistical values were calculated using t test. Units in the y axis for MVD represent CD31 + vessels per HPF.

to identify F4/80^{+} macrophages (Supplemental Figure 5A) and α-SMA^{+} fibroblasts and myofibroblasts (Supplemental Figure 5C) in both H1975 subcutaneous and H441 orthotopic tumors with BV resistance. As shown in Supplemental Figure 5, B and D, there were no significant differences in overall levels of these markers between vehicle- and BV-treated tumors at progression in either model. In vehicle-treated H441 tumors, the α-SMA staining pattern suggested a dense and desmoplastic stroma. Conversely, this pattern was no longer observed in BV-resistant tumors: α-SMA consistently localized in rounded, well-demarcated areas, indicating a pattern characteristic of, but not limited to, perivascular cells in this model. In fact, given the different localization pattern of α-SMA between BV-resistant orthotopic tumors and vehicle-treated tumors, we cannot rule out the possibility of potential changes in other cell populations of the lung microenvironment, such as mesenchymal or other stromal cells, that might contribute to the onset of resistance to VEGF inhibition.

Discussion

Early reports examining the effects of VEGF blockade and other antiangiogenic therapies raised the hopes that these agents may substantially slow or stop tumor growth, and that therapeutic resistance to these agents would be less likely to occur, at least in part, because the target was diploid and not prone to the same genetic instability as tumor cells (37, 38). However, both preclinical studies and clinical experience in lung cancer and other solid tumors (12, 17, 39–43) indicate that the vast majority of solid tumors either exhibit primary (intrinsic) resistance or will eventually acquire resistance to the effects of antiangiogenic therapy. Although to date most studies of therapeutic resistance to anticancer drugs have

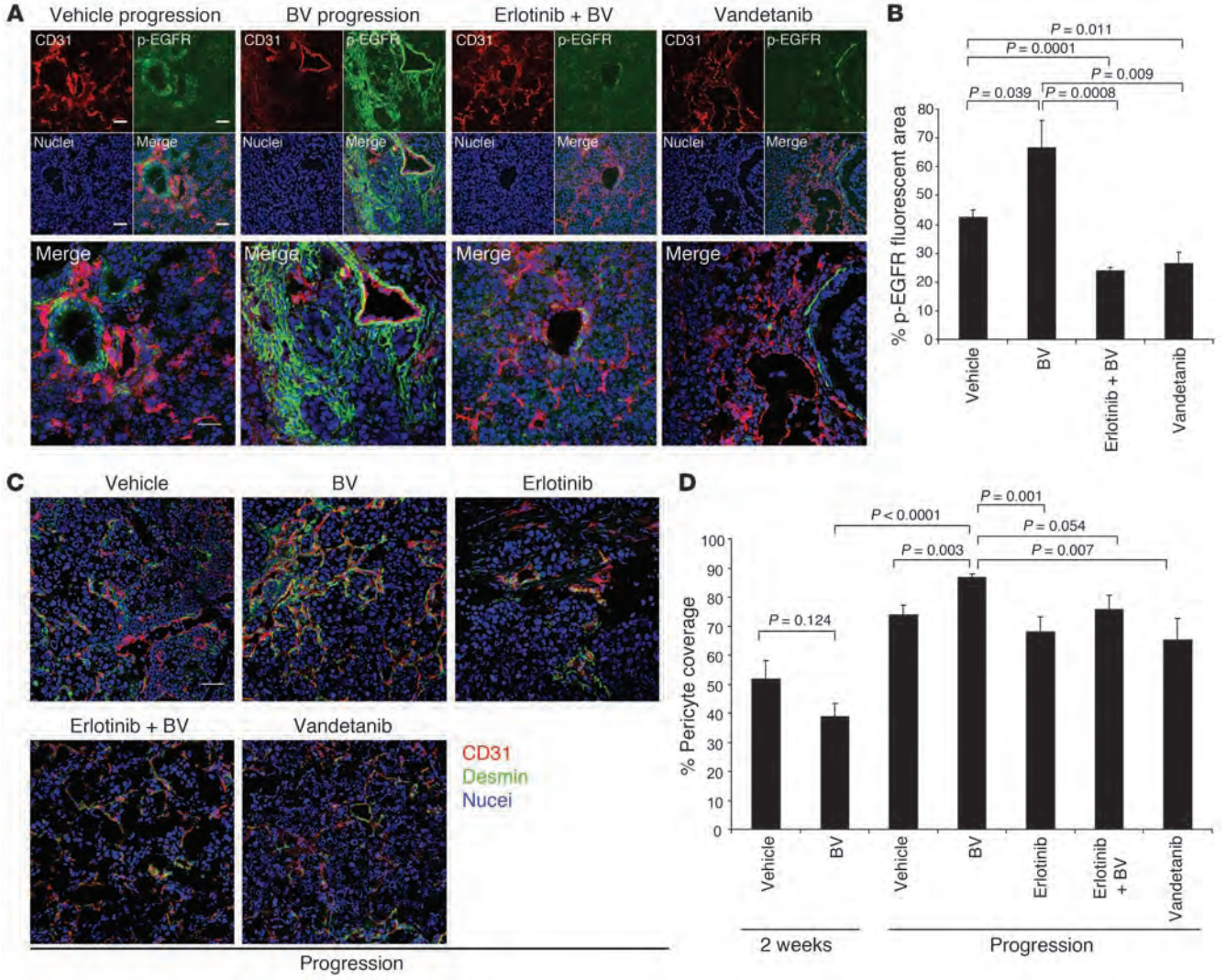

Figure 8

EGFR is activated in H441 BV-resistant tumors, and dual EGFR/VEGFR inhibition reduces pericyte coverage. (**A**) Representative microphotographs of CD31 (red), p-EGFR (green), and nuclei (blue) fluorescent staining in H441 tumors that progressed on vehicle, BV, erlotinib+BV, and vandetanib treatments, using confocal microscopy. At least 5 microphotographs were collected from all the tumor specimens in each group. Original magnification, ×200. Scale bar: 50 μm. (**B**) Percent p-EGFR fluorescent area in H441 tumors that progressed while on the indicated therapies, as determined using Alpha Innotech Software. 5–10 random microphotographs (×200) of red (CD31), green (p-EGFR), and blue (nuclei) fluorescence were collected from 5 (vehicle and BV), 6 (erlotinib+BV), and 4 (vandetanib) specimens per group. *P* values were calculated using *t* test. (**C**) Representative IF images of CD31, desmin, and nuclei in H441 tumors that progressed while on the indicated treatments, using confocal microscopy. At least 5 microphotographs were collected from all the tumor specimens per group. Original magnification, ×200. Scale bar: 50 μm. (**D**) Percent pericyte coverage in H441 tumors was quantified in at least 5 microscopic fields (×200) of tumor specimens. *n* = 4 (erlotinib); 5 (vehicle 2 weeks and vandetanib); 6 (BV 2 weeks and vehicle progression); 7 (BV progression and erlotinib+BV). *P* values were calculated using *t* test.

focused on the role of tumor cells, recent studies have suggested that host factors, including tumor stroma, may play an important role in resistance to angiogenesis inhibitors (14, 15, 23, 25, 42, 44).

In this study, we used mouse- and human-specific profiling of human NSCLC xenografts in mice to investigate stromal and tumor cell changes occurring in tumors that acquired resistance to BV. This analysis revealed that changes in gene expression, and particularly changes in angiogenesis-related genes, occurred predominantly in stromal and not tumor cells. This observation reinforces the notion that tumor stroma may play an important — and potentially dominant, in at least some circumstances — role in VEGF inhibitor resistance.

Pathway analyses highlighted that among these stromal changes, there were multiple genes in the *Egfr* and *Fgfr2* pathways that were upregulated in resistant tumors (e.g., *Epgn*, *Areg*, *Fgf13*, and *Fgfbp1*) and that the EGFR pathway appeared to be a central gene interaction pathway. EGFR and FGFR2 upregulation was confirmed using species-specific RT-PCR as well as IHC. As noted below, upregulation of the bFGF/FGFR2 pathway has previously been observed by our group and others in VEGF inhibitor resistance

(16, 17, 45), but to our knowledge, a role for stromal EGFR has not been reported previously. We therefore investigated this pathway in greater detail using 3 models: subcutaneous and orthotopic models of acquired resistance (H1975 and H441, respectively) and a model of relative primary resistance (A549). Tumor cells from all 3 models are known to be relatively resistant to EGFR blockade in vitro (26, 33).

In both models of acquired BV resistance, there was a significant increase in activated EGFR that largely, but not exclusively, localized on VSCs, which were predominantly pericytes (Figures 3, 5, and 8). No significant p-EGFR was detectable on VSCs of control tumors. This was accompanied by an increase in pericyte coverage and a pattern of less tortuous, normalized revascularization in the BV-resistant tumors. Dual inhibition of VEGFR and EGFR pathways reduced pericyte coverage of tumor vessels compared with BV alone, which indicates that EGFR signaling plays a functional role in pericyte coverage of tumor vessels in the models studied. Dual targeting also significantly delayed the emergence of resistance and prolonged survival in the H441 model, with similar trends observed in the H1975 model (Figures 6 and 7). To our knowledge, this is the first evidence demonstrating a potential role for EGFR signaling in pericytes or other stromal cell populations of the tumor microenvironment in resistance to VEGF pathway inhibition in murine models of NSCLC.

Consistent with our observation regarding EGFR in tumor pericytes, a recent study found that the EGFR TKI gefitinib significantly suppressed tumor-associated pericyte function (46). During the revisions of this manuscript, other investigators reported a role for the stromal heparin-binding Egf/Egfr (Hb-Egf/Egfr) signaling pathway in the progression of a pancreatic neuroendocrine tumor model of EGFR-targeted inhibition (47). The authors demonstrate that stromal cell–derived Hb-Egf activates the EGFR pathway in perivascular cells, contributing to increased pericyte coverage and angiogenesis. These reports provide further support for a role of EGFR signaling in pericyte function in tumor revascularization.

A recent study has identified a role for PDGF-C expressed by tumor-associated fibroblasts in VEGF inhibitor resistance (25) and in attenuating tumor response to anti-VEGF treatment in a model of glioblastoma (48). PDGFR signaling in pericytes has also been implicated in vessel maturation, and recent evidence indicates that VEGF signaling suppresses pericyte PDGFR signaling, inhibiting vessel maturation (49). Somewhat surprisingly, we did not observe upregulation of any PDGFRs or ligands. In contrast, we noted modest but statistically significant downregulation of the stromal genes *Pdgfa*, *Pdgfb*, and *Pdgfrb*. Given the role of the PDGF family in multiple tumor processes, including pericyte recruitment and function (50, 51), it appears that pericyte-expressed EGFR may play a complimentary or compensatory role in the increased pericyte coverage observed in the acquired resistance models. Although the current study does not address this issue, it will be interesting to determine whether increased pericyte EGFR signaling in the H441 model (in the absence of increased EGFR gene or protein levels) is driven by increased ligand production or by reduced VEGFR-driven inhibition of signaling, as observed for pericyte PDGFR.

In the A549 model, stromal EGFR was also upregulated in BV-resistant tumors, but was localized exclusively to tumor endothelium, not VSCs. As expected, dual VEGFR/EGFR inhibition did not reduce pericyte coverage in this model, but did significantly delay the emergence of resistance compared with BV alone (Figure 6). This observation highlights that a signaling pathway may play different roles in tumor stroma depending on the cellular context. Studies examining EGFR distribution on endothelium suggest that it is restricted to blood vessels supplying pathologic tissues (52), where it activates angiogenic programs (53). Others have reported that EGFR is activated on endothelium when tumor cells express EGFR ligands, such as TGF-α or EGF (54, 55).

Activation of the bFGF/FGFR2 pathway has previously been shown to be a critical regulator of the angiogenic switch (56) and to be upregulated in response to antiangiogenic therapy (17). We observed an approximately 6-fold increase in stromal *Fgfr2* gene expression in tumors with acquired resistance and, consistent with this finding, an increase in the number of FGFR2-expressing cells in these tumors. This immunoreactivity appeared to be largely, but not exclusively, on tumor endothelium. This suggests that the FGFR2 pathway may promote VEGF-independent endothelial survival, as previously observed in other preclinical models (57, 58), although we cannot rule out the possibility that it plays a role in other nonendothelial stromal cells. Circulating levels of bFGF were also elevated in the plasma of mice bearing BV-resistant tumors. This observation is notable in light of our recent observation that acquired resistance to chemotherapy and BV in colorectal cancer patients is associated with an increase in circulating bFGF (45), which suggests that similar mechanisms may be occurring in cancer patients.

The mechanisms underlying regulation of tumor stromal genes altered in resistant tumors remain to be established and are likely to differ in the various stromal cell types. Expression of many of the genes, including *CAIX*, *FGFR2* (59), and *EGFR* family members, is known to be regulated by hypoxia or to correlate with expression of HIF1α, as previously reviewed (60). One possible explanation is that BV therapy initially triggers a substantial decrease in tumor MVD and increases tumor hypoxia (61), inducing upregulation of hypoxia-dependent pathways. It is worth noting, however, that BV resistance was not associated with significant increases in many stromal genes known to be upregulated by hypoxia, and many of the genes upregulated in BV resistance are not known to be regulated by hypoxia. Hypoxia is therefore likely to be only one of many factors — both host and tumor cell dependent — likely to affect the resistant tumor and its microenvironment. These regulators of the stromal response merit further investigation.

Resistance to VEGF inhibition was also associated with different patterns of vascular remodeling in the models of acquired and primary resistance. In the H1975 model of acquired resistance, short-term treatment with BV during the sensitive phase initially induced a reduction in MVD; an increase in EC apoptosis, as observed in other studies (29, 30, 32, 62–65); and tumor shrinkage. This was followed by the development of resistance, marked by a pattern of normalized revascularization with increased MVD, reduced EC apoptosis, and a higher degree of pericyte coverage (Figure 5 and Supplemental Figure 1). These effects appeared to be VEGFR2 independent, as VEGFR2 phosphorylation remained inhibited in resistant tumors. Similar normalized revascularization was observed in the H441 orthotopic model (Figures 7 and 8). Prior studies have indicated that pericyte coverage may exert a protective effect on tumor endothelium (66, 67), potentially through the production of factors promoting endothelial survival and VEGF independence. Our findings were consistent with this hypothesis and revealed pericyte EGFR signaling to be a potential mediator of this effect.

In the A549 model of relative primary resistance, a distinct pattern of disorganized sprouting revascularization was observed in resistant tumors. This was marked by decreases in pericyte cover-

age with BV treatment and increased vessel tortuosity in resistant tumors. Unlike the acquired resistance models, stromal p-EGFR was upregulated in tumor endothelium, which suggests that the endothelium may be able to switch its dependence from VEGFR- to EGFR-driven endothelial proliferation and angiogenesis in the BV-resistant A549 xenografts, resulting in sprouting revascularization. It is worth noting that in an earlier study, we observed a similar switch (from EGFR- to VEGFR-dependent tumor endothelium) in a melanoma model (68), supporting the feasibility of this proposed mechanism. Endothelial EGFR signaling may explain, at least in part, the intrinsic relative resistance of these tumors to VEGF blockade, as well as our prior observation that A549 cells display EGFR TKI resistance in vitro, but show moderate sensitivity to EGFR inhibition when grown as xenografts (26). Other pathways that may contribute to this vascular phenotype are currently under investigation, including regulators of EC motility (e.g., HGF/c-MET) and vessel maturation (e.g., Ang-2/Tie-2). Nevertheless, this model provides evidence that there are distinct patterns of vascular remodeling that can accompany VEGF inhibitor resistance–associated tumor revascularization.

This study has a number of clinical implications for the use of VEGF inhibitors in NSCLC and other tumor types. First, it suggests that dual inhibition of the VEGFR and EGFR pathways may delay the emergence of therapeutic resistance in NSCLC. Consistent with this possibility, a recent phase III study (ATLAS) comparing the use of BV combined with erlotinib versus BV alone as maintenance therapy after chemotherapy demonstrated a significant, but modest, PFS improvement with an observed hazard ratio of 0.72 (P = 0.001; refs. 69, 70). Combined VEGFR/EGFR inhibition (via BV with erlotinib or vandetanib) has also demonstrated significantly improved PFS compared with EGFR inhibition alone (71–73). These studies showed a significant delay in tumor progression while treatment with VEGFR/EGFR inhibition was ongoing; however, significant improvements in overall survival were not observed. The explanation for this lack of durable clinical benefit is not known, but it is possible that once the dual inhibition is discontinued, these 2 pathways, or other alternative escape pathways, rapidly emerge.

The results of the present study may not be broadly generalizable to other tumor types or regimens containing chemotherapy. In a randomized phase III trial in colorectal cancer, the addition of the EGFR monoclonal antibodies panitumumab (74) or cetuxumab (75) to BV and chemotherapy showed trends toward worse clinical outcomes. Furthermore, in a recent study of colorectal cancer patients treated with BV plus chemotherapy, we observed increases in plasma bFGF, HGF, PDGF, and several myeloid factors prior to development of progressive disease (45); in contrast, in our model, bFGF was the sole factor that significantly increased. This suggests that resistance mechanisms may be disease or regimen specific.

Second, these findings raise the possibility that combinations of VEGF inhibitors with drugs targeting other potential stromal resistance pathways — such as FGFR2 — may improve treatment efficacy. Third, they suggest that the analysis of both tumor cell and stromal markers — not just tumor cell markers alone — may provide important clinical information. Fourth, they suggest that analysis of vascular patterns in VEGF inhibitor–resistant tumors may provide information regarding the underlying mechanisms of resistance.

In summary, our findings suggest that in NSCLC models, gene expression changes associated with VEGF inhibitor resistance occur predominantly in tumor stromal cells, not tumor cells, providing further evidence that tumor stroma may play an important — and potentially dominant — role in VEGF inhibitor resistance. Primary and acquired resistance may be associated with distinct patterns of vascularization, described here as normalized and sprouting patterns, and distinct patterns of stromal signaling. Finally, we identify what we believe to be a novel role for pericyte EGFR signaling in VEGF inhibitor resistance. It is worth noting, however, that although combinations of VEGF and EGFR pathway inhibition have shown promise in NSCLC, therapeutic resistance nevertheless continues to emerge, which indicates that additional resistance mechanisms remain to be uncovered.

Methods

Subcutaneous in vivo studies. All animal studies reported were approved by M.D. Anderson Cancer Center's animal care committee, which is fully accredited by the Association for Assessment and Accreditation of Laboratory Animal Care (AAALAC International). To generate tumor xenografts, A549 and H1975 tumor cells (2.0×10^6) in 100 μl HBSS were injected into the subcutaneous flanks of 4- to 8-week-old male athymic nude mice (NCI-nu). Body weights and tumor volumes were recorded twice weekly. Tumor volumes were calculated as $\pi/6 \times a^2 \times b$, where a is the smaller measurement of the tumor and b is the larger one, and expressed in cubic millimeters. When the tumor volumes reached an average of approximately 270 mm^3, mice were randomly assigned to one of the following treatment groups: (a) control i.p. injection of vehicle (PBS) twice weekly and oral (p.o.) administration of vehicle daily; (b) i.p. injection of BV (10 mg/kg) twice weekly; (c) erlotinib (100 mg/kg) p.o. daily; (d) erlotinib p.o. daily plus BV i.p. twice weekly; (e) vandetanib (50 mg/kg) p.o. daily (n = 6 [H1975] and 5 [A549] per group). Animals were sacrificed due to tumor burden. The log-rank test was performed to compare survival curves between different treatment groups using GraphPad Prism version 5.00 for Windows (GraphPad Software). For short-term treatment studies, H1975 (n = 5 per group) and A549 (n = 6 per group) tumor-bearing animals were treated for 2 weeks with vehicle and BV (10 mg/kg) and then sacrificed. The last tumor measurement was used to calculate $\Delta T/\Delta C$ (change in tumor volume relative to change in control, expressed as a percentage), as previously described (76). Tumor tissues from short- and long-term in vivo experiments were collected for IHC studies. Tumors were excised, a portion was fixed in formalin and embedded in paraffin, and another portion was embedded in OCT (Miles Inc.) and rapidly frozen in liquid nitrogen. Additional tumor sections for molecular studies were snap-frozen in liquid nitrogen. Staining with H&E was used to confirm the presence of tumor in each sample included in the analysis.

RNA microarray analysis. Total RNA was extracted from snap-frozen tissues using the *mir*Vana miRNA Isolation Kit (Ambion) according to the manufacturer's protocol. Biotin-labeled cRNA samples for hybridization were prepared using Illumina Total Prep RNA Amplification Kit (Ambion Inc.). Total RNA (1 μg) was used for the synthesis of cDNA, followed by amplification and biotin labeling. Each of 1.5 μg of biotinylated cRNAs was hybridized to both mouse WG-6v2 and human WG-6v3 Expression BeadChips (Illumina) at the same time for analysis of murine and human transcriptomes. Signals were developed by Amersham fluorolink streptavidin-Cy3 (GE Healthcare). Gene expression data were collected using an Illumina bead Array Reader confocal scanner (BeadStation 500GXDW; Illumina Inc.). Data were analyzed using the BRB-ArrayTools Version 3.7.0 Beta platform (http://linus.nci.nih.gov./BRB-ArrayTools.html). A log base-2 transformation was applied to the data set prior to data normalization. A median array was selected as the reference array for normalization, and statistical significance was set at $P < 0.01$. To evaluate the expression of genes involved in response to hypoxia, lymphangiogenesis, and angiogenesis in

BV-resistant xenografts versus controls, a list of 269 genes used in previous publications was compared (77). Genes differentially expressed between groups were determined applying univariate *t* test with estimation of the false discovery rate (FDR). Genes were determined using selection criteria of $P < 0.005$ and fold change of 1.5 or larger. Functional gene-interaction network analysis of genes differentially expressed between the mouse stroma of BV-resistant and vehicle-treated H1975 xenografts was performed using Ingenuity Pathways Analysis.

Accession numbers. Microarray data have been deposited into NCBI GEO (accession no. GSE26644).

IF. Frozen tissue sections were used to evaluate CD31, p-VEGFR2, EGFR, and desmin expression. Specimens were sectioned (8–10 μM thickness), mounted onto positively charged slides, and air-dried for 30 minutes. Tissue fixation was performed using 3 sequential immersions in ice-cold acetone, acetone-chloroform 50:50 (v/v), and acetone (5 minutes each). Slides were incubated in protein block solution containing 4% fish gelatin for 20 minutes at room temperature and then incubated overnight at 4°C with a 1:500 dilution of rat anti-mouse CD31. Sections were rinsed with PBS and then incubated for 1 hour with a goat anti-rat Alexa Fluor 594 antibody (diluted 1:1,200). Samples were rinsed with PBS, incubated for 20 minutes with protein block, and then incubated with primary antibody against p-VEGFR2 (diluted 1:400), or EGFR (diluted 1:100) or desmin (diluted 1:400) at 4°C overnight. Samples were rinsed 3 times with PBS and then incubated for 1 hour with goat anti-rabbit Alexa Fluor 488 antibody (diluted 1:1,200). After rinsing, sections were incubated with Hoechst stain (diluted 1:10,000 in PBS; Polysciences Inc.) for 2 minutes to visualize cell nuclei. Slides were mounted with a glycerol/PBS solution containing 0.1 mol/l propyl gallate (Sigma-Aldrich) to minimize fluorescent bleaching. IF microscopy was performed using a Zeiss Axioplan fluorescence microscope (Carl Zeiss Inc.) equipped with a 100-W Hg lamp and narrow bandpass excitation filters. Representative images were obtained using a cooled charge-coupled device Hamamatsu C5810 camera (Hamamatsu Photonics) and Optimas software (Media Cybernetics).

Confocal microscopy. Confocal microscopy was used in protein localization studies of CD31 and p-EGFR and of CD31 and total FGFR2 in subcutaneous murine models, and of CD31 and desmin, CD31 and p-EGFR, and F4/80 and α-SMA staining in orthotopic tumors, as previously described (78). Frozen tissues for confocal microscopy were sectioned (8–12 μm) and mounted on positively charged slides. IF staining for p-EGFR or total FGFR2 and CD31 was carried out as described above, with the exception that the Alexa Fluor 594 fluorophore used for CD31 detection was replaced with a Cy5 antibody, and the Alexa Fluor 488 fluorophore used to visualize p-EGFR or FGFR2 or desmin was replaced with a Cy3 antibody. Sytox green (diluted 1:10,000 in PBS) was used to visualize cell nuclei. Confocal fluorescence images were collected using a Zeiss LSM 510 laser scanning microscope (Carl Zeiss Inc.) equipped with an argon laser (458/477/488/514 nm, 30 mW), HeNe laser (413 nm, 1 mW and 633 nm, 5 mW), LSM 510 control and image acquisition software, and appropriate filters (Chroma Technology Corp.).

Determination of MVD, vessel tortuosity, and pericyte coverage. Tumor MVD was determined as previously described (79). In brief, we examined tumors microscopically to identify hot spots by low magnification (×100), and the mean MVD was quantified as the total number of $CD31^+$ structures observed in at least 5 higher-magnification microscopic fields per tumor (×200). For each group, tumors from 4 mice receiving short- and long-term treatment were used. As previously described (80), the tortuosity of blood vessel was calculated as $(L/S) - 1$, where L is the length of the vessel of interest and S is the straight-line distance between its endpoints. Vessel length was evaluated in 4 samples per treatment group by tracing along the midline of the blood vessels that showed up in a longitudinal cut within an image (×100), and the number of pixels was converted into distance in millimeters with NIH ImageJ (version 1.34; http://rsb.info.nih.gov/ij/). To determine the extent of pericyte coverage on the tumor vasculature, tumor sections were stained for CD31 (red) and desmin (green) as described above. 5 fields per tumor were randomly identified at original magnification ×200, and those blood vessels at least 50% covered by green desmin-positive cells were considered to be positive for pericyte coverage.

Plasma bFGF concentration analysis. bFGF levels were measured in the plasma of tumor-bearing animals by multiplex bead assay (BioRad and Millipore) in a 96-well plate according to the manufacturer's protocol. Concentrations were calculated based on a standard curve derived by performing 6 serial dilutions of a protein standard in assay diluent. Plasma samples were tested in duplicate, and the mean value was used for analysis.

Orthotopic lung adenocarcinoma model. Male 8-week-old athymic Ncr (*nu/nu*) mice were maintained in a specific pathogen–free mouse colony in accordance with regulations and standards of the Department of Agriculture and the Department of Health and Human Services. Mice were anesthetized with a combination of ketamine HCl (86 mg/kg) and xylazine (17 mg/kg) in normal saline; 100 μl solution per 10 g body weight was injected i.p. Mice were then placed in the right lateral decubitus position. The skin overlying the left chest wall in the midaxillary line was prepped with alcohol and incised (~7 mm), and the underlying chest wall was visualized. Logarithmically growing H441 cells (1×10^6 cells in single-cell suspensions of greater than 95% viability as determined by Trypan blue exclusion) in 50 μl HBSS containing 50 μg growth factor–reduced Matrigel (BD Bioscience) were injected into the left thorax at the lateral dorsal axillary line and into the left lung. After tumor cell inoculation, the skin incision was clipped, and the mice were turned to the left lateral decubitus position and observed until fully recovered. No anesthesia or surgery-related deaths occurred. 3 weeks after H441 tumor cell injection, 8 mice were euthanized for evaluation of baseline tumor volume ($n = 8$). Animals were sacrificed when moribund. Orthotopic tumors were photographed, and tissues were collected for IHC studies.

Alpha Innotech IF quantification. Alpha Innotech software (version 3.000) was used to quantify the IF signal in 5–10 random microscopic fields, depending on the tumor size, captured from at least 4 tumor specimens per group analyzed. Each microphotograph was collected using the same original magnification to obtain equal-sized images. 2 equally sized circles (area, 25,000 pixels) were randomly distributed on each microphotograph, and blue, red, and green pixel sums, averages, and background-corrected averages were obtained. The background-corrected fluorescent area of interest (green for p-EGFR, red for F4/80 and α-SMA) was normalized relative to the blue (nuclei) area for each analyzed microphotograph, and the mean ratio from all the images of each tumor specimen was calculated per treatment group.

Reagents, tumor cell lines, conditions, qRT-PCR, IHC, and LSC. See Supplemental Methods.

Statistics. Unless otherwise indicated, data are mean ± SEM. Distribution of PFS was estimated by the Kaplan-Meier method. Log-rank (Mantel-Cox) test was performed to test the difference in survival between groups. For comparison of continuous variables between 2 groups, 2-tailed Student's *t* test and Mann-Whitney-Wilcoxon test were used. A *P* value less than 0.05 was considered significant.

Acknowledgments

This study was supported in part by the Department of Defense BATTLE W81XWH-06-1-0303, Department of Defense PROSPECT award W81XWH-07-1-03060, University of Texas Southwestern Medical Center, University of Texas M.D. Anderson Cancer Center Lung SPORE NIH grant P50 CA070907 and NCI grant

P30CA016672, and research support from AstraZeneca. J.V. Heymach is a Damon Runyon-Lilly Clinical Investigator supported in part by Damon Runyon Cancer Research Foundation grant CI 24-04 and is also supported by the Physician Scientist Program at M.D. Anderson Cancer Center. We gratefully acknowledge Donna Reynolds (University of Texas M.D. Anderson Cancer Center) for providing us with cut tissue sections and helping with IHC protocols; Michael Worley (University of Texas M.D. Anderson Cancer Center) for editing the manuscript; Anderson Ryan, Juliane Jürgensmeier, and Lee Ellis for helpful scientific discussions; and AstraZeneca for providing vandetanib. Research in the laboratory of F. Ciardiello is supported by a grant from the Associazione Italiana per la Ricerca sul Cancro (AIRC).

Received for publication January 21, 2010, and accepted in revised form January 26, 2011.

Address correspondence to: John V. Heymach, Departments of Thoracic/Head and Neck Medical Oncology and Cancer Biology, University of Texas M.D. Anderson Cancer Center, Unit 432, 1515 Holcombe Blvd., Houston, Texas 77030, USA. Phone: 713.792.6363; Fax: 713.792.1220; E-mail: jheymach@mdanderson.org.

1. Folkman J, Shing Y. Angiogenesis. *J Biol Chem*. 1992;267(16):10931–10934.
2. Folkman J. Tumor angiogenesis: therapeutic implications. *N Engl J Med*. 1971;285(21):1182–1186.
3. Carmeliet P, Jain RK. Angiogenesis in cancer and other diseases. *Nature*. 2000;407(6801):249–257.
4. Ferrara N, Gerber HP, LeCouter J. The biology of VEGF and its receptors. *Nat Med*. 2003;9(6):669–676.
5. Ferrara N, Davis-Smyth T. The biology of vascular endothelial growth factor. *Endocr Rev*. 1997; 18(1):4–25.
6. Ellis LM, Hicklin DJ. VEGF-targeted therapy: mechanisms of anti-tumour activity. *Nat Rev Cancer*. 2008;8(8):579–591.
7. Kerbel RS. Tumor angiogenesis. *N Engl J Med*. 2008;358(19):2039–2049.
8. Jain RK, di Tomaso E, Duda DG, Loeffler JS, Sorensen AG, Batchelor TT. Angiogenesis in brain tumours. *Nat Rev Neurosci*. 2007;8(8):610–622.
9. Ferrara N, Hillan KJ, Gerber HP, Novotny W. Discovery and development of bevacizumab, an anti-VEGF antibody for treating cancer. *Nat Rev Drug Discov*. 2004;3(5):391–400.
10. Dvorak HF. Vascular permeability factor/vascular endothelial growth factor: a critical cytokine in tumor angiogenesis and a potential target for diagnosis and therapy. *J Clin Oncol*. 2002;20(21):4368–4380.
11. Chung AS, Lee J, Ferrara N. Targeting the tumour vasculature: insights from physiological angiogenesis. *Nat Rev Cancer*. 2010;10(7):505–514.
12. Sandler A, et al. Paclitaxel-carboplatin alone or with bevacizumab for non-small-cell lung cancer. *N Engl J Med*. 2006;355(24):2542–2550.
13. Hurwitz H, et al. Bevacizumab plus irinotecan, fluorouracil, and leucovorin for metastatic colorectal cancer. *N Engl J Med*. 2004;350(23):2335–2342.
14. Crawford Y, Ferrara N. Tumor and stromal pathways mediating refractoriness/resistance to anti-angiogenic therapies. *Trends Pharmacol Sci*. 2009;30(12):624–630.
15. Ebos JM, Lee CR, Kerbel RS. Tumor and host-mediated pathways of resistance and disease progression in response to antiangiogenic therapy. *Clin Cancer Res*. 2009;15(16):5020–5025.
16. Bergers G, Hanahan D. Modes of resistance to anti-angiogenic therapy. *Nat Rev Cancer*. 2008; 8(8):592–603.
17. Casanovas O, Hicklin DJ, Bergers G, Hanahan D. Drug resistance by evasion of antiangiogenic targeting of VEGF signaling in late-stage pancreatic islet tumors. *Cancer Cell*. 2005;8(4):299–309.
18. Graeber TG, et al. Hypoxia-mediated selection of cells with diminished apoptotic potential in solid tumours. *Nature*. 1996;379(6560):88–91.
19. Yu JL, Rak JW, Coomber BL, Hicklin DJ, Kerbel RS. Effect of p53 status on tumor response to antiangiogenic therapy. *Science*. 2002;295(5559):1526–1528.
20. Leenders WP, et al. Antiangiogenic therapy of cerebral melanoma metastases results in sustained tumor progression via vessel co-option. *Clin Cancer Res*. 2004;10(18 pt 1):6222–6230.
21. Davis DW, et al. Pharmacodynamic analysis of target inhibition and endothelial cell death in tumors treated with the vascular endothelial growth factor receptor antagonists SU5416 or SU6668. *Clin Cancer Res*. 2005;11(2 pt 1):678–689.
22. Heymach JV, et al. Phase II study of the antiangiogenic agent SU5416 in patients with advanced soft tissue sarcomas. *Clin Cancer Res*. 2004; 10(17):5732–5740.
23. Shojaei F, et al. Tumor refractoriness to anti-VEGF treatment is mediated by CD11b+Gr1+ myeloid cells. *Nat Biotechnol*. 2007;25(8):911–920.
24. Ferrara N. Role of myeloid cells in vascular endothelial growth factor-independent tumor angiogenesis. *Curr Opin Hematol*. 2010;17(3):219–224.
25. Crawford Y, et al. PDGF-C mediates the angiogenic and tumorigenic properties of fibroblasts associated with tumors refractory to anti-VEGF treatment. *Cancer Cell*. 2009;15(1):21–34.
26. Naumov GN, et al. Combined vascular endothelial growth factor receptor and epidermal growth factor receptor (EGFR) blockade inhibits tumor growth in xenograft models of EGFR inhibitor resistance. *Clin Cancer Res*. 2009;15(10):3484–3494.
27. Kobayashi S, et al. EGFR mutation and resistance of non-small-cell lung cancer to gefitinib. *N Engl J Med*. 2005;352(8):786–792.
28. Pao W, et al. KRAS mutations and primary resistance of lung adenocarcinomas to gefitinib or erlotinib. *PLoS Med*. 2005;2(1):e17.
29. Jain RK. Normalization of tumor vasculature: an emerging concept in antiangiogenic therapy. *Science*. 2005;307(5706):58–62.
30. Batchelor TT, et al. AZD2171, a pan-VEGF receptor tyrosine kinase inhibitor, normalizes tumor vasculature and alleviates edema in glioblastoma patients. *Cancer Cell*. 2007;11(1):83–95.
31. Greenberg JI, Cheresh DA. VEGF as an inhibitor of tumor vessel maturation: implications for cancer therapy. *Expert Opin Biol Ther*. 2009;9(11):1347–1356.
32. Jain RK. Normalizing tumor vasculature with anti-angiogenic therapy: A new paradigm for combination therapy. *Nat Med*. 2001;7(9):987–989.
33. Mukohara T, et al. Differential effects of gefitinib and cetuximab on non-small-cell lung cancers bearing epidermal growth factor receptor mutations. *J Natl Cancer Inst*. 2005;97(16):1185–1194.
34. Jacoby JJ, et al. Treatment with HIF-1alpha antagonist PX-478 inhibits progression and spread of orthotopic human small cell lung cancer and lung adenocarcinoma in mice. *J Thorac Oncol*. 2010;5(7):940–949.
35. Shojaei F, et al. G-CSF-initiated myeloid cell mobilization and angiogenesis mediate tumor refractoriness to anti-VEGF therapy in mouse models. *Proc Natl Acad Sci U S A*. 2009;106(16):6742–6747.
36. Shojaei F, Zhong C, Wu X, Yu L, Ferrara N. Role of myeloid cells in tumor angiogenesis and growth. *Trends Cell Biol*. 2008;18(8):372–378.
37. Boehm T, Folkman J, Browder T, O'Reilly MS. Antiangiogenic therapy of experimental cancer does not induce acquired drug resistance. *Nature*. 1997;390(6658):404–407.
38. Kerbel RS. Inhibition of tumor angiogenesis as a strategy to circumvent acquired resistance to anti-cancer therapeutic agents. *Bioessays*. 1991;13(1):31–36.
39. Heymach JV, et al. Randomized phase II study of vandetanib alone or with paclitaxel and carboplatin as first-line treatment for advanced non-small-cell lung cancer. *J Clin Oncol*. 2008;26(33):5407–5415.
40. Broxterman HJ, Lankelma J, Hoekman K. Resistance to cytotoxic and anti-angiogenic anticancer agents: similarities and differences. *Drug Resist Updat*. 2003;6(3):111–127.
41. Kerbel RS, et al. Possible mechanisms of acquired resistance to anti-angiogenic drugs: implications for the use of combination therapy approaches. *Cancer Metastasis Rev*. 2001;20(1–2):79–86.
42. Ellis LM, Hicklin DJ. Pathways mediating resistance to vascular endothelial growth factor-targeted therapy. *Clin Cancer Res*. 2008;14(20):6371–6375.
43. Heymach JV, Sledge GW, Jain RK. Tumor angiogenesis. In: Hong WK, et al., eds. *Holland–Frei Cancer Medicine 8*. Shelton, Connecticut, USA: People's Medical Publishing House–USA; 2010:149–169.
44. Ferrara N. Pathways mediating VEGF-independent tumor angiogenesis. *Cytokine Growth Factor Rev*. 2010;21(1):21–26.
45. Kopetz S, et al. Phase II trial of infusional fluorouracil, irinotecan, and bevacizumab for metastatic colorectal cancer: efficacy and circulating angiogenic biomarkers associated with therapeutic resistance. *J Clin Oncol*. 2010;28(3):453–459.
46. Iivanainen E, et al. The EGFR inhibitor gefitinib suppresses recruitment of pericytes and bone marrow-derived perivascular cells into tumor vessels. *Microvasc Res*. 2009;78(3):278–285.
47. Nolan-Stevaux O, et al. Differential contribution to neuroendocrine tumorigenesis of parallel Egfr signaling in cancer cells and pericytes. *Genes and Cancer*. 2010;1(2):125–141.
48. di Tomaso E, et al. PDGF-C induces maturation of blood vessels in a model of glioblastoma and attenuates the response to anti-VEGF treatment. *PLoS One*. 2009;4(4):e5123.
49. Greenberg JI, et al. A role for VEGF as a negative regulator of pericyte function and vessel maturation. *Nature*. 2008;456(7223):809–813.
50. Pietras K, Pahler J, Bergers G, Hanahan D. Functions of paracrine PDGF signaling in the proangiogenic tumor stroma revealed by pharmacological targeting. *PLoS Med*. 2008;5(1):e19.
51. Ostman A, Heldin CH. PDGF receptors as targets in tumor treatment. *Adv Cancer Res*. 2007;97:247–274.
52. Amin DN, Hida K, Bielenberg DR, Klagsbrun M. Tumor endothelial cells express epidermal growth factor receptor (EGFR) but not ErbB3 and are responsive to EGF and to EGFR kinase inhibitors. *Cancer Res*. 2006;66(4):2173–2180.
53. Cheng H, et al. Construction of a novel constitutively active chimeric EGFR to identify new targets for therapy. *Neoplasia*. 2005;7(12):1065–1072.
54. Wu W, et al. Expression of epidermal growth factor (EGF)/transforming growth factor-alpha by human lung cancer cells determines their response to EGF receptor tyrosine kinase inhibition in the lungs of mice. *Mol Cancer Ther*. 2007;6(10):2652–2663.
55. Kuwai T, et al. Phosphorylated epidermal growth factor receptor on tumor-associated endothelial cells is a primary target for therapy with tyrosine

kinase inhibitors. *Neoplasia*. 2008;10(5):489–500.
56. Kandel J, Bossy-Wetzel E, Radvanyi F, Klagsbrun M, Folkman J, Hanahan D. Neovascularization is associated with a switch to the export of bFGF in the multistep development of fibrosarcoma. *Cell*. 1991;66(6):1095–1104.
57. Paris F, et al. Endothelial apoptosis as the primary lesion initiating intestinal radiation damage in mice. *Science*. 2001;293(5528):293–297.
58. Karsan A, Yee E, Poirier GG, Zhou P, Craig R, Harlan JM. Fibroblast growth factor-2 inhibits endothelial cell apoptosis by Bcl-2-dependent and independent mechanisms. *Am J Pathol*. 1997;151(6):1775–1784.
59. Giatromanolaki A, et al. Relation of hypoxia inducible factor 1 alpha and 2 alpha in operable non-small cell lung cancer to angiogenic/molecular profile of tumours and survival. *Br J Cancer*. 2001; 85(6):881–890.
60. Semenza GL. Targeting HIF-1 for cancer therapy. *Nat Rev Cancer*. 2003;3(10):721–732.
61. Franco M, et al. Targeted anti-vascular endothelial growth factor receptor-2 therapy leads to short-term and long-term impairment of vascular function and increase in tumor hypoxia. *Cancer Res*. 2006; 66(7):3639–3648.
62. Roland CL, et al. Inhibition of vascular endothelial growth factor reduces angiogenesis and modulates immune cell infiltration of orthotopic breast cancer xenografts. *Mol Cancer Ther*. 2009;8(7):1761–1771.
63. Kim KJ, et al. Inhibition of vascular endothelial growth factor-induced angiogenesis suppresses tumour growth in vivo. *Nature*. 1993;362(6423):841–844.
64. Willett CG, et al. Direct evidence that the VEGF-specific antibody bevacizumab has antivascular effects in human rectal cancer. *Nat Med*. 2004;10(2):145–147.
65. Tong RT, Boucher Y, Kozin SV, Winkler F, Hicklin DJ, Jain RK. Vascular normalization by vascular endothelial growth factor receptor 2 blockade induces a pressure gradient across the vasculature and improves drug penetration in tumors. *Cancer Res*. 2004;64(11):3731–3736.
66. Lu C, et al. Impact of vessel maturation on anti-angiogenic therapy in ovarian cancer. *Am J Obstet Gynecol*. 2008;198(4):477.e1–477.e9.
67. Bergers G, Song S, Meyer-Morse N, Bergsland E, Hanahan D. Benefits of targeting both pericytes and endothelial cells in the tumor vasculature with kinase inhibitors. *J Clin Invest*. 2003;111(9):1287–1295.
68. Amin DN, Bielenberg DR, Lifshits E, Heymach JV, Klagsbrun M. Targeting EGFR activity in blood vessels is sufficient to inhibit tumor growth and is accompanied by an increase in VEGFR-2 dependence in tumor endothelial cells. *Microvasc Res*. 2008; 76(1):15–22.
69. Miller VA, O'Connor P, Soh C, Kabbinavar F. A randomized, double-blind, placebo-controlled, phase IIIb trial (ATLAS) comparing bevacizumab (B) therapy with or without erlotinib (E) after completion of chemotherapy with B for first-line treatment of locally advanced recurrent, or metastatic non-small cell lung cancer (NSCLC). *J Clin Oncol*. 2009;27(suppl):S18.
70. Kabbinavar FF, et al. Overall survival (OS) in ATLAS, a phase IIIb trial comparing bevacizumab (B) therapy with or without erlotinib (E) after completion of chemotherapy (chemo) with B for first-line treatment of locally advanced, recurrent, or metastatic non-small cell lung cancer (NSCLC). *J Clin Oncol*. 2010;28(suppl):Abstract 7526.
71. Natale RB, et al. Vandetanib versus gefitinib in patients with advanced non-small-cell lung cancer: results from a two-part, double-blind, randomized phase II study. *J Clin Oncol*. 2009;27(15):2523–2529.
72. Herbst RS, et al. Phase II study of efficacy and safety of bevacizumab in combination with chemotherapy or erlotinib compared with chemotherapy alone for treatment of recurrent or refractory non small-cell lung cancer. *J Clin Oncol*. 2007;25(30):4743–4750.
73. Hainsworth J, Herbst R. A phase III, multicenter, placebo-controlled, double-blind, randomized clinical trial to evaluate the efficacy of bevacizumab (Avastin) in combination with erlotinib (Tarceva) compared with erlotinib alone for treatment of advanced non-small cell lung cancer after failure of standard first-line chemotherapy (BETA). *J Thor Oncol*. 2008;3:S302.
74. Hecht JR, et al. A randomized phase IIIB trial of chemotherapy, bevacizumab, and panitumumab compared with chemotherapy and bevacizumab alone for metastatic colorectal cancer. *J Clin Oncol*. 2009;27(5):672–680.
75. Punt CJ, et al. Randomized phase III study of capecitabine, oxaliplatin, and bevacizumab with or without cetuximab in advanced colorectal cancer (ACC), the CAIRO2 study of the Dutch Colorectal Cancer Group (DCCG). *J Clin Oncol*. 2008; 26(suppl):180s.
76. Bao R, et al. Targeting heat shock protein 90 with CUDC-305 overcomes erlotinib resistance in non-small cell lung cancer. *Mol Cancer Ther*. 2009; 8(12):3296–3306.
77. Van den Eynden GG, et al. Differential expression of hypoxia and (lymph)angiogenesis-related genes at different metastatic sites in breast cancer. *Clin Exp Metastasis*. 2007;24(1):13–23.
78. Kuwai T, et al. Intratumoral heterogeneity for expression of tyrosine kinase growth factor receptors in human colon cancer surgical specimens and orthotopic tumors. *Am J Pathol*. 2008;172(2):358–366.
79. Weidner N, Semple JP, Welch WR, Folkman J. Tumor angiogenesis and metastasis--correlation in invasive breast carcinoma. *N Engl J Med*. 1991;324(1):1–8.
80. Stockmann C, et al. Deletion of vascular endothelial growth factor in myeloid cells accelerates tumorigenesis. *Nature*. 2008;456(7223):814–818.

Cancer Discovery Publish Ahead of Print, published on April 3, 2011 as doi:10.1158/2159-8274.CD-10-0010

RESEARCH ARTICLE

The BATTLE Trial: Personalizing Therapy for Lung Cancer

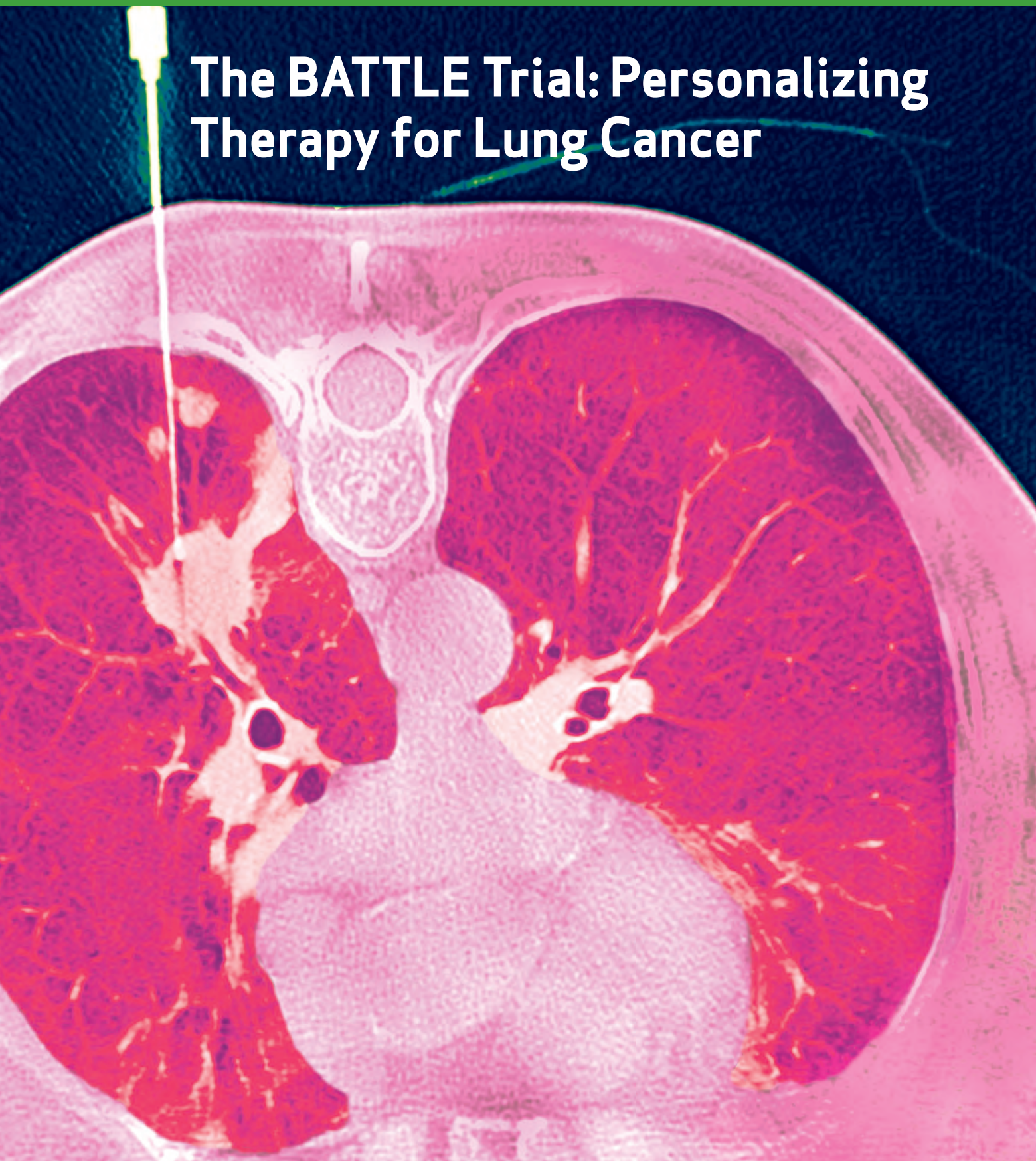

Edward S. Kim[1,], Roy S. Herbst[1,*], Ignacio I. Wistuba[1,2,*], J. Jack Lee[3,*], George R. Blumenschein Jr[1], Anne Tsao[1], David J. Stewart[1], Marshall E. Hicks[4], Jeremy Erasmus Jr[4], Sanjay Gupta[4], Christine M. Alden[1], Suyu Liu[3], Ximing Tang[1], Fadlo R. Khuri[5], Hai T. Tran[1], Bruce E. Johnson[6], John V. Heymach[1], Li Mao[7], Frank Fossella[1], Merrill S. Kies[1], Vassiliki Papadimitrakopoulou[1], Suzanne E. Davis[1], Scott M. Lippman[1,†], and Waun K. Hong[1,†]*

ABSTRACT

The Biomarker-integrated Approaches of Targeted Therapy for Lung Cancer Elimination (BATTLE) trial represents the first completed prospective, biopsy-mandated, biomarker-based, adaptively randomized study in 255 pretreated lung cancer patients. Following an initial equal randomization period, chemorefractory non–small cell lung cancer (NSCLC) patients were adaptively randomized to erlotinib, vandetanib, erlotinib plus bexarotene, or sorafenib, based on relevant molecular biomarkers analyzed in fresh core needle biopsy specimens. Overall results include a 46% 8-week disease control rate (primary end point), confirm prespecified hypotheses, and show an impressive benefit from sorafenib among mutant-*KRAS* patients. BATTLE establishes the feasibility of a new paradigm for a personalized approach to lung cancer clinical trials. *(ClinicalTrials.gov numbers: NCT00409968, NCT00411671, NCT00411632, NCT00410059, and NCT00410189.)*

SIGNIFICANCE: The BATTLE study is the first completed prospective, adaptively randomized study in heavily pretreated NSCLC patients that mandated tumor profiling with "real-time" biopsies, taking a substantial step toward realizing personalized lung cancer therapy by integrating real-time molecular laboratory findings in delineating specific patient populations for individualized treatment. *Cancer Discovery; 1(1). ©2011 AACR.*

INTRODUCTION

The leading cause of cancer-related mortality, lung cancer accounts for more U.S. deaths each year than do breast, colon, prostate, liver, and kidney cancers and melanoma combined (1). Systemic chemotherapy is the mainstay for metastatic lung cancer. Although approved therapies in this setting include a few biologic agents, subjective physician preference based on clinical characteristics such as age, gender, or performance status largely drives treatment decisions (2–4).

Tumor biomarker evaluations have recently emerged as an important factor in planning treatment for non–small cell lung cancer (NSCLC) after improved outcomes with the epidermal growth factor receptor (EGFR) tyrosine kinase inhibitors (TKI) erlotinib and gefitinib in patients with NSCLC harboring *EGFR* mutations (5–8). Notwithstanding this success, biologic agents have not been effective in many randomized trials in NSCLC. There is a paucity of effective predictive markers of drug sensitivity or resistance, due in large part to difficulties in prospectively obtaining baseline tumor tissue in patients with metastatic NSCLC. In patients with pretreated NSCLC, tumor biomarker evaluation is frequently based on the tissue obtained at diagnosis and may not reflect the current state of biomarkers after treatment with chemotherapy.

In the novel phase II Biomarker-integrated Approaches of Targeted Therapy for Lung Cancer Elimination (BATTLE) program of personalized medicine (ClinicalTrials.gov numbers: NCT00409968, NCT00411671, NCT00411632, NCT00410059, and NCT00410189) reported in this article, we prospectively biopsied tumors and, based on tumor markers, used adaptive randomization to assign NSCLC patients to the treatment with greatest potential benefit based on cumulative data (Fig. 1). The signaling pathways and targeted

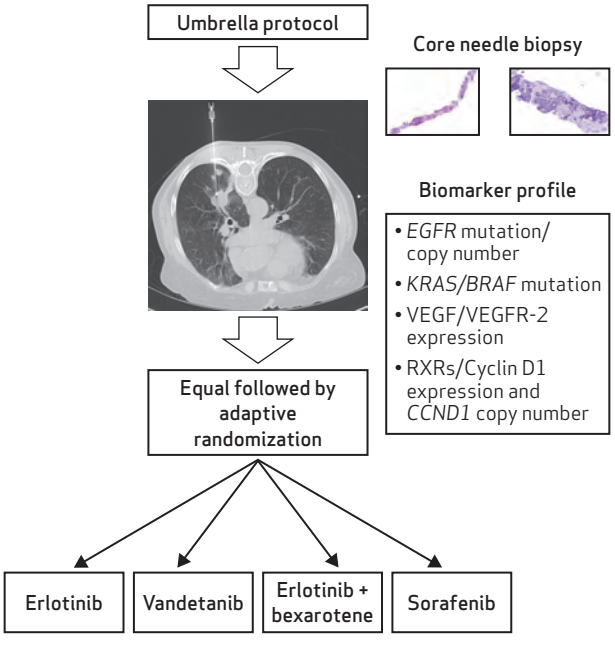

Figure 1. Schema for BATTLE study.

Authors' Affiliations: [1]Departments of Thoracic/Head and Neck Medical Oncology, [2]Pathology, [3]Biostatistics, and [4]Diagnostic Radiology, The University of Texas MD Anderson Cancer Center, Houston, Texas; [5]Winship Cancer Center, Emory University, Atlanta, Georgia; [6]Dana-Farber Cancer Institute, Boston, Massachusetts; and [7]University of Maryland, Baltimore, Maryland.

*These authors contributed equally to this article.

†These authors are co-senior authors of this article.

Note: Supplementary data for this article are available at Cancer Discovery Online (http://www.aacrjournals.org).

Corresponding Author: Waun K. Hong, The University of Texas MD Anderson Cancer Center, 1515 Holcombe Blvd., Houston, TX 77030. Phone: 713-794-1441; Fax: 1-713-792-4654; E-mail: whong@mdanderson.org

doi: 10.1158/2159-8274.CD-10-0010

agents were selected on the basis of the highest scientific and clinical interest at the time (2005) and included EGFR (erlotinib), KRAS/BRAF (sorafenib), retinoid–EGFR signaling (bexarotene and erlotinib), and vascular endothelial growth factor receptor [VEGFR; vandetanib (refs. 9–12)]. All of these compounds were being tested in the phase II or III setting and thus were appropriate for treatment of patients with advanced NSCLC. Testing the feasibility of performing core biopsy procedures in pretreated patients with advanced disease and utilizing real-time biomarker analyses for treatment were major challenges in BATTLE and, if successful, were proposed as major steps toward personalizing therapy for patients with NSCLC.

RESULTS

Patient Characteristics

A total of 341 patients were enrolled in the BATTLE study between November 30, 2006, and October 28, 2009, with equally random assignments for the first 97 patients and adaptive randomization for the remaining 158. The numbers of randomized patients per treatment arm were 59 (erlotinib), 54 (vandetanib), 37 (erlotinib plus bexarotene), and 105 (sorafenib). Seventeen patients were randomly assigned twice, and 1 patient 3 times. Eighty-six patients could not be randomly assigned because of intercurrent illnesses (n = 29) or worsening overall condition (n = 22), conditions preventing a biopsy (n = 17), or choice of an alternative treatment (n = 18; Fig. 2).

Notable patient characteristics included 83 patients (33%) with prior brain metastases, 116 (45%) with prior treatment with an EGFR TKI, and a median of 2 prior chemotherapies (Table 1). Our patient population was reflective of a heavily pretreated NSCLC population, with 44% (102 patients) having progression as their best response to prior therapy. Supplementary Table S1 lists the distribution of individual biomarkers. The prevalence of mutations in our study population included 15% *EGFR* and 20% *KRAS*. Forty-two patients had inadequate tissue for biomarker analysis, and 2 patients were negative for all study biomarkers.

Efficacy

The overall 8-week disease control rate (DCR) in 244 patients eligible for this analysis was 46% (Table 2); median progression-free survival (PFS) was 1.9 months [95% confidence interval (CI), 1.8–2.4]; median overall survival (OS) was 8.8 months (95% CI, 6.3–10.6); and 1-year survival was 35% (Supplementary Fig. S1). The median patient follow-up was 10.3 months. There were no complete responses and only

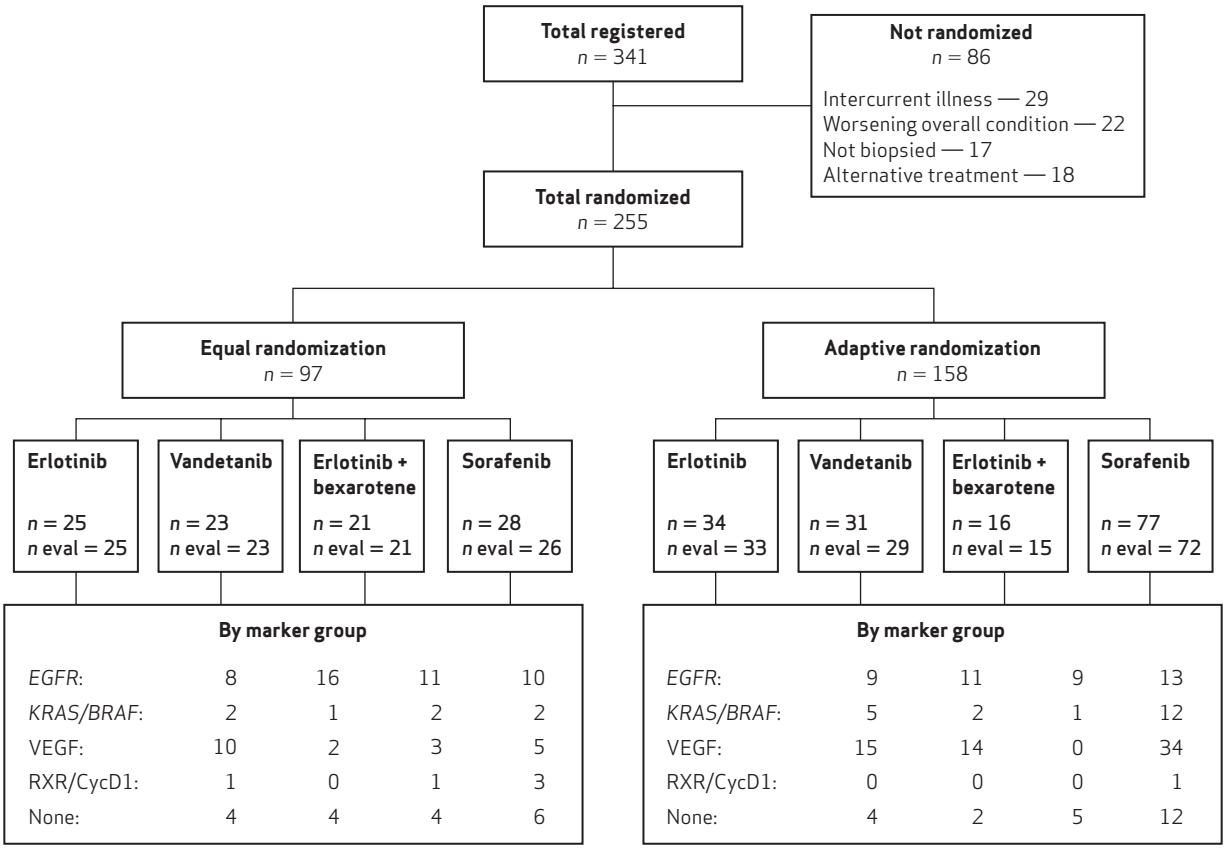

Figure 2. CONSORT diagram of the BATTLE study.

Table 1. Patient characteristics by treatment

		All	Erlotinib ($n = 59$)	Vandetanib ($n = 54$)	Erlotinib + bexarotene ($n = 37$)	Sorafenib ($n = 105$)
		n (%)	*n* (%)	*n* (%)	*n* (%)	*n* (%)
Age	≤50	41 (16%)	5 (8%)	11 (20%)	6 (16%)	19 (18%)
(mean, 62; range, 26–84)	51–60	73 (29%)	23 (39%)	15 (28%)	11 (30%)	24 (23%)
	61–70	86 (34%)	19 (32%)	19 (35%)	11 (30%)	37 (35%)
	>70	55 (22%)	12 (20%)	9 (17%)	9 (24%)	25 (24%)
Gender	Female	118 (46%)	26 (44%)	29 (54%)	12 (32%)	51 (49%)
	Male	137 (54%)	33 (56%)	25 (46%)	25 (68%)	54 (51%)
Ethnicity	Caucasian	209 (82%)	51 (86%)	41 (76%)	31 (84%)	86 (82%)
	Hispanic	16 (6%)	2 (3%)	7 (13%)	0 (0%)	7 (7%)
	African American	16 (6%)	3 (5%)	2 (4%)	4 (11%)	7 (7%)
	Asian	14 (5%)	3 (5%)	4 (7%)	2 (5%)	5 (5%)
Smoker	Current	23 (9%)	9 (15%)	5 (9%)	3 (8%)	6 (6%)
	Former	177 (69%)	41 (69%)	31 (57%)	32 (86%)	73 (70%)
	Never	55 (22%)	9 (15%)	18 (33%)	2 (5%)	26 (25%)
Histology	Adenocarcinoma	160 (63%)	31 (53%)	35 (65%)	23 (62%)	71 (68%)
	Squamous	46 (18%)	16 (27%)	7 (13%)	6 (16%)	20 (19%)
	Others	49 (19%)	12 (20%)	12 (22%)	8 (22%)	14 (13%)
Prior erlotinib therapy	No	139 (55%)	59 (100%)	9 (17%)	37 (100%)	34 (32%)
	Yes	116 (45%)	0 (0%)	45 (83%)	0 (0%)	71 (68%)
ECOG performance status	0	22 (9%)	5 (8%)	9 (17%)	2 (5%)	6 (6%)
	1	197 (77%)	44 (75%)	36 (67%)	30 (81%)	87 (83%)
	2	36 (14%)	10 (17%)	9 (17%)	5 (14%)	12 (11%)
Prior cytotoxic chemotherapy	1	95 (37%)	25 (42%)	21 (39%)	18 (49%)	31 (30%)
(median, 2; range, 1–6)	2	84 (33%)	20 (34%)	17 (31%)	12 (32%)	35 (33%)
	3	40 (16%)	9 (15%)	7 (13%)	4 (11%)	20 (19%)
	4	24 (9%)	4 (7%)	6 (11%)	2 (5%)	12 (11%)
	5	9 (4%)	1 (2%)	2 (4%)	1 (3%)	5 (5%)
	6	3 (1%)	0 (0%)	1 (2%)	0 (0%)	2 (2%)

Table 2. Eight-week disease control status by treatment and marker groups

Number of patients with disease control / total number of patients (%)

Marker group	Treatment				Total
	Erlotinib	Vandetanib	Erlotinib + bexarotene	Sorafenib	
EGFR	6/17 (35%)	11/27 (41%)[a]	11/20 (55%)[a]	9/23 (39%)	37/87 (43%)
KRAS/BRAF	1/7 (14%)	0/3 (0%)	1/3 (33%)	11/14 (79%)[a]	13/27 (48%)
VEGF/VEGFR-2	10/25 (40%)[a]	6/16 (38%)	0/3 (0%)	25/39 (64%)[a]	41/83 (49%)
RXR/Cyclin D1	0/1 (0%)	0/0 (NA)	1/1 (100%)[a]	1/4 (25%)	2/6 (33%)
None	3/8 (38%)	0/6 (0%)	5/9 (56%)[a]	11/18 (61%)[a]	19/41 (46%)
Total	20/58 (34%)	17/52 (33%)	18/36 (50%)	57/98 (58%)	112/244 (46%)

[a] Cells showing effective treatments within specific marker groups defined as the probability of DCR given data is 80% or greater. Only 1 patient in the RXR/CycD1 marker group received erlotinib + bexarotene.

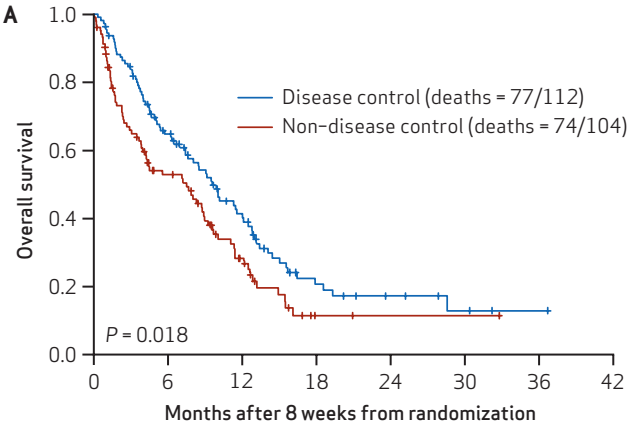

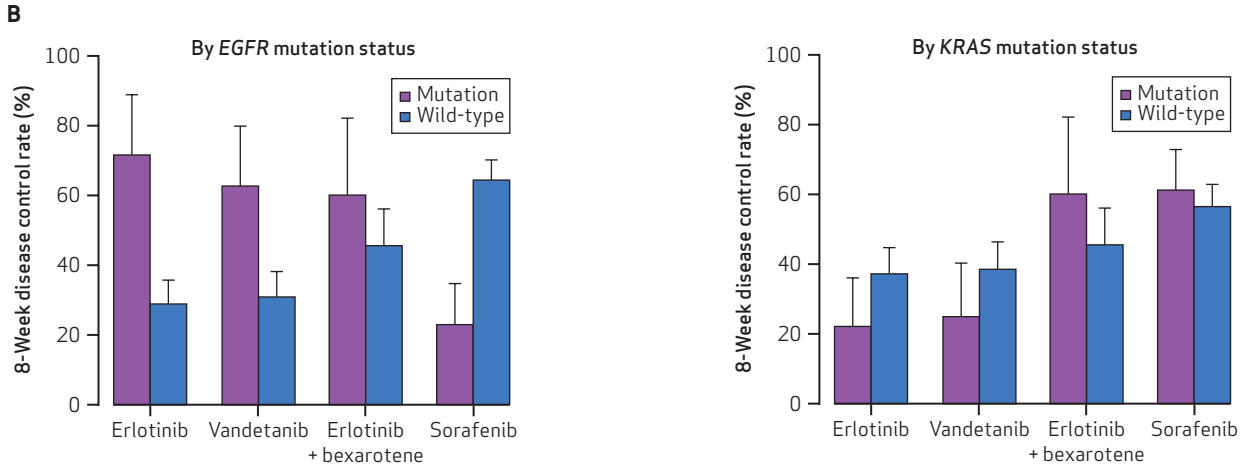

Figure 3. Major efficacy results of BATTLE study. **A**, landmark analysis of overall survival for patients with or without 8-week disease control. The landmark time point is set at 8 weeks; i.e., time 0 is at 8 weeks after randomization. **B**, 8-week disease control rates (in %) by treatment in patients with tumors harboring wild-type or mutated *EGFR* (left) and *KRAS* (right) genes.

9 partial responses in these heavily pretreated patients. In an 8-week landmark analysis, the median survival of patients with 8-week disease control (DC) was 9.6 months (95% CI, 7.4–12.5), compared with 7.5 months (95% CI, 4.2–9.2) for patients without 8-week DC (Fig. 3A; $P = 0.018$). The overall 8-week DCRs were 34% (erlotinib), 33% (vandetanib), 50% (erlotinib plus bexarotene), and 58% (sorafenib). Effective treatment–marker-group pairings, defined as having a 0.8 posterior probability of exceeding a DCR of 30%, were as follows: erlotinib in the VEGF/VEGF receptor 2 (VEGFR-2) group; vandetanib in the *EGFR* group; erlotinib plus bexarotene in the *EGFR*, retinoid X receptor (RXR)/Cyclin D1, and no-marker groups; and sorafenib in the *KRAS/BRAF*, VEGF/VEGFR-2, and no-marker groups (Table 2).

In addition to analysis of prespecified marker groups, we also studied effects of individual markers on treatment efficacy. In confirmation of our prespecified scientific hypotheses, individual markers that predicted a better 8-week DC of treatment [versus the marker's opposite status (absence or presence)] were *EGFR* mutations for erlotinib ($P = 0.04$), high VEGFR-2 expression for vandetanib ($P = 0.05$), and high Cyclin D1 expression for erlotinib plus bexarotene ($P = 0.01$). Exploratory predictive marker analysis results were as follows: a better 8-week DC with *EGFR* amplification for erlotinib plus bexarotene ($P = 0.006$); a worse 8-week DC with *EGFR* mutation ($P = 0.01$) or high *EGFR* polysomy ($P = 0.05$) for sorafenib; and, compared with the combined other treatments, sorafenib had a higher DCR (64% versus 33%) in *EGFR*–wild-type patients ($P < 0.001$) and a non-statistically significant trend toward better DCR (61% versus 32%) in mutant-*KRAS* patients ($P = 0.11$; Fig. 3B). In addition, in the *KRAS/BRAF* marker group, sorafenib had a 79% DCR compared to a 14% DCR with erlotinib ($P = 0.016$).

Toxicity

All 4 treatments were well tolerated, each having toxicity consistent with prior reports. Treatment-related grade 3–4 toxicity was 6.5% (Supplementary Table S2). Average compliance in each arm was >95%. Sorafenib produced the most toxicity, which caused discontinuation of treatment in 19% and dose reductions in 21% of sorafenib-treated patients (Supplementary Table S3). Lung biopsy was well tolerated by the 139 patients who underwent the procedure, with pneumothorax in 11.5%, and only 1 grade 3 event, which required overnight hospitalization.

DISCUSSION

The phase II randomized BATTLE trial made important clinical discoveries and demonstrated the feasibility of its novel design for advancing personalized treatment of NSCLC. BATTLE is the first completed prospective, biopsy-mandated, biomarker-based, adaptively randomized clinical study in patients with pretreated, advanced lung cancer. The trial data validated prespecified scientific hypotheses

regarding predictive biomarkers for targeted agents and identified potential new predictive markers. The BATTLE study is important in demonstrating several key points: 1) establishing the feasibility of performing biopsies and real-time biomarker analyses in previously treated lung cancer patients; 2) identifying interactions between the treatments and markers (e.g., DCR of 79% with sorafenib but only 14% with erlotinib in the *KRAS/BRAF* marker group) for guiding adaptive randomization; and 3) confirming the prespecified hypotheses of treatment efficacy in the presence of individual markers related to the treatments' mechanism of action.

EGFR mutations have been adopted as a predictive biomarker for directing NSCLC patient treatment with EGFR TKIs but are present in only 10% to 15% of the lung cancer population. Results from the vast majority of chemotherapy-based clinical trials in NSCLC, which continue to treat NSCLC as a homogeneous disease, have been disheartening, and personalized trials targeting molecular NSCLC characteristics of individual patients may be a viable option for improving treatment outcomes.

We showed that 8-week DC status is a good surrogate for OS in previously treated patients, as also reported by the Southwest Oncology Group during BATTLE (13). This clinically relevant, short-term, surrogate end point facilitated the rapid integration of outcome data into adaptive randomization, confirming its utility for personalizing treatment assignments. In addition, the short-term nature of the 8-week DC end point was not considered to be affected by patients who had received multiple prior treatments before BATTLE. Our overall response rate of 4% is reflective of a heavily pretreated NSCLC population and consistent with other published studies in this population (5, 9, 14).

Results of the BATTLE study support the potential of various biomarkers to predict the sensitivity or resistance of patients to targeted agents. Sorafenib was active against tumors with mutated or wild-type *KRAS*, but had a worse DCR (compared with other study agents) in patients with *EGFR* mutations. As expected (5–7, 15–17), erlotinib was beneficial in patients with mutated-*EGFR* tumors. Erlotinib plus bexarotene improved DC in patients with a higher expression of Cyclin D1, suggesting a potential role for bexarotene in lung cancer treatment (11); similar to sorafenib, the combination also improved DC in the *KRAS*-mutant patient population. Future randomized, controlled studies are needed to further confirm the predictive value of these biomarkers. These findings (e.g., association of increased expression of Cyclin D1 with benefit from treatment with bexarotene and erlotinib, and sorafenib's activity in patients with both *KRAS*-mutant and *KRAS*–wild-type tumors) have fueled enthusiasm to further test these compounds in future clinical trials.

Biomarker profiles may differ between early-stage and advanced lung tumors. In current practice, biomarker profiles are determined from the original diagnostic tissue and may not reflect the current tumor biomarker status after receiving treatments, thus hampering decision making for personalized treatment. The present study performed real-time biopsies for assessing the current status of tumor biomarkers in patients, thus validating the feasibility of this paradigm-shifting approach.

The BATTLE approach could be expanded to develop personalized cytotoxic therapy. ERCC1 or RRM1 protein overexpression can help direct cytotoxic therapy, but these markers are not widely used in the clinical setting; other cytotoxic-therapy markers need further elucidation (18, 19). We mandated at least 2 core needle biopsies (CNB) in BATTLE and collected additional tissue and blood for discovering new biomarkers, including gene signatures, which may help further define patient populations sensitive to specific cytotoxic and biologic treatments.

Our study has some important limitations. First, and probably most important, our biomarker groups were less predictive than were individual biomarkers, which diluted the impact of strong predictors in determining treatment probabilities. For example, *EGFR* mutations were far more predictive than was the overall *EGFR* marker group. The unfortunate decision to group the EGFR markers also impacted the other marker groups and their interactions with other treatments, resulting in a suboptimal overall DCR as described. Second, several of the prespecified markers (e.g., RXR) had little, if any, predictive value in optimizing treatment selections. This limitation will be addressed in future studies by not grouping or prespecifying biomarkers prior to initiating these biopsy-mandated trials. In addition, adaptive randomization, which assigns more patients to the more effective treatments within each biomarker group, only works well with a large differential efficacy among the treatments (as evident in the *KRAS/BRAF* group), but its role is limited without such a difference (e.g., in the other marker groups). Allowing prior use of erlotinib was another limitation and biased treatment assignments; in fact, the percentage of patients previously treated with erlotinib steadily increased during trial enrollment. Overall, 45% of our patients were excluded from the 2 erlotinib-containing arms because of prior EGFR TKI treatment. As erlotinib is a standard of care therapy in NSCLC second-line, maintenance, and front-line settings, the number of patients receiving this targeted agent will likely continue to increase.

The BATTLE approach requires a highly integrated team of multidisciplinary investigators and should be implemented at specialized centers in carefully designed clinical trials. However, once a validated biomarker predicting benefit of treatment is identified, conducting this type of study in both academic and community environments will help promote the use of biomarkers to select patients for optimal treatment assignments.

While proving that the BATTLE-type platform is feasible, we have also learned several important lessons from our initial experience that have and will impact the design and conduct of future BATTLE studies focused on pretreated NSCLC populations. A forthcoming study (BATTLE-2) of targeted agents in pretreated patients with advanced NSCLC will further refine our experience with this approach. In BATTLE-2, we prespecify an extremely limited set of markers and will use the first half of the study population (approximately 200 patients) to conduct prospective testing of biomarkers/signatures. Upon completing this analysis, the "best" (most predictive) markers and signatures will be used to guide patient assignments to the most favorable matched treatments in the second half of the study (approximately 200 patients). Patients enrolled would be screened for *EGFR* mutations and *ALK*

translocations (20). If positive, they would not be eligible for enrollment in this study but would be referred to other ongoing trials testing agents targeting those mutations. We believe this is an ethical design and would allow patients to be exposed to additional novel therapies for lung cancer treatment.

BATTLE is the first completed prospective, adaptively randomized study in heavily pretreated NSCLC patients that mandated tumor profiling with real-time CNBs, demonstrating the feasibility of this approach and creating a new paradigm for translational research. This trial took a substantial step toward realizing personalized lung cancer therapy by integrating real-time molecular laboratory findings in delineating specific patient populations for individualized treatment. BATTLE accumulated increasing probabilities of a positive treatment outcome and showed the potential of its mandatory-biopsy design for developing specific predictive biomarkers and associated treatments for subsequent definitive clinical testing. This approach will be important for future evaluations of new molecular targets and predictive biomarkers (21–23). The successful completion of BATTLE reported in this article will potentially facilitate the implementation of future trials of personalized treatments in lung and other cancers with even more efficient designs, as a forerunner in the quest for discovery of novel cancer treatments.

METHODS

Patient Population

We recruited patients with pretreated NSCLC at the University of Texas MD Anderson Cancer Center (MDACC) who agreed to a baseline tumor biopsy procedure. Eligibility also included age ≥18 years and adequate performance status (ECOG grade 0–2). Prior treatment with erlotinib was allowed, but such patients were excluded from the erlotinib-containing study arms, and stable (for at least 4 weeks) or treated brain metastases were permitted. Patients with multiple lines of prior therapy were eligible if they had adequate performance status. Radiographic imaging of tumors was reviewed to determine suitability for biopsy. All participants provided written informed consent. Other eligibility criteria appear in the Supplementary Data.

Study Design

BATTLE was a randomized phase II, single-center, open-label study in patients with advanced NSCLC refractory to prior chemotherapy (Fig. 1). Following molecular tumor-biomarker assessments, patients were randomly assigned to oral treatment with erlotinib (150 mg once daily; Tarceva, OSIP/Genentech), vandetanib (300 mg once daily; Zactima, AstraZeneca), erlotinib (150 mg once daily) plus bexarotene (400 mg/m^2 once daily; Targretin, Eisai), or sorafenib (400 mg twice daily; Nexavar, Bayer/Onyx). The primary end point was the DCR at 8 weeks. Secondary end points included response rate, PFS, OS, and toxicity. Planned exploratory objectives were each treatment's efficacy in relation to patient biomarker profiles.

The Institutional Review Boards of MDACC and the U.S. Department of Defense approved the study, which was monitored by an independent Data and Safety Monitoring Board.

Biopsy, Molecular Analysis, and Biomarker Grouping

An interventional radiologist used computed tomography or ultrasound guidance to obtain fresh CNB tumor specimens from each patient (Supplementary Data). The procedure yielded 1 to 3 tissue cores approximately 1 mm in diameter and 1.2 to 1.8 cm long (average length, 1.5 cm). Each CNB specimen was divided at collection into 2 portions: 1) tissue for clinical-trial biomarker analysis (at least 1 core), and 2) tissue for future gene expression and proteomic biomarker analysis (at least 1 core). A critical study aspect was the concurrent collection of additional CNB tissue samples, which were prepared simultaneously with the study specimens, for future discovery of novel biomarkers.

The CNB tissue specimens designated for clinical-trial biomarker analysis were formalin-fixed immediately in the interventional radiology suite and transported to the research laboratory for processing and subsequent histologic and biomarker analyses. Molecular pathologist I. Wistuba (MDACC) reviewed formalin-fixed, paraffin-embedded, and hematoxylin-and-eosin (H&E)–stained histologic sections within 24 hours of collection to assess the presence, quantity, quality, and histologic type of tumor tissue. Each histology section considered adequate for biomarker analysis had ≥200 malignant cells.

Tumor specimens from the mandatory CNB procedure (minimum of 2 cores; see Supplementary Data) were tested for the following 11 prespecified biomarkers: mutations of *EGFR*, *KRAS*, and *BRAF*; copy numbers (by FISH) of *EGFR* and the *Cyclin D1* gene (*CCND1*); and protein expression levels of VEGF, VEGFR-2, RXRs α, β, and γ, and Cyclin D1. The MDACC Thoracic Molecular Pathology Research Laboratory performed these biomarker tests (see Supplementary Data), reporting results within 2 weeks of each biopsy procedure. Biomarker choices and criteria for classifying each biomarker test as positive or negative were prespecified prior to starting this study on the basis of data available in 2005 (15–17, 24, 25). Patients and investigators were blinded to the biomarker results until the patient was taken off the study.

Five biomarker groups were established and ranked for predictive value (based on evidence available at trial initiation) from 1 (highest) to 5 (lowest), as follows: 1) *EGFR* mutation and/or *EGFR* amplification/high polysomy; 2) *KRAS* or *BRAF* mutation; 3) VEGF and/or VEGFR-2 overexpression; 4) RXR α, β, or γ overexpression and/or Cyclin D1 overexpression and/or *CCND1* amplification; or 5) no study biomarkers. Each patient was assigned to one of these groups; patients with biomarkers in more than one group were assigned to the group with the highest ranking. Our prespecified hypothesis was that each treatment regimen would be efficacious for patients presenting markers related to the treatment's mechanism of action. Namely, erlotinib, sorafenib, vandetanib, and erlotinib plus bexarotene would work for patients with *EGFR* mutation/amplification, *KRAS* or *BRAF* mutation, VEGF and/or VEGFR-2 overexpression, and RXR receptor overexpression and/or Cyclin D1 overexpression/amplification, respectively.

Biopsy Procedure

Written informed consent was obtained from each patient before each biopsy. Coagulopathies were corrected prior to biopsy. All biopsies were performed under computed tomographic or sonographic guidance by a board-certified interventional radiologist with the patient in the prone, supine, or lateral decubitus position, depending on the location of the lesion. During the biopsy, patients received either local anesthesia or monitored, moderate sedation. Patients' skin was aseptically prepared and draped, and 1% lidocaine was administered subcutaneously for local anesthesia. A coaxial biopsy technique was used for all patients. With image guidance to evaluate the needle's trajectory, an 18- or 19-gauge guide needle (Cook) was inserted through the skin and advanced to a position close to the target lesion. After imaging confirmation of the needle tip's position, 2 or 3 core biopsy samples were obtained with a 20-gauge biopsy needle (Quick-core; Cook). The samples were handed over to the appropriate research personnel for handling and processing.

After the biopsy procedure, patients were monitored by the nursing staff in the radiology department's recovery area. In patients

who underwent a lung or mediastinal biopsy, an upright inspiratory posteroanterior chest radiograph was obtained within 30 minutes of the biopsy procedure. In the absence of a pneumothorax, the procedure included a second chest radiograph 3 hours after the biopsy. If the initial chest radiograph showed a pneumothorax, a follow-up radiograph was obtained after 1 hour. Chest tubes were inserted if the pneumothorax size was >30%, the pneumothorax increased in size, or patients experienced pain, shortness of breath, or a decrease in oxygen saturation.

Biomarker Methodology

To evaluate 11 molecular biomarkers (Supplementary Table S1) using the formalin-fixed paraffin-embedded (FFPE) CNB tissue specimens, 13 5-μm histology sections were obtained, as follows: 1) H&E histology analysis ($n = 1$ section); 2) DNA extraction for mutation analyses (*EGFR*, *KRAS*, and *BRAF*; $n = 1$ or 2 sections); 3) FISH analysis (*EGFR* and *CCND1*; $n = 2$ sections); and 4) immunohistochemistry (IHC) analysis (VEGF, VEGFR-2, Cyclin D1, RXRα, RXRβ, and RXRγ; $n = 6$ sections). All specimens were assigned an identification number linked to the clinical trial identification number for subsequent processing in the laboratory. Certification of the presence of adequate tumor tissue in the FFPE tissue specimens by histologic examination was performed within 24 to 48 hours, and analysis of the 11 molecular biomarkers was performed, completed, and reported, in most cases, within 14 days.

Microdissection and DNA extraction Malignant tumor cells were manually microdissected from 4 sequential 5-μm-thick H&E-stained FFPE histology sections. DNA was extracted using 25 μL of Pico Pure TM DNA Extraction solution (Arcturus) containing proteinase K and incubated at 65°C for 24 hours. Subsequently, proteinase K inactivation was performed by heating samples at 95°C for 10 minutes.

Mutation analysis Mutations of *EGFR* (exons 18–21), *KRAS* (exons 1, codons 12 and 13; and exon 2, codon 61), and *BRAF* (exons 11 and 15) were studied using DNA extracted from microdissected FFPE tumor cells. The DNA sequences were PCR amplified using primers shown in Supplementary Table S1. Each PCR amplification was performed in 30 μL of volume containing 2 μL of DNA (approximately 100 ng of genomic DNA), 0.3 of μM forward and reverse primers, and 15 μL of HotStarTaq (1.5 units of DNA polymerase) Master Mix (Qiagen) for 40 cycles at 94°C for 30 seconds, for 30 seconds at the primer pairs' annealing temperature (Supplementary Table S1), and at 72°C for 45 seconds, followed by 7 minutes of extension at 72°C. All PCR products were directly sequenced using Applied Biosystems PRISM dye terminator cycle sequencing method (Perkin-Elmer). All sequence variants were confirmed by independent PCR amplifications from at least 2 independent DNA extractions, and sequenced in both directions.

EGFR and CCND1 copy number analysis Copy number of both genes was analyzed using FISH. For *EGFR*, gene copy number per cell was analyzed using the LSI EGFR SpectrumOrange/CEP7 SpectrumGreen Probe (Abbott Molecular), as previously described (16). For *CCND1*, the Vysis LSI *CCND1* (SO)/CEP11 DNA probe set (Abbott Molecular) was used. For both FISH analyses, histology sections were incubated at 56°C overnight and deparaffinized by washing in CitriSolv (Fisher Scientific). After incubation in denaturing solution containing 70% formamide and 2× SSC buffer, pH 7.0, at 73°C for 5 minutes, the histology sections were digested with proteinase K (0.25 mg/mL in 2× SSC) at 37°C for 15 to 25 minutes, rinsed in 2 × SSC (pH 7.0) at room temperature for 5 minutes, and dehydrated using ethanol in a series of increasing concentrations (70%, 85%, 100%). The probe set was applied onto the selected area, per the manufacturer's instructions, on the basis of the tumor foci seen on each slide. The hybridization area was covered with a glass coverslip and then sealed with rubber cement. The slides were incubated at 80°C for 10 minutes for co-denaturation of chromosomal and probe DNA and then placed in a humidified chamber at 37°C for 20 to 24 hours to allow hybridization to occur. Posthybridization washes were performed in 1.5-M urea and 0.1× SSC (pH, 7.0–7.5) at 45°C for 30 minutes and in 2× SSC for 2 minutes at room temperature. After the samples were dehydrated in a series of increasing ethanol concentrations, 4',6'-diamidino-2-phenylindole (0.15 mg/mL) in Vectashield Mounting Medium (Vector Laboratories) was applied for chromatin counterstaining.

For both genes, fluorescence signals were scored in at least 50 nonoverlapping interphase nuclei per tumor, and the section of the area was guided by images of the H&E-stained section. The number of copies of *EGFR* and chromosome 7 probes was assessed independently using a fluorescence microscope (Cytovision platform, Genetix). The number of copies of *CCDN1* and chromosome 11 probes was assessed independently using a fluorescence microscope (Cytovision platform, Genetix).

For *EGFR*, cases were classified into 6 FISH strata according to the frequency of cells with the *EGFR* gene copy number and referred to the chromosome 7 centromere, as follows: 1) disomy (≤3 copies in <10% of cells); 2) low trisomy (3 copies in 10%–40% of cells, 4 copies in <10% of cells); 3) high trisomy (3 copies in >40% of cells, 4 copies in <10% of cells); 4) low polysomy (≥4 copies in 10%–40% of cells); 5) high polysomy (≥4 copies in 40% of cells); and 6) gene amplification (ratio of *EGFR* gene to chromosome ≥2, presence of tight *EGFR* gene clusters and 15 copies of *EGFR* per cell in 10% of the analyzed cells). The high polysomy and gene amplification categories were considered to be high *EGFR* copy number, and the other categories were considered to be nonincreased *EGFR* copy number, as previously published (24, 26).

For *CCDN1*, cases were considered to have gene copy number gain when the average ratio of *CCND1* copy number to chromosome 11 centromere copy number was >1, or when clusters of *CCND1* signals were observed in >20% of nuclei, as previously published (27).

IHC analysis Protein expression of VEGF, VEGFR-2, RXRα, RXRβ, RXRγ, and Cyclin D1 was determined by IHC. For VEGF, VEGFR-2, RXRα, RXRβ, and RXRγ proteins, combined expression of cytoplasmic and membrane staining was assessed, and for RXRα and Cyclin D1 proteins, expression of nuclear staining was examined. Commercially available antibodies were used, as follows: VEGF, rabbit polyclonal antibody (Santa Cruz Biotechnology, Inc.), dilution 1:200; VEGFR-2, mouse monoclonal antibody (Santa Cruz Biotechnology, Inc.), dilution 1:200; RXRα, rabbit polyclonal antibody (Santa Cruz Biotechnology, Inc.), dilution 1:300; RXRβ, rabbit polyclonal antibody (Upstate), dilution 1:100; RXRγ rabbit polyclonal antibody (Santa Cruz Biotechnology, Inc.), dilution 1:200; and Cyclin D1, rabbit monoclonal antibody (clone SP4; Thermo Scientific), dilution 1:100.

All immunostaining was performed using automated stainers (DakoCytomation). Sections 5-μm thick were deparaffinized, rehydrated, and washed with PBS. Antigens were retrieved with 0.01-M citrate buffer (pH 6.0; DakoCytomation) for 30 minutes in a steamer. Samples were blocked for endogenous activity in 3% hydrogen peroxide-PBS, avidin–biotin solution (Zymed), and serum-free protein block (DakoCytomation) before incubation at room temperature with the primary antibody for 60 minutes for VEGF, RXRα, and RXRγ, and 65 minutes for VEGFR-2, RXRβ, and Cyclin D1. The sections were then washed in Tris-buffered saline (pH 7.4) and incubated with goat antirabbit biotinylated immunoglobulin (DakoCytomation). After incubation with the secondary antibody, the sections were incubated with the avidin-biotin-peroxidase complex (DakoCytomation) and developed with 3, 3′-diaminobenzidine. The sections were then rinsed in distilled water, counterstained with Mayer's hematoxylin,

and mounted for evaluation. Surgically resected FFPE NSCLC tumor tissue specimens with known expression of the markers were used as positive controls. The same FFPE tissues processed without the primary antibody were used as negative controls.

Biomarker scoring For VEGF, VEGFR-2, RXRα, RXRβ, and RXRγ proteins, combined expression of cytoplasmic and membrane staining was assessed, and for RXRα and Cyclin D1 proteins, expression of nuclear staining was examined. All expression was assessed using semiquantitative analysis of intensity and extension. For cytoplasmic/membrane expression, the percentage of positive tumor cells in the cytoplasm/membrane (0%–100%) was multiplied by the intensity of staining (0–3); therefore, the possible overall score ranged from 0 to 300. Cytoplasmic and membrane expression scores >100 were considered positive for VEGF and VEGFR-2, and scores >200 were considered positive for RXRβ and RXRγ. Nuclear expression was evaluated for any positive immunostaining, which was expressed in percentage. A nuclear score >30% was considered positive for RXRα, and a nuclear score >10% was considered positive for Cyclin D1.

Serum Collection

Samples were collected from consenting patients at baseline and after each cycle of treatment. Venous blood was collected at the following time points: baseline (pretreatment), end of cycles 1 and 2, and every 2 cycles thereafter until the patient went off protocol. At each time point, 8 mL of venous blood was collected into an EDTA-based Vaccutainer and plasma was separated via centrifugation, 1500 RPM for 15 minutes at 4°C within 30 minutes of collection. The resultant plasma was aliquoted into 3 prelabeled cryovials and stored at −70°C until analysis.

Statistical Analysis

The accrual goal was 250 randomized patients to achieve a sample size of 200 evaluable patients with complete marker profiles, which would allow an 80% power, with a 20% type I error rate, to identify effective treatments within each marker group. A high type I error rate prevented missing any potentially effective treatments that could be confirmed in larger, future studies (28).

The primary end point was the 8-week DCR [complete or partial response or stable disease via Response Evaluation Criteria in Solid Tumors (RECIST) (29)], which we compared with the historical 30% DCR estimate in similar patients (14). Treatment efficacy (a positive finding) was defined as >0.80 probability of achieving >30% DCR.

The statistical design was based on adaptive randomization under a Bayesian hierarchical model that would increasingly assign patients into treatments with the greatest potential for efficacy based on individual biomarker profiles (28). We planned to randomly assign at least the initial 80 patients equally to the 4 treatments, to allow at least 1 patient in each marker group to complete treatment, thus providing sufficient data to estimate the prior probability of DC for subsequent patients. Subsequent randomization "switched" to an adaptive algorithm, which incorporated the data of each patient evaluated at the 8-week time point (treatment, biomarker group, and 8-week DCR) into recalculations of the posterior probability of efficacy for treatments in relation to biomarker groups. This scheme adapts randomization probabilities for each of the 4 treatments from an equal chance, that is, 25% per treatment, to chances determined by biomarkers of >25% (high predicted DC) or <25% (low predicted DC).

Bayesian adaptive randomization bases treatment assignments on accumulating data within the trial, allowing more patients to be assigned to more effective therapies and fewer patients to be assigned to less effective therapies. This "learn-as-we-go" approach leveraged accumulating patient data to improve the treatment outcome. This trial design also allows the suspension of underperforming treatments in marker groups, as stipulated for our trial if the probability of a DCR >50% was <0.1 (detailed statistical assumptions can be found in ref. 28). The study was not designed to test the efficacy of equal versus adaptive randomization in improving DCR.

Standard statistical methods included the Fisher's exact test for contingency tables and log-rank test for survival data, in addition to calculating the Bayesian posterior probability. Each randomized patient represented a unit of the analysis. Time-to-event end points (e.g., OS) were censored at the time of a subsequent randomization for patients randomly assigned more than once.

Randomization

After categorization into marker groups, patients were randomly assigned to 1 of the 4 treatment arms. The initial cohort of eligible patients was randomly assigned to the 4 arms without regard to their respective marker groups (except for patients who had prior treatment with erlotinib, who were excluded from the 2 erlotinib-containing arms). These patients were assessed for associations between their marker groups and DC, giving a "prior" probability of the DCR for a given treatment in a given marker group. Patients enrolled after the initial cohort were randomly assigned to treatment according to a Bayesian adaptive algorithm, which incorporated the prior probability and DC data into a "posterior" probability of the DCR for a given treatment; the resulting posterior probability was continually updated per accumulating data on the associations between the DC and biomarkers of patients.

Clinical Assessments

Patients were evaluated clinically at the end of each treatment cycle (defined as lasting 4 weeks), and underwent imaging studies every 2 cycles, or every 8 weeks. Patients who progressed could reenter the clinical trial and be reassigned randomly to treatment if still eligible and agreeable to a new biopsy.

A radiologist independently assessed DC, which was defined as a complete or partial response or stable disease according to the RECIST (29) at the end of 8 weeks (start of treatment to end of second treatment cycle). PFS was assessed from the date of randomization to the earliest sign of disease progression or death from any cause. OS was assessed from the date of randomization until death from any cause. Tumor response was assessed every 8 weeks until disease progression. Toxicity was assessed in accordance with the National Cancer Institute Common Terminology Criteria for Adverse Events, version 3.0.

Disclosure of Potential Conflicts of Interest

A. Tsao received commercial research support from Bristol-Myers Squibb, Merck, and Novartis and served on the advisory board for Genentech and Roche; B. Johnson served as consultant for AstraZeneca, Genentech, and Pfizer; D. Stewart received honoraria from AstraZeneca; E. Kim received commercial research support from AstraZeneca and Genentech and served as a consultant for AstraZeneca, Bayer, and Genentech; G. Blumenschein received commercial research support from Amgen, Bayer, Exelixis, GlaskoSmithKline, and Pfizer and served as a consultant for Amgen, Bayer, and GlaskoSmithKline; J. Heymach received commercial research support and served on the advisory board for AstraZeneca; I. Wistuba received commercial research support from AstraZeneca, Genentech, and Pfizer; R. Herbst received commercial research support and served as a consultant for AstraZeneca and Genentech; and V. Papadimitrakopoulou served on the advisory boards of Amgen and GlaxoSmithKline.

Acknowledgments

We gratefully acknowledge the patients who participated in the study, as well as Jeffrey Lewis for programming and database management support; Dawn Chalaire and Sunita Patterson for editorial assistance;

the Faith, Family and Friends Foundation; Rexanna's Foundation; Mayberry Memorial Foundation; Stading Family Foundation; Hewett Foundation; Cohen-Reinach Family Charitable Foundation; and the National Foundation for Cancer Research. We also thank the MD Anderson Data Safety and Monitoring Board chaired by Dr. Donald A. Berry for monitoring the trial.

Grant Support

This research was supported in part by the Department of Defense Grant W81XWH-6-1-0303 and by the National Institutes of Health through MD Anderson's Cancer Center Support Grant P30 CA016672.

Received September 28, 2010; revised December 2, 2010; accepted December 20, 2010; published OnlineFirst April 3, 2011.

REFERENCES

1. Jemal A, Siegel R, Xu J, Ward E. Cancer statistics, 2010. CA Cancer J Clin 2010; 60:277–300.
2. Herbst RS, Heymach JV, Lippman SM. Lung cancer. N Engl J Med 2008;359:1367–80.
3. Sandler A, Gray R, Perry MC, Brahmer H, Schiller JH, Dowlati, A, et al. Paclitaxel-carboplatin alone or with bevacizumab for non-small-cell lung cancer. N Engl J Med 2006;355:2542–50.
4. Scagliotti GV, Parikh P, von Pawel J, Biesma B, Vansteenkiste J, Manegold C, et al. Phase III study comparing cisplatin plus gemcitabine with cisplatin plus pemetrexed in chemotherapy-naive patients with advanced-stage non-small-cell lung cancer. J Clin Oncol 2008;26:3543–51.
5. Kim ES, Hirsh V, Mok T, Socinski MA, Gervais R, Wu YL, et al. Gefitinib versus docetaxel in previously treated non-small cell lung cancer (INTEREST): a randomized Phase III trial. Lancet 2008;372:1809–18.
6. Douillard JY, Shepherd FA, Hirsh V, Mok T, Socinski MA, Gervais R, et al. Molecular predictors of outcome with gefitinib and docetaxel in previously treated non-small-cell lung cancer: data from the randomized Phase III INTEREST trial. J Clin Oncol 2010;28:744–52.
7. Mok TS, Wu YL, Thongprasert S, Yang CH, Chu DT, Saijo N, et al. Gefitinib or carboplatin-paclitaxel in pulmonary adenocarcinoma. N Engl J Med 2009;361:947–57.
8. Rosell R, Moran T, Queralt C, Porta R, Cardenal F, Camps C, et al. Screening for epidermal growth factor receptor mutations in lung cancer. N Engl J Med 2009;361:958–67.
9. Shepherd FA, Pereira JR, Ciuleanu T, Tan EH, Hirsh V, Thongprasert S, et al. Erlotinib in previously treated non–small-cell lung cancer. N Engl J Med 2005;353:123–32.
10. Schiller JH, Lee JW, Hanna NH, et al. A randomized discontinuation phase II study of sorafenib versus placebo in patients with non-small cell lung cancer who have failed at least two prior chemotherapy regimens: E2501. J Clin Oncol 2008;26(May 20 Suppl; abstr 8014)
11. Dragnev KH, Tian M, Cyrus J, Galimberti F, Memoli V, Buset AM, et al. Bexarotene plus erlotinib suppresses lung carcinogenesis independently of KRAS mutations in two clinical trials and transgenic models. Cancer Prev Res (Phila) In press, 2011.
12. Natale RB, Bodkin D, Govindan R, Aleckman BG, Rizvi NA, Capó A, et al. Vandetanib versus gefitinib in patients with advanced non–small-cell lung cancer: results from a two-part, double-blind, randomized phase II study. J Clin Oncol 2009;27:2523–9
13. Lara PN, Redman MW, Kelly K, Edelman MJ, Williamson SK, Crowley JJ, et al. Disease control rate at 8 wk predicts clinical benefit in advanced non-small-cell lung cancer: results from Southwest Oncology Group randomized trials. J Clin Oncol 2009;26:463–7.
14. Fossella FV, DeVore R, Kerr RN, Crawford J, Natale RR, Dunphy F, et al. Randomized phase III trial of docetaxel versus vinorelbine or ifosfamide in patients with advanced non-small-cell lung cancer previously treated with platinum-containing chemotherapy regimens. The TAX 320 Non-Small Cell Lung Cancer Study Group. J Clin Oncol 2000;18:2354–62.
15. Paez JG, Janne PA, Lee JC, Tracy S, Greulich H, Gabriel S, et al: EGFR mutations in lung cancer: correlation with clinical response to gefitinib therapy. Science 2004;304:1497–500.
16. Tsao MS, Sakurada A, Cutz JC, Zhu CQ, Kamel-Reid S, Squire J, et al. Erlotinib in lung cancer: molecular and clinical predictors of outcome. N Engl J Med 2005;353:133–44.
17. Lynch TJ, Bell DW, Sordella R, Gurubhagavatula S, Okimoto RA, Brannigan BW, et al. Activating mutations in the epidermal growth factor receptor underlying responsiveness of non-small-cell lung cancer to gefitinib. N Engl J Med 2004;350:2129–39.
18. Zheng Z, Chen T, Li X, Haura E, Sharma A, Bepler G, et al. DNA synthesis and repair genes *RRM1* and *ERCC1* in lung cancer. N Engl J Med 2007;356:800–8.
19. Reynolds C, Obasaju C, Schell MJ, Li X, Zheng Z, Boulware D, et al. Randomized phase III trial of gemcitabine-based chemotherapy with in situ RRM1 and ERCC1 protein levels for response prediction in non-small cell lung cancer. J Clin Oncol 2009;34:5808–15.
20. Shaw AT, Yeap BY, Mino-Kenudson M, Digumarthy SR, Costa DB, Heist RS, et al. Clinical features and outcome of patients with non-small-cell lung cancer who harbor EML4-ALK. J Clin Oncol 2009;27:4247–53.
21. Simon G, Sharma A, Li X, Hazelton T, Welsh F, Williams C, et al. Feasibility and efficacy of molecular analysis-directed individualized therapy in advanced non-small-cell lung cancer. J Clin Oncol 2007;19:2741–6.
22. Lee JJ, Gu X, Liu S. Bayesian adaptive randomization designs for targeted agent development. Clin Trials 2010;7:584–96.
23. Turke AB, Zejnullahu K, Wu YL, Song Y, Dias-Santagata D, Lifshits E, et al. Preexistence and clonal selection of MET amplification in EGFR mutant NSCLC. Cancer Cell 2010;17:77–88.
24. Cappuzzo F, Hirsch FR, Rossi E, Bartolini S, Ceresoli GL, Bemis L, et al. Epidermal growth factor receptor gene and protein and gefitinib sensitivity in non-small-cell lung cancer. J Natl Cancer Inst 2005;97:643–55.
25. Edelman MJ, Smith R, Hausner P, Doyle LA, Kalra K, Kendall J, et al. Phase II trial of the novel retinoid, bexarotene, and gemcitabine plus carboplatin in advanced non-small cell lung cancer. J Clin Oncol 2005;24:5774–8.
26. Hirsch FR, Dziadziuszko R, Thatcher N, Mann H, Watkins C, Parums DV, et al. Epidermal growth factor receptor immunohistochemistry: comparison of antibodies and cutoff points to predict benefit from gefitinib in a phase 3 placebo-controlled study in advanced non small-cell lung cancer. Cancer 2008;112:1114–21.
27. Uzawa N, Sonoda I, Myo K, Takahashi K, Miyamoto R, Amagasa T. Fluorescence in situ hybridization for detecting genomic alterations of cyclin D1 and p16 in oral squamous cell carcinomas. Cancer 2007;110:2230–9.
28 Zhou X, Liu S, Kim ES. Bayesian adaptive design for targeted therapy development in lung cancer—a step toward personalized medicine. Clin Trials 2008;5:181–93.
29. Therasse P, Arbuck SG, Eisenhauer EA, Wanders J, Kaplan RS, Rubenstein L, et al. New guidelines to evaluate the response to treatment in solid tumors: European Organization for Research and Treatment of Cancer, National Cancer Institute of the United States, National Cancer Institute of Canada. J Natl Cancer Inst 2000;92:205–16.

Endocrinology. First published ahead of print March 29, 2011 as doi:10.1210/en.2010-0693

Differential Impacts of Insulin-Like Growth Factor-Binding Protein-3 (IGFBP-3) in Epithelial IGF-Induced Lung Cancer Development

Woo-Young Kim, Mi-Jung Kim,* Hojin Moon,* Ping Yuan, Jin-Soo Kim, Jong-Kyu Woo, Guangcheng Zhang, Young-Ah Suh, Lei Feng, Carmen Behrens, Carolyn S. Van Pelt, Hyunseok Kang, J. Jack Lee, Waun-Ki Hong, Ignacio I. Wistuba, and Ho-Young Lee

Departments of Thoracic Head and Neck Medical Oncology (W.-Y.K., J.-S.K., J.-K. W., G.Z., C.B., W.-K.H., I.I.W., H.-Y.L.), Pathology (M.-J.K., P.Y., C.B., I.I.W.), Genetics (Y.-A.S.), Biostatistics (L.F., J.J.L.), and Veterinary Medicine and Surgery (C.S.V.P.), The University of Texas M.D. Anderson Cancer Center, and The University of Texas Graduate School of Biomedical Sciences (J.J.L., H.-Y.L.), Houston, Texas 77030; College of Pharmacy (H.-Y.L.), Seoul National University, Seoul 151-742, Korea; School of Pharmacy (W.Y.K.), Sookmyung Women's University, Seoul 140-742, Korea; Department of Mathematics and Statistics (H.M.), California State University, Long Beach, California 90840; and Columbia University College of Physicians and Surgeons (H.K.), New York, New York 10032

The IGF axis has been implicated in the risk of various cancers. We previously reported a potential role of tissue-derived IGF in lung tumor formation and progression. However, the role of IGF-binding protein (IGFBP)-3, a major IGFBP, on the activity of tissue-driven IGF in lung cancer development is largely unknown. Here, we show that IGF-I, but not IGF-II, protein levels in non-small-cell lung cancer (NSCLC) were significantly higher than those in normal and hyperplastic bronchial epithelium. We found that IGF-I and IGFBP-3 levels in NSCLC tissue specimens were significantly correlated with phosphorylated IGF-IR (pIGF-IR) expression. We investigated the impact of IGFBP-3 expression on the activity of tissue-driven IGF-I in lung cancer development using mice carrying lung-specific human *IGF-I* transgene (*Tg*), a germline-null mutation of *IGFBP-3*, or both. Compared with wild-type ($BP3^{+/+}$) mice, mice carrying heterozygous ($BP3^{+/-}$) or homozygous ($BP3^{-/-}$) deletion of *IGFBP-3* alleles exhibited decreases in circulating IGFBP-3 and IGF-I. Unexpectedly, IGF^{Tg} mice with 50% of physiological IGFBP-3 ($BP3^{+/-}$; IGF^{Tg}) showed higher levels of pIGF-IR/IR and a greater degree of spontaneous or tobacco carcinogen [4-(methylnitrosamino)-1-(3-pyridyl)-1-butanone]-induced lung tumor development and progression than did the IGF^{Tg} mice with normal ($BP3^{+/+;}$ IGF^{Tg}) or homozygous deletion of *IGFBP-3* ($BP3^{-/-}$; IGF^{Tg}). These data show that IGF-I is overexpressed in NSCLC, leading to activation of IGF-IR, and that IGFBP-3, depending on its expression level, either inhibits or potentiates IGF-I actions in lung carcinogenesis. **(*Endocrinology* 152: 0000–0000, 2011)**

The IGF play a pivotal role in cell proliferation, survival, and metabolism, and their signaling is associated with cancer, because it is required for cell transformation. IGF-I is unique among cellular growth factors in being synthesized by the liver and peripheral tissues, thus being both a tissue growth factor and an endocrine hormone (1–3). The IGF-I receptor (IGF-IR) binds to both IGF-I and IGF-II, and activated IGF-IR transfers the activated signal, mainly through phosphatidylinositol 3-kinase/AKT and MAPK (2, 3). The IGF-II receptor binds to IGF-II but has no in-

ISSN Print 0013-7227 ISSN Online 1945-7170
Printed in U.S.A.

doi: 10.1210/en.2010-0693 Received June 23, 2010. Accepted March 8, 2011.

* M.-J. K. and H.M. contributed equally to this research.

Abbreviations: hIGF-I, Human IGF-I; IGFBP, IGF-binding protein; IGF-IR, IGF-I receptor; IHC, immunohistochemical; mIGF, murine IGF; NNK, 4-(methylnitrosamino)-1-(3-pyridyl)-1-butanone; NSCLC, non-small-cell lung cancer; pIGF-IR, phosphorylated IGF-IR; TMA, tissue microarray.

trinsic tyrosine kinase activity. Thus, the effects of IGF are mediated mainly through the IGF-IR.

Epidemiological studies have found that a high serum level of IGF-I is a risk factor for several types of cancer, including lung (4), prostate (5), breast (premenopausal) (6), and colon cancers (7). However, following studies have shown inconsistent findings regarding the link between the serum levels of IGF-I and lung cancer risk (4, 8, 9). The impact of the serum level of IGF-I on the risk of developing lung cancer, therefore, remains ambiguous. We have recently demonstrated that airway lung epithelial cells produce IGF (IGF-I and -II) in an autocrine manner, leading to deregulation of IGF-IR activation (10). Additionally, we showed that lung-specific overexpression of IGF-I in mouse promotes lung tumor development and progression, which is accelerated by the tobacco carcinogens 4-(methylnitrosamino)-1-(3-pyridyl)-1-butanone (NNK) and benzo[*a*]pyrene. These findings indicate the importance of peripheral tissue-derived IGF-I in lung cancer development, providing an explanation for the apparent inconsistent findings (4, 8, 9) in which circulating IGF were mainly analyzed.

IGF bioavailability is regulated by a family of six IGF-binding proteins (IGFBP), of which IGFBP-3 is the major IGF carrier protein in the serum (11). Previous studies have demonstrated that the serum IGF-I level in mice is significantly reduced when IGFBP-3, IGFBP-4, and IGFBP-5 are lost (12), and reduced levels of circulating IGF-I delay the onset of mammary tumor formation and suppress growth and metastasis of colon cancer (13, 14). In another murine model, however, prostate tumor development was suppressed by increased levels of circulating IGFBP-3 (15). In addition to its modulatory effect on IGF action, IGFBP-3 has IGF-independent antiproliferative and proapoptotic effects (16). These findings have led investigators to question whether IGFBP-3 plays a positive or negative role in IGF-promoted tumor development.

The association between high plasma levels of IGFBP-3 and reduced lung cancer risk was reported years ago (17). Recent studies have also demonstrated that inverse correlation between circulating IGFBP-3 and lung cancer risk (8, 18). However, other studies showed positive correlation between IGFBP-3 level and lung cancer risk (19). Therefore, the association between circulating levels of IGFBP-3 and the risk of lung cancer is not conclusive yet.

In the current study, we determined 1) the expression of the IGF-I and IGF-II in human non-small-cell lung cancer (NSCLC) and adjacent normal tissues and correlated that expression with the activation of IGF-IR/IR, 2) the link between IGFBP-3 expression and IGF-IR/IR activation in the lungs, and 3) the impact of IGFBP-3 expression levels in IGF-I-mediated pathogenesis of spontaneous and NNK-initiated lung carcinogenesis by using tissue microarrays (TMA) of human NSCLC and a mouse model of lung carcinogenesis composed of a lung-specific human *IGF-I* transgene (IGF^{Tg}) with or without a germline-null mutation of IGFBP-3. The data described herein demonstrate the positive and negative impacts of IGFBP-3 on IGF-IR activation in tumor development and progression.

Materials and Methods

Case selection and TMA construction

Archived formalin-fixed, paraffin-embedded normal/preneoplastic tissue samples and tumor samples resected from patients with NSCLC were obtained from the previously described tissue bank at The University of Texas M.D. Anderson Cancer Center (10). Tissue specimens had been collected between 1997 and 2003 from 353 lung tumors (234 adenocarcinomas and 119 squamous cell carcinomas) and were classified according to the 2004 World Health Organization classification system (20).

To assess the immunohistochemical (IHC) expression of IGF-I, IGF-II, and phosphorylated IGF-IR (pIGF-IR)/IR in the early pathogenesis of NSCLC, we studied formalin-fixed, paraffin-embedded material placed in TMA from 52 normal bronchial epithelia, 61 bronchial hyperplasias, and 32 squamous dysplasia and carcinomas *in situ* as well as 52 normal alveoli, 37 atypical adenomatous hyperplasias, and four cases of alveolar bronchiolization. After histological examination, TMA were constructed from selected NSCLC specimens by obtaining three 1-mm-diameter cores from each tumor. The clinicopathological features of lung cancer cases studied are shown in Supplemental Table 1 (published on The Endocrine Society's Journals Online web site at http://endo.endojournals.org).

IHC staining and evaluation of TMA

IHC staining procedures were performed as described previously (10). Cytoplasmic expression was blindly analyzed and quantified by two independent pathologists (P.Y. and I.I.W.), who were also unaware of the patients' outcomes, using a four-value scale of staining intensity (0, 1+, 2+, and 3+) and a percentage (0–100%) for extent of reactivity. A final cytoplasmic expression score was obtained by multiplying the intensity and extent of reactivity values (range, 0–300). Nuclear expression was quantified on a range of 0–100, according to the percentage of positive nuclei among all tumor or epithelial cells present in the TMA core specimens. The antibodies used for the staining were the following: IGF-I (Santa Cruz Biotechnology, Santa Cruz, CA), IGF-II (Upstate/Millipore, Billerica, MA), IGFBP-3 (Diagnostic Systems Laboratories, Webster, TX), and pIGF-IR/IR (Invitrogen, Carlsbad, CA).

Mice

Mice carrying lung-specific human IGF^{Tg} in *FVB/NJ* background were described previously (10, 21). Briefly, IGF^{Tg} mice convey the DNA encoding 3.7 kb of human surfactant protein C gene promoter region followed by the cDNA of human *IGF-I* and express human IGF-I (hIGF-I) in alveolar type II cells of lung, not in the plasma. Germline mutant *IGFBP-3* mice (12) were a gift from Dr. John Pintar (Rutgers University, Piscataway, NJ).

The *IGFBP-3* null mutation was transferred to *FVB/NJ*-background mice via backcrossing six times. Male *IGFBP-3* heterozygous mutant *IGF* transgenic ($BP3^{+/-}$;IGF^{Tg}) mice were mated to female *IGFBP-3* heterozygous ($BP3^{+/-}$) mice to produce the following six genotypes: $BP3^{+/+}$, $BP3^{+/-}$, $BP3^{-/-}$, $BP3^{+/+}$;IGF^{Tg}, $BP3^{+/-}$;IGF^{Tg}, and $BP3^{-/-}$;IGF^{Tg}. *IGF* transgene genotyping was performed as previously described (10, 21). An *IGFBP-3* forward primer, an *IGFBP-3* reverse primer, and a *Neo* reverse primer (TGTCCTCACTCCTATCTGGGA, ACTCCAGGGACTCTGGTCTTC, and TCGGCAGGAGCAAGGTGAGAT, respectively) were used for *IGFBP-3* genotyping. All mouse maintenance and experiments were performed according to a protocol preapproved by M.D. Anderson's Institutional Animal Care and Use Committee.

Histology and IHC of mouse lung tissues

At age 14–15 months, mice were euthanized for pathological examination of their lungs. Lung tissue specimens were fixed in formalin, dehydrated, and processed for embedding in paraffin. Every 20th 5-μm section of the paraffin blocks (20 sections total per mouse) was evaluated after hematoxylin and eosin staining by two pathologists including one animal pathologist. Adenoma and adenocarcinoma were diagnosed according to histological criteria described previously (10).

Statistical analysis

Statistical analysis of IGF-I, IGF-II, IGFBP-3, and pIGF-IR/IR expression levels was performed according to patient baseline characteristics. The independent-samples *t* test or ANOVA test were used to compare these expressions in different subgroups defined by categorical variables. Pearson correlation coefficient was used to estimate the correlation between the IGF-I/II and pIGF-IR/IR expression scores. The Student's *t* test and Fisher exact test were performed to compare the lung tumor development in mice. All of the statistical tests performed were two sided, and *P* values ≤ 0.05 were considered statistically significant. If the *P* value was >0.05 but <0.10, we considered the difference to represent a trend in the data and noted this trend. All analyses were conducted using SAS (SAS Institute, Cary, NY) or SPSS (SPSS, Chicago, IL).

ELISA

Serum levels of murine IGF (mIGF) and IGFBP-3 (mIGFBP-3) were measured by using a sandwich method with the following antibodies: antimouse IGF-I, biotinylated antimouse IGF-I, antimouse IGFBP-3, and biotinylated antimouse IGFBP-3 (R&D Systems, Minneapolis, MN; FAF02, BAF791, MAB775, and BAF775, respectively). The ELISA plate and avidin/*para*-nitrophenylphosphate were obtained from Corning (Lowell, MA) and Invitrogen, respectively. The sensitivities of the ELISAs were 0.3 and 4 ng/ml for mIGF and mIGFBP-3, respectively. The serum IGF was extracted by using a standard acid-ethanol extraction method (22). No cross-reactivity between hIGF and mIGF was observed.

Results

IGF axis protein expression is associated with lung cancer

We have shown overexpression of IGF (IGF-I and -II) and pIGF-IR/IR in human preneoplastic bronchial epithelial lesions and in lung tumors formed in mice with lung-specific overexpression of IGF-I (10), suggesting that an increase in autocrine IGF level and subsequent activation of IGF-IR are common events in the early stages of lung cancer development. These findings led us to hypothesize that tissue-derived IGF could promote progression of lung cancer. To test the hypothesis, we performed IHC analysis to evaluate expression of IGF in TMA, which were composed of 353 biopsy specimens of lung adenocarcinoma (n = 234) and squamous cell carcinoma (n = 119) and the adjacent normal tissues. A summary of the clinicopathological features of this study with the staining is described in Supplemental Table 1. Consistent with previous findings (10), IGF-I and -II staining was primarily cytoplasmic (Fig. 1). Although IGF-I staining was not associated with age, sex, or race of the patients (Supplemental Table 2), IGF-II staining was associated with gender, with a higher level in male patients. Interestingly, the expression level of IGF-I was significantly higher in NSCLC tissues than in normal tissue specimens, whereas IGF-II staining did not show such difference (Fig. 2A).

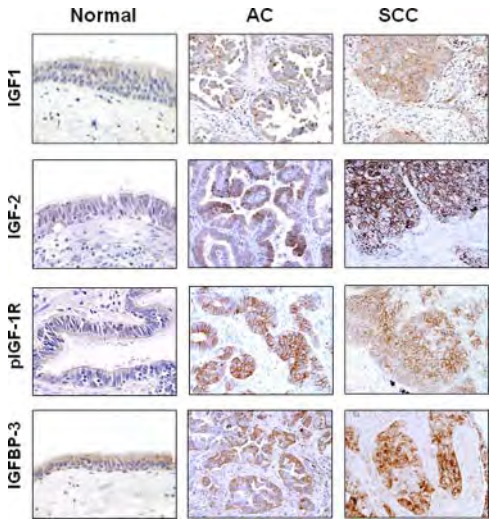

FIG. 1. Expression of IGF-I, IGF-II, pIGF-IR, and IGFBP-3 in specimens of human NSCLC. Adenocarcinomas (AC), squamous cell carcinomas (SCC), and adjacent normal tissues are shown after IHC staining.

To assess whether the increased levels of IGF were associated with activation of IGF-IR, we performed IHC analysis in the same cohort of NSCLC patients using an antibody against pIGF-IR/IR (Tyr^{1131}/Tyr^{1146}); staining appeared in the cell membrane and/or cytoplasm in 35.4% of the specimens (102 of 288 cases) (Fig. 1). Expressions of IGF-I, but not IGF-II, were significantly correlated with levels of pIGF-IR/IR staining in the membrane suggests that tissue-derived IGF-I could, in part, account for activation of IGF-IR/IR in NSCLC. However, the correlation was not robust (Fig. 2B), suggesting that other factors could have been involved in the regulation of IGF-IR/IR phosphorylation in NSCLC. In addition to the well-

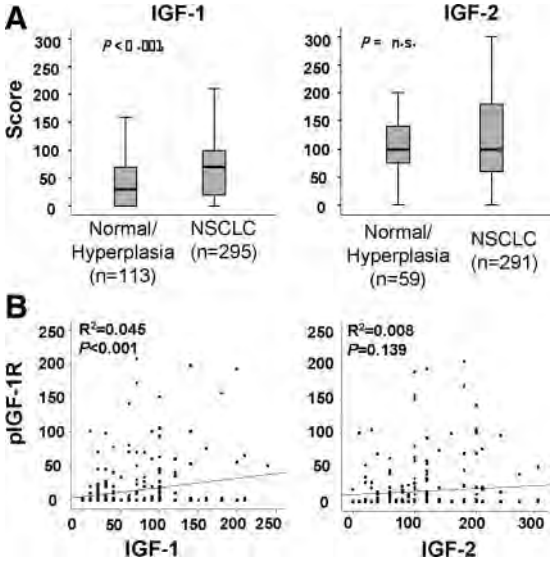

FIG. 2. IGF-I and IGF-II expression and IGF-IR activation in NSCLC. A, Expression of IGF-I and IGF-II in cancer specimens and normal/hyperplastic lung tissues; B, correlation among IGF-I, IGF-II, and pIGF-IR/IR expression levels. Positive correlations were observed between IGF-I and pIGF-IR/IR but not between IGF-II and pIGF-IR/IR. n.s., Not significant; R^2, Pearson's coefficient.

known function in regulating bioavailability of IGF, IGFBP-3 is believed to potentiate IGF-I-induced signaling and proliferative activities depending on cellular context (23). However, the stimulatory effects of IGFBP-3 has remained elusive in NSCLC. Hence, we evaluated IGFBP-3 expression in the same specimens and assessed correlation between levels of staining for pIGF-IR/IR and IGFBP-3. We observed that the specimen that expresses IGFBP-3 at the highest quartile expresses greater pIGF-IR/IR than do the specimens at first or second to third quartile (Fig. 3). This result suggests a possibility that high expression of IGFBP-3 is associated functionally with activated IGF-IR/IR signaling in NSCLC.

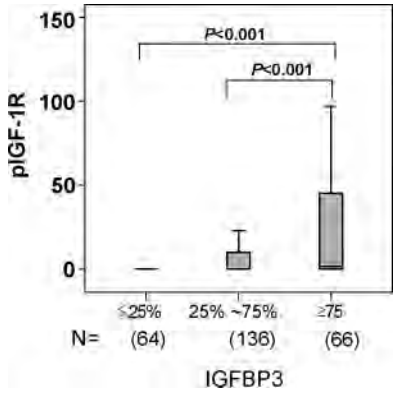

FIG. 3. Elevated pIGF-IR/IR expression in higher IGFBP-3-expressing NSCLC specimens. The box plot shows pIGF-IR/IR expression levels among 266 cases of NSCLC. The specimen with the highest quartile expression of IGFBP-3 (n = 66, ≥75%) showed significantly higher pIGF-IR/IR expression compared with the specimen with the lowest quartile expression of IGFBP-3 (n = 64, ≤25%) or medium expression of IGFBP-3 (n = 136, 25–75%). The *boxes* represent the central two quartiles (first and third quartiles), and the *bar within the box* represents the median value of pIGF-IR/IR staining.

Circulating IGF-I level is dependent on level of IGFBP-3 expression but does not determine level of IGF-IR activation in peripheral lung tissues

IGFBP-3 has been suggested to induce both inhibition and potentiation of IGF activity, whereas results from *in vivo* studies largely support the concept that IGFBP-3 enhances IGF activity by providing a stable serum reservoir of bioactive IGF-I (16, 24). Given the controversial findings on the impact of IGFBP-3 on IGF action in tumor development (13–15), we decided to investigate the role of IGFBP-3 in lung pathogenesis promoted by tissue-derived IGF in a more defined system using a transgenic mouse model. To this end, we generated mice with lung-specific IGF-I overexpression and variable levels of IGFBP-3 expression. The breeding scheme and nomenclature of the mice in this study are shown in Fig. 4A. Offspring genotypes occurred at expected Mendelian ratios; the offspring were fertile and had normal growth rates, suggesting that the genetic changes did not alter normal development. We first determined whether germline deletion of *IGFBP-3* resulted in changes in the levels of IGFBP-3 and IGF in circulation. A mouse IGFBP-3-specific ELISA showed no detectable levels of IGFBP-3 in the serum of $BP3^{-/-}$ and $BP3^{-/-}$;IGF^{Tg} mice (Fig. 4B) as expected. $BP3^{+/-}$ and $BP3^{+/-}$;IGF^{Tg} mice, which lost one allele of the *IGFBP-3* gene, had approximately 50% lower serum levels of IGFBP-3 than wild-type ($BP3^{+/+}$) mice. A mouse IGF-specific ELISA revealed that the serum levels of mIGF-I in $BP3^{+/-}$ and $BP3^{-/-}$ mice were about 80 and 45% of those in the $BP3^{+/+}$ mice, respectively, regardless of the lung-specific expression of the human *IGF-I* transgene (Fig. 3C). The serum levels of hIGF-I in the IGF^{Tg} mice were under the detection limit (6 ng/ml), indicating no significant hIGF-I secretion into circulation (data not shown). Thus, we had six cohorts with three expression levels of systemic IGF-I and IGFBP-3, with or without the lung-specific *IGF-I* transgene, as summarized in Supplemental Table 3. We examined the expression levels of pIGF-IR/IR in the lungs of these six mice groups. IHC staining analysis of pIGF-IR and IGF-IR on the lung tissues revealed that pIGF-IR staining levels normalized by that of total IGF-IR levels in the $BP3^{+/-}$;IGF^{Tg} mice group were greatest among all of the groups (Supplemental Fig. 1 and Fig. 4D), suggesting the partial loss of IGFBP-3 was more effective in activating IGF-IR than was the complete loss of IGFBP-3.

Impact of variable levels of IGFBP-3 on the effects of tissue-derived IGF-I in lung tumor development

We assessed whether changes in IGFBP-3 expression affect lung tumor development and progression in IGF^{Tg}

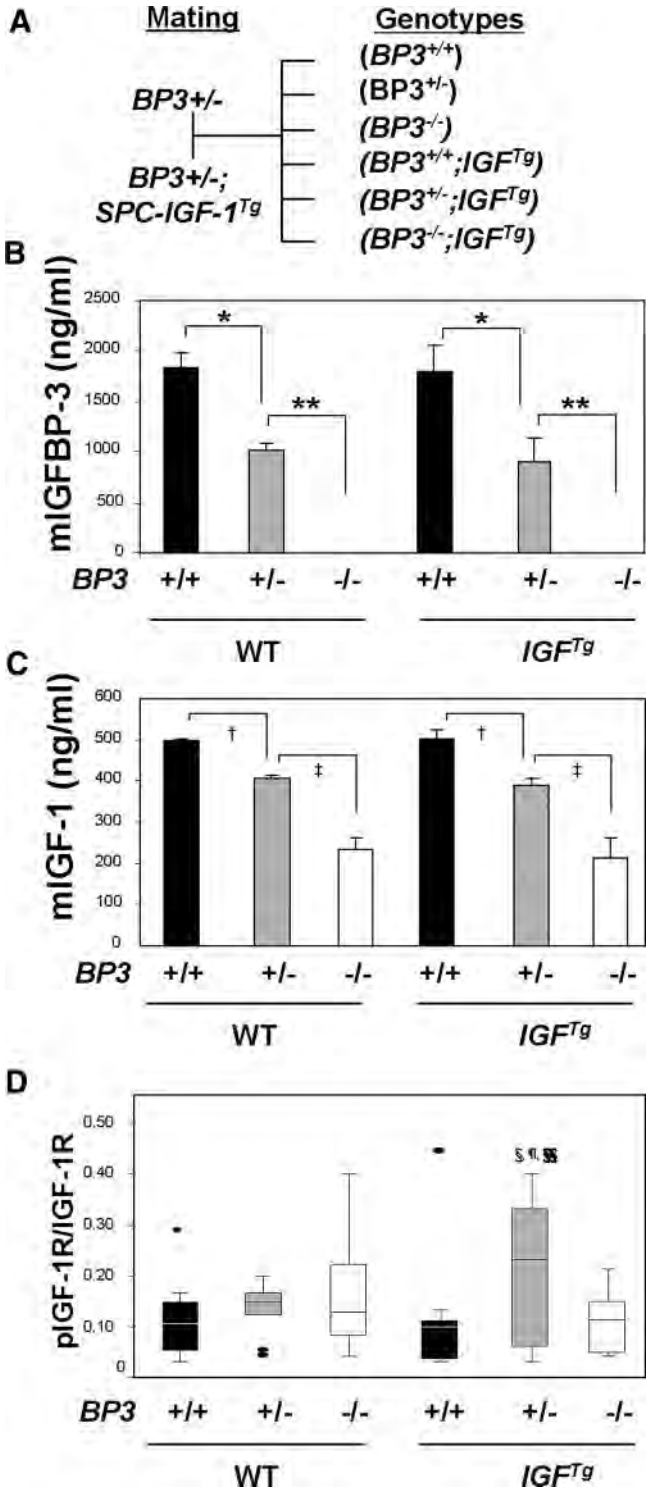

FIG. 4. The status of IGF and IGFBP-3 concentrations in serum and IGF-IR/IR activation in lungs of *IGF* transgenic and *IGFBP-3*-null mice. A, Schematic of mating strategy used to get mice with the six genotypes of *IGF* and *IGFBP-3*; n = 4 in each group, triplicate samples. B, Expression level of IGFBP-3 in serum. *, $P < 0.01$; **, $P < 0.001$. C, Circulating expression levels of mIGF. †, $P < 0.01$; ‡, $P < 0.001$; n = 4 in each group, triplicate samples. D, IHC analysis of total IGF-IR and pIGF-IR expression on bronchial epithelium. Blindly scored expression levels of pIGF-IR *vs.* IGF-IR are plotted for the mice genotypes. Each *bar* represents median, quartile, and range. Student's *t* test was used to obtain *P* values (§, ¶, §§, $P < 0.05$ compared with $BP3^{+/+}$, $BP3^{+/-}$;IGF^{Tg}, and $BP3^{-/-}$;IGF^{Tg}, respectively); n = 10 in each group. WT, Wild type.

mice. Because the tumor incidence in *FVB*-background mice increases with age (25), we ensured that the mice in each group were comparable in age at the time of analysis. Because a few IGF^{Tg} mice develop benign tumors (adenoma) at over 1 yr of age (10, 21), we evaluated 14- to 15-month-old mice. Gross appearance of representative dissected lungs is shown in the *left panels* of Fig. 5. We were able to find several small lung tumors across all genotypes, including control mice, consistent with previous findings in age-matched mice with *FVB* background (25). The tumors in the wild-type mice were small and all ad-

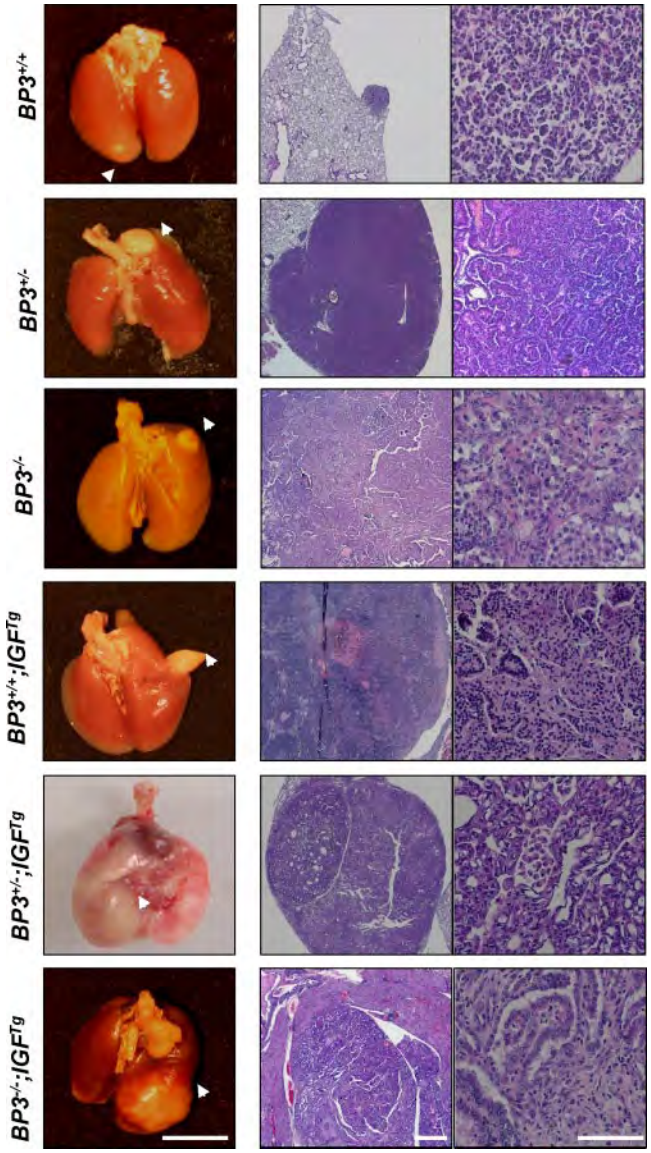

FIG. 5. Lung tumor development in *IGFBP-3* mutant and/or IGF^{Tg} mice. Profiles of spontaneous lung adenocarcinomas from 14- to 15-month-old *IGFBP-3* mutant and/or IGF^{Tg} mice. All tumors were histologically evaluated after sectioning and hematoxylin and eosin staining. *Top* ($BP3^{+/+}$), Papillary adenomas; all others, adenocarcinomas. Magnification, ×4 (*left panels*), ×25 (*middle panels*), and ×400 (*right panels*). Notable are the invasive cancer cells in $BP3^{+/-}$;IGF^{Tg} and $BP3^{-/-}$;IGF^{Tg} mice. *Scale bars*, 3 mm (*left panels*), 200 μm (*middle panels*), and 100 μm (*right panels*).

enomas (Fig. 5, *top*). Tumors larger than 3 mm in diameter and histological feature of adenocarcinoma were observed only in mice with the *IGF* transgene with and without the *IGFBP-3* deletion mutation (Fig. 5). Intensive quantitative and pathological microscopic analysis of the lungs of mice (n = 305) of all six genotypes ($BP3^{+/+}$, $BP3^{+/-}$, $BP3^{-/-}$, $BP3^{+/+}$;IGF^{Tg}, $BP3^{+/-}$;IGF^{Tg}, and $BP3^{-/-}$;IGF^{Tg}; n = 49, 53, 46, 82, 34, and 41, respectively) revealed that mice with *IGF-I*^{Tg} and/or the *IGFBP-3* deletion mutation had a greater incidence of spontaneous lung tumors than $BP3^{+/+}$ mice (Fig. 6A). Furthermore, $BP3^{+/-}$;IGF^{Tg} mice showed the greatest tumor incidence and multiplicity (Fig. 6, A and B) than any of the other genotypes. Specifically, they showed a significantly greater mean tumor multiplicity than did $BP3^{+/+}$;IGF^{Tg} ($P < 0.05$) or $BP3^{-/-}$;IGF^{Tg} ($P < 0.01$) mice, suggesting that IGF-I-induced lung tumor formation is enhanced by reduction, but not complete loss, of IGFBP-3 expression. To assess the impact of IGFBP-3 levels on IGF-I-promoted lung tumor progression, we performed histopathological analysis of tumor tissues from mice in the six cohorts. No adenocarcinomas were observed in the $BP3^{+/+}$ mice, whereas mice from all other groups had developed adenocarcinomas and adenomas at the time of dissection. Consistent with their having the greatest tumor incidence and multiplicity, the $BP3^{+/-}$;IGF^{Tg} mice exhibited the most frequent incidence and multiplicity of adenocarcinomas (Fig. 5, C and D).

Impact of variable levels of IGFBP-3 on adenocarcinoma progression in mice with lung-specific IGF-I overexpression

Upon finding that pIGF-IR was activated by tissue IGF expression or loss of one *IGFBP-3* allele, we questioned whether the effect of IGF-IR signaling on lung cancer is at the initiation of lung carcinogenesis or at progression to lung cancer. To address this question, we explored the impact of changes in IGFBP-3 expression on lung cancer development initiated by the tobacco carcinogen NNK. Mice were treated with NNK (3 μmol, ip, once a week for 7 wk) from 8 months of age, and the resulting tumors were examined 6 months later (Fig. 6). The incidence of neoplastic lesions (hyperplasia, adenoma, and adenocarcinoma) reached 80–90% and did not differ significantly among the six genotypes (Fig. 7A). The NNK exposure enhanced lung cancer development in $BP3^{+/-}$, $BP3^{-/-}$, $BP3^{+/-}$;IGF^{Tg}, and $BP3^{-/-}$;IGF^{Tg} mice; NNK-treated mice showed about 2- to 3-fold increases in incidence and multiplicity of adenocarcinomas compared with untreated mice (compare Figs. 6 and 7). In contrast, NNK-exposed $BP3^{+/+}$ and $BP3^{+/+}$;IGF^{Tg} mice showed no detectable difference in tumor progression compared with the unexposed mice. Consistent with their having the greatest spontaneous tumor incidence and multiplicity (Fig. 6), $BP3^{+/-}$;IGF^{Tg} mice revealed the greatest malignant tumor (adenocarcinoma) development than did any other genotype. However, the difference from the $BP3^{-/-}$;IGF^{Tg} mice did not reach statistical significance. It is possible that the advantage in tumor development in the $BP3^{+/-}$;IGF^{Tg} mice over the $BP3^{-/-}$;IGF^{Tg} mice was lost in the NNK-induced cancer formation, or the difference was simply because the size of the experimental group was not big enough to reveal the difference (total 88 in the NNK-

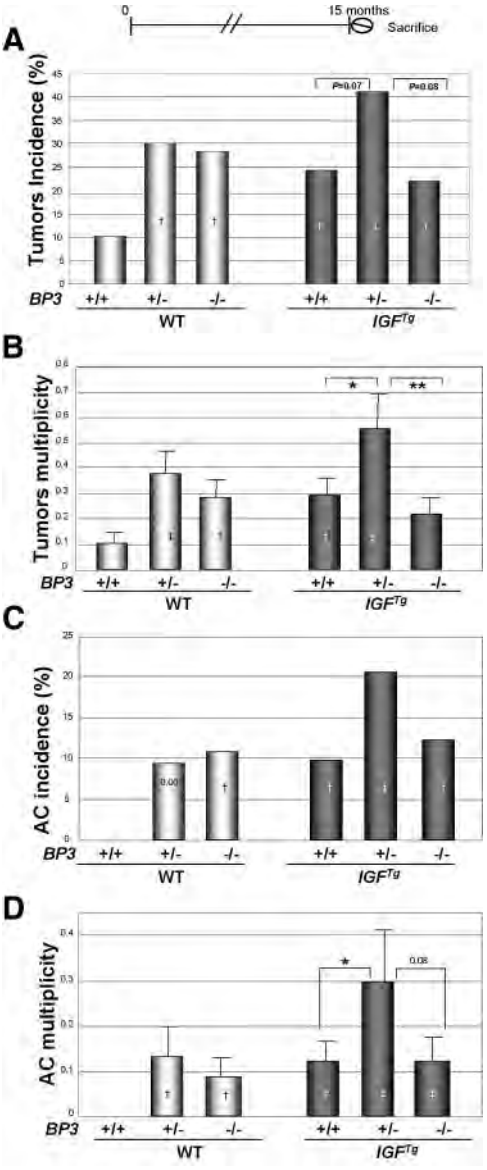

FIG. 6. Expression of *IGF* and *IGFBP-3* and lung tumor development. A, Incidence (percentage) of tumor [adenoma plus adenocarcinoma (AC)] formation per mouse; B, multiplicity of tumors per mouse; C, incidence (percentage) of AC formation per mouse; D, multiplicity of AC per mouse. The Fisher exact test (incidence) and Student's *t* test (multiplicity) were used to obtain *P* values. †, $P < 0.05$; ‡, $P < 0.01$ compared with $BP3^{+/+}$; *, $P < 0.05$; **, $P < 0.01$ compared with $BP3^{+/+}$;IGF^{Tg} or $BP3^{-/-}$;IGF^{Tg}, respectively. *P* values >0.05 but <0.1 are noted. WT, Wild type.

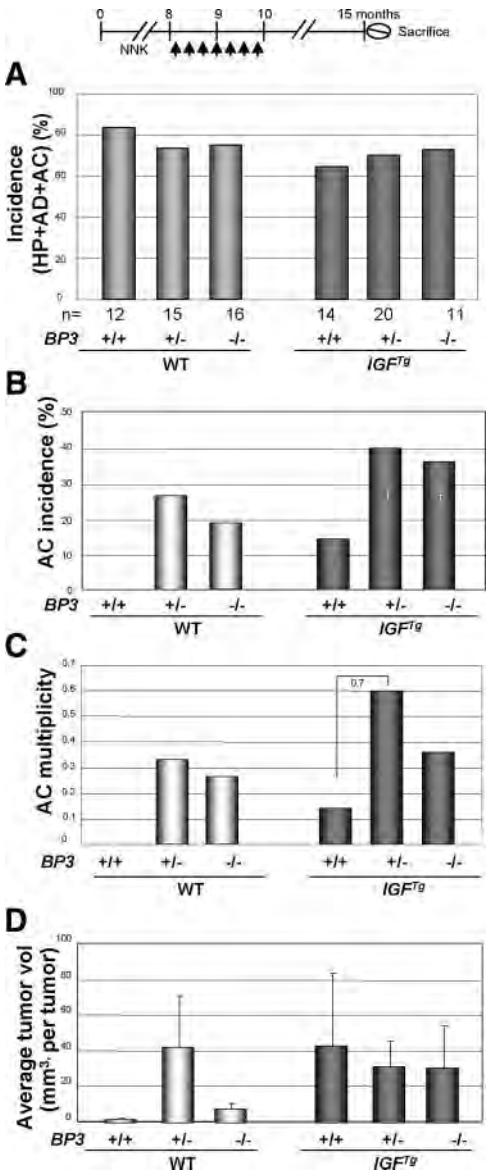

FIG. 7. Expression of IGF and IGFBP-3 and lung tumor promotion. A, The incidence of pathological lesions including hyperplasia (HP), adenomas (AD), and adenocarcinomas (AC) in mice treated with NNK are combined and shown by genotype; B and C, incidence (percentage) (B) and multiplicity (C) of AC formation per mouse (*, $P < 0.05$; P values >0.05 but <0.1 are noted); D, the average volume of the tumors. The Fisher exact test (incidence) and Student's t test (multiplicity and average tumor volume) were used to obtain P values. (†, $P < 0.05$; ‡, $P < 0.01$ compared with $BP3^{+/+}$; *, $P < 0.05$, compared with $BP3^{+/+}$;IGF^{Tg}; P values >0.05 but <0.1 are noted). WT, Wild type.

treated group in Fig. 7, and a total of 305 were used in the spontaneous tumor group in Fig. 6).

The facts that IGF-IR activation was strongest and the lung tumor development and progression are greatest in the $BP3^{+/-}$;IGF^{Tg} mice (Figs. 4D, 6A, and 7B) clearly indicate that neither high level of expression nor complete depletion of IGFBP-3 promotes activation of IGF-IR and development of lung cancer. Notably, average tumor volume did not show a significant difference among the IGF^{Tg}, $BP3^{+/-}$;IGF^{Tg}, and $BP3^{-/-}$;IGF^{Tg} mice (Fig. 7D), suggesting that reduced levels of IGFBP-3 expression are implicated in the progression but not the growth of lung tumors.

Discussion

IGFBP-3 has been associated with both inhibitory and stimulating activity of proliferation and apoptosis in a variety of human cancer cells (26–32). Several *in vitro* studies have noted switches of IGFBP-3 bioactivity from antiproliferative to proliferative (33, 34) or from proapoptotic to antiapoptotic (35, 36). Hence, characterization of IGFBP-3's impact on cell proliferation and apoptosis is an area of active research. This study shows *in vivo* evidence that IGFBP-3 can have stimulatory or inhibitory effects on IGF bioactivity and tumor formation and progression in the lung depending on its expression level. Through the use of tumor samples from patients with NSCLC, we found that 1) the levels of tissue-derived IGF-I significantly correlated with pIGF-IR/IR in tumor samples from patients with NSCLC, although the correlation was not robust, and 2) IGFBP-3 expression levels positively correlated with pIGF-IR/IR expression. Through the use of lung-specific *IGF-I* transgenic mice (21) in which expression of IGFBP-3 was suppressed by knocking out the *IGFBP-3* genes, we further demonstrated that IGFBP-3 has a positive and a negative role in IGF-I actions and lung carcinogenesis depending on its expression level. It is likely that, if expressed at physiological levels, IGFBP-3 binds to IGF, leading to suppression of IGF actions on cell proliferation. When expressed at the decreased levels, IGF should be rapidly released from IGFBP-3, resulting in activation of the IGF-IR pathway. When IGFBP-3 is completely lost, however, IGF-I, which requires IGFBP-3 for stability, is degraded quickly, leading to IGF-IR inactivation.

Several investigations have shown the importance of IGF-IR signaling in the development of human cancers. A case-control study using samples from lung cancer patients and control subjects showed that high plasma levels of IGF-I were associated with an increased risk of lung cancer (4). A prospective cohort study, however, did not support the importance of circulating IGF-I and IGFBP-3 in lung cancer risk (8, 9). The inconsistency of these findings could be due to the fact that local production of IGF was not considered in those analyses. Our previous and current findings show that 1) expression of IGF and an associated activation of IGF-IR/IR were significantly increased in human bronchial preneoplastic (10) and NSCLC specimens compared with normal bronchial tis-

sue samples, and 2) lung tumor formation and progression is increased in mice with lung-specific IGF^{Tg}, especially when exposed to tobacco carcinogens (10).

Because tissue IGF bioactivity is regulated in large part by IGFBP-3, IGFBP-3 has been expected to be a major determinant of IGF action. Indeed, the case-control retrospective and prospective studies have found inverse correlations between circulating levels of IGFBP-3 and the risk of developing lung cancer (4, 8). IGFBP-3 has also been shown to suppress the activity of IGF-I at the tissue level *in vitro* and *in vivo* (37). We have demonstrated that overexpression of IGFBP-3 introduced by an adenoviral vector suppresses IGF-IR activation and induces apoptosis in NSCLC cells *in vitro* and *in vivo* (26). These findings indicate the inhibitory effects of IGFBP-3 on the action of IGF-I in cancer. However, occasional positive correlation between circulating IGFBP-3 and premenopausal breast cancer has been reported (38, 39). Furthermore, there is ample evidence for high expression of IGFBP-3 in a variety of cancer types, including breast, prostate, and renal cancers (40–43). Moreover, tumor size or a malignant phenotype correlate with IGFBP-3 expression levels in a number of cancers (36, 40, 42, 44, 45). These controversial findings could have been due to the complex role of IGFBP-3 in IGF-I action (46, 47) and IGF-independent suppressive effects on cell growth (48) as well as its procancerous activity regardless of its role in regulating bioavailability of IGF (23, 49).

In the present study, we show high tissue expression of IGFBP-3 in a positive correlation with pIGF-IR level in NSCLC, suggesting that increased levels of IGFBP-3 could be implicated in the activation of IGF-IR. Because the antibody we used for the human TMA for pIGF-IR detection recognizes the activated form of both IGF-IR and IR, it is possible that the signaling we observed includes the activated form of IR. IGF-IR and IR, which form heterodimers and can be activated by IGF, are closely related in structure (50) and function (51–53). Hence, the positive correlation between expression levels of IGFBP-3 and pIGF-IR/IR in NSCLC shown in the current study suggests that increased levels of IGFBP-3 could have played a positive role in activation of the IGF signaling pathway.

To determine the actual impact of IGFBP-3 expression on the bioactivity of IGF-I and lung tumorigenesis, we established a mouse model with various levels of IGFBP-3 expression (normal, reduced, and absent) by mating IGF^{Tg} mice (21) with *IGFBP-3* knockout mice. We observed that 50% ($BP3^{+/-}$) or complete loss ($BP3^{-/-}$) of IGFBP-3 expression led to reduction in serum level of IGF-I by about 19–23 or 54–58%, respectively. Given that 80% of circulating IGF bind to IGFBP-3 (16), decreases of less than 60% in the level of circulating IGF-I in the $BP3^{-/-}$ mice indicated possible compensation by other IGFBP family members. However, we were not able to detect any compensatory increase of IGFBP, including IGFBP-2 and -4, in $BP3^{+/-}$ and $BP3^{-/-}$ mice (data not shown). Nevertheless, given a previous finding of significantly delayed carcinogenesis/cancer cell growth in liver-specific IGF-null mice (13), which had only 10–25% of the normal serum IGF level, we expected that the 19–58% reduction in the level of circulating IGF-I would suppress lung cancer development. However, the mice with reduced or loss of IGFBP-3 expression ($BP3^{+/-}$, $BP3^{-/-}$) had obviously greater overall tumor incidence and multiplicity than in the wild-type mice ($BP3^{+/+}$) mice. These results, which contradict previous reports showing a positive correlation between circulating IGF-I and cancer development (54), indicate the importance of tissue-derived (rather than serum) IGF-I in its bioavailability in lung epithelial cells during the process of lung tumor formation. The increased tumor incidence in $BP3^{+/-}$ and $BP3^{-/-}$ mice compared with that in $BP3^{+/+}$ mice could have resulted from the decrease or loss of IGFBP-3's IGF-I-independent antiproliferative activity, but the greater tumor development and progression in $BP3^{+/-}$ mice than in $BP3^{-/-}$ mice does not support that notion. Our observations, including 1) the increased tumor incidence and multiplicity in $BP3^{+/-}$ mice, especially when IGF-I was overexpressed in the lung, and 2) the accelerated tumor progression in $BP3^{+/-}$;IGF^{Tg} mice compared with $BP3^{+/+}$;IGF^{Tg} mice or $BP3^{-/-}$;IGF^{Tg} mice provide novel *in vivo* evidence that support a significant role for IGFBP-3 in potentiating IGF action.

The accelerated tumor progression in $BP3^{+/-}$;IGF^{Tg} mice could have resulted simply from accelerated transformation of lung epithelial cells and/or enhanced initiation and promotion of lung tumors owing to activation of IGF-IR. However, $BP3^{+/-}$;IGF^{Tg} mice had the greater multiplicity of adenocarcinomas with local invasion than did $BP3^{+/+}$;IGF^{Tg} mice or $BP3^{-/-}$;IGF^{Tg} mice after lung tumor initiation was synchronized by NNK injection. These findings strongly imply a role of IGFBP-3 in both lung tumor formation and progression. The advanced pathogenesis in $BP3^{+/-}$;IGF^{Tg} mice can be explained by increased net tissue bioavailability of IGF-I regardless of the loss of circulating IGF-I as a benefit from partial depletion of tissue levels of IGFBP-3. Supporting this hypothesis is our finding that $BP3^{+/-}$;IGF^{Tg} mice had greater IGF-IR activation than did $BP3^{+/+}$;IGF^{Tg} mice. However, the more severe phenotype and the greater IGF-IR activation in $BP3^{+/-}$;IGF^{Tg} mice than in $BP3^{-/-}$;IGF^{Tg} mice supports the protective role of IGFBP-3 in IGF action; *e.g.* the complete loss of IGFBP-3 could have resulted in the suppression of IGF signaling. These results

emphasize the critical function of IGFBP-3 as a reservoir for IGF bioactivity as suggested by the previous reports in certain contexts (16, 24). Another possible explanation is that IGFBP-3 mediates procancer activity through unknown novel mechanisms independent of its modulation of IGF signaling. Indeed, IGFBP-3 directly interacts with the integrin or caveolin and propagates the mitotic signal downstream (49). Nevertheless, these findings suggest that IGFBP-3 can either suppress or enhance lung tumor formation and progression depending on the level of expression.

In summary, our findings using human patient tumor specimens and an *in vivo* mouse system demonstrate that 1) expression of IGF-I is higher in NSCLC than in normal tissue, 2) lung tumor development and progression are mainly regulated by levels of tissue-derived IGF-I but not circulating IGF-I, 3) decreased but not completely absent expression of IGFBP-3 elevates local availability of IGF-I in lung tissue and increases the risk of lung cancer, and 4) IGFBP-3 may not only suppress but also enhance IGF-I actions on and risk of developing lung cancer. In light of these issues, further studies with liver- and lung-specific IGFBP-3-null mice are warranted to confirm the role of IGFBP-3 in lung cancer development. Our findings also indicate that attempts to modulate serum or tissue levels of IGFBP-3 in cancer therapy must be approached with caution.

Acknowledgments

Address all correspondence and requests for reprints to: Ho-Young Lee, Ph.D., College of Pharmacy, Seoul National University, Sillim 9 Dong, 599 Kwanakro, Kwanak-Gu, Seoul 151-742, Korea. E-mail: hylee135@snu.ac.kr.

This work was supported by National Institutes of Health Grants R01 CA109520 and CA100816-01A1 (to H.-Y. L.) and in part by grants from the National Foundation for Cancer Research, the Department of Defense, the VITAL program (W81XWH-04-1-0142), and the BATTLE program (W81XWH-06-1-0303) (to W.-K.H.).

Current address for M.-J.K.: Department of Pathology, University of Ulsan College of Medicine, Asan Medical Center, Seoul 138-736, Korea.

Disclosure Summary: The authors do not have any conflicts of interest to disclose.

References

1. **Yakar S, Liu JL, Stannard B, Butler A, Accili D, Sauer B, LeRoith D** 1999 Normal growth and development in the absence of hepatic insulin-like growth factor I. Proc Natl Acad Sci USA 96:7324–7329
2. **Pollak MN** 2004 Insulin-like growth factors and neoplasia. Novartis Found Symp 262:84–98; discussion 98–107, 265–108
3. **Pollak M** 2008 Insulin and insulin-like growth factor signalling in neoplasia. Nat Rev Cancer 8:915–928
4. **Yu H, Spitz MR, Mistry J, Gu J, Hong WK, Wu X** 1999 Plasma levels of insulin-like growth factor-I and lung cancer risk: a case-control analysis. J Natl Cancer Inst 91:151–156
5. **Chan JM, Stampfer MJ, Giovannucci E, Gann PH, Ma J, Wilkinson P, Hennekens CH, Pollak M** 1998 Plasma insulin-like growth factor-I and prostate cancer risk: a prospective study. Science 279:563–566
6. **Hankinson SE, Willett WC, Colditz GA, Hunter DJ, Michaud DS, Deroo B, Rosner B, Speizer FE, Pollak M** 1998 Circulating concentrations of insulin-like growth factor-I and risk of breast cancer. Lancet 351:1393–1396
7. **Ma J, Pollak M, Giovannucci E, Chan JM, Tao Y, Hennekens C, Stampfer MJ** 2000 A prospective study of plasma levels of insulin-like growth factor I (IGF-I) and IGF-binding protein-3, and colorectal cancer risk among men. Growth Horm IGF Res 10(Suppl A):S28–S29
8. **London SJ, Yuan JM, Travlos GS, Gao YT, Wilson RE, Ross RK, Yu MC** 2002 Insulin-like growth factor I, IGF-binding protein 3, and lung cancer risk in a prospective study of men in China. J Natl Cancer Inst 94:749–754
9. **Lukanova A, Toniolo P, Akhmedkhanov A, Biessy C, Haley NJ, Shore RE, Riboli E, Rinaldi S, Kaaks R** 2001 A prospective study of insulin-like growth factor-I, IGF-binding proteins-1, -2 and -3 and lung cancer risk in women. Int J Cancer 92:888–892
10. **Kim WY, Jin Q, Oh SH, Kim ES, Yang YJ, Lee DH, Feng L, Behrens C, Prudkin L, Miller YE, Lee JJ, Lippman SM, Hong WK, Wistuba II, Lee HY** 2009 Elevated epithelial insulin-like growth factor expression is a risk factor for lung cancer development. Cancer Res 69:7439–7448
11. **Firth SI, Kaufman PL, De Jean BJ, Byers JM, Marshak DW** 2002 Innervation of the uvea by galanin and somatostatin immunoreactive axons in macaques and baboons. Exp Eye Res 75:49–60
12. **Ning Y, Schuller AG, Bradshaw S, Rotwein P, Ludwig T, Frystyk J, Pintar JE** 2006 Diminished growth and enhanced glucose metabolism in triple knockout mice containing mutations of insulin-like growth factor binding protein-3, -4, and -5. Mol Endocrinol 20:2173–2186
13. **Wu Y, Yakar S, Zhao L, Hennighausen L, LeRoith D** 2002 Circulating insulin-like growth factor-I levels regulate colon cancer growth and metastasis. Cancer Res 62:1030–1035
14. **Wu X, Tortolero-Luna G, Zhao H, Phatak D, Spitz MR, Follen M** 2003 Serum levels of insulin-like growth factor I and risk of squamous intraepithelial lesions of the cervix. Clin Cancer Res 9:3356–3361
15. **Silha JV, Sheppard PC, Mishra S, Gui Y, Schwartz J, Dodd JG, Murphy LJ** 2006 Insulin-like growth factor (IGF) binding protein-3 attenuates prostate tumor growth by IGF-dependent and IGF-independent mechanisms. Endocrinology 147:2112–2121
16. **Baxter RC** 1994 Insulin-like growth factor binding proteins in the human circulation: a review. Horm Res 42:140–144
17. **Yu H, Rohan T** 2000 Role of the insulin-like growth factor family in cancer development and progression. J Natl Cancer Inst 92:1472–1489
18. **Wakai K, Ito Y, Suzuki K, Tamakoshi A, Seki N, Ando M, Ozasa K, Watanabe Y, Kondo T, Nishino Y, Ohno Y** 2002 Serum insulin-like growth factors, insulin-like growth factor-binding protein-3, and risk of lung cancer death: a case-control study nested in the Japan Collaborative Cohort (JACC) Study. Jpn J Cancer Res 93:1279–1286
19. **Spitz MR, Barnett MJ, Goodman GE, Thornquist MD, Wu X, Pollak M** 2002 Serum insulin-like growth factor (IGF) and IGF-binding protein levels and risk of lung cancer: a case-control study nested in the beta-Carotene and Retinol Efficacy Trial Cohort. Cancer Epidemiol Biomarkers Prev 11:1413–1418
20. **Beasley MB, Brambilla E, Travis WD** 2005 The 2004 World Health

Organization classification of lung tumors. Semin Roentgenol 40: 90–97
21. **Frankel SK, Moats-Staats BM, Cool CD, Wynes MW, Stiles AD, Riches DW** 2005 Human insulin-like growth factor-IA expression in transgenic mice promotes adenomatous hyperplasia but not pulmonary fibrosis. Am J Physiol Lung Cell Mol Physiol 288:L805–L812
22. **Chestnut RE, Quarmby V** 2002 Evaluation of total IGF-I assay methods using samples from type I and type II diabetic patients. J Immunol Methods 259:11–24
23. **Martin JL, Lin MZ, McGowan EM, Baxter RC** 2009 Potentiation of growth factor signaling by insulin-like growth factor-binding protein-3 in breast epithelial cells requires sphingosine kinase activity. J Biol Chem 284:25542–25552
24. **Clemmons DR** 1997 Insulin-like growth factor binding proteins and their role in controlling IGF actions. Cytokine Growth Factor Rev 8:45–62
25. **Huang P, Duda DG, Jain RK, Fukumura D** 2008 Histopathologic findings and establishment of novel tumor lines from spontaneous tumors in FVB/N mice. Comp Med 58:253–263
26. **Lee HY, Chun KH, Liu B, Wiehle SA, Cristiano RJ, Hong WK, Cohen P, Kurie JM** 2002 Insulin-like growth factor binding protein-3 inhibits the growth of non-small cell lung cancer. Cancer Res 62:3530–3537
27. **Baxter RC** 2001 Signalling pathways involved in antiproliferative effects of IGFBP-3: a review. Mol Pathol 54:145–148
28. **Oh Y, Müller HL, Lamson G, Rosenfeld RG** 1993 Insulin-like growth factor (IGF)-independent action of IGF-binding protein-3 in Hs578T human breast cancer cells. Cell surface binding and growth inhibition. J Biol Chem 268:14964–14971
29. **Rajah R, Valentinis B, Cohen P** 1997 Insulin-like growth factor (IGF)-binding protein-3 induces apoptosis and mediates the effects of transforming growth factor-beta1 on programmed cell death through a p53- and IGF-independent mechanism. J Biol Chem 272: 12181–12188
30. **Bhattacharyya N, Pechhold K, Shahjee H, Zappala G, Elbi C, Raaka B, Wiench M, Hong J, Rechler MM** 2006 Nonsecreted insulin-like growth factor binding protein-3 (IGFBP-3) can induce apoptosis in human prostate cancer cells by IGF-independent mechanisms without being concentrated in the nucleus. J Biol Chem 281:24588–24601
31. **Butt AJ, Fraley KA, Firth SM, Baxter RC** 2002 IGF-binding protein-3-induced growth inhibition and apoptosis do not require cell surface binding and nuclear translocation in human breast cancer cells. Endocrinology 143:2693–2699
32. **Liu B, Lee HY, Weinzimer SA, Powell DR, Clifford JL, Kurie JM, Cohen P** 2000 Direct functional interactions between insulin-like growth factor-binding protein-3 and retinoid X receptor-α regulate transcriptional signaling and apoptosis. J Biol Chem 275:33607–33613
33. **Butt AJ, Martin JL, Dickson KA, McDougall F, Firth SM, Baxter RC** 2004 Insulin-like growth factor binding protein-3 expression is associated with growth stimulation of T47D human breast cancer cells: the role of altered epidermal growth factor signaling. J Clin Endocrinol Metab 89:1950–1956
34. **Firth SM, Fanayan S, Benn D, Baxter RC** 1998 Development of resistance to insulin-like growth factor binding protein-3 in transfected T47D breast cancer cells. Biochem Biophys Res Commun 246:325–329
35. **McCaig C, Perks CM, Holly JM** 2002 Intrinsic actions of IGFBP-3 and IGFBP-5 on Hs578T breast cancer epithelial cells: inhibition or accentuation of attachment and survival is dependent upon the presence of fibronectin. J Cell Sci 115:4293–4303
36. **Granata R, Trovato L, Garbarino G, Taliano M, Ponti R, Sala G, Ghidoni R, Ghigo E** 2004 Dual effects of IGFBP-3 on endothelial cell apoptosis and survival: involvement of the sphingolipid signaling pathways. FASEB J 18:1456–1458
37. **Ali O, Cohen P, Lee KW** 2003 Epidemiology and biology of insulin-like growth factor binding protein-3 (IGFBP-3) as an anti-cancer molecule. Horm Metab Res 35:726–733
38. **Krajcik RA, Borofsky ND, Massardo S, Orentreich N** 2002 Insulin-like growth factor I (IGF-I), IGF-binding proteins, and breast cancer. Cancer Epidemiol Biomarkers Prev 11:1566–1573
39. **Yu H, Jin F, Shu XO, Li BD, Dai Q, Cheng JR, Berkel HJ, Zheng W** 2002 Insulin-like growth factors and breast cancer risk in Chinese women. Cancer Epidemiol Biomarkers Prev 11:705–712
40. **Rocha RL, Hilsenbeck SG, Jackson JG, Lee AV, Figueroa JA, Yee D** 1996 Correlation of insulin-like growth factor-binding protein-3 messenger RNA with protein expression in primary breast cancer tissues: detection of higher levels in tumors with poor prognostic features. J Natl Cancer Inst 88:601–606
41. **Singh D, Febbo PG, Ross K, Jackson DG, Manola J, Ladd C, Tamayo P, Renshaw AA, D'Amico AV, Richie JP, Lander ES, Loda M, Kantoff PW, Golub TR, Sellers WR** 2002 Gene expression correlates of clinical prostate cancer behavior. Cancer Cell 1:203–209
42. **Yu H, Levesque MA, Khosravi MJ, Papanastasiou-Diamandi A, Clark GM, Diamandis EP** 1996 Associations between insulin-like growth factors and their binding proteins and other prognostic indicators in breast cancer. Br J Cancer 74:1242–1247
43. **Chuang ST, Patton KT, Schafernak KT, Papavero V, Lin F, Baxter RC, Teh BT, Yang XJ** 2008 Over expression of insulin-like growth factor binding protein 3 in clear cell renal cell carcinoma. J Urol 179:445–449
44. **Granata R, Trovato L, Lupia E, Sala G, Settanni F, Camussi G, Ghidoni R, Ghigo E** 2007 Insulin-like growth factor binding protein-3 induces angiogenesis through IGF-I- and SphK1-dependent mechanisms. J Thromb Haemost 5:835–845
45. **Hansel DE, Rahman A, House M, Ashfaq R, Berg K, Yeo CJ, Maitra A** 2004 Met proto-oncogene and insulin-like growth factor binding protein 3 overexpression correlates with metastatic ability in well-differentiated pancreatic endocrine neoplasms. Clin Cancer Res 10: 6152–6158
46. **De Mellow JS, Baxter RC** 1988 Growth hormone-dependent insulin-like growth factor (IGF) binding protein both inhibits and potentiates IGF-I-stimulated DNA synthesis in human skin fibroblasts. Biochem Biophys Res Commun 156:199–204
47. **Conover CA** 1992 Potentiation of insulin-like growth factor (IGF) action by IGF-binding protein-3: studies of underlying mechanism. Endocrinology 130:3191–3199
48. **Gill ZP, Perks CM, Newcomb PV, Holly JM** 1997 Insulin-like growth factor-binding protein (IGFBP-3) predisposes breast cancer cells to programmed cell death in a non-IGF-dependent manner. J Biol Chem 272:25602–25607
49. **Burrows C, Holly JM, Laurence NJ, Vernon EG, Carter JV, Clark MA, McIntosh J, McCaig C, Winters ZE, Perks CM** 2006 Insulin-like growth factor binding protein 3 has opposing actions on malignant and nonmalignant breast epithelial cells that are each reversible and dependent upon cholesterol-stabilized integrin receptor complexes. Endocrinology 147:3484–3500
50. **Lawrence MC, McKern NM, Ward CW** 2007 Insulin receptor structure and its implications for the IGF-1 receptor. Curr Opin Struct Biol 17:699–705
51. **Belfiore A** 2007 The role of insulin receptor isoforms and hybrid insulin/IGF-I receptors in human cancer. Curr Pharm Des 13:671–686
52. **Belfiore A, Frasca F, Pandini G, Sciacca L, Vigneri R** 2009 Insulin receptor isoforms and insulin receptor/insulin-like growth factor receptor hybrids in physiology and disease. Endocr Rev 30:586–623
53. **Heuson JC, Legros N** 1972 Influence of insulin deprivation on growth of the 7,12-dimethylbenz (a) anthracene-induced mammary carcinoma in rats subjected to alloxan diabetes and food restriction. Cancer Res 32:226–232
54. **Wu X, Yu H, Amos CI, Hong WK, Spitz MR** 2000 Joint effect of insulin-like growth factors and mutagen sensitivity in lung cancer risk. J Natl Cancer Inst 92:737–743

Bayesian adaptive randomization designs for targeted agent development

J. Jack Lee, Xuemin Gu and Suyu Liu

Clin Trials 2010 7: 584 originally published online 22 June 2010
DOI: 10.1177/1740774510373120

CLINICAL TRIALS *PRESENTATION* *Clinical Trials* 2010; **7**: 584–596

Bayesian adaptive randomization designs for targeted agent development

J Jack Lee, Xuemin Gu and Suyu Liu

Background With better understanding of the disease's etiology and mechanism, many targeted agents are being developed to tackle the root cause of problems, hoping to offer more effective and less toxic therapies. Targeted agents, however, do not work for everyone. Hence, the development of target agents requires the evaluation of prognostic and predictive markers. In addition, upon the identification of each patient's marker profile, it is desirable to treat patients with best available treatments in the clinical trial accordingly.

Methods Many designs have recently been proposed for the development of targeted agents. These include the simple randomization design, marker stratified design, marker strategy design, efficient targeted design, etc. In contrast to the frequentist designs with equal randomization, we propose novel Bayesian adaptive randomization designs that allow evaluating treatments and markers simultaneously, while providing more patients with effective treatments according to the patients' marker profiles. Early stopping rules can be implemented to increase the efficiency of the designs.

Results Through simulations, the operating characteristics of different designs are compared and contrasted. By carefully choosing the design parameters, types I and II errors can be controlled for Bayesian designs. By incorporating adaptive randomization and early stopping rules, the proposed designs incorporate rational learning from the interim data to make informed decisions. Bayesian design also provides a formal way to incorporate relevant prior information. Compared with previously published designs, the proposed design can be more efficient, more ethical, and is also more flexible in the study conduct.

Limitations Response adaptive randomization requires the response to be assessed in a relatively short time period. The infrastructure must be set up to allow timely and more frequent monitoring of interim results.

Conclusion Bayesian adaptive randomization designs are distinctively suitable for the development of multiple targeted agents with multiple biomarkers. *Clinical Trials* 2010; **7**: 584–596. http://ctj.sagepub.com

Introduction

With better understanding of the disease causing mechanisms, many targeted agents are being developed recently to tackle the root cause problem of the disease with the hope to offer more effective and less toxic therapies. For example, cytotoxic chemotherapy has been used in treating cancer for over 50 years. Many cytotoxic agents take effects by impairing mitosis and are more effective for fast-dividing cells such as cancer. However, as a result, fast-dividing normal cells are also being killed indiscriminately, which results in substantial toxicity. Targeted agents, on the other hand, have specific 'targets' that the drugs attack [1]. For example, imatinib is highly effective in chronic myelogenous leukemia (CML) because CML is fueled by the *bcr-abl* protein and imatinib

Department of Biostatistics, The University of Texas M. D. Anderson Cancer Center, Houston, TX, USA
Author for correspondence: J Jack Lee, PhD, Department of Biostatistics, The University of Texas M.D. Anderson Cancer Center, 1400 Pressler Street, Unit 1411, Houston, TX 77030, USA. E-mail: jjlee@mdanderson.org

10.1177/1740774510373120

inhibits it [2]. Trastuzumab works well in a subset of breast cancer patients presented with HER-2 [3]. The development of target agents requires the evaluation of the corresponding markers for their use in predicting the treatment efficacy and/or toxicity. In addition, it is desirable to identify each patient's marker profile in order to provide the best available treatments accordingly [4,5].

Thanks to the knowledge explosion in this genomic era, many disease-causing mechanisms and the corresponding drugable targets are identified. Pharmaceutical companies and research institutions are engaged in screening thousands and thousands of compounds or combinations to identify potentially effective ones [6]. It poses a huge challenge to test numerous putative agents with only limited patient resources [7]. The co-development of the associated markers is equally challenging. Key questions to be investigated include the following: Does the treatment work for all patients or only in a subset of patients with certain marker profiles? Are there markers available which can help us to evaluate the treatment's efficacy and/or toxicity? In cases when the treatment only works in a small fraction of marker-positive patients, the overall treatment effect may be low and the drug could be abandoned. Furthermore, we often do not know what these markers are and accurate assays to measure them may not exist. The amount of resources it takes and the time pressure make the drug development even more difficult.

Another challenge faced by clinical trial practitioners is the competing interest between individual ethics and group ethics. Based on individual ethics, patients should be assigned to the best available treatment, and the total number of successes in the trial should be maximized. Because the best available treatment is yet to be defined during the study, the response-based adaptive randomization (AR) can be applied to enhance individual ethics [8–10]. On the other hand, according to group ethics, the statistical power of a trial should be maximized such that, after the trial, a better treatment is defined for the general population. This is typically accomplished by applying equal randomization (ER), in which the individual need of patients in the trial to receive the best available treatment is largely ignored. A good clinical trial design should strike a balance between individual ethics and group ethics [11,12].

In targeted agent development, we want to find out whether the treatment works or not. If the treatment does not work in all patients, does the treatment work in a subset of patients? Are there markers which can be used to identify such subsets? Can markers be measured accurately and timely? Can the trial be conducted in smaller number of patients and a decision can be reached earlier? Can we treat patients better during the trial based on patients' marker profile? In facing these voluminous challenges, how do we move forward? Traditional clinical trial designs are more rigid and can only answer a small number of well-formulated questions. How can we do better? We need a design that is accurate in decision making and inference drawing, efficient in requiring smaller number of patients or shorter trial duration, and ethical in that patients are treated with best available treatments during the trial. The design must be flexible in that it is amendable to change during its course. In short, we are looking for a smart design that can meet all these challenges. Because most of the facts are not known at the beginning of the trial, adaptive designs allow us to continue to learn and adapt during the trial [13–16].

We argue that Bayesian framework is particularly suitable for adaptive designs because the inference does not depend on a particular, preset sampling scheme. It allows frequent analyses and monitoring of the trial's interim data. It can incorporate prior information easily. Under a hierarchical model, it can 'borrow strength' across similar groups. Via simulations, one can choose the design parameters to obtain desirable frequentist properties, for example, controlling types I and II error rates [17–23].

Many frequentist designs have been proposed recently for the development of target agents [24–26]. In contrast to the frequentist designs with ER, we propose novel Bayesian adaptive randomization (BAR) designs to allow evaluating the treatment and marker effect simultaneously while treating more patients with more effective treatments according to patients' biomarker profiles. Early stopping rules can be implemented to increase the efficiency of the designs. These designs will be studied in more details in the following sections.

BAR applied in designs with two treatments, no markers

To illustrate how response-based AR works under the Bayesian framework, we first study a simple case of testing the response rates between two treatments with no markers. Assume p_i is the response rate, x_i is the number of responders, and n_i is the total number of patients for treatment i, $i=1, 2$. Based on the standard binomial distribution, we have $X_i \sim$ binomial(n_i, p_i). With a conjugate beta prior distribution for p_i taken as $f_0(p_i) = \text{beta}(a_0, b_0)$, the posterior distribution of p_i can be easily calculated as $f(p_i) = \text{beta}(a_0 + x_i, b_0 + n_i - x_i)$. A decision rule can be set to compare the response rate between the two treatments. For example, we conclude that treatment 1 is better than treatment

2 if $\Pr(p_1 > p_2) > 0.975$ and treatment 2 is better than treatment 1 if $\Pr(p_2 > p_1) > 0.975$. Otherwise, we conclude that treatments 1 and 2 are not significantly different.

The standard study design is to equally randomize patients between the two treatments and compare the result at the end of study. The AR, on the other hand, assumes that patients are enrolled over time, and one can use the interim results to preferentially allocate more patients into the more effective treatment. There are many choices for the randomization ratio. For example, the probability of randomizing the next patient into treatment 1 can be chosen as $\hat{p}_1^{\lambda}/(\hat{p}_1^{\lambda} + \hat{p}_2^{\lambda})$ or $\Pr(p_1 > p_2)^{\lambda}/(\Pr(p_1 > p_2)^{\lambda} + \Pr(p_2 > p_1)^{\lambda})$, where $\hat{p}_i$ is its posterior mean and λ is the tuning parameter. Note that when $\lambda = 0$, it corresponds to ER. When $\lambda = \infty$, it becomes the 'play-the-winner' design, in which the next patient is assigned to the current winner treatment based on the available data and no randomization is involved. The larger the λ is, the more imbalance the randomization will be.

Figure 1 shows the randomization probability and the observed response rate over time for five simulated trials in the setting, where $p_1 = 0.1$, $p_2 = 0.3$, and $n = 80$. We also assume that patients are enrolled sequentially and the response status is known instantaneously. With ER, the randomization probabilities converge to 0.5 as the trial moves along (upper left panels). The observed response rates converge to 0.1 and 0.3 (their corresponding true values) for treatments 1 and 2, respectively (bottom left panels). The right panels show the performance of AR. With AR, we first equally randomize 20 patients and afterward adaptively randomize the next 60 patients. The AR probability to treatment 1 is $\hat{p}_1/(\hat{p}_1 + \hat{p}_2)$. After 20 patients, the randomization ratio decreases for treatment 1 and increases for treatment 2, depicting that more patients are randomized into the better treatment.

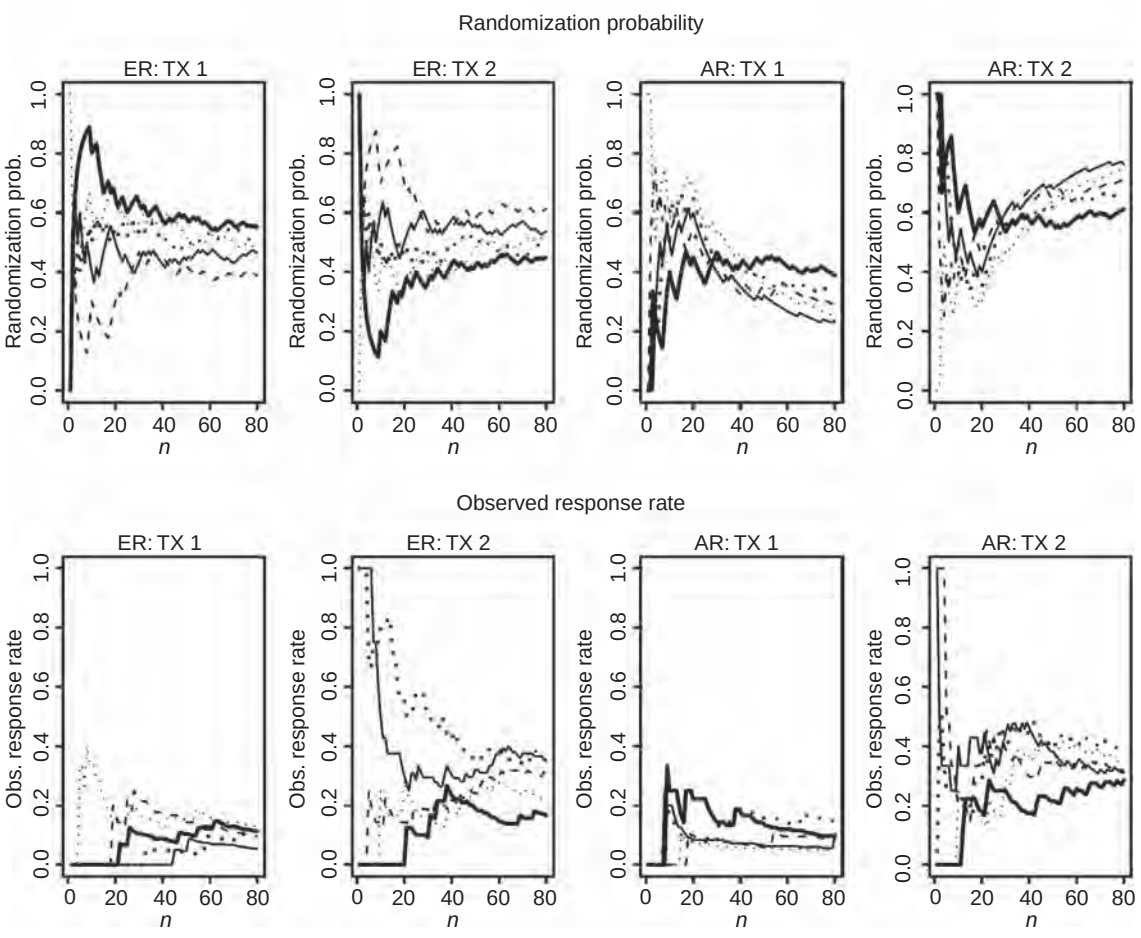

Figure 1 Randomization probability and observed response rate plotted over sequentially enrolled patients under the equal randomization (ER) and adaptive randomization (AR) designs. The probabilities of response in treatment 1 (TX1) and treatment 2 (TX2) are 0.1 and 0.3, respectively. For the AR design, AR starts after the first 20 patients are equally randomized

Table 1 Operating characteristics for two-arm Bayesian equal and adaptive randomization designs with and without early stopping

	ER		AR		AR w/early stopping ($N_{max} = 200$)		AR w/early stopping ($N_{max} = 250$)	
	H_0	H_1	H_0	H_1	H_0	H_1	H_0	H_1
N1	100	100	100	46	98	42	122	46
N2	100	100	100	154	97	125	121	150
N	200	200	200	200	195	167	243	196
Pr(declare TX1 better)	0.02	0	0.04	0	0.05	0	0.05	0
Pr(declare TX2 better)	0.03	0.83	0.04	0.75	0.05	0.76	0.05	0.85
Pr(early stopping)	0	0	0	0	0.04	0.34	0.04	0.44
Pr(randomized in arm 2)	0.50	0.50	0.50	0.77	0.50	0.75	0.50	0.77

H_0: $p_1 = p_2 = 0.3$; H_1: $p_1 = 0.3$, $p_2 = 0.5$.

The resulting observed response rates also converge to their corresponding true values as the trial continues.

Table 1 shows the operating characteristics for four designs with 5000 simulation studies using the AR program developed at M. D. Anderson Cancer Center (http://biostatistics.mdanderson.org/SoftwareDownload/). The four designs are (1) ER with $N = 200$ without early stopping, (2) AR with $N = 200$ without early stopping, (3) AR with $N_{max} = 200$ and early stopping, and (4) AR with $N_{max} = 250$ and early stopping. We evaluate the treatment effect by comparing the posterior distribution of the probability of response, for example, treatment 1 is claimed to be better if $\Pr(p_1 > p_2) > \tau$, where τ is a cutoff of the probability treatment 1 being better than treatment 2. An early stopping rule is implemented using a cutoff of 0.999, and at the end of study, a cutoff of 0.975 is used to make inference of the treatment efficacy. The performance of each method under the null hypothesis of $p_1 = p_2 = 0.3$ and the alternative hypothesis of $p_1 = 0.3$, $p_2 = 0.5$ are studied. Without early stopping, ER yields 5% type I error rate and 83% power under the null and alternative hypotheses, respectively. With AR, the type I error rate is slightly higher (8%), and the power is a bit lower (75%) due to the imbalance of treatment assignment. Under H_1, the averaged numbers of patients randomized into treatments 1 and 2 are 46 and 154, respectively. The result illustrates the trade-off between individual ethics and group ethics. AR enhances the individual ethics by assigning 77% of patients to the better treatment comparing to 50% by ER. However, due to imbalance in treatment allocation, the power is reduced from 83% to 75%.

One way to increase the study efficiency is to incorporate early stopping rules. Based on the interim result, if there is convincing evidence that one treatment is better than another, there is no need to continue the study. One can stop the trial early and announce the study result. Therefore, early stopping not only saves the sample size but can also allow better treatment to be adopted earlier in the general population. With AR and early stopping, the type I error rate rises again slightly to 10%, and there is a 4% chance of stopping the trial early under the null hypothesis. Under the alternative hypothesis, 34% of the time the trial will be stopped early. The averaged sample size is reduced from 200 to 167. The power and proportion of patients assigned to treatment 2 are comparable to AR without early stopping. To remedy the lower power resulting from imbalance due to AR, one can increase the maximum sample size. When the maximum sample size is increased to 250, the power is raised to 85%. The expected sample size is 196 with 77% of the patients receiving better treatment. Comparing to ER, the averaged number of patients treated in the trial is comparable. However, under the alternative hypothesis, AR with early stopping can result in both higher power and treating more patients with effective treatment, that is, getting the best from both worlds. We can also add early futility stopping rules to further reduce the expected sample size under the null hypothesis.

BAR and Frequentist's designs applied in designs with two treatments, one marker

In the targeted agent development, putative markers play a role in guiding the selection of treatment. By convention, markers can be broadly classified as prognostic or predictive. A prognostic marker is a marker that is associated with the patient's disease outcome regardless of treatment or in patients receiving standard care. For example, early-stage patients tend to do better than late-stage patients in cancer no matter what treatment is given. Patients with good performance status are

Table 2 Response rates for two treatments and one marker in five scenarios

TX	Scenario 1 MK		Scenario 2 MK		Scenario 3 MK		Scenario 4 MK		Scenario 5 MK	
	−	+	−	+	−	+	−	+	−	+
1	0.2	0.2	0.2	0.4	0.2	0.2	0.2	0.2	0.1	0.3
2	0.2	0.2	0.2	0.4	0.4	0.4	0.2	0.6	0.2	0.6

likely to do better than patients with poor performance status, and so on. In contrast, a predictive marker for a treatment is a marker that can predict the treatment outcome based on the marker status. For example, it is well established that lung cancer patients with EGFR mutation tend to do better than patients without mutation if they are given tyrosine kinase inhibitor such as gefitinib or erlotinib. The treatment does not work well in patients without mutation because they do not have the 'target' for the targeted agent to work on [27].

In the case with two treatments, one binary marker with a binary outcome, we illustrate that the BAR can be applied to achieve the following three goals: (1) test whether the marker is prognostic or predictive, (2) test whether the new treatment works better than the standard treatment in all patients or in patients within certain marker subsets, and (3) treat patients better in the trial by assigning more patients to the more effective treatment based on the patients' marker status. Most of the standard frequentist designs can also achieve the first two goals.

Table 2 depicts five illustrative scenarios. Assume treatment 1 (TX1) is the standard treatment and treatment 2 (TX2) is a new targeted agent. All patients are evaluated for their marker status (− or +) before randomization. We assume that there are no measurement errors in marker status, and the outcome is binary and the result can be observed quickly. Scenario 1 shows the null case in which regardless of the patients' marker status or the treatment assignment, the response rate (p) is 0.2 in all cases. Scenario 2 shows that the marker is prognostic, where $p = 0.4$ in M+ patients, which is better than $p = 0.2$ in M− patients regardless of treatments. On the other hand, scenario 3 shows the case where there is a treatment effect but no marker effect. Scenario 4 gives an example that the marker is predictive but not prognostic. The new treatment does not work in M− patients ($p = 0.2$) but works very well in M+ patients ($p = 0.6$). Lastly, scenario 5 shows the case where the marker is both prognostic and predictive. Comparing to the standard treatment, the new treatment works slightly better in the M− patients but much better in M+ patients ($p = 0.2$ vs. 0.1 and 0.6 vs. 0.3, respectively).

Several designs have been proposed in the literature for evaluating targeted agent in this setting. We compare the operating characteristics of five recently proposed designs, namely, the simple randomization design, the marker stratified design, the marker strategy design [28], the efficient targeted design [24,25] and the BAR design. The schematic diagram of these designs is given in Figure 2. In the simple randomization design, patients are randomized equally into the standard or the targeted treatment without the knowledge of the marker status. Simple randomization design can be used to test the overall treatment effect in the whole patient population. Conditional on the post hoc analysis by patients' marker status, it can also be used to test treatment effect in the M− and M+ patients separately. However, the marker distribution may not be balanced between the two treatment groups for small samples. If markers are measured retrospectively, a higher missing rate could occur. On the other hand, the marker stratified design requires that marker values be obtained at baseline. Upon stratifying on marker status, patients are equally randomized into the standard and targeted treatments. The prognostic effect of the marker can be tested by comparing A versus C. Testing A versus B or C versus D can be used to assess the treatment effects in patients within each marker group. The predictive effect can be tested by comparing the odds of treatment response between M− and M+ patients (A/B vs. C/D). In the marker strategy design, patients are first randomized between strategies. Patients randomized into the nonstrategy arm either receive the standard treatment or can be randomized equally to the standard and targeted treatments. The latter design is used for comparing with other designs. For patients randomized into the marker strategy arm, the treatment assignment is deterministic. M− patients receive standard treatment, whereas M+ patients receive targeted treatment. The differential effect of the two strategies can be compared by testing A + B versus C + D. The comparison between A and B can test the treatment effect in the unselected population. Similarly, the treatment effect in the selected population can be tested by the comparison between C and D. Efficient targeted design is an enrichment design that only treats M+ patients in the trial. M− patients are treated off protocol.

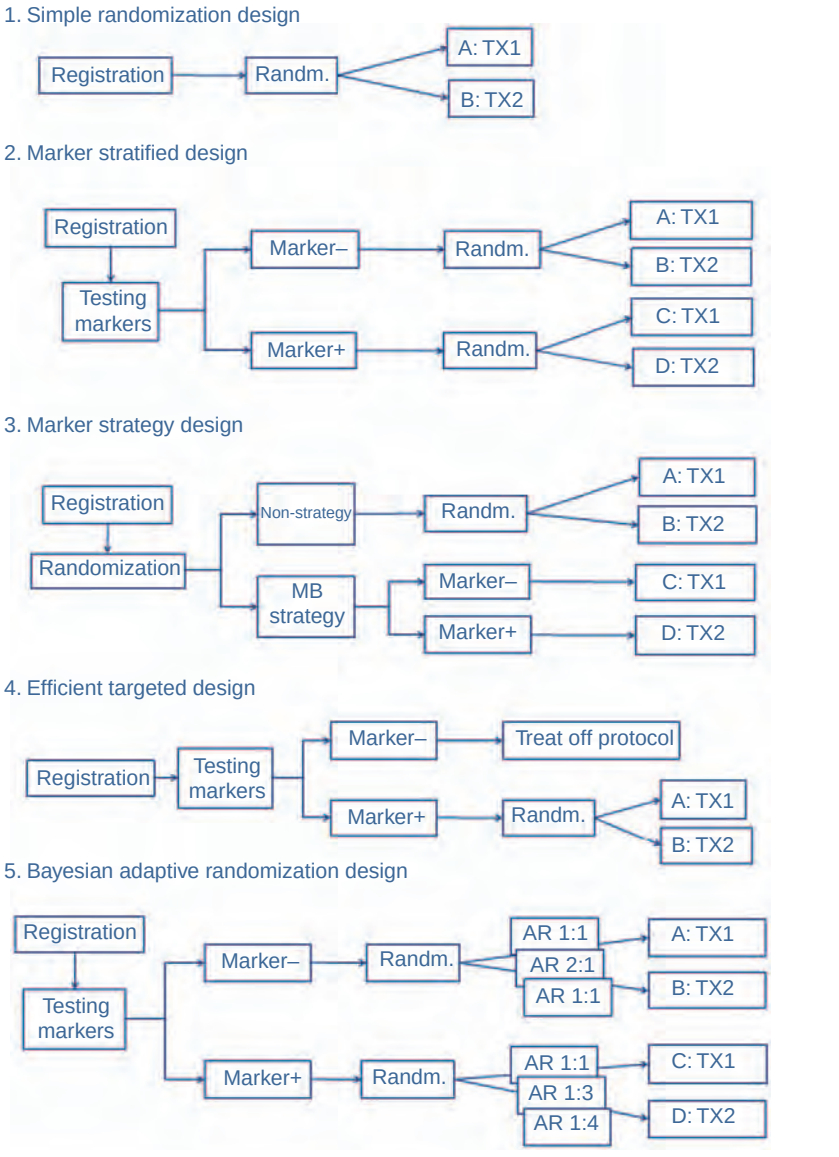

Figure 2 Schematic diagram for the five designs for the development of targeted agents

It can answer the question whether targeted treatment works in the M+ patients, but its effectiveness in M− patients cannot be assessed.

BAR design is a model-based approach, where the treatment effects are evaluated in marker groups progressively. The design structure is similar to marker stratified design, where randomization is conducted conditionally on marker status. However, instead of using ER, covariate-adjusted AR by marker is applied to allocate more patients to the putatively superior treatment.

With two marker groups and two treatments, logistic regression can be applied to test for the marker effect, the treatment effect, and their interaction. The model can be formulated as follows. For patient *i*, we assume:

$$\begin{aligned} &\Pr(Y_i = 1) = \theta_i \\ &\log\left(\frac{\theta_i}{1-\theta_i}\right) = \beta_0 + \beta_M M_i + \beta_T T_i + \beta_I M_i \cdot T_i, \end{aligned} \quad (1)$$

where Y_i is the response indicator, θ_i is the probability of response, M_i is the marker indicator, and T_i is the treatment indicator. For the BAR design, we assume that the parameters follow a multivariate normal distribution with a non-informative (NI) prior. Simulation studies are performed to evaluate the operating characteristics of the above designs.

Table 3 Operating characteristics for five designs in testing the marker effect, treatment effect, and marker by treatment interaction (marker predictive effect)

Scenario	Design	Marker effect			Treatment effect						MK × TX interaction[b]	Overall response rate
		In TX1[a]	In TX2	Overall	In MK(−)	In MK(+)	Overall	In STR(−)	In STR(+)	STR(−) vs. STR(+)		
1	Simple randomization	0.04	0.02	0.06	0.04	0.02	0.06				0.05	0.20
	Marker stratified	0.04	0.02	0.06	0.03	0.02	0.06				0.05	0.20
	Marker strategy	0.03	0.00	0.03	0.03	0.00	0.03	0.05	0.05	0.05	0.03	0.20
	Efficient target					0.04						0.20
	Bayesian AR	0.03	0.02	0.05	0.02	0.04	0.06				0.03	0.20
2	Simple randomization	0.46	0.45	0.71	0.04	0.02	0.06				0.05	0.30
	Marker stratified	0.47	0.47	0.72	0.03	0.03	0.06				0.05	0.30
	Marker strategy	0.40	0.28	0.56	0.03	0.02	0.04	0.06	0.46	0.05	0.04	0.30
	Efficient target					0.05	0.05					0.40
	Bayesian AR	0.46	0.43	0.71	0.02	0.03	0.05				0.04	0.30
3	Simple randomization	0.04	0.02	0.06	0.46	0.45	0.70				0.05	0.30
	Marker stratified	0.04	0.02	0.06	0.46	0.47	0.72				0.04	0.30
	Marker strategy	0.03	0.02	0.05	0.38	0.25	0.54	0.46	0.46	0.05	0.04	0.30
	Efficient target					0.47						0.30
	Bayesian AR	0.02	0.03	0.05	0.36	0.38	0.62				0.02	0.34
4	Simple randomization	0.04	0.95	0.95	0.04	0.95	0.95				0.64	0.30
	Marker stratified	0.04	0.95	0.95	0.03	0.94	0.95				0.62	0.30
	Marker strategy	0.03	0.86	0.86	0.03	0.84	0.84	0.46	0.95	0.25	0.46	0.35
	Efficient target					0.95						0.40
	Bayesian AR	0.02	0.98	0.98	0.04	0.87	0.87				0.50	0.35
5	Simple randomization	0.54	0.95	0.98	0.15	0.75	0.79				0.08	0.30
	Marker stratified	0.54	0.95	0.98	0.15	0.74	0.78				0.08	0.30
	Marker strategy	0.52	0.86	0.93	0.19	0.60	0.66	0.46	1.00	0.10	0.05	0.33
	Efficient target					0.75						0.45
	Bayesian AR	0.40	0.98	0.99	0.19	0.66	0.71				0.06	0.34

[a]Testing whether marker is prognostic. [b]Testing whether marker is predictive. The statistical power and overall response rate are shown in five scenarios. TX, treatment; MK, marker; STR, strategy.

We run 5000 simulations for the frequentist designs and 1000 simulations for the Bayesian design. We assume that the total sample size is 150 and the M+ probability of 0.5. Table 3 gives the statistical power for testing the marker effect, the treatment effect, and the marker by treatment interaction (i.e., whether the marker is predictive). For the marker strategy design, because patients' marker status is assumed to be available, we carry out the *post hoc* logistic regression analysis to test for the above effects. In addition, we report the results of testing whether the treatment works in patients randomized into non-strategy and strategy approaches, and the power for comparing the two strategies. The last column shows the averaged overall response rate in all patients enrolled in the trial. All the frequentist tests are carried out at a two-sided 5% significance level.

For the BAR design, we let the first 50 patients to be equally randomized, so we can obtain initial estimates of the parameters. Starting from the 51st patient, patients are randomized to treatment 1 with probability $\hat{p}_1/(\hat{p}_1+\hat{p}_2)$, where $\hat{p}_i$ is the current estimate of the response rate in treatment i, $i=1, 2$. At the end of study, a parameter β is considered significantly different from 0 if $\Pr(\beta > 0) > \tau$, where β represents for β_T in testing treatment effect in M− patients, for $\beta_T+\beta_I$ in testing treatment effect in M+ patients, for β_M in testing marker effect in TX1, and for $\beta_M+\beta_I$ in testing marker effect in TX2. An overall treatment effect is defined as TX2 is better than TX1 in either M− or M+ patients or in the whole group. Similar definition is applied for the overall marker effect. The cutoff τ is selected to correspond to 5% type I error rate under the null hypothesis.

In scenario 1, when there is no marker effect or treatment effect, the statistical power (type I error) is between 0 and 0.06 in all settings. The overall response rate is indeed 0.2 in all settings. In our case with the M+ proportion being 0.5, the performance of the simple randomization design and the marker stratified design (both are ER designs) is essentially identical.

For scenario 2, ER design shows the power for testing the marker effect is about 46% in each treatment subgroups and about 71% in all patients. Due to the imbalanced allocation in the marker strategy design (approximately 37.5% in the M−, TX1 and M+, TX2; and 12.5% in M−, TX2 and M+, TX1), the corresponding powers are reduced. Because there is no treatment effect, the powers for testing the treatment effect are around the levels of type I error rates in the null case in all designs.

In scenario 3, when there is a treatment effect but no marker effect, all designs show the power for

testing the marker effect is hovering around the 5% type I error rate. The power for testing the overall treatment effect is higher in the ER design (about 71%) than the marker strategy design (54%) as shown earlier. The power for testing the treatment effect using the efficient targeted design is only 47% because it screens out the M− patients.

In scenario 4, when marker is predictive but not prognostic, the type I errors for testing the marker's prognostic effect and the treatment effect in M− patients are all less than 5% for all designs. The powers for testing the marker effect in TX2 patients or treatment effect in M+ patients are greater than 90% for the ER design and the efficient targeted design but in the mid-80% range for the marker strategy design. The power for testing the marker's predictive effect (i.e., marker by treatment interaction) is about 63% for the ER designs and only 46% for the marker strategy design.

In scenario 5, when the marker is both prognostic and predictive, the powers for testing the marker effect and the treatment effect are all greater than the nominal significance level. The performance of the efficient targeted design is similar to the ER designs and is better than the marker strategy design.

For the marker strategy design, we also evaluate the treatment effect in patients assigned to nonstrategy arm, strategy arm, and the power for comparing strategy versus nonstrategy arm. For scenario 2, the power for testing the treatment effect in patients assigned to the strategy approach arm is 46%. This means that taking the marker strategy approach, there is evidence showing that patients assigned to the targeted agent fare better than patients assigned to the standard treatment. Hence, it may lead to an erroneous conclusion that the targeted agent works better than the standard treatment. The difference is, in fact, due to the marker effect and not the treatment effect. The strategy approach leads to a total confounding between marker and treatment. Hence, when difference is observed, it is not known whether it is attributed to the marker or the treatment. Another important observation is that, for the marker strategy design, the power for testing strategy versus no-strategy approaches is consistently low in all scenarios. Even in scenarios 4 and 5, when the marker is predictive, the powers are only 25% and 10%, respectively. The low power is a result of a significant overlap in treatment assignments between the two.

For the BAR design, we choose the cutoff value $\tau = 0.983$ to control the type I error rate to 0.05. For scenario 2, the powers of the BAR design for testing the marker effect are comparable to the ER design. For scenario 3, the power of the BAR design for testing the treatment effect is slightly lower than the ER design (62% vs 70% for testing overall treatment effect). Due to AR, the slight loss of power can also be seen in scenarios 4 and 5 (87% vs 95% and 71% vs 79%, respectively).

We also compare the overall response rate in all designs. For scenario 2, efficient targeted design has 40% response rate because only M+ patients are enrolled. In scenario 3, BAR gave the best result with a response rate of 34%. For scenario 4, efficient targeted design yields a response rate of 40%, while the marker strategy design and BAR give a response rate of 35%. Likewise, in scenario 5, efficient targeted design has the highest overall response rate (45%), followed by BAR (34%), marker strategy design (33%), and ER (30%). ER design has the lowest response rate in all scenarios.

BAR applied in designs with multiple treatments and multiple markers

BAR design can be applied to settings when multiple markers are involved in evaluating the effect of multiple treatments. To illustrate its use, we give an example when two markers are used for evaluating four treatments. Specifically, we recently designed a biomarker-based clinical trial in advanced-staged lung cancer patients. Building upon a similar trial called BATTLE (Biomarker-Integrated Approaches of Targeted Therapy of Lung Cancer Elimination) [28], our BATTLE-2 trial is to test four treatments with multiple biomarkers. The primary endpoint is the 8-week disease control rate (DCR) defined as patients without progression by the end of 8 weeks after randomization [29]. The trial was designed with a total sample size of 320 in two stages (160 patients per stage). There are four treatments, namely, erlotinib, erlotinib + an AKT inhibitor, erlotinib + an IGFR inhibitor, and an AKT inhibitor + a MEK inhibitor. In stage 1, two well established markers (EGFR mutation and K-ras mutation) are used to guide the patient allocation. Patients will be adaptively randomized in stage 1 based on the two markers. From stage 1, more putative and discovery markers are identified to refine the predictive model, which will then be used in adaptively randomizing patients in stage 2.

We use only the stage 1 part to illustrate how BAR can be applied in this setting. The design has one more complication: two types of patients are recruited – erlotinib-naïve who have not been exposed with erlotinib and erlotinib-resistant who had prior erlotinib treatment but failed. Per design, erlotinib-naïve patients can be randomized in any one of the four treatments, but erlotinib-resistant patients is excluded from erlotinib only treatment, and can only be randomized into one of the three combination treatments.

The statistical model is given below. Let X_i be a $n \times q$ design matrix, n is the total number of patients, q is the total number of parameter including

intercept, J is the total number of treatments, and K is the total number of markers. Under the framework of the logistic model, the DCR p_i for the ith patient can be expressed as follows:

$$\begin{aligned}\text{logit}(p_i) &= X_i\ \beta = \alpha_1 \\ &+ \sum_{j=2}^{J} \alpha_j T_{ij} + \sum_{k=1}^{K} \beta_k M_{ik} + \sum_{j=2}^{J}\sum_{k=1}^{K} \gamma_{kj} M_{ik} T_{ij} \\ &+ \left(\alpha'_1 + \sum_{j=2}^{J} \alpha'_j T_{ij} + \sum_{k=1}^{K} \beta'_k M_{ik} + \sum_{j=2}^{J}\sum_{k=1}^{K} \gamma'_{kj} M_{ik} T_{ij} \right) \cdot Z_i,\end{aligned} \tag{2}$$

where T_{ij} is the indicator for the experimental treatments (TX2, TX3, or TX4), M_{ik} is the indicator for positive marker status, and Z_i is the indicator for erlotinib-resistant patient.

For erlotinib-naïve patients, the probability of patient being assigned to the jth treatment is proportional to $\Pr(p_j > p_{j'}, j' \in \{1,2,3,4 | j' \neq j\})$. For erlotinib-resistant patients, allocation to TX1 is prohibited, and the probability of patient being assigned to TX2, TX3, or TX4 is proportional to $\Pr(p_j > p_{j'}, j' \in \{2,3,4 | j' \neq j\})$.

Our main interest is to test for the effect of new treatments (TX2, TX3, TX4) versus the standard treatment (TX1) in the following settings.

(1) Evaluation of the marginal treatment effect in all patients

The marginal treatment effect will be tested using model (3) with only treatment and marker main effect present:

$$\text{logit}(p_i) = \alpha_1 + \alpha_2 T_{i2} + \alpha_3 T_{i3} + \alpha_4 T_{i4} + \beta_1 M_{i1} + \beta_2 M_{i2} \tag{3}$$

Experimental treatment, TX j ($j = 2, 3, 4$) will be claimed as having a significant marginal treatment effect in all patients if $\Pr(\alpha_j > 0) > \tau$, where τ is the threshold cutoff value for posterior inference. That is, we call the experimental treatment better than the standard if the probability of the DCR in the experimental treatment being greater than the DCR in the standard treatment is greater than τ.

(2) Evaluation of the marginal treatment effect in erlotinib-resistant and in erlotinib-naïve patients

The marginal treatment effect in the erlotinib-resistant and in the erlotinib-naïve patients will be tested using model (4), which include Z_i:

$$\begin{aligned}\text{logit}(p_i) = {} & \alpha_1 + \alpha_2 T_{i2} + \alpha_3 T_{i3} + \alpha_4 T_{i4} + \beta_1 M_{i1} \\ & + \beta_2 M_{i2} + (\alpha'_1 + \alpha'_2 T_{i2} + \alpha'_3 T_{i3} + \alpha'_4 T_{i4} \\ & + \beta'_1 M_{i1} + \beta'_2 M_{i2}) \cdot Z_i\end{aligned} \tag{4}$$

TX j ($j = 2, 3, 4$) will be claimed as having a significant marginal treatment effect in naïve patients if $\Pr(\alpha_j > 0) > \tau$ and in resistant patients if $\Pr(\alpha_j + \alpha'_j > 0) > \tau$.

(3) Evaluation of the treatment effects in erlotinib-resistant and in erlotinib-naïve patients in different marker groups

It is assumed that, among erlotinib-naïve patients, M1+ patients will have a better response to the experimental treatments than M1− patients. If there are no marginal treatment effects in either the overall patient population or erlotinib-naïve or erlotinib-resistant patients, we will further evaluate the treatment effect in erlotinib-naive patients expressing particular markers using the full model in Equation (2).

Experimental treatment j ($j = 2, 3, 4$) will be claimed as having a significant treatment effect in erlotinib-naïve and marker k positive patients if $\Pr(\alpha_j + \gamma_{kj} > 0) > \tau$ and in erlotinib-resistant and marker k positive patients if $\Pr(\alpha_j + \gamma_{kj} + \alpha'_j + \gamma'_{kj} > 0) > \tau$.

Simulations are conducted with 2000 runs for each scenario to evaluate the operating characteristics. For each run, a total of 5000 Markov chain Monte Carlo iterations after 5000 burn-in draws are used to make posterior inferences. We assume 44% of the 160 patients are erlotinib resistant and the remaining 56% are erlotinib-naïve based on our prior data. We also assume that the EGFR mutation rate and K-ras mutation rate are both at 20%, and they are independent to each other. Two priors were used to evaluate the operating characteristics: (1) a NI independent normal (0, 100) prior is used for all parameters; (2) same as in (1) but an informative beta prior for the erlotinib only treatment in the erlotinib-resistant patients. Because no erlotinib-resistant patients are assigned to the erlotinib only arm, when testing the treatment efficacy in resistant patients with the NI prior option, the inference is essentially based on comparing the treatment effects of experimental arms to a very diffuse prior centered at 0.5, which could yield a very low power. Therefore, the use of a NI prior may not be reasonable. The very reason that we do not assign erlotinib-resistant patients into the erlotinib only arm is because the treatment does not work in this setting. Sim et al. [30] reported data from 16 patients who were treated with gefitinib first, followed by erlotinib upon gefitinib failure. The DCR was 69% in the gefitinib treatment and 25% in the subsequent erlotinib treatment. We implement this information through our second prior option,

Table 4 Assumed 8-week disease control rate under the null and alternative hypotheses for erlotinib-resistant and -naïve patients by marker status in the BATTLE-2 design

Markers		Erlotinib-naïve				Erlotinib-resistant		
M_1	M_2	TX1	TX2	TX3	TX4	TX2	TX3	TX4
Under null hypothesis								
−	−	0.3	0.3	0.3	0.3	0.1	0.1	0.1
+	−	0.6	0.6	0.6	0.4	0.2	0.2	0.1
−	+	0.1	0.1	0.1	0.1	0.1	0.1	0.1
Under alternative hypothesis								
−	−	0.3	0.6	0.6	0.6	0.5	0.5	0.5
+	−	0.6	0.9	0.9	0.7	0.6	0.6	0.6
−	+	0.1	0.3	0.3	0.5	0.3	0.3	0.5

Table 5 Observed averaged number of patients under the null and alternative hypotheses for erlotinib-resistant and naïve patients by marker status in the BATTLE-2 design

Markers		Erlotinib-naïve				Erlotinib-resistant		
M_1	M_2	TX1	TX2	TX3	TX4	TX2	TX3	TX4
Under null hypothesis								
−	−	15.2	14.0	14.5	13.3	14.9	15.6	14.6
+	−	3.9	3.9	3.3	3.4	3.7	3.5	4.1
−	+	2.9	5.1	3.6	2.8	4.5	3.7	2.9
+	+	0.8	1.1	0.8	0.8	1.0	0.9	0.9
Under alternative hypothesis								
−	−	10.0	15.9	15.9	15.7	14.8	14.8	15.4
+	−	3.3	4.1	3.6	3.4	4.0	3.8	3.5
−	+	2.1	4.9	3.3	4.0	3.9	3.2	4.0
+	+	0.7	1.1	0.8	0.9	1.0	0.9	0.9

the beta prior. To discount the weight of the historical data, we assume that the DCRs for the erlotinib treatment in the erlotinib-resistant patients follow beta prior distributions with an effective sample size of 5. The order of magnitude of treatment effect in the literature is similar to the ones shown in Table 4.

The total numbers of patients randomized into each marker by treatment combinations are given in Table 5. Under the null hypothesis, the numbers of patients treated in each arm are very similar to each other as expected. Under the alternative hypothesis, for naïve patients, the numbers of patients in the erlotinib arm is smaller than the combination arms because the combination arms have higher DCRs.

Table 6 shows the statistical power for testing the treatment effect under various settings. An overall treatment effect is defined as significant if the effect is shown in either marginal effect (for all patients or for subgroup of patients) or in any marker-positive patients. If any of TX 2, 3, and 4 have significant effect, the trial will be claimed as a success. For the Bayesian design, a cutoff value τ is chosen to declare the test result being 'significant'. We chose τ such that the type I error rate under the null hypothesis for testing treatment effect of experimental arm versus erlotinib only arm is 10%. For NI prior, $\tau = 0.982$, and for the beta prior, $\tau = 0.984$.

With the NI prior, the powers for testing TX 2, 3, and 4 being better than TX1 are 0.632, 0.592, and 0.622, respectively. The power gains are mainly from the erlotinib-naïve patients as it is evident that the power gain from the erlotinib-resistant patients is essentially nil. This is due to the nature of the NI prior and no resistant patients are assigned to the erlotinib only arm to update information. In contrast, even with a weak informative beta prior (with an effective sample size of 5), we gain power for testing the treatment effect in the resistant patients. The power for testing TX 2, 3, and 4 being effective increased to 0.787, 0.861, and 0.801, respectively. The overall family-wise type I

Table 6 Statistical power for testing the treatment effect under the null and alternative hypotheses for erlotinib-resistant and -naïve patients by marker status in the BATTLE-2 adaptive randomization design using the Bayesian logistic regression

Prior	Scenario	Cutoff	TX	Margin	Naïve margin	Resistant margin	Naïve MK (−,−)	Naïve MK (+,−)	Naïve MK (−,+)	Resistant MK (−,−)	Resistant MK (+,−)	Resistant MK (−,+)	Overall	All TX
NI	Null	0.982	2	0.004	0.040	0.000	0.035	0.046	0.014	0.000	0.000	0.000	0.098	0.184
			3	0.004	0.034	0.000	0.034	0.052	0.011	0.001	0.001	0.001	0.093	
			4	0.004	0.018	0.000	0.033	0.010	0.002	0.000	0.000	0.000	0.044	
	Alternative		2	0.302	0.463	0.003	0.348	0.293	0.083	0.004	0.004	0.000	0.632	0.865
			3	0.316	0.442	0.001	0.358	0.263	0.098	0.003	0.009	0.000	0.592	
			4	0.375	0.440	0.002	0.348	0.102	0.244	0.003	0.004	0.011	0.622	
Beta5	Null	0.984	2	0.003	0.038	0.000	0.033	0.041	0.013	0.000	0.001	0.000	0.091	0.174
			3	0.003	0.033	0.010	0.030	0.049	0.009	0.000	0.001	0.001	0.095	
			4	0.004	0.016	0.000	0.030	0.009	0.001	0.000	0.000	0.001	0.039	
	Alternative		2	0.291	0.447	0.277	0.336	0.277	0.071	0.271	0.211	0.039	0.787	0.987
			3	0.299	0.432	0.579	0.338	0.243	0.087	0.299	0.230	0.050	0.861	
			4	0.357	0.423	0.040	0.337	0.096	0.225	0.311	0.208	0.207	0.801	

Cutoff values for posterior probability were chosen to control the type I error rates for comparing TX 2, 3, 4 to TX1 under the null hypothesis to 10%.

Table 7 Statistical power for testing the treatment effect under the null and alternative hypotheses for all patients and for erlotinib-naïve patients by marker status in the frequentist's equal randomization designs

Scenario	TX	Margin	Naïve margin	Naïve MK (−,−)	Naïve MK (+,−)	Naïve MK (−,+)	Overall	All TX
Null	2	0.007	0.054	0.044	0.018	0.003	0.097	0.200
	3	0.006	0.058	0.053	0.018	0.001	0.099	
	4	0.004	0.036	0.050	0.004	0.001	0.071	
Alternative	2	0.579	0.644	0.487	0.076	0.031	0.741	0.923
	3	0.593	0.651	0.495	0.081	0.035	0.756	
	4	0.639	0.650	0.495	0.021	0.135	0.758	

A *p*-value cutoff for the Fisher's exact test was chosen to control the type I error rates for comparing TX 2, 3, 4 to TX1 under the null hypothesis to 10%.

error rate is 0.184 and 0.174 for the NI and beta prior, respectively. The corresponding overall power is 0.865 and 0.987.

To compare the performance of the Bayesian design with frequentist's design, Table 7 shows the corresponding statistical power using the Fisher's exact test. Because there is no data in the erlotinib-resistant group treated with erlotinib, we show the results based on the whole group (margin) and for the naïve patients only. Fisher's exact test is chosen because the maximum likelihood estimators from logistic regressions often failed due to the small sample size and no events in biomarker subgroups. The overall power is 0.923, which is higher than the Bayesian design with a NI prior but lower than the Bayesian design with an informative prior.

Discussion

For developing targeted agents, it is indeed challenging to ask for a design that is accurate, efficient, ethical, and flexible. Through simulation studies, we have compared the performance of various frequentist designs and the BAR design. For the frequentist designs, simple randomization design and marker stratified design have similar operating characteristics, but the marker stratified design can ensure that treatments are equally assigned in each marker group, and the prospective evaluation of markers can improve the completeness and accuracy of the marker data. Efficient targeted design only tests the treatment efficacy in selected marker group(s); hence, it reduces the trial sample size. It is most efficient when there is sufficient evidence that the treatment is most likely to work only in the selected marker groups and unlikely to work in the other groups. However, in most settings, the answers to these questions remain unknown. This is exactly the reason why we need to conduct clinical trials in the first place. Although the efficient targeted design can test the treatment effect in the selected group, the effect in other marker groups cannot be assessed. Marker strategy design may sound like a reasonable approach, but due to the

confounding between the marker effect and the treatment effect, the design cannot accurately attribute the difference in outcomes to marker, treatment, or their combinations. The design also has very little power in comparing the strategy versus nonstrategy approaches.

BAR design allocates more patients in more effective treatments as the trial progresses and information accumulates. It continues to learn about the effects of markers, treatments, and their interactions along the trial and adjusts the randomization proportion accordingly. By carefully calibrating the design parameters, types I and II errors can be controlled for the Bayesian designs. AR can result in mild loss in statistical power due to imbalance allocation between treatment groups. It, however, gains efficiency through modeling and the appropriate use of the prior information. Larger sample size in more effective treatments can also result in higher precision in estimating the corresponding treatment effects. Furthermore, adding futility or efficacy early stopping rules can reduce the sample size. Although the BAR designs yield only incremental improvements over the frequentist's counterparts, Bayesian approach provides a uniform way of setting up complex problems, parameter estimation, and inference making. Bayesian framework also allows more flexible study conduct, such as dropping ineffective treatments and adding new treatments, because the inference is based on the data (conformed with the likelihood principle) and does not depend on a fixed sampling plan.

The validity of the Bayesian models that we have discussed, however, depends on the proper model specification and the assumed parameters. Extensive simulations should be conducted to evaluate the operating characteristics of the design under various settings. A conservative approach should be taken in choosing the sample size and in controlling type I errors. Highly complex models may gain efficiency but lack robustness. Model checking and sensitivity analysis are required to ensure that the model provides adequate fit for the data.

Early phase of drug developing is about discovery and learning. Adaptive design provides an ideal platform for learning and enables the investigators to continue to learn about the new agents' clinical activities during the trial and apply this knowledge to better treat patients in real time. It can increase the study efficiency, allow flexibility in study conduct, and provide better treatment to study participants, which is a step toward personalized medicine.

One limitation of the response-based AR is that it requires the response to be assessed in a relatively short time period. Infrastructure setup is necessary to allow more frequent monitoring of interim results. Extra steps need to be taken to ensure the integrity of the study conduct, for example, timely and objective evaluation of endpoints. Due to the large number of tests, the overall false positive rate may increase. Results found in one trial need to be confirmed in other trials, which includes the validation of both the predictive markers and the treatment efficacy. Upon the identification of efficacious treatments and corresponding markers, a more focused confirmatory trial can be designed accordingly.

The success of Bayesian adaptive trials requires an integrated multidisciplinary research team of clinical investigators, who see patients and perform biopsies, basic scientists who run the biomarker analysis, computer programmers who build Web-based database applications, and statisticians who provide the design and implementation of AR.

In summary, Bayesian designs can be more ethical and efficient by incorporating AR and early stopping rules. The proposed new designs incorporate rational learning from the interim data for randomization and making decisions on treatment efficacy. BAR designs are distinctively suitable for the development of multiple targeted agents with multiple biomarkers. Although it requires more efforts on trial design, simulation, setting up the infrastructure, trial conduct, analysis, and reporting, Bayesian designs have gain increasing popularity recently and have been implemented in many settings [23,28]. In reviewing papers demonstrating that Bayesian clinical trials are currently in action, Gonen has aptly titled his editorial 'Bayesian clinical trials: no more excuses' [31].

Acknowledgements

The paper was based on a presentation in the University of Pennsylvania Annual Conference on Statistical Issues in Clinical Trials: Targeted Clinical Trials on April 29th, 2009. This work was supported in part by the Department of Defense grant W81XWH-06-1-303 and a National Cancer Institute grant CA 16672. JJL is Kenedy Foundation Chair in Cancer Research at M. D. Anderson Cancer Center. The authors also thank M. Victoria Cervantes for her editorial assistance.

References

1. **Kummar S, Gutierrez M, Doroshow JH, Murgo AJ.** Drug development in oncology: classical cytotoxics and molecularly targeted agents. *Br J Clin Pharmacol* 2006; **62**: 15–26.
2. **O'Hare T, Deininger MW.** Toward a cure for chronic myeloid leukemia. *Clin Cancer Res* 2008; **14**: 7971–74.
3. **Buzdar AU.** Role of biologic therapy and chemotherapy in hormone receptor- and HER2-positive breast cancer. *Ann Oncol* 2009; **20**: 993–99.
4. **Chackalamannil S, Desai MC.** Personalized medicine – a paradigm for a sustainable pharmaceutical industry? *Curr Opin Drug Discov Devel* 2009; **12**: 443–45.
5. **Fine BM, Amler L.** Predictive biomarkers in the development of oncology drugs: a therapeutic industry perspective. *Clin Pharmacol Ther* 2009; **85**: 535–38.

6. **Tepper RI, Roubenoff R.** The role of genomics and genetics in drug discovery and development. In: Willard HF, Ginburg GS (eds). *Genomic and Personalized Medicine*. Academic Press, San Diego, CA, 2009, pp. 335–56.
7. **Cooley ME, Sarna L, Brown JK, *et al*.** Challenges of recruitment and retention in multisite clinical research. *Cancer Nurs* 2003; **26**: 376–86.
8. **Rosenberger WF, Lachin JM.** *Randomization in Clinical Trials: Theory and Practice*, Wiley, New York, 2002.
9. **Hu F, Rosenberger WF.** Optimality, variability, power: evaluating response-adaptive randomization procedures for treatment comparisons. *J Am Stat Assoc* 2003; **98**: 671–78.
10. **Hu F, Rosenberger WF.** *The Theory of Response-Adaptive Randomization in Clinical Trials*, Wiley, Hoboken, NJ, 2006.
11. **Thall PF.** Ethical issues in oncology biostatistics. *Stat Methods Med Res* 2002; **11**: 429–48.
12. **Berry DA.** Bayesian statistics and the efficiency and ethics of clinical trials. *Stat Sci* 2004; **19**: 175–87.
13. **Chow S-C, Chang M.** *Adaptive Design Methods in Clinical Trials*. Chapman and Hall/CRC, Boca Raton, FL, 2007.
14. **Chang M.** *Adaptive Design Theory and Implementation Using SAS and R*. Chapman and Hall/CRC, Boca Raton, FL, 2008.
15. **Berry DA.** Adaptive trial design. *Clin Adv Hematol Oncol* 2007; **5**: 522–24.
16. **Biswas A.** Adaptive designs for binary treatment responses in phase III clinical trials: controversies and progress. *Stat Methods Med Res* 2001; **10**: 353–64.
17. **Biswas S, Liu DD, Lee JJ, Berry DA.** Bayesian clinical trials at the University of Texas M. D. Anderson Cancer Center. *Clin Trials* 2009; **6**: 205–16.
18. **Goodman SN.** Introduction to Bayesian methods I: measuring the strength of evidence. *Clin Trials* 2005; **2**: 282–90.
19. **Louis TA.** Introduction to Bayesian methods II: fundamental concepts. *Clin Trials* 2005; **2**: 291–94.
20. **Berry DA.** Introduction to Bayesian methods III: use and interpretation of Bayesian tools in design and analysis. *Clin Trials* 2005; **2**: 295–300.
21. **Spiegelhalter DJ, Abrams KR, Myles JP.** *Bayesian Approaches to Clinical Trials and Health-Care Evaluation*. John Wiley & Sons, Chichester, West Sussex, UK, 2004.
22. **Berry DA.** A guide to drug discovery: Bayesian clinical trials. *Nat Rev Drug Discov* 2006; **5**: 27–36.
23. **Berry DA.** Statistical innovations in cancer research. In: Holland J, Frei T, *et al*. (eds). *Cancer Medicine* (7th edn), Decker BC, London, 2005, pp. 411–25.
24. **Simon R, Maitournam A.** Perspective evaluating the efficiency of targeted designs for randomized clinical trials. *Clin Cancer Res* 2004; **10**: 6759–63.
25. **Maitournam A, Simon R.** On the efficiency of targeted clinical trials. *Stat Med* 2005; **24**: 329–39.
26. **Sargent DJ, Conley BA, Allegra C, Collette L.** Clinical trial designs for predictive marker validation in cancer treatment trials. *J Clin Oncol* 2005; **23**: 2020–27.
27. **Dahabreh IJ, Linardou H, Siannis F, *et al*.** Somatic EGFR mutation and gene copy gain as predictive biomarkers for response to tyrosine kinase inhibitors in non-small cell lung cancer. *Clin Cancer Res* 2010; **16**: 291–303.
28. **Zhou X, Liu S, Kim ES, *et al*.** Bayesian adaptive design for targeted therapy development in lung cancer – a step toward personalized medicine. *Clin Trials* 2008; **5**: 181–93.
29. **Lara Jr PN, Redman MW, Kelly K, *et al*.** Disease control rate at 8 weeks predicts clinical benefit in advanced non-small-cell lung cancer: results from Southwest Oncology Group randomized trials. *J Clin Oncol* 2008; **26**: 463–67.
30. **Sim SH, Han S-W, Oh D-Y, *et al*.** Erlotinib after gefitinib failure in female never-smoker Asian patients with pulmonary adenocarcinoma. *Lung Cancer* 2009; **65**: 204–07.
31. **Gönen M.** Bayesian clinical trials: no more excuses. *Clin Trials* 2009; **6**: 203–04.

Cancer Discovery Publish Ahead of Print, published on April 3, 2011 as doi:10.1158/2159-8274.CD-11-0036

IN THE SPOTLIGHT

The BATTLE Trial: A Bold Step toward Improving the Efficiency of Biomarker-Based Drug Development

Eric H. Rubin, Keaven M. Anderson, and Christine K. Gause

Summary: Successful completion of the Biomarker-integrated Approaches of Targeted Therapy for Lung Cancer Elimination (BATTLE) trial, reported in this issue of *Cancer Discovery*, is an important advance in the effort to improve clinical trial approaches to the simultaneous development of new therapeutics with matching diagnostic tests so that patients most likely to benefit from these therapies can be identified. *Cancer Discovery; 1(1). ©2011 AACR.*

Commentary on Kim et al., p. OF42 (1).

THE PROBLEM THAT BATTLE WAS DESIGNED TO SOLVE

Advances in basic cancer research have led to a widely used discovery and development approach for drugs designed to inhibit specific cancer pathways. However, clinical trial designs have not kept pace with basic research advances, and use of traditional, histology-based, "all-comers" phase I and II trial designs for these drugs has led typically to failure in phase III studies or demonstration of "success" based on statistically significant but clinically questionable benefit in an all-comers population. For example, Table 1 lists 9 drugs that failed in 13 phase III trials of unselected (i.e., in the absence of a diagnostic test that predicts tumor responsiveness to a drug) patients with non–small cell lung cancer (NSCLC) during or after the completion of the BATTLE study (1). Indeed, only 2 drugs that target signaling pathways have been approved by the FDA for the treatment of unselected NSCLC patients: erlotinib [small molecule inhibitor of the epidermal growth factor receptor (EGFR) tyrosine kinase] and bevacizumab [monoclonal antibody targeting vascular endothelial growth factor (VEGF)]. Clearly, the approach to developing these kinds of drugs for NSCLC and other cancers needs to change, or we will continue to waste precious clinical trial resources in futile studies.

Authors' Affiliation: Merck Research Laboratories, North Wales, Pennsylvania

Corresponding Author: Eric H. Rubin, Merck Research Laboratories, 351 North Sumneytown Pike, North Wales, PA 19454. Phone: 267-305-1717; Fax: 267-305-6042; E-mail: eric_rubin@merck.com

doi: 10.1158/2159-8274.CD-11-0036

Table 1. Signaling pathway–targeting compounds that failed in phase III trials involving unselected NSCLC patients

Agent	Target	Trial design
Bexarotene	RXR	Add-on to vinorelbine/cisplatin
Sorafenib	Multikinase	Add-on to carboplatin/paclitaxel
		Add-on to gemcitabine/cisplatin
Vandetanib	Multikinase	Add-on to erlotinib
		Add-on to docetaxel[a]
		Add-on to pemetrexed
Bevacizumab	VEGF	Add-on to erlotinib
Cediranib	VEGFR	Add-on to carboplatin/paclitaxel
Figitumumab	IGF1R	Add-on to carboplatin/paclitaxel
		Add-on to erlotinib
Lonafarnib	Farnesyltransferase	Add-on to carboplatin/paclitaxel
PFS3512676	TLR9	Add-on to carboplatin/paclitaxel
Vadimezan	Tumor vasculature	Add-on to carboplatin/paclitaxel

NOTE: Shading indicates compounds that were studied in the BATTLE trial.

Abbreviations: RXR, retinoid X receptor; TLR9, Toll-like receptor 9.

[a]Met primary progression-free survival end point of a hazard ratio <0.80; no difference in overall survival.

Although this problem is well recognized and frequently discussed, in practice little has changed in the use of traditional phase I and II trial designs in cancer drug development. In part, this lack of change has resulted from the difficulty of selecting a diagnostic test to identify responsive patient subgroups in early clinical trials, and even when a test has been selected, it has often been incorrect. A good example is the selection of EGFR protein expression to predict responsiveness to the EGFR-targeting antibody cetuximab. This choice was rational, based on preclinical studies of the antibody–receptor interaction (2), but subsequent studies indicated that EGFR protein expression, as assessed by immunohistochemical (IHC) analyses, is not a useful predictor for responsiveness to cetuximab in the clinic (3). Similarly, although intuitively appealing and supported by preclinical experiments (4), insulin-like growth factor 1 receptor (IGF1R) protein expression alone has not been useful in selecting patients who will benefit from treatment with IGF1R-targeting antibodies (5). These kinds of errors are, in some measure, due to the frequent depiction of cancer pathways as relatively simple, well-understood linear networks, when in reality our understanding of these pathways, and their perturbation by therapeutics, remains poor. In addition, agnostic, systems biology approaches to identifying "molecular signatures" for responsive patient subgroups have been hampered by the requirement for relatively large clinical datasets for signature validation, which are not available in early phase I and II trials of a new anticancer agent. Further, molecular signatures derived from preclinical studies have not yet proved reliable for predicting benefit in the clinic (6, 7). Thus, despite major advances in understanding cancer biology over the past 30 years, only 8 diagnostic tests used to select responsive patient subgroups are included in cancer drug labels (estrogen receptor IHC, HER-2 IHC/DNA hybridization assay, EGFR IHC, C-KIT IHC, BCR-ABL chromosome, PML-RAR chromosome, 5 del chromosome, and RAS mutation), with only 3 of these FDA approved (HER-2 IHC/DNA hybridization assay, EGFR IHC, and C-KIT IHC).

BATTLE TRIAL DESIGN AND WHAT WE CAN LEARN FROM A DRUG DEVELOPMENT PERSPECTIVE

The BATTLE trial investigators must be recognized and congratulated as bold innovators in their efforts to move beyond traditional clinical trial designs that are ineffective in simultaneously developing a new therapeutic and a matching diagnostic test. The investigators showed that treatment allocation based on results from multiple assays performed on computed tomography–guided biopsy specimens is feasible and associated with minimal safety risk. The study used an adaptive randomization design for this allocation, which was based on ongoing analyses of the rate of 8-week disease control obtained for 20 biomarker-treatment groups (4 treatments, with 5 biomarker groups, yields 20 combinations; the number of patients in some groups was small, as shown in Table 2 of ref. 1). The results indicate that 8 of the 20 biomarker–treatment matches met the predefined criterion for efficacy: a >80% probability of achieving a >30% 8-week disease control rate (DCR; ref. 1). Some matches that met the efficacy criterion are consistent with our current understanding of markers predictive for drug efficacy, such as *KRAS/BRAF* mutations predicting for response to sorafenib (8). However, other matches are more difficult to understand, including the finding that the highest DCR for erlotinib (40%) was in the VEGF/VEGFR-2 biomarker group. One might have expected the highest DCR for erlotinib to have been in the EGFR biomarker group (which had a 35% DCR that did not meet the efficacy criterion).

Another consideration is that issues with the BATTLE study design complicate interpretation of results. First, as noted by the investigators, partial exclusion of patients with previous erlotinib treatment confounded the adaptive randomization process because these patients could be randomized to only 2 of the 4 treatment arms. Second, technical qualifications of the assays used for biomarker grouping were not reported; thus, the choice of cutoffs for these assays (to determine whether a patient's tumor was "positive" or "negative" for a given biomarker group) could be questioned. These issues make it difficult to conclude that predictive biomarkers have been identified for the treatments. In addition, although the authors assert that the study "validated prespecified hypotheses regarding predictive biomarkers," the precise biomarker hypotheses, as well as associated type I and type II statistical errors, are not clear. Thus, the study should be considered as generating a hypothesis rather than as confirming a particular biomarker hypothesis.

From a drug developer perspective, it is of interest to ask whether BATTLE results will influence development plans for the investigational drugs included in the study, or whether BATTLE results might have altered development plans if the results had been available before phase III studies were initiated for bexarotene, sorafenib, or vandetanib, all of which yielded negative results in an unselected NSCLC population (Table 1). With regard to future development, although it is not clear whether the manufacturers of bexarotene, sorafenib, or vandetanib will initiate confirmatory studies in biomarker-defined patient populations identified in BATTLE as potentially responsive to these drugs, 2 BATTLE-like studies have been initiated recently, with support from multiple pharmaceutical companies: BATTLE-FL (front line; NCT01263782) and BATTLE-2 (NCT01248247). BATTLE-FL involves lung cancer patients who are chemotherapy naïve for metastatic disease and includes the combination of pemetrexed and carboplatin as a "control group," with other treatment arms involving addition of anti-VEGF (bevacizumab), anti-EGFR (cetuximab), or anti-IGF1R (cixutumumab) antibodies to the pemetrexed + carboplatin backbone. Similar to BATTLE, BATTLE-2 involves previously treated lung cancer patients and includes erlotinib and sorafenib treatment arms as well as 2 other investigational treatments: a combination of the AKT inhibitor MK-2206 with the MEK inhibitor AZD6244 and a combination of MK-2206 with erlotinib. As noted in the article by Kim and colleagues (1), this study involves an approach to biomarker selection and tumor classification that is different from the approach of the BATTLE trial. In the first half of the study, clinically validated biomarkers (such as *KRAS* mutation) will define biomarker groups to be used in adaptive treatment allocation. A limited set of additional prespecified biomarkers will be evaluated in tumor

Table 2. Alternative approach to BATTLE

Traditional single-arm phase II trial	Biomarker eligibility requirement	Estimated proportion of eligible patients (%)	Sample size needed without early stopping	Expected sample size with early stopping
Erlotinib	*EGFR* mutation	15	133	100
Vandetanib	VEGFR-2 overexpression (IHC score >100)	40	50	38
Erlotinib + bexarotene	RXRα overexpression (nuclear IHC score >30)	80	25	19
Sorafenib	*KRAS* or *BRAF* mutation	22	91	68
			Total = 299	Total = 225

NOTE: This alternative approach uses 4 separate Simon 2-stage phase II trials that treat only biomarker-positive patients.

biopsies. After analysis of results, biomarkers considered to be potentially predictive for response to each experimental treatment will be selected for use in treatment allocation decisions in the second half of the study.

ALTERNATIVE APPROACHES TO CODEVELOPMENT OF A NEW THERAPEUTIC WITH A MATCHING PREDICTIVE DIAGNOSTIC TEST

Although it is not difficult to point out flaws in the BATTLE trial and to question the significance of results in terms of subsequent development of drugs and biomarkers included in the trial, it is more problematic to suggest an alternative, more efficient approach to codevelopment of new therapeutics with matching predictive biomarkers.

Two major innovations of the BATTLE trial are its operational and statistical approaches. From an operational perspective, BATTLE successfully pioneered an ambitious goal of incorporating 4 different treatment arms (requiring cooperation of 4 different pharmaceutical companies) and 5 different biomarker classifiers within a single study, with treatment allocation based on results of a diagnostic biopsy. Considerable operational efficiency is gained by the lack of "screen failures" versus a traditional approach to selecting only biomarker-positive patients for separate phase II studies. For example, using a traditional single-arm phase II Simon 2-stage approach with null and alternative hypotheses that match those of BATTLE—the null hypothesis is a DCR of 30%, and the alternative hypothesis is a DCR of 50%, with 20% type I error rate and 80% power—with treatment of only biomarker-positive patients in each phase II study (using the data in Supplementary Table S1 of ref. 1 to calculate the frequency of biomarker-positive patients), up to 299 patients would need to be enrolled and undergo biopsy (to obtain 20 biomarker–positive patients for each treatment), compared with the 200 patients required for BATTLE (ref. 9; Table 2). Even with an assumption that all separate phase II studies would stop early, 225 patients (on average) would be needed (Table 2).

Furthermore, among the 4 treatment arms in the BATTLE trial, erlotinib was the only one FDA approved for lung cancer before initiation of the trial. As described previously (10), if the erlotinib arm is viewed as a control group, then additional operational efficiency is gained by inclusion of 3 experimental treatments with 1 control treatment in a single study, as opposed to the traditional approach of separate randomized phase II trials, each comparing one experimental treatment to erlotinib.

The second major innovation of the BATTLE trial is the statistical approach, using adaptive rather than equal randomization. Adaptive randomization allowed selection of the best treatment arm for each enrolled patient based on accumulating knowledge of the DCR for each of the 20 biomarker–treatment matches evaluated in the study. Simulations performed by the BATTLE statisticians indicate that, even with a requirement for equal randomization among approximately the first 90 of 200 patients (to avoid early skewing of the adaptive randomization process), the adaptive randomization approach provides higher expected overall DCRs than does an equal randomization approach (9). The adaptive approach is attractive to both patients and physicians because it epitomizes the idea of "personalized medicine." Notably, a similar approach is used in the Investigation of Serial Studies to Predict Your Therapeutic Response with Imaging and Molecular Analysis 2 (I-SPY 2) trial, which involves patients with newly diagnosed breast cancer who are eligible for neoadjuvant treatment with a taxane (11).

A caveat regarding the use of adaptive randomization is that the differences in expected DCRs for adaptive versus equal randomization in the BATTLE trial simulations were relatively small (9), and that Korn and Freidlin (12) have reported similar simulations for 2-arm studies, in which the advantages of adaptive versus equal randomization (or alternate fixed randomization, such as 2:1) in the probability of disease control were found to be quite small and of questionable advantage from a trial design perspective.

An alternative approach to BATTLE, using fixed randomization with a similar number of patients, can be used to

determine whether codevelopment of an experimental agent with a matching diagnostic test should move forward. For example, we consider a 240-patient trial with equal randomization comparing 3 experimental groups with a common control, with 5 distinct biomarker subpopulations equally distributed across the treatment groups (yielding 20 biomarker–treatment matches, as in BATTLE). A set of decision rules may be constructed on the basis of observed P values, comparing each experimental treatment with the control. If the test in the all-comers population is not significant at a prespecified threshold (e.g., $P > 0.2$), then further development may not be considered; conversely, further development of an experimental treatment in all comers might be considered if the test is significant (e.g., $P < 0.05$). An observed trend toward statistical significance (e.g., $0.05 \leq P < 0.20$) could trigger a comparison of the experimental treatment with the control in each biomarker subpopulation, with additional development in a specific subpopulation considered if $P < 0.05$. Using this example and assuming a DCR of 30% in all but one biomarker subpopulation for a given experimental treatment, we see that an underlying 80% DCR would be required to have a >50% probability of moving an experimental treatment forward, either in a biomarker subpopulation or in an all-comers population. Although an 80% DCR may seem high, precedence for this kind of efficacy exists in well-matched biomarker–treatment combinations (such as *BRAF* mutation and the BRAF inhibitor PLX4032) and is arguably an appropriate expectation for further development of new therapeutics with matching diagnostic tests.

Statistical designs different from those of BATTLE and I-SPY 2 have been proposed for randomized trials that include predictive biomarker hypotheses (13, 14). These designs do not require a prespecified biomarker test used for treatment assignment, which avoids the screen failure problem described above. The cross-validated adaptive signature design (14) is particularly attractive because it can test multiple biomarkers in a large trial with many clinical end points in the true population of interest. Statistical validity of selected subgroups is characterized by evaluating the signature selection procedure among multiple (e.g., 10) nonoverlapping groups, forming a 90% sample for each complement to the 10% subsample for training and using the 10% sample to test how well the predicted model works. Combining variability across these samples gives a composite predictive value of the signature selection procedure. Although signatures in the 10 subsets evaluated will vary, they presumably will predict patient outcomes and treatment benefit similarly well; that is, they are all different, but similar, "versions of the truth." Not having to prespecify a set of biomarkers to test before enrollment has the major advantage of accommodating how little we often know at the beginning of a pivotal trial about which subgroups may benefit from a novel treatment regimen.

In summary, successful completion of the BATTLE study is an important milestone in the war against cancer. Biomarker-based approaches like those of BATTLE and I-SPY 2, as well as fixed randomization alternatives, represent major advances in trial design that should accelerate identification of predictive biomarkers for novel therapeutics.

Disclosure of Potential Conflicts of Interest

No potential conflicts of interest were disclosed.

Published OnlineFirst April 3, 2011.

REFERENCES

1. Kim ES, Herbst RS, Wistuba II, Lee JJ, Blumenschein GR Jr, Tsao A, et al. The BATTLE Trial: personalizing therapy for lung cancer. Cancer Discovery 2011;1:OF42–OF51.
2. Goldenberg A, Masui H, Divgi C, Kamrath H, Pentlow K, Mendelsohn J. Imaging of human tumor xenografts with an indium-111-labeled anti-epidermal growth factor receptor monoclonal antibody. J Natl Cancer Inst 1989;81:1616–25.
3. Chung KY, Shia J, Kemeny NE, Shah M, Schwartz GK, Tse A, et al. Cetuximab shows activity in colorectal cancer patients with tumors that do not express the epidermal growth factor receptor by immunohistochemistry. J Clin Oncol 2005;23:1803–10.
4. Gong Y, Yao E, Shen R, Goel A, Arcila M, Teruya-Feldstein J, et al. High expression levels of total IGF-1R and sensitivity of NSCLC cells in vitro to an anti-IGF-1R antibody (R1507). PLoS One 2009;4:e7273.
5. Gualberto A, Dolled-Filhart M, Gustavson M, Christiansen J, Wang YF, Hixon ML, et al. Molecular analysis of non-small cell lung cancer identifies subsets with different sensitivity to insulin-like growth factor I receptor inhibition. Clin Cancer Res 2010;16: 4654–65.
6. Baggerly K, Coombes K. Deriving chemosensitivity from cell lines: forensic bioinformatics and reproducible research in high-throughput biology. Ann Appl Stat 2009;3:1309–34.
7. Potti A, Dressman HK, Bild A, Riedel RF, Chan G, Sayer R, et al. Genomic signatures to guide the use of chemotherapeutics. Nat Med 2006;12:1294-300.
8. Wilhelm SM, Carter C, Tang L, Wilkie D, McNabola A, Rong H, et al. BAY 43-9006 exhibits broad spectrum oral antitumor activity and targets the RAF/MEK/ERK pathway and receptor tyrosine kinases involved in tumor progression and angiogenesis. Cancer Res 2004;64:7099–109.
9. Zhou X, Liu S, Kim ES, Herbst RS, Lee JJ. Bayesian adaptive design for targeted therapy development in lung cancer—a step toward personalized medicine. Clin Trials 2008;5:181–93.
10. Freidlin B, Korn EL, Gray R, Martin A. Multi-arm clinical trials of new agents: some design considerations. Clin Cancer Res 2008;14:4368–71.
11. Barker AD, Sigman CC, Kelloff GJ, Hylton NM, Berry DA, Esserman LJ. I-SPY 2: an adaptive breast cancer trial design in the setting of neoadjuvant chemotherapy. Clin Pharmacol Ther 2009;86:97–100.
12. Korn EL, Freidlin B. Outcome-adaptive randomization: is it useful? J Clin Oncol 2011;29:771–6.
13. Baker SG, Sargent DJ. Designing a randomized clinical trial to evaluate personalized medicine: a new approach based on risk prediction. J Natl Cancer Inst 2010;102:1756–9.
14. Freidlin B, Jiang W, Simon R. The cross-validated adaptive signature design. Clin Cancer Res 2010;16:691–8.

Cancer Discovery Publish Ahead of Print, published on April 3, 2011 as doi:10.1158/2159-8274.CD-11-0044

IN THE SPOTLIGHT

A New BATTLE in the Evolving War on Cancer

Lecia V. Sequist[1,2], Alona Muzikansky[1,3], and Jeffrey A. Engelman[1,2]

Summary: The Biomarker-integrated Approaches of Targeted Therapy for Lung Cancer Elimination (BATTLE) trial couples real-time molecular interrogation of cancer specimens with an adaptive Bayesian clinical trial design. *Cancer Discovery; 1(1). ©2011 AACR.*

Commentary on Kim et al., p. OF42 (6).

The landscape of non–small cell lung cancer (NSCLC) diagnosis and treatment has dramatically changed in the past few years owing to the successful pairing of biomarker-defined cohorts of patients with targeted therapeutics: namely, *EGFR* mutations as biomarkers of benefit from epidermal growth factor receptor (EGFR) tyrosine kinase inhibitors (TKI) and *EML-ALK* translocations as biomarkers of benefit from ALK TKIs (1, 2). Testing NSCLC patients for these and other biomarkers at the time of diagnosis is becoming more routine because it affects decisions about treatment as well as patient outcomes (3). These examples also underscore the value of exploring biomarkers during early clinical trials with targeted therapies. However, most novel targeted therapies studied in NSCLC clinical trials are not administered as initial therapies but rather as second, third, or later lines of treatment. Clinical trial designs frequently do not mandate tumor tissue from all patients but attempt *post hoc* analyses of biomarker status among those with available tissue from the original diagnostic biopsy, typically 25% to 45% of the study population (1, 4, 5). Not only is this "strategy of convenience" not comprehensive, but it also risks inaccurate conclusions if intervening treatments have altered the biologic and/or biomarker status since the time of the archival biopsy specimen. Capturing the biomarker status for all participants at the time of drug administration maximizes the chances of discovering the relationship between putative biomarkers and response to novel treatments. In this issue of *Cancer Discovery*, Kim and colleagues (6) describe their landmark effort to accomplish these goals within the framework of the Biomarker-integrated Approaches of Targeted Therapy for Lung Cancer Elimination (BATTLE) trial.

BATTLE was designed as an umbrella structure, within which 4 separate therapeutic clinical trials for NSCLC were nested: erlotinib, vandetanib, erlotinib plus bexarotene, and sorafenib. All NSCLC patients entering the BATTLE program (at the time of second-line therapy or beyond) first underwent a core tumor biopsy for the purpose of obtaining up-to-date biomarker status and then were randomized to one of the 4 treatment arms. Biomarker analysis was done in real time, with a large panel of mutation, gene copy number, and immunohistochemistry analyses performed on each sample. The results of these studies grouped patients into predefined biomarker signature groups, which could then be used to evaluate treatment–biomarker interactions. The initial 97 patients were randomized equally into the 4 different treatments, with a 25% chance of being placed into each treatment arm. Results from these 97 patients were then assessed, comparing the outcome of interest—8-week disease control rate (DCR)—with the biomarker status within each treatment arm. With this information, future randomization probabilities were adjusted (rather than being equal) using a Bayesian model. This adjustment means that if a patient was found to have a particular biomarker signature on biopsy, he or she would have a >25% chance of being randomized to a treatment on which prior patients with the same biomarker signature had done well with respect to 8-week DCR. The pattern continually repeated, so that the more patients with a particular signature did well on a particular therapy, the higher the probability of being assigned to that therapy for subsequent similar patients. The authors planned to benchmark the BATTLE 8-week DCR against the historical rate of 30% for similar patients. The study was not designed to determine if significant associations existed between particular biomarkers and treatments.

The innovative adaptive randomization design attempts to increase the opportunity for each patient to receive the most effective experimental treatment possible, a feature that is attractive to potential patients and their oncologists alike. However, this type of Bayesian design has not yet been used in clinical research with the frequency required to establish robust standard practices. Some concerns have arisen that adaptive randomization may worsen the precision of estimates of treatment effect by increasing variability, mainly owing to unequal subject allocation to the treatment arms (7). The potential caveats of the Bayesian design aside, the authors deserve tremendous praise for accomplishing this Herculean task. The difficulty in establishing the infrastructure and multidisciplinary collaborations necessary to successfully carry out 255 core needle biopsies with real-time multiplexed genotype and other biomarker analyses cannot be overstated.

Authors' Affiliations: [1]Harvard Medical School; [2]Massachusetts General Hospital Cancer Center; and [3]Department of Biostatistics, Massachusetts General Hospital, Boston, Massachusetts

Corresponding Author: Jeffrey A. Engelman, Massachusetts General Hospital Cancer Center, CNY 149, 13th Street, Charlestown, MA 02129. Phone: 617-724-7298; Fax: 617-724-9648; E-mail: jengelman@partners.org

doi: 10.1158/2159-8274.CD-11-0044

This study showed that these procedures were safe (<1% incidence of serious complications among patients undergoing lung biopsy) and that real-time biomarker assessment is possible (83% of patients could be categorized into one of the predefined biomarker signature cohorts). Had the authors designated feasibility as an end point for the BATTLE trial, they would likely have met their benchmarks. The University of Texas MD Anderson Cancer Center (Houston, Texas) has shown that trials mandating pretreatment biopsies coupled with complex real-time biomarker analysis are feasible.

The primary end point of the trial, 8-week DCR, has been shown previously to be a reasonable surrogate for overall survival (8). The authors chose this somewhat unconventional end point because the adaptive randomization design requires an end point that can be rapidly determined for each patient, to facilitate the Bayesian algorithm going forward. The overall 8-week DCR was 46% among 244 evaluable patients. When examining 8-week DCR by treatment arm, they observed 34% for erlotinib, 33% for vandetanib, 50% for erlotinib + bexarotene, and 58% for sorafenib. The study did not report the 8-week DCR among the initial cohort of patients assigned to treatment by equal randomization because, as the authors point out, the study was not designed or powered to assess this crucial question. However, these data would be useful to determine whether the Bayesian trial design truly did affect patient outcomes and steer patients toward the most effective therapies. Because these initial observations formed the basis for adaptive randomization used in the rest of the trial, an appreciation of the magnitude of variation among the initial cohort would increase general confidence in the potential benefits of this adaptive randomization study design.

The BATTLE investigators did report treatment efficacy by biomarker signature groups. The results from the large number of biomarkers assessed on each patient were condensed into 4 biologically relevant groups, and the biomarker-positive versus biomarker-negative couplets were then analyzed by treatment arm. Significant biomarker–treatment relationships were defined as those in which the biomarker-positive group had an 80% probability of achieving better outcomes than the historical 8-week DCR of 30%. This threshold turned out to have a relatively low sensitivity, as 8 of the 20 pairs they examined had a significant biomarker–treatment relationship. However, setting the bar low is acceptable in this sort of hypothesis-generating exercise and allows the investigators to observe correlations that might not have been envisioned *a priori*. In fact, one of the most interesting findings from the BATTLE study is the promising biomarker–treatment relationship between *KRAS* or *BRAF* mutation–positive patients and sorafenib therapy (79% of the biomarker-positive patients had 8-week DCR). It seems likely that the adaptive randomization design enhanced the ability to make this observation by aggregating these patients into the sorafenib arm. A total of 27 patients were positive for the *KRAS/BRAF* biomarker signature, and half of them ($n = 14$) were assigned to sorafenib. Examined from the opposite perspective, the BATTLE design directed *KRAS*-positive patients away from the other 3 treatment arms, which all included EGFR inhibitors; this strategy was likely beneficial because previous data have demonstrated that EGFR TKIs are ineffective against *KRAS* mutant cancers (5, 9, 10). Although BATTLE does not definitively confirm a relationship between *KRAS* mutations and sorafenib efficacy, it certainly provides the impetus for ongoing validation studies as well as future studies to assess more potent inhibitors of the RAF/MEK/ERK signaling axis in these cancers.

It is notable that decisions about how to define biomarker groupings at the outset of the trial may have obscured the ability to make some observations. As the authors point out, the most obvious example of this is the pairing of *EGFR* mutations with *EGFR* gene copy number into a single group. At the time BATTLE was designed, this seemed a reasonable strategy because both biomarkers were considered predictive for benefit from EGFR TKIs. However, it has now become clear that *EGFR* mutations are much more reliable for identifying patients who will benefit from EGFR TKI therapy (11), and the aggregation with *EGFR* gene copy number likely muted the relationship observed between the *EGFR* biomarker group and erlotinib-based therapies. It is not known at this time if other grouping decisions may have influenced the observations in a similar way. This point highlights the concern that a large and complex research structure such as BATTLE, with an umbrella framework and multiple nested treatment studies, does not have the agility to adapt quickly as knowledge outside the trial advances. For example, the *ALK* translocation story developed all the way from the bench to the bedside during the course of the BATTLE trial (2, 12). The investigators acknowledge this development and plan to exclude patients with *ALK* translocations from future BATTLE studies so that they will be steered toward ALK-directed therapies; one hopes that other such biomarker–treatment combination success stories will develop over the course of subsequent BATTLE studies, and the investigators will need to be mindful to build strategies for identifying and triaging these patients into their future designs.

It remains challenging to define the exact circumstances in which the Bayesian trial design will more rapidly identify clinically significant biomarker–targeted therapy relationships, compared with the more common clinical trial designs, such as prospective biomarker-directed trials (e.g., crizotinib in ALK-translocated cancers) or careful retrospective examination of specific biomarkers in conventional targeted therapy trials (13–15). The BATTLE study design may provide a more distinct advantage in the study of novel drugs without clearly understood mechanisms of action or in situations when the biologic characteristics of the target are uncertain. In these situations, real-time, complex biomarker analyses may accelerate the identification and further testing of potential biomarker–therapy relationships. Conversely, when hypotheses about the drug target and its biologic features are well understood, the adaptive randomization strategy may be less efficient than either prospective biomarker-directed trials addressing mature hypotheses or conventional targeted therapy studies in less restricted patient populations that incorporate retrospective analyses of well-defined biomarkers.

In summary, the BATTLE trial offers proof that, with a concerted, determined effort, we can successfully raise the bar for lung cancer clinical trials research to include

comprehensive pretreatment biopsies and genotyping for all participants. We believe that such efforts have great potential to exponentially increase our understanding of patients who benefit from targeted therapies and are likely to accelerate and improve the drug development process. Although it remains to be determined when an adaptive randomization design such as the one used by BATTLE investigators ultimately increases the efficiency of discovery, these investigators have clearly set a new standard for acquiring tissue and performing comprehensive biomarker evaluation in real time. The rest of us will have no valid excuses when future compelling trials demand the same.

Disclosure of Potential Conflicts of Interest

No potential conflicts of interest were disclosed.

Published OnlineFirst April 3, 2011.

REFERENCES

1. Mok TS, Wu YL, Thongprasert S, Yang CH, Chu DT, Saijo N, et al. Gefitinib or carboplatin-paclitaxel in pulmonary adenocarcinoma. N Engl J Med 2009;361:947–57.
2. Kwak EL, Bang YJ, Camidge DR, Shaw AT, Solomon B, Maki RG, et al. Anaplastic lymphoma kinase inhibition in non-small-cell lung cancer. N Engl J Med 2010;363:1693–1703.
3. Azzoli CG, Baker S Jr, Temin S, Pao W, Aliff T, Brahmer J, et al. American Society of Clinical Oncology Clinical Practice Guideline update on chemotherapy for stage IV non-small-cell lung cancer. J Clin Oncol 2009;27:6251–66.
4. Tsao MS, Sakurada A, Cutz JC, Zhu CQ, Kamel-Reid S, Squire J, et al. Erlotinib in lung cancer—molecular and clinical predictors of outcome. N Engl J Med 2005;353:133–44.
5. Eberhard DA, Johnson BE, Amler LC, Goddard AD, Heldens SL, Herbst RS, et al. Mutations in the epidermal growth factor receptor and in KRAS are predictive and prognostic indicators in patients with non-small-cell lung cancer treated with chemotherapy alone and in combination with erlotinib. J Clin Oncol 2005;23:5900–9.
6. Kim ES, Herbst RS, Wistuba II, Lee JJ, Blumenschein GR Jr, Tsao A, et al. The BATTLE trial: personalizing therapy for lung cancer. Cancer Discovery 2011;1:OF42–OF51.
7. Thall PF, Wathen JK. Practical Bayesian adaptive randomisation in clinical trials. Eur J Cancer 2007;43:859–66.
8. Lara PN Jr, Redman MW, Kelly K, Edelman MJ, Williamson SK, Crowley JJ, et al. Disease control rate at 8 weeks predicts clinical benefit in advanced non-small-cell lung cancer: results from Southwest Oncology Group randomized trials. J Clin Oncol 2008;26:463–7.
9. Massarelli E, Varella-Garcia M, Tang X, Xavier AC, Ozburn NC, Liu DD, et al. KRAS mutation is an important predictor of resistance to therapy with epidermal growth factor receptor tyrosine kinase inhibitors in non-small-cell lung cancer. Clin Cancer Res 2007;13:2890–6.
10. Jackman DM, Miller VA, Cioffredi LA, Yeap BY, Jänne PA, Riely GJ, et al. Impact of epidermal growth factor receptor and KRAS mutations on clinical outcomes in previously untreated non-small cell lung cancer patients: results of an online tumor registry of clinical trials. Clin Cancer Res 2009;15:5267–73.
11. Fukuoka M, Wu Y, Thongprasert S, Yang CH, Chu DT, Saijo N, et al. Biomarker analyses from a phase III, randomized, open-label, first-line study of gefitinib (G) versus carboplatin/paclitaxel (C/P) in clinically selected patients (pts) with advanced non-small cell lung cancer (NSCLC) in Asia (IPASS). J Clin Oncol 2009;27 Suppl: abstract 8006.
12. Soda M, Choi YL, Enomoto M, Takada S, Yamashita Y, Ishikawa S, et al. Identification of the transforming EML4-ALK fusion gene in non-small-cell lung cancer. Nature 2007;448:561–6.
13. Sequist LV, Gettinger S, Senzer NN, Martins RG, Jänne PA, Lilenbaum R, et al. Activity of IPI-504, a novel heat-shock protein 90 inhibitor, in patients with molecularly defined non-small-cell lung cancer. J Clin Oncol 2010;28:4953–60.
14. Sequist LV, Akerley W, Brugger W, Ferrari D, Garmey EG, Gerber DE, et al. Final results from ARQ 197–209: a global randomized placebo-controlled phase 2 clinical trial of erlotinib plus ARQ 197 versus erlotinib plus placebo in previously treated EGFR-inhibitor naïve patients with advanced non-small cell lung cancer (NSCLC). Paper presented at European Society for Medical Oncology Congress; October 8–11, 2010; Milan, Italy.
15. Spigel DR, Ervin TJ, Ramlau R, Daniel DB, Goldschmidt JH, Krzakowski M, et al. Randomized, phase II, multicenter, double-blind, placebo-controlled study evaluating MetMAb, an antibody to Met receptor, in combination with erlotinib, in patients with advanced non-small-cell lung cancer (OAM4558g). Paper presented at European Society for Medical Oncology Congress; October 8–11, 2010; Milan, Italy.

37 An epithelial to mesenchymal transition (EMT) gene expression signature identifies Axl as an EMT marker in non-small cell lung cancer (NSCLC) and head and neck cancer (HNC) lines and predicts response to erlotinib

ORAL

L. Byers *J. Wang, L. Diao, J. Yordy, L. Girard, M. Story, K. Coombes, J. Weinstein, J. Minna, J. Heymach*

MD Anderson Cancer Center, Thoracic/Head and Neck Medical Oncology Houston TX USA; MD Anderson Cancer Center, Bioinformatics and Computational Biology Houston TX USA; MD Anderson Cancer Center

Background: Epithelial/mesenchymal transition (EMT) is associated with loss of cell adhesion molecules such as E-cadherin and increased invasion, migration, and proliferation in epithelial cancers. In non-small cell lung cancer (NSCLC), EMT is associated with worse prognosis and resistance to EGFR inhibitors. Despite the clinical implications, no gold standard exists for classifying a cancer as epithelial or mesenchymal. The goal of this study was to develop a robust EMT gene expression signature and test its correlation with drug response.

Materials/Methods: The EMT signature was derived in 54 DNA fingerprinted NSCLC cell lines profiled on Affymetrix U133A, B, and Plus2.0 arrays and tested on the Illumina WGv2 and WGv3 platforms and in an independent set of head and neck cancer lines (HNC). E-cadherin and other protein levels were quantified by reverse phase protein array and correlated with the first principal component of the EMT signature. IC50s were determined for NSCLC cell lines by MTS assay.

Results: Expression of 76 genes (the EMT signature) correlated with mRNA expression of known EMT markers E-cadherin, vimentin, N-cadherin, or fibronectin 1 and was bimodally distributed across the NSCLC panel. Classification of the NSCLC lines as epithelial or mesnchymal by the EMT signature agreed for 51/52 cell lines tested on both Affymetrix and Illumina platforms. In an independent validation set of 62 HNC lines, the signature identified a subset of six mesenchymal cell lines. The EMT signature score correlated well with E-cadherin protein levels in NSCLC ($r = 0.90$) and HNC ($r = 0.73$). mRNA levels for Axl, a tyrosine kinase receptor associated with EMT in breast cancer, had the most negative correlation with E-cadherin ($r = -0.45$) of any signature gene after ZEB1 and vimentin and was positively correlated with vimentin ($r = 0.60$) and N-cadherin ($r = 0.54$) expression. Higher Axl total protein was confirmed in NSCLC and HNC mesenchymal-like cell lines. Mesenchymal phenotype (classified by the EMT signature) was more strongly correlated with NSCLC erlotinib resistance ($p = 0.028$) than E-cadherin mRNA or protein level.

Conclusions: An EMT gene expression signature accurately classifies cell lines as epithelial or mesenchymal-like across three microarray platforms and two cancer types and identifies Axl as a novel EMT marker in NSCLC and HNC. The EMT signature was a better predictor of erlotinib resistance than single mRNA or protein markers such as E-cadherin.

American Society of Clinical Oncology
www.asco.org

Sorafenib treatment efficacy and KRAS biomarker status in the Biomarker-Integrated Approaches of Targeted Therapy for Lung Cancer Elimination (BATTLE) trial.

Sub-category:
Metastatic

Category:
Lung Cancer - Metastatic

Meeting:
2010 ASCO Annual Meeting

Session Type and Session Title:
General Poster Session, Lung Cancer - Metastatic

Abstract No:
7609

Citation:
J Clin Oncol 28:15s, 2010 (suppl; abstr 7609)

Author(s):
R. S. Herbst, G. R. Blumenschein Jr., E. S. Kim, J. Lee, A. S. Tsao, C. M. Alden, S. Liu, D. J. Stewart, I. I. Wistuba, W. K. Hong; University of Texas M. D. Anderson Cancer Center, Houston, TX

Abstract:

Background: BATTLE is a phase II study to prospectively use biomarkers (BM) to guide treatment selection in patients (PTS) with advanced non-small cell lung cancer (NSCLC). This report details a subset analysis of the 8-week disease control rate (DCR) of PTS treated with sorafenib (S) relative to their BM status. **Methods:** In this phase II, multi-arm study, PTS with pretreated NSCLC, ECOG PS 0-2, consented to fresh core needle biopsies to test, in a research lab, 11 biomarkers related to 4 molecular pathways in NSCLC (*EGFR*, *KRAS*, and *BRAF* gene mutation [PCR-based sequencing], EGFR and Cyclin D1 copy number [FISH], and 6 proteins via IHC [VEGF/R and RXR receptors/Cyclin D1]). PTS were randomized, based on eligibility and BM grouping, into 1 of 4 treatments (erlotinib [E], sorafenib, vandetinab and erlotinib plus bexarotene). PTS randomized to the S arm received S 400 mg orally twice daily until tumor progression or an unacceptable toxicity. Tumor evaluations were performed at baseline and every 8 weeks. The primary objective was to assess DCR. **Results:** 105 PTS were randomized to receive S: 82% Caucasian, 51% male, 68% adenocarcinoma, 13% squamous cell carcinoma, ECOG status was 0-1 in 89% of PTS. 31 PTS had dose reduction/discontinuation of S. The most common reasons were hand-foot syndrome (n = 6), hemoptysis (n = 5), fatigue, and rash (n = 2 each). DCR for PTS treated with S was 58% (57 in 98 pts with outcome). No responses were observed. In PTS with the presence of a *KRAS* mutation, DCR was 61% (11/18), in contrast to 31% (4/13) in *KRAS*-mutated PTS treated with regimens with E. In PTS with an *EGFR* mutation, DCR was significantly lower (23%, 3/13) when compared to those PTS without the mutation (64%, n = 43/67) (p = 0.012). PTS with EGFR high-polysomy had a lower DC than those who did not (27%, 3/11; 62%, 42/68) (p = 0.048). **Conclusions:** DCR was improved in PTS treated with S who had *KRAS* mutations when compared to those who had *EGFR* mutations or copy number gain. This result suggests that PTS who have *KRAS* mutations may derive benefit from treatment with S, while those who have *EGFR* mutation/copy number gain may do worse. Supported by DoD grant W81XWH-6-1-0303.

Abstract Disclosures

Faculty & Discussant Disclosures

Annual Meeting Planning Committee Disclosures

Abstracts that were granted an exception in accordance with ASCO's Conflict of Interest Policy are designated with a caret symbol (^) here and in the printed Proceedings.

Associated Presentation(s):

1. Sorafenib treatment efficacy and KRAS biomarker status in the Biomarker-Integrated Approaches of Targeted Therapy for Lung Cancer Elimination (BATTLE) trial.

Meeting: 2010 ASCO Annual Meeting
Presenter: Roy S. Herbst
Session: Lung Cancer - Metastatic (General Poster Session)

Other Abstracts in this Sub-Category:

1. Weekly paclitaxel combined with monthly carboplatin versus single-agent therapy in patients age 70 to 89: IFCT-0501 randomized phase III study in advanced non-small cell lung cancer (NSCLC).

Meeting: 2010 ASCO Annual Meeting Abstract No: 2 First Author: E. A. Quoix
Category: Lung Cancer - Metastatic - Metastatic

2. Clinical activity of the oral ALK inhibitor PF-02341066 in ALK-positive patients with non-small cell lung cancer (NSCLC).

Meeting: 2010 ASCO Annual Meeting Abstract No: 3 First Author: Y. Bang
Category: Lung Cancer - Metastatic - Metastatic

3. Randomized, open-label study of pemetrexed/carboplatin followed by maintenance pemetrexed versus paclitaxel/carboplatin/bevacizumab followed by maintenance bevacizumab in patients with advanced non-small cell lung cancer (NSCLC) of nonsquamous histology.

Meeting: 2010 ASCO Annual Meeting Abstract No: TPS290 First Author: R. Zinner
Category: Lung Cancer - Metastatic - Metastatic

More...

Abstracts by R. S. Herbst:

1. Final results from a phase I, dose-escalation study of PX-866, an irreversible, pan-isoform inhibitor of PI3 kinase.

Meeting: 2010 ASCO Annual Meeting Abstract No: 3089 First Author: A. Jimeno
Category: Developmental Therapeutics - Experimental Therapeutics - Other Novel Agents

2. First-in-human phase I study of the oral PI3K inhibitor BEZ235 in patients (pts) with advanced solid tumors.

Meeting: 2010 ASCO Annual Meeting Abstract No: 3005 First Author: H. Burris
Category: Developmental Therapeutics - Experimental Therapeutics - Other Novel Agents

3. Results from a phase I, dose-escalation study of PX-478, an orally available inhibitor of HIF-1α.

Meeting: 2010 ASCO Annual Meeting Abstract No: 3076 First Author: R. Tibes

Category: Developmental Therapeutics - Experimental Therapeutics - Other Novel Agents

More...

Presentations by R. S. Herbst:

1. Sorafenib treatment efficacy and KRAS biomarker status in the Biomarker-Integrated Approaches of Targeted Therapy for Lung Cancer Elimination (BATTLE) trial.

Meeting: 2010 ASCO Annual Meeting
Presenter: Roy S. Herbst
Session: Lung Cancer - Metastatic (General Poster Session)

2. Customizing Therapy for Localized NSCLC

Meeting: 2009 ASCO Annual Meeting
Discussant: Roy S Herbst, MD, PhD
Session: Lung Cancer - Local-Regional and Adjuvant Therapy (Poster Discussion Session)

3. Vandetanib plus docetaxel vs docetaxel as 2nd-line treatment for patients with advanced non-small-cell lung cancer (NSCLC):a randomized, double-blind Phase III trial (ZODIAC)

Meeting: 2009 ASCO Annual Meeting
Presenter: Roy S Herbst, MD, PhD
Session: Lung Cancer - Metastatic (Oral Abstract Session)

More...

***Educational Book Manuscripts by R. S. Herbst*:**

1. Novel Therapeutic Options for Non-Small-Cell Lung Cancer (Second-Line and Subsequent Therapy)

Source: 2003 Educational Book
Category: Lung Cancer

More...

Print this Page

Presentation Abstract

Abstract Number:	LB-88
Presentation Title:	**Gene expression signatures predictive of clinical outcome and tumor mutations in refractory NSCLC patients (pts) in the BATTLE trial (Biomarker-integrated Approaches of Targeted Therapy for Lung Cancer Elimination)**
Presentation Time:	Sunday, Apr 03, 2011, 3:45 PM - 4:05 PM
Location:	Room W415 B/C, (Valencia Ballroom), Orange County Convention Center
Author Block:	*John V. Heymach*, *Pierre Saintigny*, *Edward S. Kim*, *Lauren A. Byers*, *J. Jack Lee*, *Kevin Coombes*, *Lixia Diao*, *Jing Wang*, *Hai Tran*, *You H. Fan*, *Anne Tsao*, *George R. Blumenschein Jr.*, *Vassiliki A. Papadimitrakopoulou*, *Ximing Tang*, *Michael Story*, *Yang Xie*, *Luc Girard*, *John Weinstein*, *Li Mao*, *John D. Minna*, *Roy Herbst*, *Scott M. Lippman*, *Waun K. Hong*, *Ignacio I. Wistuba*. UT MD Anderson Cancer Center, Houston, TX, UT Southwestern Medical Center at Dallas, Dallas, TX, University of Maryland Dental School, Baltimore, MD
Abstract Body:	**Background**: There are currently no established markers to identify pts bearing wild-type EGFR who are likely to benefit from erlotinib (ERLO). The EGFR and Kras pathways, and epithelial to mesenchymal transition (EMT), have been associated with response/resistance to EGFR inhibitors. We developed gene signatures for these pathways and tested whether they were predictive of disease control (DC) and tumor mutations using gene expression profiles from pts in the BATTLE trial, and developed novel markers for ERLO benefit in wt EGFR pts. **Methods:** Gene expression profiles (Affymetrix HG1.0ST) from pretreatment core needle biopsies (CNBs) were obtained from 101 BATTLE pts. Pathways signatures were developed using independent datasets from resected NSCLC pts and cell lines. A robust EGFR mutation signature was derived by comparing genes differentially expressed in mutated and wt *EGFR* lung adenocarcinoma from 3 independent institutions, and validated in three independent sets, both *in vivo* and *in vitro*. A KRAS signature was similarly derived. An EMT signature was derived by identifying genes with a bimodal distribution and correlated with known EMT genes (E-cadherin, vimentin, N-cadherin, FN-1) using 54 NSCLC cell lines, and validated in an independent panel of HN cell lines and across different platforms. A novel 5-gene signature was derived using erlotinib-treated BATTLE patients with or without 8 week DC, the primary study endpoint. **Results:** The EGFR and Kras signatures predicted *EGFR* and *Kras* mutations, respectively, in BATTLE patients (AUC 0.72 by ROC analysis, p=0.03 for EGFR; AUC 0.67, p=0.0.01 for KRas signature). In pts with wt *EGFR* and *Kras*, the EMT and 5-gene, but not the EGFR or KRas signatures, were associated with improved DC in ERLO treated pts (EMT signature: 64% for epithelial vs 10% mesenchymal groups, p=0.02; 5-gene: 83% vs 0%, p=<.001) and progression-free survival (PFS). The EGFR, EMT and 5-gene signatures were also significantly associated with in vitro sensitivity to ERLO in NSCLC cell lines. LCN2/NGAL, part of the 5-gene signature, was found to be associated with the epithelial phenotype. Potential therapeutic targets associated with mesenchymal phenotype including Axl were identified by the EMT signature. **Conclusions:** Gene expression profiling from CNBs is a feasible approach for predicting response and identifying activated oncogenic pathways and potential therapeutic targets in refractory NSCLC pts. EGFR and Kras signatures predicted mutation status but, in wt *EGFR* patients, did not predict efficacy. EMT and a novel 5-gene signature including LCN2/NGAL were predictive of DC in pts with wt EGFR treated in BATTLE and merit further investigation as markers of benefit for EGFR inhibitors.
Webcast:	http://webcast.aacr.org/portal/p/2011annual/9787

American Association for Cancer Research
615 Chestnut St. 17th Floor
Philadelphia, PA 19106

Print this Page

American Association for Cancer Research 102nd ANNUAL MEETING
April 2-6, 2011 • Orange County Convention Center, Orlando, Florida

Presentation Abstract

Presentation Number:	PL01-03
Presentation Title:	The landscape of cancer prevention: Personalized approach in lung cancer
Presentation Time:	Sunday, Apr 03, 2011, 10:00 AM -10:30 AM
Location:	West Hall D, Orange County Convention Center
Author Block:	*Waun Ki Hong*, *Edward S. Kim*, *J. Jack Lee*, *Ignacio Wistuba*, *Scott Lippman*. UT MD Anderson Cancer Ctr., Houston, TX
Webcast:	http://webcast.aacr.org/portal/p/2011annual/518

Abstract Body:

Recent data indicate that lung cancer causes over 1.3 million deaths worldwide each year, over 157,000 deaths in the U.S. alone. Although the overall incidence of cancer in the U.S. has decreased (1.3 % for men; 0.5% for women) largely because of declines in breast, prostate, lung, and colon cancer, lung cancer in women is increasing.

Tobacco causes more than 30% of cancer, not just of the lung but in at least 12 other cancers, including the head and neck, esophagus, pancreas, stomach, and bladder. Smoking cessation is an important approach for decreasing cancer risk but is not sufficient because 50% of new lung cancers arise in former smokers. The molecular mechanisms of lung-cancer pathogenesis in former smokers are under intense investigation.

Cancer screening and early detection have made substantial progress in cervical, colorectal, breast, prostate, and lung cancers. Very recently, the National Lung Screening Trial (NLST) demonstrated that spiral chest CT scanning reduced lung-cancer mortality by 20% in heavy smokers. This finding is extremely important and should be capitalized on by complementary targeted lung-cancer chemoprevention strategies that could further improve public health.

The fundamental concept of cancer chemoprevention, defined by Sporn as the use of pharmacologic agents to impede, arrest, or reverse carcinogenesis at earlier, preinvasive stages, was based on the biological understanding that genetic and epigenetic alterations through multistep carcinogenesis and field effects of carcinogen exposure lead to cancer. These biologic processes comprise the hallmarks of cancer development that were well described by Hanahan and Weinberg - evasion of apoptosis, self sufficiency of growth signals, insensitivity to antigrowth signals, strong replication potential, and sustained angiogenesis.

Cancer prevention trials of single or combined molecular-targeted agents in the breast, prostate, and colorectum and of vaccines in cervical cancer have met with very positive results. Several agents are currently approved by the Food and Drug Administration (FDA) for treating precancerous lesions or reducing the risk of cancer. These agents include bacillus Calmette-Guérin (BCG) in the bladder, hormone-related modulators to prevent breast cancer, nonsteroidal anti-inflammatory drugs to prevent colorectal and skin cancers, and human papillomavirus vaccines to prevent cervical cancer. Other agents, not FDA approved, also are established for reducing cancer risk in definitive phase III prevention trials.

Despite the availability of these agents to reduce some cancer risks, many are not accepted for cancer prevention by the public because of concerns over their toxicity and the need for long-term treatment. These agents can have paradoxical biologic effects; e.g., tamoxifen reduces estrogen-receptor-positive breast cancer but increases endometrial cancer, and finasteride reduces prostate cancer incidence but appeared in initial reports to induce high-grade prostate cancer. Therefore, cancer chemoprevention, in contrast to chemoprevention of cardiovascular disease with statins or antihypertensive agents, is highly controversial even in the setting of high-risk individuals. This controversy should be openly debated in regard to agent risk versus prevented-cancer risk and agent benefit versus agent risk in the primary, secondary, and tertiary prevention settings.

Lung cancer is the most lethal major cancer, with a 16% 5-year survival rate despite aggressive combined-modality treatment. This grim statistic has provided a strong rationale for conducting lung cancer chemoprevention trials over the last two decades and for the extraordinary efforts to prevent smoking and treat smoking addiction. Many chemopreventive agents (e.g., beta-carotene and vitamin A and E) were selected for clinical trials based largely on epidemiologic data; many were tested in large randomized controlled trials that produced quite disappointing results. Major reasons for the negative findings of these trials were a lack of understanding of the molecular underpinnings, heterogeneity of the targeted carcinogenesis and insufficient identification of the drivers of cancer development that could serve as molecular targets.

Lung cancer incidence by smoking status is as follows: former smokers, 50%; current smokers, 40%; and non-smokers, 10 %. Lung cancer in non- or former smokers is related to *EGFR* mutations and EML-ALK fusion as major drivers toward lung carcinogenesis. Therefore, the rationale for using EGFR inhibitors as chemopreventive agents in mutated-*EGFR* lung cancer is strong based on the field effect of mutant *EGFR* in normal epithelium adjacent to the tumor.

Lung cancer presents one of the biggest challenges and one of the greatest opportunities to make an impact on the global burden of cancer in the future. Our increased understanding of the biology of lung cancer has enabled us to develop biologic risk models and identify new targeted agents for the adjuvant or preventive settings that will enable more personalized chemoprevention.

Recent data provide a proof of principle of the potential of pharmacogenetics to personalize cancer prevention. These data come from genotyping studies in, for example, the head and neck (isotretinoin), colorectum (aspirin, celecoxib, statins), prostate (selenium), and bladder (BCG). Similar personalized genotyping approaches are being applied to research in tobacco dependence and cancer therapy.

We have investigated personalized targeted therapy in advanced lung cancer in our Biomarker-integrated Approaches of Targeted

Therapy for Lung Cancer Elimination (BATTLE) trial. Lessons learned from BATTLE are trickling down in a reverse migration to the development of a BATTLE prevention strategy. We are in the process of developing a biologic risk model for recurrence and second primary tumors (SPTs) through our Department of Defense (DoD)-supported lung cancer prevention programs, with parallel efforts to identify molecular drivers of recurrence as drug targets. The BATTLE program could have several roles in the prevention setting: A model of trial design, with its innovative Bayesian statistical design and emphasis on biomarker discovery; a discovery platform for targets, as provided by its analyses of multiple blood and tissue biomarkers; and a source of experience with targeted agents such as sorafenib. Sorafenib is a well-tolerated oral multi-kinase inhibitor with potent antiangiogenic activity. Studies of biomarkers predicting a benefit from sorafenib in the BATTLE study show a trend towards improved disease control in patients with *KDR* and *PDGFR* amplification, and BATTLE evidence also shows that circulating angiogenic factors may predict for efficacy of antiangiogenic agents such as sorafenib. The lessons we have learned from the BATTLE program may help us in studying sorafenib and other agents for cancer chemoprevention.

The first approach toward personalized lung cancer chemoprevention should occur in the tertiary prevention setting of patients with a history of resected lung cancer due to the high risk of these patients and their accessibility for molecular studies in tumor and adjacent tissue. These patients are at high risk for recurrence and SPTs, which can be histologically and molecularly similar or even indistinguishable from one another. Histologically normal tissue near a tumor often has molecular abnormalities due to field "cancerization" and/or clonal spread that may lead to a second cancer. Though predictive and prognostic signatures have been described in patients with, or at a high risk of, lung cancer, none are currently used clinically.

Using all that we have learned from our BATTLE and biological risk-modeling experience, we propose a personalized chemoprevention trial in the tertiary setting of resected lung cancer: Biomarker-integrated Approaches of Targeted Lung-cancer Elimination (BATTLE) Adjuvant and Prevention Trial. Following resection of adenocarcinoma, biomarker analyses would be performed on tumors and adjacent epithelium. Treatment groups would be determined by the molecular drivers of tumorigenesis. Patients whose tumors are driven by *EGFR* mutations could receive an EGFR inhibitor; *KRAS* and *BRAF* mutations, a Ras/Raf inhibitor; EML4-ALK translocation, an ALK inhibitor; VEGFR overexpression, vandetanib or other VEGFR inhibitors. Patients with alterations in the PI3K pathway could receive an Akt inhibitor. Primary endpoints would be recurrence and SPTs. Secondary endpoints would be tolerability, biomarker modulation, and correlation of biomarker modulation with outcome. Issues of dosing and informative biomarkers for patient selection must be optimized before this trial can begin; nevertheless, the basic BATTLE prevention design likely will become more common in the future, as our understanding of the biology of lung cancer tumorigenesis improves.

In this opening plenary session, specific strategic directions of personalized targeted chemoprevention, including study design issues of the use of spiral lung CT screening, targeted agents, and clear endpoints, will be discussed thoroughly.

American Association for Cancer Research
615 Chestnut St. 17th Floor
Philadelphia, PA 19106

Print this Page

Presentation Abstract

Abstract Number:	955
Presentation Title:	Specific forms of mutant *KRAS* predict patient benefit from targeted therapy in the BATTLE-1 clinical trial in advanced non-small cell lung cancer
Presentation Time:	Sunday, Apr 03, 2011, 4:20 PM - 4:35 PM
Location:	Room W311 E-H, Orange County Convention Center
Author Block:	Nate T. Ihle[1], Roy S. Herbst[1], Edward S. Kim[1], Ignacio I. Wistuba[1], J.Jack Lee[1], George R. Blumenschein, Jr.[1], Anne S. Tsao[1], Lu Chen[1], Shuxing Zhang[1], Christine M. Alden[1], Ximing Tang[1], Suyu Liu[1], David J. Stewart[1], Vassiliki Papadimitrakopoulou[1], John V. Heymach[1], Hai T. Tran[1], Marshall E. Hicks[1], Jeremy J. Erasmus[1], Sanjay Gupta[1], John D. Minna[2], Jill Larsen[2], Scott M. Lippman[1], Waun Ki Hong[1], Garth Powis[1]. [1]The University of Texas MD Anderson Cancer Center, Houston, TX; [2]The University of Texas Southwestern Medical Center, Dallas, TX
Abstract Body:	Mutant *KRAS* (mut-*KRAS*) is present in 17-25% of all human cancers, where it plays a critical role in driving cancer cell growth and resistance to therapy. Despite numerous attempts, there is still no effective therapy for mut-*KRAS* tumors. Understanding the signaling mechanisms activated by mut-*KRAS* and finding agents to inhibit mut-*KRAS* signaling are important unmet needs in cancer therapy today. The recently completed BATTLE-1 clinical trial, a prospective, multi-arm, biopsy-mandated, biomarker-driven, clinical trial in advanced refractory non-small cell lung cancer (NSCLC), found that mut-*KRAS* did not accurately predict patient outcome (progression-free survival) to targeted intervention. This finding contradicted published evidence for such a relationship from colon cancer and some previous NSCLC studies. We explored more specifically the nature of the *KRAS* mutations, which are primarily found at codons 12 and 13, where different base substitutions lead to alternate amino acid (aa) substitutions. NSCLC has a much higher proportion of mut-*KRAS* G12C(cysteine) aa substitutions (47%) due to carcinogens in tobacco smoke, and only 15% mut-*KRAS* have G12D(aspartate). These data contrast those in other solid tumors, such as colon or pancreas, which predominantly manifest mut-*KRAS* G12D (50%) and only 9% mut-*KRAS* G12C. In a subset analysis of the BATTLE-1 data, we showed significantly worse progression-free survival in patients with mut-*KRAS* G12C, versus other mut-KRAS including G12D (p=.041) and who were treated with erlotinib, vandetanib or sorafenib. In a panel of NSCLC cell lines with known mut-*KRAS* aa substitutions to identify pathways activated by the different mut-*KRAS* genotypes, we found that mut-*KRAS* G12D activates both PI-3-K and MEK signaling, while mut-*KRAS* G12C does not and alternatively activates PKCζ and RAL signaling. This finding was confirmed in immortalized human bronchial epithelial (HBEC) cells stably transfected with wt-*KRAS* or different forms of mut-*KRAS*. Our molecular modeling studies show that the different conformation imposed by mut-*KRAS* G12C could lead to altered association with downstream signaling transducers, compared to mut-*KRAS* G12D. The significance of the findings for developing mut-*KRAS* therapies is profound, since it suggests that not all mut-*KRAS* may be addictive; and that different combinations of inhibitors of downstream signaling may be needed for different mut-KRAS.
CME Designation:	CME-Designated

American Association for Cancer Research
615 Chestnut St. 17th Floor
Philadelphia, PA 19106

Print this Page

Presentation Abstract

Abstract Number:	1122
Presentation Title:	Insulin receptor expression and survival of patients with non-small cell lung cancer
Presentation Time:	Monday, Apr 04, 2011, 8:00 AM -12:00 PM
Location:	Exhibit Hall A4-C, Poster Section 6
Poster Section:	6
Poster Board Number:	8
Author Block:	Jin-Soo Kim, Edward S. Kim, Diane Liu, J. Jack Lee, Luisa Solis, Carmen Behrens, Scott Lippman, Waun Ki Hong, Ignacio I. Wistuba, Ho-Young Lee. University of Texas M.D. Anderson Cancer Center, Houston, TX
Abstract Body:	Purpose: The purpose of this study was to characterize insulin receptor (IR) and insulin-like growth factor-1 receptor (IGF-1R) expression in patients with non-small cell lung cancer (NSCLC). Methods: A total of 459 patients who underwent curative resection of NSCLC were studied (median follow-up duration, 4.01 years). Expression of the IR and IGF-1R protein in tumor specimens was assessed immunohistochemically using tissue microarrays. Results: The cytoplasmic IR score was higher in patients with adenocarcinoma (ADC) than in those with squamous cell carcinoma (SCC) whereas cytoplasmic IGF-1R was higher in patients with SCC than those with ADC. Neither IR nor IGF-1R expression was associated with sex, smoking history, or clinical stage. Patients with positive IR or IGF-1R expression levels had poor recurrence-free (3.8 vs. 3.3 years; 3.8 vs. 2.0 years, respectively) but similar overall survival durations. Patients with high expression levels both IR and IGF-1R had shorter recurrence-free and overall survival compared to those with low levels of IR and/or IGF-1R expression. IGF-1R and IR expressions were negatively correlated with survival duration of patients with ADC and SCC, respectively. Finally, a multivariate analysis revealed the impact of IR, but not IGF-1R, as an independent prognostic predictor of survival: hazard ratio (HR) for OS, 1.005 (95% confidence interval [CI], 1.001 - 1.010], HR for RFS, 0.608 (95% CI, 1.001 - 1.009) when tested as a continuous variable. Conclusions: Overexpression of IR, but not IGF-1R, appears to foretell a poor survival among patients with NSCLC, especially those with SCC. Thus, expression of IR has a negative prognostic value and future clinical trials with therapy interventions of IR regulation should be under the consideration for this patient population.

American Association for Cancer Research
615 Chestnut St. 17th Floor
Philadelphia, PA 19106

This is the program for the 2010 Joint Statistical Meetings in Vancouver, British Columbia.

Abstract Details

Activity Number:	360
Type:	Contributed
Date/Time:	Tuesday, August 3, 2010 : 10:30 AM to 12:20 PM
Sponsor:	Biometrics Section
Abstract - #307615	
Title:	Design, Implementation, and Results for a Bayesian Adaptive Randomization Trial for Targeted Therapy in Lung Cancer
Author(s):	Suyu Liu*+ and J. Jack Lee
Companies:	MD Anderson Cancer Center and MD Anderson Cancer Center
Address:	1400 Pressler St., Houston, TX, 77030,
Keywords:	Bayesian adaptive design ; clinical trial ; hierachical Bayes model
Abstract:	The BATTLE trial applies response adaptive randomization (AR) to identify promising treatment agents for lung cancer patients. A hierarchical Bayes model is used to characterize disease control rates in four treatment arms by incorporating biomarkers. After an equal randomization phase, patients were adaptively randomized to treatments based on the posterior disease control rates. A web-based application has been developed to conduct this trial. We have successfully randomized 255 patients, characterized the treatment efficacy and identified the associated predictive markers. The adaptive randomization, however, did not work as well as we planned. We will report the lessons learned from running this innovative trials for personalizing medicine. Practical considerations for running a successful Bayesian adaptive trial will be given.

The address information is for the authors that have a + after their name.
Authors who are presenting talks have a * after their name.

Back to the full JSM 2010 program

2010 JSM Online Program Home

Print this Page

Presentation Abstract

Abstract Number:	4109
Presentation Title:	A 5-gene signature (sig) predicts clinical benefit from erlotinib in non-small cell lung cancer (NSCLC) patients (pts) harboring wild-type (wt) EGFR & KRAS
Presentation Time:	Tuesday, Apr 05, 2011, 1:00 PM - 5:00 PM
Location:	Exhibit Hall A4-C, Poster Section 13
Poster Section:	13
Poster Board Number:	1
Author Block:	Pierre Saintigny[1], Lixia Diao[1], Jing Wang[1], Luc Girard[2], Steven H. Lin[1], Kevin R. Coombes[1], Suyu Liu[1], J. Jack Lee[1], John N. Weinstein[1], Yang Xie[2], You H. Fan[1], Xi Ming Tang[1], Edward S. Kim[1], Roy S. Herbst[1], Anne Tsao[1], George R. Blumenschein[1], Li Mao[3], Scott M. Lippman[1], John D. Minna[2], Waun Ki Hong[1], Ignacio I. Wistuba[1], John V. Heymach[1]. [1]UT M.D. Anderson Cancer Ctr., Houston, TX; [2]UT SouthWestern Medical Center, Dallas, TX; [3]University of Maryland, Baltimore, MD
Abstract Body:	Background: Despite a low response rate, erlotinib (E) improves survival in a subset of NSCLC pts with wt EGFR but there are no established markers for identifying pts likely to have clinical benefit. We hypothesized that a gene expression sig could be used for this purpose. Material and Methods: We used pretreatment gene expression profiles (Affymetrix HG1.0ST) from 101 chemo-refractory pts in our Biomarkers-Integrated Approaches of Targeted Therapy for Lung Cancer Elimination (BATTLE) treated with E, E+bexarotene (EB), sorafenib (S), or vandetanib (V). 24 cases of wt EGFR & KRAS tumors treated with E or EB were compared to train the signature (two-sided t-test), using the primary end-point of the trial [8-week disease control (8wDC)]. Principal component (PC) analysis and a logistic regression model were used to develop the sig. Gene expression profiles from 108 NSCLC cell lines (Illumina), with available E IC50 (N=94) and DNA methylation profiling (N=66, Illumina), were used for in vitro studies. Results: 113 genes were differentially expressed between pts with or without 8wDC (false discovery rate 30%; P=0.004). Leave-one-out cross validation with various gene list lengths produced a 5-gene sig, including lipocalin 2 (LCN2), with a specificity, sensitivity and accuracy of 80% to predict 8wDC. In pts treated with E or EB, using the median sig score, the 8wDC rate in the sig-positive group was 83% compared with 0% in the sig-negative group; the sig did not predict 8wDC in pts treated with S or V (Mantel-Haenszel chi-squared test P=0.023). The improvement in 8wDC in the sig-positive group translated to an increased progression-free survival (PFS) (hazard ratio=0.12, 95% confidence interval: 0.03-0.46, P=0.001; log-rank P=0.0004; median PFS: 12.5 weeks vs. 7.2 weeks). We tested the sig in an independent set of 47 wt EGFR&KRAS cell lines. It predicted E sensitivity with an area under the curve of 78% (P=0.002). The first PC of the sig and the IC50 for E were correlated (r=-0.47, P=0.0009). In 108 NSCLC cell lines, LCN2 gene expression was bimodal and correlated with the IC50 for E (r=-0.46, P=0.001). Degree of methylation and expression level of LCN2 were inversely in wt EGFR & KRAS NSCLC cells (r=-0.79, P<0.0001, N=33). Cell lines with completely unmethylated LCN2 were more sensitive to E compared to those with LCN2 full methylation (N=36) (P=0.006); the difference remained significant in wt EGFR & KRAS cell lines (P=0.014). Conclusion: We identified a 5-gene sig predictive of PFS benefit in NSCLC pts with wt EGFR & KRAS treated with E, but not S or V The sig was also predictive of E sensitivity in vitro. LCN2 was the strongest individual marker of sensitivity and may be epigenetically regulated.

American Association for Cancer Research
615 Chestnut St. 17th Floor
Philadelphia, PA 19106

BATTLE Manuscript Updates

1. BATTLE Primary Paper (E Kim) –In press, *Cancer Discovery*; publication online April 2011 and in 1st issue July 2011.
2. Erlotinib trial (E Kim/P Saintigny) – manuscript is being drafted with an estimated submission date of May 2011.
3. Erlotinib and Bexarotene trial (E Kim/W William) – "Erlotinib and Bexarotene for Advanced Non-Small Cell Lung Cancers." Statistical analysis was received and Dr. William is working to complete the draft with a submission date of May 2011.
4. Sorafenib trial (G Blumenschein) – Dr. Blumenschein has sent a draft of the manuscript to Dr. Hong for review. Further statistical analysis is needed before submission.
5. Vandetanib trial (A Tsao) – Dr. Tsao is waiting to receive the statistical report from Suyu before she can complete the draft. Plan to submit Spring 2011.
6. Elderly Analysis paper – Dr. Tsao is waiting to receive the statistical report from Suyu before she can complete the draft. Plan to submit Spring 2011.
7. CAF analysis (H Tran) – Dr. Tran confirmed that he has 1 additional plate left to re-analyze by multiplex magnetic beads (to be completed this week). He will send the data to Dr. Lee's group for biostatistical analysis.
8. EGFR (P Saintigny) - "An EGFR mutation signature reveals features of the EGFR-dependent phenotype and identifies MACC1 as an EGFR mutant-associated regulator of MET" was rejected by *Cancer Cell*. Additional experiments have been/are being performed to allow a resubmission to Cancer Cell in the next few months, if the editors are receptive, including an additional *in vitro* study (they now have knockdown data in 3 EGFR mutant cell lines, versus only one in the original manuscript). They will also enhance clinical relevance by applying the signature and looking at MACC1 gene expression in the entire BATTLE gene expression (both platforms).
9. EMT (L Byers) – "An epithelial-mesenchymal transition (EMT) gene signature predicts sensitivity to erlotinib and identifies new EMT-associated therapeutic targets in non-small cell lung cancer**."** Lauren Averett Byers, Jing Wang, Pierre Saintigny, Lixia Diao, John Yordy, Luc Girard, Mike Story, Mike Peyton, Li Shen, Youhong Fan, Uma Giri, Praveen K. Tumula, Edward Kim, Roy Herbst, J. Jack Lee, Scott Lippman, Kian Ang, Gordon B. Mills, Waun K. Hong, John N. Weinstein, Ignacio I. Wistuba, Kevin R. Coombes, John D. Minna, John V. HeymachDr. Byers stated that she sent the draft to Dr. Heymach for review and edits before the manuscript is sent to the full author list.
10. KRAS (N Ihle/G Powis) – "Substitutions in the KRas oncogene determine protein behavior: Implications for signaling and clinical outcome." Nate T. Ihle, Lauren A Byers, Edward S. Kim, Pierre Saintigny, J. Jack Lee, Suyu Liu, Jill E Larsen, Lixia Diao, Kevin R Coombes, Lu Chen, Shuxing Zhang, Mena F Abdelmelek, Ximing Tang, Vassiliki Papadimitrakopoulou, John D. Minna, Scott M. Lippman, Waun K. Hong, Roy S. Herbst, Ignacio I. Wistuba, John V. Heymach, Garth Powis. Submitted to Journal of National Cancer Institute (JNCI). The manuscript was submitted to JNCI on 3/29/11 and is currently waiting on the review.
11. 5-Gene Signature (P Saintigny) – "A 5-gene signature (sig) predicts clinical benefit from erlotinib in non-small cell lung cancer (NSCLC) patients (pts) harboring wild-type (wt)

EGFR & KRAS." Dr. Saintigny reported that the paper will focus on lipocalin 2, and no more on the signature. The paper is already drafted, but we are waiting for Jack Lee's report on lipocalin 2 expression in the whole population of the trial using immunohistochemistry. Overexpression and downregulation experiments of lipocalin 2 expression are ongoing in collaboration with Dr. Arlinghaus lab: lipocalin 2 knockdown in HCC827 (EGFR mutant) decrease erlotinib-induced apoptosis which fit their hypothesis; similar experiments are ongoing in EGFR wild type cell lines in the lab and he is working with them to finish the draft for submission.

12. Biomarker paper - Dr. Wistuba is drafting the paper with an estimated submission date of May 2011.
13. Non-clinical trial related:
    a. R Lotan's papers
        1. "Subcellular Localization of Retinoid Receptors Correlates with Prognosis in a subset of NSCLCs." A draft is written and he will distribute the final version for review this week.
        2. "Tyrosine Phosphorylation of the Tumor Suppressor Protein GPRC5A by Epidermal Growth Factor Receptor Activation Inhibits its Activity." Projected time for completion is about 3 months to allow for additional data analysis.
    b. HY Lee papers
        1. "Differential Impacts of IGFBP-3 in Epithelial IGF-induced Lung Cancer Development." Woo-Young Kim, Mi-Jung Kim, Hojin Moon, Ping Yuan, Jin-Soo Kim, Jong-Kyu Woo, Guangcheng Zhang, Young-Ah Suh, Lei Feng, Carmen Behrens, Carolyn S. Van Pelt, Hyunseok Kang, J. Jack Lee, Waun-Ki Hong, Ignacio I. Wistuba, and Ho-Young Lee. Endocrinology, 2011 Mar 29. [Epub ahead of print]
        2. "Prognostic impact of Insulin Receptor Expression on Survival of Patients with Non-Small Cell Lung Cancer." Jin-Soo Kim, Edward S. Kim, Diane Liu, J. Jack Lee, Luisa Solis, Carmen Behrens, Scott M. Lippman, Waun Ki Hong, Ignacio I. Wistuba, and Ho-Young Lee, submitted to Cancer, 2011
    c. B Johnson – One publication **"**A novel, highly sensitive antibody allows for the routine detection of ALK-rearranged lung adenocarcinomas by standard immunohistochemistry.**"** Mino-Kenudson M, Chirieac LR, Law K, Hornick JL, Lindeman N, Mark EJ, Cohen DW, Johnson BE, Jänne PA, Iafrate AJ, Rodig SJ. *Clin Cancer Res*. 2010 Mar 1;16(5):1561-71. No further manuscripts planned.
    a. F Khuri – They are continuing to accrue to our RAD001 pre-op trial.
        1. Xu C-X, Yue P, Owonikoko TK, Ramalingam SS, Khuri FR, and Sun S-Y. The combination of RAD001 and NVP-BEZ235 exerts synergistic anticancer activity against non-small cell lung cancer *in vitro* and *in vivo*. PLoS One, under review.
        2. Xu C-X, Zhao L, Yue P, Fang G, Tao H. Owonikoko TK, Ramalingam SS, Khuri FR, and Sun S-Y. Augmentation of NVP-BEZ235's anticancer

activity against human lung cancer cells by blockage of autophagy. Mol Cancer Ther, under review.